UNIVERSIDADE
BEIRA INTERIOR

The recent acceleration of the Universe:
Exploring the hidden essence of the Cosmos

Imanol Albarran Payo

Tese para obtenção do Grau de Doutor em
Física
(3º ciclo de estudos)

Orientador: Prof. Doutora Mariam Bouhmadi-López
Co-orientador: Prof. Doutor João Pedro de Jesus Marto

Maio de 2021

Provas públicas realizadas no dia 20 de abril de 2021

Composição do júri:

- Doutor Paulo Jorge da Silva Almeida (presidente)

- Doutora Mariam Bouhmadi-López

- Doutor Claus Kiefer (arguente)

- Doutora María del Prado Martín-Moruno (arguente)

- Doutor José Manuel Pé-Curto Velhinho

- Doutor João Pedro Trancoso Gomes Rosa

To my loving parents

Acknowledgements

First of all, I want to express my most sincere gratitude to my supervisor Dr. Mariam Bouhmadi-López for all the work and efforts done in order to drive me from the master thesis till the present day. I should declare that all the walked path would have never been possible without her help and assistance. During the last six years I learnt a large amount of issues about the most intriguing aspects of life, beyond theoretical physics where She has shown to be an excellent investigator and a hard worker researcher, She granted me most of the crucial lessons to face in life. Her courage had been a source of inspiration. In addition, She gave me the opportunity to meet with researchers from all around the world, visit places I could have never visited in any other way and a vast amount of experiences that have broaden my mind. I want to thank as well my co-supervisor Dr. João Pedro de Jesus Marto for his invaluable help along my stay at Universidade da Beira Interior (UBI), in Covilhã. His absolute disposal and comprehension has made easier the stay in a foreign country. I have to declare that I will have never reached to this point if it were not for my supervisors.

Along my stay in Covilhã, I had the opportunity to meet with other students whom I want to express my gratitude: To Sravan Kumar Korumilli, for giving me moments of passionate discussion about any scientific subject. To João Morais for his lessons on computations and personal assistance. To Amine Bouali and Che-Yu Chen, for their kindy personality and hard work in collaboration in projects. I want to thank as well Hugo Nunes and Nivaldo Martins for their invaluable human capital and for improving a comfortable cohabitation in Covilhã.

Not less important, I would thank my parents who helped me on the most difficult economical and personal moments, their help will always be invaluable. I will be eternally grateful for their comprehension and patience. It is worthy to mention as well the spirits of my close friends in Bilbao: *Txika, Janis, Moli, López, Ekaitz, Eder, Joan Arkaitz, Pablo, Ibai* and the crew of people that engross the most beautiful experiences at my homeland. Special gratitude to Iñaki Zarza and the family Lozano-Rodríguez for being sensitive and careful with me.

In addition, I want to thank the Santader Totta UBI fellowship I had in my first year, it really helped me at the beginning of my PhD.

All these people had collaborated along the path that takes where I am now. From the most important pillars to the last grain of sand, I keep all them in my hearth.

The true sign of intelligence is not knowledge but imagination
- Albert Einstein

Oak leaves by Florentino Albarran, 2020.

Resumo

A tese presente tem por objetivo estudar e comparar três modelos com energia escura fantasma, onde cada um induz um cenário cosmológico extremo de extinção do Universo. Escolhemos identificar esses três modelos como: modelo A, modelo B e modelo C, enquanto as extinções cósmicas correspondentes são conhecidas como *Big Rip* (BR), *Litlle Rip* (LR) e *Little Sibling of the Big Rip* (LS), respetivamente. Encaramos o BR como uma verdadeira singularidade, uma vez que esta acontece ao fim de um intervalo de tempo cósmico finito, enquanto identificamos o LR e LS como acontecimentos abruptos, porque estes ocorrem ao fim de intervalo de tempo cósmico que tende para infinito. Contudo, é reconhecido que em tais acontecimentos abruptos, mais cedo ou mais tarde, todas as estruturas ligadas serão inevitavelmente destruídas e, portanto, o Universo iria confrontar-se com uma destruição total num intervalo de tempo cósmico finito.

Numa primeira abordagem ao assunto da tese, considerámos a fenomenologia das soluções de fundo e as perturbações de primeira ordem cosmológicas para os modelos de energia escura fantasma acima mencionados. Adicionalmente, usámos o largamente conhecido modelo ΛCDM como padrão em relação ao qual se estimam os desvios dos modelos considerados. Uma vez que o conteúdo de energia escura está presente, evitamos o surgimento das instabilidades associadas através da decomposição da pressão da energia escura nas contribuições adiabáticas e não adiabáticas. Calculamos, através de métodos numéricos, a evolução das quantidades perturbadas para um Universo contendo radiação, matéria e energia escura. Estes cálculos são feitos assumindo um ponto de partida bem no interior da era dominada pela radiação até ao futuro longínquo. Subsequentemente, prevemos o espetro de potência atual e a taxa de crescimento f_{σ_8} para cada modelo. Tais quantidades observáveis são, então, comparadas com os dados observacionais correntes de modo a encontrar indícios que nos permitiriam distinguir os diversos modelos na época atual. Por forma a completar o estudo, impusemos constrangimentos observacionais aos modelos de energia escura fantasma com o ΛCDM para obter um conjunto consistente de parâmetros. Por um lado, descobrimos que embora o ΛCDM se ajuste melhor às observações, os modelos aqui considerados seguem de muito perto esse bom ajuste do modelo padrão. Por outro lado, descobrimos que estes modelo genuínos de energia escura fantasma induzem uma inversão de sinal do potencial gravítico para fatores de escala muito grandes. Este facto pode ser interpretado como a força da gravidade se tornar efetivamente repulsiva num futuro distante. Finalmente, estudámos os efeitos de variar a velocidade efetiva do som da energia escura nas perturbações.

Numa segunda abordagem, partimos do princípio que é expectável que os efeitos quânticos se tornem importantes quando o Universo se aproxima de uma singularidade cósmica futura, o que se afigura o destino certo nos modelos considerados anteriormente. Infelizmente, não dispomos ainda de uma teoria quântica da gravidade consistente para completar a nossa visão sobre os acontecimentos mais dramáticos no fim da vida do Universo. É esperado que com a ajuda de uma teoria tão fundamental, como a teoria quântica do campo gravítico, os cenários singulares previstos na Relatividade Geral sejam naturalmente evitados. Assim, abordámos o problema da remoção das singularidades cosmológicas adotando uma abordagem quântica. A quantização é implementada através da equação de Wheeler-DeWitt e a imposição da condição fronteira de DeWitt, isto é, considerando que a função de onda se anula perto da singularidade. Analisámos cada modelo considerando várias ordens dos fatores na construção dos observáveis

na equação de Wheeler-DeWitt, resolvendo-a para vários conteúdos da energia escura dados por (i), um fluido perfeito, e (ii), um campo escalar. Adicionalmente, considerámos estes modelos no contexto da teoria de gravidade modificada *Eddington-inspired-Born-Infeld* e aplicámos a abordagem quântica, acima descrita, para remover as singularidades clássicas.

Deste modo, esta tese é dividida em duas partes principais, uma clássica, onde descrevemos as soluções de fundo e as perturbações desse fundo para os três modelos genuínos de energia escura fantasma e, uma segunda parte onde estudamos a remoção quântica das singularidades resultantes destes modelos.

Dado que a UBI permite que se apresente uma tese que inclua uma introdução, um conjunto de capítulos baseados em trabalhos publicados durante o Doutoramento e as conclusões, nós seguimos principalmente esse formato.

Palavras-chave

Universo tardio, energia escura, teoria da gravitação modificada, teorias de Palatini, perturbações cosmológicas, cosmologia quântica, dados de observação.

Abstract

The present thesis is aimed to disclose three genuine phantom Dark Energy (DE) models where each of them induce a particular cosmic doomsday. We have named these models as model A, model B and model C, while the corresponding induced cosmic events are known as Big Rip (BR), Little Rip (LR) and Little Sibling of the Big Rip (LS), respectively. We regard a BR as a true singularity since it takes place at a finite cosmic time, while we have coined LR and LS as *abrupt events*, since they occur at infinite cosmic time. Nevertheless, it is well known that in such abrupt events sooner or later all the bound structures would unavoidably torn away, and therefore, the Universe would face a total destruction at a finite cosmic time.

On the one side, we have addressed the background phenomenology and the first order cosmological perturbations for the phantom DE models above mentioned. In addition, we have made use of the widely known ΛCDM model as a guideline to measure deviations among the models. Given that a DE content is present, we avoid the associated instabilities at the perturbative level by applying the method of DE pressure decomposition in its adiabatic and non-adiabatic contributions. We compute, by means of numerical methods, the evolution of the perturbed quantities for a Universe filled with radiation, matter and DE. Such computations are carried from well inside the radiation dominated era to the far future. Then, we predict the current matter power spectrum and f_{σ_8} growth rate for each model. The latter mentioned observable quantity is compared with the current observational data in order to find footprints that could allow us to distinguish between the mentioned models. For the sake of completeness, we have fitted observationally these phantom DE models together with ΛCDM in order to constrain the parameters characterising the models. On the one hand, we have found that despite that ΛCDM still gives the best fit, it is closely followed by the models studied in the present thesis. On the other hand, we have found that these genuine phantom models induce a sign switch of the gravitational potential at very large scale factors. This fact could be understood as gravity becoming effectively repulsive in the far future. Finally, we have studied the effects of DE speed of sound on the perturbations.

On the other side, it is expected that quantum effects will become important when the Universe approaches a future cosmic singularity, which is the case of those events addressed in the present thesis. Unfortunately, we have not yet a consistent theory of quantum gravity to deal with the most dramatic effects that would take place at the end of the Universe. It is expected that such a fundamental quantum theory of gravity will naturally avoid those singularities present in the classical theory of General Relativity (GR). We have rather addressed the issue of cosmological singularity avoidance within the context of a quantum approach. The quantisation is carried via Wheeler-DeWitt (WDW) equation and imposing the DeWitt (DW) boundary condition, i.e. the wave function vanishes close to the singularity. We have analysed each model by considering different factor orderings and solving the WDW equation for a DE content given by (i), a perfect fluid, and (ii), a scalar field. In addition, we have addressed these phantom models in the context of the Eddington-inspired-Born-Infeld (EiBI) modified theory of gravity and applied the same quantisation methods above mentioned to analyse the avoidance of singularities from a quantum point of view.

Therefore, this thesis is divided in two main parts, a classical part, where we present the back-

ground and perturbations of three genuine phantom models, and a second part, where we address the avoidance of singularities induced by such models from a quantum point of view.

Given that UBI allows to present the thesis as an introduction, a set of chapters based on the published works during the PhD and the conclusions, we have followed mainly this format.

Keywords

The late-universe, dark energy, modified gravity, Palatini theories, cosmological perturbations, quantum Cosmology, observational data.

List of publications

This dissertation is based on the following publications (with referee):

- Albarran, Imanol and Bouhmadi-López, Mariam, "Quantisation of the holographic Ricci dark energy model," *JCAP* **1508** (2015) 051, arXiv:1505.01353 [gr-qc].
- Albarran, Imanol and Bouhmadi-López, Mariam and Cabral, Francisco and Martín-Moruno, Prado, "The quantum realm of the "Little Sibling" of the Big Rip singularity," *JCAP* **1511** (2015) 044, arXiv:1509.07398 [gr-qc].
- Albarran, Imanol and Bouhmadi-López, Mariam and Kiefer, Claus and Marto, João and Vargas Moniz, Paulo, "Classical and quantum cosmology of the little rip abrupt event," *Phys. Rev. D* **94** (2016) no.6, 063536 , arXiv:1604.08365 [gr-qc].
- Albarran, Imanol and Bouhmadi-López, Mariam and Morais, João, "Cosmological perturbations in an effective and genuinely phantom dark energy Universe," *Phys.Dark Univ.* **16** (2017) 94-108 , arXiv:1611.00392 [astro-ph.CO].
- Albarran, Imanol and Bouhmadi-López, Mariam and Chen, Che-Yu and Chen, Pisin "Doomsdays in a modified theory of gravity: A classical and a quantum approach," *Phys. Lett. B* **772** (2017) 814-818 , arXiv:1703.09263 [gr-qc].
- Albarran, Imanol and Bouhmadi-López, Mariam and Morais, João "What if gravity becomes really repulsive in the future?," *Eur.Phys.J.C* **78** (2018) 260 , arXiv:1706.01484 [gr-qc].
- Albarran, Imanol and Bouhmadi-López, Mariam and Chen, Che-Yu and Chen, Pisin "Quantum cosmology of Eddington-Born-Infeld gravity fed by a scalar field: The big rip case," *Phys.Dark Univ.* **23** (2019) 100255 , arXiv:1811.05041 [gr-qc].
- Bouali, Amine and Albarran, Imanol and Bouhmadi-López, Mariam and Ouali, Taoufik "Cosmological constraints of phantom dark energy models," *Phys.Dark Univ.* **26** (2019) 100391 , arXiv:1905.07304 [astro-ph.CO].
- Albarran, Imanol and Bouhmadi-López, Mariam and Chen, Che-Yu and Chen, Pisin "Eddington-inspired-Born–Infeld tensorial instabilities neutralized in a quantum approach," *Eur.Phys.J.C* **80** (2020) 33 , arXiv:1911.03935 [gr-qc].
- Albarran, Imanol and Bouhmadi-López, Mariam and Marto, João "The Speed of sound in phantom DE models". To be submitted for publication soon.

In addition, we have published the following proceedings (also with referee):

- Albarran, Imanol and Bouhmadi-López, Mariam and Morais, João, "Cosmological Perturbations in Phantom Dark Energy Models," *Universe* **3** no. 1, (2017) 22.
- Albarran, Imanol and Bouhmadi-López, Mariam and Cabral, Francisco and Martín-Moruno, Prado, "The Avoidance of the Little Sibling of the Big Rip Abrupt Event by a Quantum Approach," *Galaxies* **6** no. 1, (2018) 21.

Contents

List of Abbreviations

GR	General Relativity
DE	Dark Energy
DM	Dark Matter
ΛCDM	Λ cold dark matter
dS	de Sitter
BAO	Baryon Acoustic Oscillations
WMAP	Wilkinson Microwave Anisotropic Probe
CMB	Cosmic Microwave Background
EoS	Equation of State
GCG	Generalised Chaplying Gas
BR	Big Rip
BF	Big Freeze
SS	Sudden Singularity
LR	Little Rip
LS	Little Sibling of the Big Rip
QM	Quantum Mechanics
QC	Quantum Cosmology
WDW	Wheeler DeWitt
DW	DeWitt
HRDE	Holographic Ricci Dark Energy
BO	Born-Oppenheimer
WKB	Wentzel-Kramers-Brillouin
LB	Laplace-Beltrami
EiBI	Eddington-inspired-Born-Infeld

1

Introduction

All my life through, the new sights of Nature made me rejoice like a child

– Marie Curie

1.1 The classical Universe

Cosmology has experimented a significant progress since its boost with Einstein's GR in 1915. The first evidences that endorse the reliability of GR, for instance, explained the anomaly of the mercury's perihelium precession and the apparent position of stars during a solar eclipse [1]. A century later, the gravitational waves predicted by GR were measured for the first time as a result of an extraordinary collaboration work, which probed the shortest distance ever measured [2]. Certainly, the technological development of the last century has played an important role on the improvement of the observational aspect of Cosmology. During this time, some of the hiding features of the current Universe were revealed. Let us mention briefly those that have changed completely the initial knowledge we had of the cosmos.

1.1.1 A brief history of cosmology: from the first revelations to the current knowledge

In 1929 Hubble computed the current expansion rate of the Universe by using the redshift of the Cepheid star cluster [3]. He also computed the redshift of the star-light coming from other astronomical objects, identifying them as galaxies and regarding the milky way as just another common galaxy in the vast Universe [4]. The electromagnetic Doppler effect was the clearest evidence of a dynamical Universe rather than a static one, contrary to the most widely accepted idea on the scientific community including Einstein believes. In fact, the cosmological constant introduced by Einstein was motivated to counteract the natural gravitational attraction of standard matter, i.e. matter that fulfill the strong energy condition $\rho + p > 0$, $\rho + 3p > 0$, where ρ stands for the energy density and p for the pressure. In 1922 the soviet scientist Alexander Friedmann solved the Einstein equations for a homogeneous and isotropic Universe filled with standard matter pointing out an expanding Universe for open and flat spatial curvature while for closed geometry the Universe is finite and recollapses after reaching a maximum size. Meanwhile, the Belgium scientist Georges Lemaître was already working on the theory of "the primeval atom", where the notion of a very hot and dense early Universe was introduced for the first time [5]. This idea is considered the precursor of the Big Bang theory. The theory continued along the path laid by Friedmann while it was observationally supported by the existence of the Cosmic Microwave Background (CMB) radiation, first detected by Penzias and Wilson in 1965 [6]. Such radiation corresponds to a black body emission at $2.625\ K$ at present, while small fluctuations reaching up to ten thousandth $\pm 10^{-3}\ K$. In 1933 Fritz Zwicky proposed, for the first time, the existence of Dark Matter (DM) between galaxies [7], however, the clearest evidences were not found till the late 70's when Vera Rubin observed the rapid rotation curves of galaxies [8].

Subsequent observations, based on gravitational lensing, pointed to the presence of an exotic matter that do not interacts with radiation as usual baryonic matter does, altough it contributes to the universal energy budget as ordinary matter [7–9]. Finally, in 1998, observations of supernova type Ia pointed out that the Universe is currently experiencing a phase of accelerated expansion [10–12], corroborated by further observations as the Wilkinson Microwave Anisotropy Prove (WMAP) and Baryon Acoustic Oscillations (BAO) [13–17]. The energy source responsible for such speed up is still unknown, which is the reason for coining it DE. Indeed, it represents roughly 70% of the total energy budget of the Universe. The remaining 30% corresponds mainly to the contribution of matter wherein only a tiny 5% corresponds to baryonic matter. The contribution of radiation could be neglected at present since it corresponds to an insignificant 0.008% [15].

According to what was just exposed above, in the most optimistic perspective, we barely know from a fundamental point of view 5% of the total composition of the Universe. However, it can be said that we are lucky for living in particular conditions, where the horizon covers large distances giving us the possibility to "watch" the evolution of the Universe from the distant past to the present epoch. The current expansion rate is set to be roughly $H_0 \sim 70$ Km Mpc^{-1}s^{-1}. This value establishes, at the present time, the size of the observable part of the Universe as a ball with a 95 giga light years diameter, holding inside up to the last scattering surface and further. This value is crucial, at first, because the observations of very distant galaxies give us a photography of the past scenarios, but secondly, because a detailed view of the CMB grant us the opportunity to draw a chronology of the different stages faced by the Universe from the very early epochs.

The age of the Universe is roughly 14 Gyr. The radiation dominated epoch finished after the first 0.3 Myr years and, since then, after the decoupling the thermal radiation started to travel freely with almost no interaction with matter. The matter dominated epoch covers almost the rest of the Universe existence until recently, where a new stage has started with the DE domination epoch, characterised by a late-time acceleration. In addition, considering small fluctuations in the CMB radiation and applying the Galilean principle, we can assume the Universe as isotropic and homogeneous on large scale. In fact, the Universe becomes effectively homogeneous at scales larger than 100 Mpc [18].

1.1.2 The fate of the Universe: future cosmic events

Our understanding of the Universe has improved significantly, but in turn, each discovery brings more questions to be addressed. Probably, solving the mysterious dark side of the Universe (the origins of DE and DM) has become one of the most important open problems in modern cosmology and in theoretical physics in general. While the fundamental nature of radiation and baryonic matter is well known, the "hidden sides" of DM and DE are still open questions.

How DE works is not clear. Fortunately, we are not blind at this aspect; it is possible to infer its behaviour by analysing the history of the expansion of the Universe. Some theories consider DE as an hypothetical fluid with negative pressure called "quintessence" [19–21]. The Equation of State (EoS) parameter of DE (the ratio between the pressure and the energy density of the DE fluid), w_{d}, could be constant or time dependent but it must be smaller than $-1/3$ in order to induce acceleration. Assuming an EoS parameter constant and equal to -1 is equivalent to

incorporate into the gravitational action the widely known cosmological constant. Surprisingly, such paradigm, known as ΛCDM (which incorporate as well the DM contribution) is the model that better fits the observations [13–15, 18]. However, from a theoretical point of view it has some problems as: (i) the so called cosmological constant problem; the mismatch between the large vacuum energy density predicted by particle physics in comparison with the observed one. Such a difference reaches up to 120 orders of magnitude and it can be considered nowadays as the worst prediction ever made in physics. (ii), the coincidence problem; why DM and DE are almost of the same order and are currently dominating the expansion of the Universe.

An interesting way to avoid the aforementioned hurdle is by invoking the so called "k-essence" model, which consist in incorporating a non-canonical correction to the kinetic term of the scalar field [22–26]. This produces a scenario where the EoS parameter could stay below -1. Therefore, the null energy condition, $0 \leq \rho + p$, would not be satisfied. The scenarios described by such an energy condition are known as phantom models. Surprisingly, they represent an excellent option among the paradigms deviating from the widely analysed ΛCDM model since the best fits of the EoS parameter of DE give values close but less to -1 [13–15, 18].

The discovery of an accelerated Universe has pointed out the possibility of a future doomsday not characterised by a gravitational collapse but by a Universal Rip. The acceleration is so strong that the Universe could face a cosmological singularity in the far future, i.e. some of the cosmological parameters, as the energy density, for instance, are expected to blow up. The Big Bang is probably the most well known cosmological singularity, it takes place in the early Universe where the Hubble parameter and its cosmic time derivatives blow up when the size of the Universe is too small in the initial stage of its evolution. With the advent of DE, the future expansion of the Universe could be different from a Big Crunch. For example, let us addreess first the asymptotic evolution of one of the hottest model in the market, ΛCDM. On that case, the curvature of Universe would reach a constant non vanishing value in the future. While getting colder and colder when heading to such an asymptotic state [27]. Within this scenario, despite the fact that objects are progressively far away from each other, the Universe would be asymptotically de Sitter (dS). Consequently, hypothetical future observations will detect a CMB radiation corresponding to a black body emission below the current temperature. In addition, their comoving Hubble horizon ($1/aH$) will be smaller than the horizon holding us at present. Note that this is the predicted scenario as long as the the DE EoS parameter fulfils $w_{\mathsf{d}} = -1$ everywhere and at any time. However, the smallest variation on the EoS of DE from that value can induce a wide range of very different types of cosmological singularities or abrupt events. Within this context, from now on we will call such an event a "true curvature singularity", when the event happens at a finite cosmic time from the present. On the other hand, we will call it an "abrupt event", when such an event happens at an infinite cosmic time.

Despite the fact that, in an abrupt event, the singularity occurs at an infinite cosmic time, all the bound structures are unavoidably destroyed at a finite cosmic time [28]. As a simple example, one could imagine first our galaxy being teared apart from the local group, then, at some point, the dissociation of the solar system would follow and at the end the decomposition of atoms would take place. The following is a list of some well known curvature future singularities and abrupt events[i]:

[i] It is well known that in such kind of abrupt events, quantum effects are expected to become important and, therefore, it will be necessary to implement a well motivated quantum treatment. We will address

- **Big Rip (BR):** In this kind of singularity the scale factor, the Hubble rate and its higher orders cosmic time derivatives blow up at a finite cosmic time [28–35]. For example, in these models, an effective DE EoS constant parameter below $w < -1$ leads the Universe towards this kind of doomsday. The name Big Rip was first coined by Caldwell in [28] and it has been extensively studied in [36–40] where several authors have analysed differents setups of DE (See [36–38, 40, 41] and the extensive list of references therein). The quantum realm for this singularity was first addressed in [42] and later on studied in detail in [43, 44].

- **Big Freeze (BF):** In this type of singularity the Hubble rate and its cosmic time derivatives diverge not only at a finite cosmic time but at a finite scale factor as well. Indeed, the energy density and the pressure blow up at such an event. The model that induces this kind of singularity was first suggested in [45, 46] where the DE component is driven by a phantom Generalised Chaplying Gas (GCG). In [47] the authors study the casuistic and analyse the different final abrupt events depending on the parameters choice. The name of BF was coined in the work [46]. In ref [48], the authors address the corresponding quantum analysis and singularity avoidance.

- **Sudden singularity (SS):** In this kind of singularity the scale factor and the Hubble rate remain finite while the higher cosmic time derivatives of the Hubble rate diverge at finite cosmic time. It was obtained, for example, in the late time acceleration assisted by a tachyonic scalar field [49] or in interacting models in [50]. The DE component can be described by standard type GCG, as in the case of the previously mentioned BF singularity. However, we can have two scenarios depending on the nature of the matter considered. On the one hand, and in in contrast with the BF singularity, if a phantom type matter is present it induces a past singularity also known as *big démarrage* [48, 51] where the acceleration evolve very fast from negative to positive values. On the other hand, if a standard type matter is considered, it leads the Universe to a future singularity also known as a *big brake* because the deceleration blows up, i.e. the Universe moves from a positive accelerated stage to an infinitely negative acceleration [49, 52]. In fact, it was studied before BF singularity [53–55] while quantum studies were addressed first in [56] and later on in [48, 51, 57].

- **Type IV (IV):** In this type of singularity, the scale factor, the Hubble rate and its first cosmic time derivative remain constant while the higher cosmic time derivatives of the Hubble rate blow up at finite cosmic time [47, 58, 59]. It was first analysed in [47] where the authors analyse a particular model that, depending upon the value of the parameters, give rise to a rich variety of future singularities, including the previously aforementioned singularities. Moreover, for a type IV to occur in a GCG it is necessary to restrict the value of a particular parameter [60] in such a way that despite the curvature is finite, its derivatives might not be well defined (See [61] and the extensive list of references therein). This class of singularity is also present in modified theories of gravity [62]. In addition, the quantum realm for this particular cosmic event was analysed in [63] where the authors address the quantisation within the framework of the WDW equation.

- **Little Rip (LR):** In this abrupt event the scale factor, the Hubble rate and its cosmic time derivatives blow up at an infinite cosmic time. It could be understood as the soft version of the BR since it is reached at an infinite cosmic time. Despite the this abrupt event takes place at an infinite cosmic time, all the bound structures will be unavoidably ripped apart

this issue in detail later on.

Singularity	t	a	H	$\dot{H}$	$\ddot{H}$	$V(\phi)$	Tip	Kro
BR	t_{br}	∞	∞	∞	∞	$e^{\alpha\phi}$	S	S
BF	t_{bf}	a_{bf}	∞	∞	∞	ϕ^{γ_1}	W	S
SS	t_{ss}	a_{ss}	H_{ss}	∞	∞	ϕ^{γ_2}	W	W
IV	t_{iv}	a_{iv}	H_{iv}	$\dot{H}_{iv}$	∞	ϕ^{γ_3}	W	W
LR	∞	∞	∞	∞	∞	ϕ^4	W	W
LS	∞	∞	∞	$\dot{H}_{ls}$	0	ϕ^2	W	W

Table 1.1: Table with the most well known DE singularities and their diverging parameters. The first column denotes the singularities or abrupt events. The second set of columns denotes the diverging parameters where t, a, H, $\dot{H}$ and $\ddot{H}$ are, respectively; the cosmic time, the scale factor, the Hubble rate and the first and second cosmic time derivatives of the Hubble rate. The third column corresponds to the expression for the dominant term of the potential when mapping the fluid into a phantom scalar field nearby the singularity. Note that the factor α is positive. The γ factors are real numbers with the following conditions: $\gamma_1, \gamma_2 < -2$, and $\gamma_3 \neq 2(p-1)/(p+1)$ where p is an integer. The last couple of columns point out the classification depending upon *Tipler* (Tip) or *Krolak* (Kro) criteria, where S stands for strong and W for weak.

at a finite cosmic time. It was first discovered in [64] as a result of applying quadratic corrections into the Lagrangian and later on rediscovered in a brane-world model [65], and applied as a DE model in [66] where the name of "Little Rip" was coined by Frampton *et al*. Subsequently, it was studied in [67] where the authors reproduce a LR by considering bulk viscosity and in [68] as a modified $f(R)$ theory of gravity.

- **Little Sibling of the Big Rip (LSBR):** In this class of abrupt event the scale factor and the Hubble parameter blow up at an infinite cosmic time while the first cosmic time derivative of the Hubble rate remains constant. It is even smoother than the above mentioned LR abrupt event. It was first introduced in [69] where the authors include a detailed study about the fate of different bound structures. Finally, the quantum avoidance was addressed in [70, 71].

Aside from the above mentioned singularities and abrupt events, the so called *w singularities* and *Q singularities* have been found. In the former case, the EoS parameter blows up at a finite cosmic time and scale factor while the Hubble rate vanishes and its cosmic time derivative stands finite. It is worth to mention that this class of events could be found as well on the so called Type IV singularity. The second branch of singularities are only found in models where different kind of components interact with each other, where in addition, the resulting interacting term, usually denoted by Q, blows up. As has been pointed out in [61], within both subset of singularities aside from the singularities present at the background level, instabilities could appear at the perturbative level leading to a dramatic growth of DE perturbations or giving rise to a speed of sound above the speed of light.

Looking at the above classification the reader could figure out a hierarchy which would be based on the number of the diverging parameters and more precisely, on the order of the diverging cosmic time derivative of the Hubble rate. In this sense, the BR is at the top while a type IV singularity stands at the bottom. In the case of the LR and LSBR abrupt events, it is conceivable that as they occur at an infinite cosmic time, they are softer than those true singularities happening at a finite cosmic time. The third column of table 1.1 shows the dominant term of the potential when mapping the fluid into a phantom scalar field. First of all, we remind that

singularities like a BF, SS and type IV, can be achieved with a GCG model where the induced singularity depends on the particular value of the chosen parameters [60]. As can be seen, the effective potential for a BR singularity corresponds to an exponential potential while the rest of the singularities and abrupt events are mapped to a power law potential, where the latter, characterises the class of singularity. At first glance, it is clear that once again, the BR singularity is the stronger singularity, however, the rest of the singularities and abrupt events do not show the same hierarchy visualised in the examples before. Nonetheless, there is not a particular way to classify such cosmological singularities [46, 47, 61, 72–74]. While we have established the diverging parameters as the basis for classifying those doomsdays, in the literature one could find often such events classified as "strong" or "weak" depending upon the *Tipler* or *Krolak* criteria [75, 76]. The strength of a singularity is determined by taking into account the tidal forces on a volume element falling on a geodesic near the singularity. On the one hand, Tipler criteria establishes that a singularity is strong if the volume element vanishes when the singularity occurs [75]. Therefore, only the BR singularity is strong while the rest of singularities and abrupt events are considered weak. On the other hand, Krolak criteria says that a singularity is strong if the proper time derivative of the volume element is negative when approaching the singularity [76]. A detailed analysis (done, for example, in [61, 77, 78]) shows that not only BR but BF type singularities are regarded as strong as well. The mismatch is due to the fact that the Tipler criteria are more restrictive since it is applied to the volume element. After all, both classifications points out that the BR drives the Universe to the most dramatic doomsday while the other cosmological events are weaker (with the exception of the BF depending on the chosen criteria). We consider that a classification of the cosmological events depending on the divergence of the Hubble parameter could be more intuitive.

It is worthy to point out some of the interesting fact about the phantom nature of those models inducing abrupt events. On the one hand, singularities as BF, SS and Type IV can be achieved with phantom or standard models [46–48]. On the other hand, the BR, LR and LSBR are genuinely phantom, i.e. they only occur in models where phantom matter is present. There is an exception in the case of the LSBR where it was found in a model with a three-form field [71, 79].

1.1.3 Describing the current speed up: parametric models

A further approach to explain the late-time acceleration consists on the so called parametric models [80–83], where the relevant cosmological quantities are parametrised through a dynamical variable around a particular value, usually, the present time. They were designed to analyse the dynamics at low orders of some of the most relevant cosmological quantities. As it is the case of the DE EoS parameter, where the variation of the cosmological constant is questioned. For instance, on the well known Chevallier-Polarski-Linder (CPL) model the DE EoS parameter is parametrised as an arbitrary function of the scale factor (or equivalently the redshift) [80, 81]. In the same way, other models have been suggested with more intricate functions as it is the case of the models introduced in [84, 85] or using logarithmic and power law functions as in the works [86, 87].

Parametric models have been widely studied given their viability to describe DE phenomenology. The new phase entered by the Universe is understood as a recent phenomena where the parametrisation is usually expanded around the vicinity of the present time (as we mentioned before) and often with a standard and a phantom fluid. Those models contain a set of param-

eters that should be fitted to observational data. Moreover, different parametrisations could return very similar footprints resulting in the impossibility to distinguish models beyond the statistics, which often, could lead us to ambiguities due to eventual coincidences. In this sense, it is worth to mention those parametrisations dealing with future cosmic singularities [85, 88–91] where an extended parametrisation is carried such that it encompasses a wide span in time ranging from the future singularity to the present and matching the past edge with the matter domination era. It is expected that those models which are more restrictive when fitting them to data to be in turn more reliable since they avoid possible numeric coincidences on fitting. Nevertheless, this thesis does not focus on parametrised models since they go beyond the scope of the present work.

1.1.4 From background to perturbations

Although ΛCDM is the model that better fits the observations there is no reason to exclude other models that could describe suitably the current speed up. Given that the observations slightly support a Universe driven by a phantom type of DE rather than a standard one, we felt encouraged to study in deep those pure phantom paradigms. So the motivation of this work lays on focusing on genuine phantom models, studying in detail the induced doomsdays (the BR singularity and the LR and LSBR abrupt events). These phantom models could be understood as deviations of the ΛCDM paradigm and therefore, good candidates to describe appropriately the late time acceleration.

A useful tool, to check the validity of the models, consists on the computation of the perturbations. The perturbations can be visualised as the small fluctuations on the CMB temperature that grow as the Universe expands. The hottest regions evolve leading to large concentrations of matter, as well as galaxy clusters, while the coldest regions end up in vast voids.

Following the Helmholtz theorem, the space-time perturbations can be decomposed into scalar, vector, and tensor perturbations where in total, there are ten perturbations (four scalars, two-component purelly rotational two vector fields, and a two-component traceless spatially symmetric tensor field). Gauge fixing can significantly simplify the problem by removing four degrees of freedom, where each one is generated by the coordinate transformations in the chosen basis. In the perturbation theory it is often used the Newtonian gauge (also known as the longitudinal gauge or shear free gauge [23, 92]) and the comoving Newtonian gauge which are closely related via time-time transformations. The suitable choice of a Newtonian gauge provides two vanishing scalars and a vanishing vector field leaving the problem with only six degrees of freedom (two scalars, a two-components vector field and a two-components tensor field). Vectorial contributions are present at the lowest orders of cosmological perturbations but it is well known that they vanish in the early Universe and cannot be produced during the inflationary era at the first order of the cosmological perturbations [23, 92]. Tensorial perturbations correspond to gravitational waves, so their contribution is negligible as well. Therefore, the remaining two scalars are the main contribution to the inhomogeneities at first order in the cosmological perturbations. Such scalars, known as Bardeen potentials, arise as the gravitational source on the Newtonian limit. As stated before, an observer in the Newtonian frame is blind against the expansion while the peculiar velocity of the objects moving around (or velocity field, if a fluid description is preferred) transforms like a pure rotational vector field. The assumption of a vanishing anisotropic stress tensors on the local energy momentum tensor leads to the equality

between Bardeen potentials, leaving just one Bardeen potential as the single degree of freedom at the first order approach. This potential is usually named as the gravitational potential since it coincides with Newtonian gravity which satisfies the Poisson equation [23, 92].

Depending on the evolution of the chosen model, the distribution of matter could be different in such a way that the imprints left are distinguishable. The obtained results are compared with the observational data where statistical methods tell us how close is the prediction from the observed Universe. Therefore, the flourishing new models dealing with the late-time acceleration brings, in turn, the mandatory work of constraining the model parameters and a detailed analysis of the perturbations. Nevertheless, while the perturbations of the models inducing a BR have been extensively studied, this is not the case of the models inducing a LR or a LSBR. A BR inducing model could simply be achieved assuming a DE fluid with an effective EoS parameter constant and below -1. Several observational fits have been made within this setup, as is the case of the so called wCDM models [18].

Beside the background parameters, the induced perturbations can be used in order to get the best values for the parameters of the model. In addition, the initial conditions is often a discussed issue. What is known is that most models present a very low dependence with respect to the initial conditions, this fact could be a hint of the existence of attractors which, independetly of the choice of the initial conditions, drive the Universe towards the same stage at present time [24, 47, 93–98]. There are several approaches to describe the perturbations in a DE dominated regime. For example, the DE perturbations can be neglected since they are very small in comparison with matter induced inhomogeneities [88–91]. The strategy consists in computing the observable quantities as for example, the matter power spectrum and the growth rate. This pair provide useful data about the distribution of matter. Unfortunately, in most of the cases the imprints of different DE models on such observables are insignificant. Consequently, important efforts have been made to improve the accuracy of the observations, particularly, on scrutinising the DE sector as it is the case of the upcoming Euclid mission [99, 100].

Special emphasis has been put into constraining the EoS parameter of DE because, at the end, it determines the dynamics of the unknown energy source responsible of the recent speed up. Nevertheless, in addition to the EoS parameter, there is another important parameter that plays a key role on the perturbation dynamics: The squared speed of sound, $\tilde{c}_s^2$, which is defined as the variation of the pressure over the variation of the energy density, $\tilde{c}_s^2 = \delta p/\delta\rho$. For fluids, with a negative EoS parameter, it is recommendable to decompose the pressure on its adiabatic and non-adiabatic contributions [16, 101], giving rise to a couple of new parameters known as the adiabatic squared speed of sound, c_a^2, and the rest-frame squared speed of sound, c_s^2. While the first one is defined as $c_a^2 = p'/\rho'$ (as far the EoS is well defined), when computing perturbations, the c_s^2 parameter is regarded as a free parameter which can take any real value from 0 to 1. In a scalar field interpretation, it is often set equal to one [16, 101]. However, one of the most striking problems when dealing with the squared speed of sound lays on defining a well behaved function. By definition, the squared speed of sound diverge at the phantom crossing. We recall that for a single scalar field it is impossible to describe at the same time standard and phantom matter. Moreover, when describing a mixture of standard and phantom matters the effective squared speed of sound corresponding to the mixture blows up when the total EoS parameter crosses the phantom barrier, that is, when the EoS parameter pass over the phantom bisection, $w_{\text{tot}} = -1$ [21, 59, 102, 103]. In fact, the aforementioned Euclid mission is aimed to measure

these parameters precisely in order to get an accurate view of the dark sector [99, 100, 104].

The strategy followed in our perturbation analysis consists into describing a Universe filled with radiation, matter and a DE fluid with a well defined EoS parameter from the radiation dominated epoch to the far future. The motivation of imposing a DE existence at small scales, even if its presence is completely negligible, is supported by the need of fixing the initial conditions when computing the cosmological perturbations of the model. The adiabatic conditions are presumed to be satisfied at the beginning, i.e. far enough to be at a completely radiation dominated era but detached from the early inflationary ages[ii].

Bearing in mind that each separated component introduces two independent variables; the matter density contrast and the peculiar velocity of the corresponding fluid, we therefore build a set of six dynamical equations coming from the conservation equations. This means that the problem needs up to six initial conditions. We assume adiabatic conditions between the different components [23, 92]. These conditions, together with some approximations, conform the set of equations establishing the initial values of the different components. Using numerical methods, we estimate the matter power spectrum and the $f\sigma_8$ growth rate. The results are confronted with the observations, more precisely with the results for the ΛCDM model, as a guidance, whereby deviations with respect to other models are obtained [105–107].

1.1.5 Beyond Einstein's GR: modified theories of gravity

The possibility of modifying Einstein's GR at large scales is attractive from a theoretical point of view provided that it can explain the late-time acceleration as it can explain the early inflationary era through Starobinsky model [108]. Some of the aforementioned cosmological singularities have been found on modified gravity models as is the case of the BR in [109–111] LR in [68, 112–116] and the LSBR in [117].

However, at present time, the description of the current Universe concerning small scales, GR has shown to be the best approach (without any modification). Since the birth of cosmology with Einstein's GR, several tests have been performed in order to check the reliability of the theory. During decades, different experiments have shown the solidity of GR improving the results and increasing the accuracy more and more. Currently, GR has passed successfully several tests with a significant accuracy at scales up to the solar system [118–120].

Faced with the robustness of the theory, there is no choice unless to conclude that in case of existing a deviation from GR at present cosmic time, it should be at very large scales. One could expect that in the upcoming years GR will be proved to be correct at larger scales. In this sense, we will consider GR as a fundamental law that governs the nature of the cosmos, while modified theories of gravity, although interesting from the point of view that they could explain the late-time acceleration, have not been verified fully and they constitute a set of approaches only relevant at very large scales. Therefore, we will focus on the original GR theory regarding most of modified theories of gravity outside the scope of this thesis. Nevertheless, some approaches

[ii] In the very early epochs, let us say, like the inflationary era, some of the most dramatic effects should be taken into account as could be for example, quantum effects and particle creation. We stand far away from such a phase of the Universe but inside enough a radiation dominated epoch where the chosen initial conditions are imposed.

like the so called EiBI theory will be handled later on, mostly, motivated to address the quantum realm.

Regarding the classical scope of the EiBI theory, this approach is based first, on Eddington suggestion of a functional where the connection is the main gravitational field [121]. As a result of this theory, an alternative metric emerges, the so called "auxiliary metric". The vacuum solutions are equivalent to those obtained from the Hilbert-Einstein action [122]. Second in the EiBI gravity, a Born-Infeld like structure Lagrangian is suggested [123, 124]. In this way, for small values of the Ricci scalar the Einstein's functional is recovered while for large values of the Ricci scalar the action approaches Eddington's action [122]. Despite the success of Eddington's approach, the theory is incomplete since it does not include the matter fields [122]. In most of the approaches a minimal coupling is considered, however, there have been several suggestions for a metric matter coupling beside the minimal way [125–127]. The theory presents interesting features. On the one hand, the merging auxiliary metric could absorb the singularities arising in the true metric, in such a way that those abrupt events prevalent in GR could be avoided in a natural way. The issue of cosmological singularities on a EiBI context have been deeply studied in [128–131], where the authors address the quantum analysis close to some of the most known singularities. On the other hand, within this approach some of the solutions point to a minimum size of the Universe, which plays an important role in introducing bouncing solutions on the EiBI context [132, 133].

The perturbations induced within the framework of the EiBI theory were analysed in detail in [134–137]. In addition, it has been recently shown that the singularities on the auxiliary metrics are related with instabilities on the true metric at the perturbative level [138]. However, quantum effects might smooth those instabilities [139]. In addition, it has been shown that some of the models can be observationally constrained and tested at solar system scales or in the vicinity of compact stars [135, 136, 140–146].

1.2 The quantum Universe

Paying attention to the efforts done to shed some light on the dark sector of the Universe one could figure out the scientific significance, and not least, the possible technological development behind the mysterious essence that drives the cosmos. The discovery of an accelerated Universe, and the novel questions related with it, has become the problem of the century. For sure those that will solve this problem will write a new chapter in history, opening the doors for the entire Humanity to a new age of scientific progress. This does not mean however, that all questions will be answered. It is widely assumed that a phantom dominated Universe will most likely face a singularity or an abrupt event, where all the bound structures will unavoidably ripped apart at a finite future cosmic time. Sooner or later, all the Universe as we know it will end in a cosmic doomsday. This scenario could lead to a second quantum era, understanding the first quantum era as the scenario in which a singularity launched the Universe at the beginning, i.e. The Big Bang. It is clear that future singularities tell us about the end of the Universe rather than its origin. In both singular events, quantum effects are expected to dominate the dynamics and therefore, a classical description would not be enough to describe suitably such a Universe.

While we have so far focused on a classical approach to describe an accelerated Universe,

a quantum point of view will be brought into the discussion. The discovery of an accelerated Universe and, in turn, the possibility of an open range of future singularities implies the need of a Quantum Cosmology (QC) theory more imperative than ever. The main motivation in considering a quantum point of view consists on solving, or at least alleviate, the singularities present in GR. The hope is that a consistent theory of QC should, in principle, avoid such abrupt events by means of quantum phenomena.

1.2.1 Quantum cosmology: from the classical scope to the quantum realm

The idea of handling the Universe as a whole is inspiring from a quantum point of view. If it is possible to apply quantum mechanics (QM) to every system with a well defined Hamiltonian, it should be possible to apply QM to the whole Universe as well, provided of course, by a well defined Hilbert space wherein the wave functions, Ψ_n, represent the eigenvectors with their corresponding eigenvalues, E_n, that set the energy levels. The problem looks simple at first glance but nowadays represents one the most difficult hurdle to deal with. One main difficulty consists on how to address the variable of time. In GR the time is just a metric variable, as it could be, for example, the position. However, in QM theory the position is an operator while time is regarded as an external and absolute variable on which all the rest of the observables depend. Hence, the question on how to deal with time is an important question that demands a suitable answer. In order to give an appropriate approach to this inquiry many attempts have been carried [147–150]. However, so far there is not a fully consistent quantum theory of gravity. Therefore, it will be amazing to setup a robust quantum theory that unify all the forces in the Universe. It would be, at the end, the theory of everything, the philosopher's stone enabling us to understand how the whole Universe works from the microscopic realm to the global scope. That is the reason for searching stubbornly such a physical theory.

As already mentioned, we have not yet a suitable approach to handle appropriately cosmology according to QM, that is, we did not find yet the correct principles to address in a consistent way the framework of QC. However, there are some approaches that give us some hints on how to proceed [151–153]. Nowadays, there are three important approaches to tackle GR within a quantum scope: (i) string theory, (ii) loop quantum cosmology and (iii) WDW equation. The first approach considers the point like particles as vibrating strings [154–164]. The second approach suggests a space-time metric chained by a spin network at microscopic scales (up to the Planck length) [165–175]. The third one promotes the Hamiltonian constraints through metric variables, where time is just taken as a metric variable as in GR [176–183].

1.2.2 The quantum approach: the WDW equation

The objective of this thesis is to work on the third approach, i.e. WDW equation. The WDW equation is the cosmological analogous to the Schrödinger equation in QM. It was first suggested by Bryce DeWitt in 1967 as an approach for quantising gravity on the basis of a canonical formulation of gravity [176] and inspired on the quantisation techniques of Hamiltonian dynamics by Paul Dirac [184]. The Hamiltonian and momentum constraints play an essential role here. First, the Hamiltonian is obtained starting from the Lagrangian by the usual Legendre transformations of classical mechanics. The Lagrangian in turn, comes from a physically motivated action within a particular theory. The transition from classical to quantum realm consists in promoting the conjugate momenta as operators acting on a set of wave functions, where the latter are the

solutions to the WDW equation. The dynamics is obtained by means of a vanishing Hamiltonian [151, 152, 176] and ultimately, the choice of a factor ordering completely determines the shape of the wave function. There is not a single way to address the later procedure and one has the free choice to adopt a particular ordering. Hence, the investigated models should be taken with caution since they lead to different results depending on the chosen ordering, so we should understand those methods more as a reliable approach rather than a consistent theory. In this sense, it is often preferred the Laplace-Beltrami (LB) operator, for the reason that it leads to a kinetic term invariant under transformations of the configuration space as it is the case of Srchödinger equation in QM [151]. Finally, the DW boundary condition is imposed, which requires that the wave function should vanish at singular regions (as it is the case of an infinite potential wall on QM) [151, 152].

As an initial example, the first action to be addressed would be the Hilbert-Einstein action. Taking a FLRW metric background, one could deduce that the scale factor is the only degree of freedom. The underlying interpretation is that the scale factor plays the role of time, so it indirectly suggests at least, a second degree of freedom. For example, incorporating different scalar fields enrich the variables of the phase space dimension where the wave function spreads, together with the subsequent quantum phenomena as for example, tunnelling effects across classically forbidden regions. Therefore,the WDW equation could be understood as a canonical approach to quantum gravity rather than a closed physical theory. So one could figure out that we are dealing with a rather simple description by means of a toy model. Nevertheless and not by accident, as a first approach it is shown to be successful enough to avoid those singularities arising in several DE models and modified theories of gravity. Therefore, those results can be interpreted as valuable hints of singularity avoidance within a possible framework of QC theory instead as a proof in itself.

In the present thesis, we have followed the quantum analysis based on WDW equation for a FLRW Universe and applied over those purely phantom-matter induced singularities (read Big Rip, Little Rip and Little Sibling of the Big Rip). The target consists in achieving a solution which also fulfils with the DW boundary conditions, that is, the wave function vanishes when reaching the abrupt event. For those descriptions involving more variables than the scale factor as the single degree of freedom (for example by incorporating a scalar field), a Born-Oppenheimer (BO) approximation simplifies quite the total differential equation. At the beginning, this approximation was motivated to solve multi-atomic systems like molecules. Its cosmological analogous has shown to be valid by neglecting the back reaction of the matter fields on the gravitational part [185], that is, the matter fields change faster than the gravitational fields do, so the former ones are considered as the fast degrees of freedom while the latter are regarded as slow degrees of freedom [151, 185–187].

More generally, given an action with an appropriate boundary term, the Lagrangian and the conjugate momenta (together with the Hamiltonian) are completely defined. So the WDW equation could be applied to any system with a well defined action or at least, with a consistent Hamiltonian. On this sense some modified theories of gravity have gained some attention, like the so called EiBI gravity.

The EiBI theory has shown to be an interesting alternative that has gained a lot of attention on the last decade. Rather than its origin and modifications, we have mainly focused on the quan-

tum analysis of those abrupt events induced by genuine phantom models within the framework of WDW equation [188, 189]. In addition, we have contemplated tensorial instabilities in [139], where our quantum analysis suggest that those instabilities are removed. In this part of the thesis, we have analysed in deep the models which respond to genuinely phantom paradigms i.e. a phantom type of matter is present.

1.3 Outline of the present thesis

The thesis is divided in two main parts. First, the classical part, where the subject of cosmological perturbations is addressed. Second, the quantum part, where the avoidance of DE singularities is tackled. Therefore the outline of this work runs as follows: On the one hand, the classical part holds the chapters 2-6. In chapter 2, we present the background of three genuine phantom models, coined as model A, model B and model C. In addition, we introduce the first order linear perturbations and the computational methods used in the present thesis to calculate the perturbations. In chapter 3, we present the results of the perturbations for the three phantom models together with the predicted observational quantities as the matter power spectrum and the $f\sigma_8$ growth rate. We compare the DE models and try to find footprints that could allow us to distinguish between them. In addition, we compute the perturbations for the widely accepted ΛCDM model as well, in order to use it as a standard model to measure the deviations of the DE models. In chapter 4, we constrain observationally the model parameters of those phantom DE models using, by consistency, the same dataset. Here, we compute the relevant parameters involved in the ΛCDM paradigm as well, in order to use it as a comparison model. We not only predict the matter power spectrum and the $f\sigma_8$ growth rate but go beyond via the measure of the relative deviations of the perturbation quantities with respect to ΛCDM. In chapter 5, we compare two DE model with a constant EoS parameter: barely deviating from the ΛCDM model, one corresponds to a standard fluid while the other is a phantom fluid. Motivated by the previous works, we focus on the far future where the gravitational potential could switches the sign depending if a standard or a phantom model is chosen. In chapter 6, we compute all the perturbation variables when varying the effective speed of sound parameter, c^2_{sd}, from 0 to 1. In order to find the footprints induced by different models with varying c^2_{sd} parameter, we compute the deviations with respect to $c^2_{\mathsf{sd}} = 1$ of the main observational quantities as the matter power spectrum and the $f\sigma_8$ growth rate. As in the previous chapter, we focus on the far future and study how the c^2_{sd} parameter affects the gravitational potential sign switch.

On the other hand, the quantum part holds the chapters 7-13. In chapter 7, we introduce the WDW equation and derive the quantum Hamiltonian considering a DE fluid driven by i) a perfect fluid and ii) by a scalar field. In chapter 8, we study the Holographic Ricci DE (HRDE) model, which it is effectively described by a DE content with a constant EoS parameter below -1 and therefore, induces a BR singularity. Then, by means of the WDW equation we get the wave function fulfilling the DW boundary condition. In chapter 9, we not only study the classical behaviour of a DE scalar field leading the Universe to a LR abrupt event, but we study the quantum avoidance in the context of the WDW equation. We have made use of the BO approximation and obtained the solution to the total wave function. We have found vanishing solutions at the vicinity of the LR abrupt event, fulfilling in this way the DW boundary condition. In chapter 10,

we proceed in the same way as in the previous chapters and try to find a wave function of the Universe vanishing at the vicinity of the LS abrupt event. Here, we represent the DE content by i) a perfect fluid and ii) by a scalar field. In addition, we have made use of different factor orderings and obtained the resulting wave function. In chapter 11, we start from the action suggested by the EiBI theory, which considers the connection and the metric separated fields. The DE content is described by two type of models leading the Universe to the abrupt events of LR and LS. We apply a quantum geometrodynamical approach by performing an appropriate Hamiltonian, where the latter is derived from the Lagrangian by the well known Legendre transformations. Then, we study in the context of WDW equation the quantum avoidance of such abrupt events, i.e. the fulfillment of the DW boundary condition, by considering two different factor orderings. In addition, we compute the expected value of the auxiliary scale factor proving the avoidance of the LR and LS abrupt events. In chapter 12, we follow the path of the previous work but in this case, we consider a more fundamental degree of freedom corresponding to a phantom scalar field which, in turn, induces a BR singularity at large scales. In addition, we include an analysis of the constraints of the system. Once again, the quantisation is done in the context of the WDW equation where the conjugate momenta acts like operators over the wave function via a factor ordering choice. On the other hand, we make use of some approximations like the BO approximation. In chapter 13, like in the previous works, we perform a study of the quantum avoidance in the context of WDW equation and within the EiBI theory. However, in contrast to the previous chapters, we focus on the Big Bang primordial singularity rather than on future ones. We study the cases of a Universe filled by a perfect fluid or a scalar field, where in addition, we take into account the branch of solutions for a negative coupling constant, κ. Once we get the wave function, we check if the DW boundary condition is satisfied. This will ensure that the tensorial instabilities are prevented from a quantum point of view. Finally, in chapter 14, we present our main conclusions. In addition, to complete the thesis, we include the appendix A, where we get the full expression for the statefinders parameters, appendix B, where we show detailed calculations of the perturbations, and appendix C, where we perform the main approximations and their corresponding justification carried in the quantum part of the present thesis.

2

Background models and first order perturbations

No one is dumb who is curious. The people who don't ask questions remain clueless throughout their lives

– Neil deGrasse Tyson

2.1 introduction

Cosmology has made a long way on the last years with the impressive amount of observations and theoretical advancements. Yet, it still faces many challenging questions like the fundamental cause of the recent acceleration of the Universe, which was found with SNeIa observations almost twenty years ago [10, 11], and afterwards confirmed by several types of cosmological and astrophysical observations (see for example [13] for a recent account on this issue). The simplest approach which is in agreement with the current observations is to assume a cosmological constant that started recently to dominate the late-time energy density budget of the Universe [14]. But then the issues *of why is it so tiny?* and *why this cosmological constant has begun to be important only right now?* have to be addressed as well (see for example: [190–193]). Another, equally important, issue is what happens if the cosmological constant is not quite constant? This has led to a great interest in exploring other possible scenarios to explain the late-time acceleration of the cosmos by invoking either an additional matter component in the Universe, which we name DE [22, 23, 194], or by modifying appropriately the laws of gravity (for a recent account on this issue see, for example, [195, 196] and the extensive list of references provided therein).

We will focus on the third question: *what happens if the cosmological constant is not quite constant?* More precisely, we will address this question on the framework of the cosmological perturbations and for some DE models whose equations of state; i.e., the ratio between its pressure and its energy density, deviate slightly from the one corresponding to a cosmological constant[i]. Before proceeding let us remind the following well known fact: if the EoS parameter of DE deviates from -1, the Universe fate might be quite different from the one corresponding to an empty de Sitter Universe. In particular, if the EoS parameter of DE is smaller than -1, i.e., DE is apparently (at least from an effective point of view) not fulfilling the null energy condition, several future singularities or abrupt events might correspond to the cosmic doomsday of the Universe. Amazingly, some of these models are in accordance with current data [85].

On the other hand, the theory of cosmological perturbations is a cornerstone of nowadays cosmology. It provides us with a theoretical framework which allows us to determine, for example, the CMB predicted from an early inflationary era or compute the matter power spectrum and the growth rate of matter in order to make a comparison with the observational results. In

[i] This chapter corresponds mainly to our publication [105]

addition, it allows us to compute the evolution and possible clustering of DE perturbations and investigate their effect on the growth of DM. Even though no perturbations of DE have so far been detected, and are in fact absent in the ΛCDM model, the existence of a great number of experiments aiming to probe the physics of the late-Universe, like the DE Survey [197] and the Euclid mission [100], suggests that a thorough study and characterisation of such effects can be proven to be important to understand the nature of this mysterious fluid that drives the acceleration of the Universe. With this mindset, on this work we analyse the perturbative effects of phantom DE models [ii] and look for observational fingerprints that could be used as a mean to favour or disregard such models.

There are three genuinely phantom DE fates; i.e., which happens if and only if a phantom DE component is present: BR [28–35], LR [47, 55, 59, 64–67, 201] and LS [47, 55, 59, 64–67, 201].

We will consider three models which share in common the fact that in the (far) future all the structures in the Universe would be ripped apart in a finite cosmic time [66, 69]. The classical singular asymptotic behaviour of these DE models has led us to a quantum cosmological analysis of these setups [42, 44, 70, 202, 203]. In these works, it was concluded that once the Universe enters in a genuinely quantum phase; i.e., where coherence and entanglement effects are important, the Universe would evade a doomsday *à la rip*. This applies even to the smoother version of these singular behaviours corresponding to a LS [202] (see also [48, 51, 57, 63, 204]).

We will as well present the equations that describe the cosmological perturbations of these models. the numerical results will be shown in the next chapter.

2.2 Background models

In this section, we briefly review the different models that, at the background level, lead to distinct future cosmological abrupt events: (i) BR, (ii) LR and (iii) LS. For each of these models, we begin by presenting an EoS for DE that can originate such genuinely phantom abrupt events in the future, while ensuring that the background evolution follows closely that of ΛCDM until the present time. These models should be interpreted as an effective description of a more fundamental field, therefore, even though at the background level they might be defined by a barotropic fluid, the same should not be assumed at the perturbative level. In fact, as we will discuss below, in order to avoid non-physical instabilities we will explicitly break the adiabaticity of the DE perturbations. Bearing in mind, from now on, the approach that we will follow, we next describe the effective background models that we will contemplate.

Let us consider a homogeneous and isotropic Universe described by the Friedmann-Lemaître-Robertson-Walker (FLRW) metric:

$$ds^2 = -dt^2 + a^2(t)\left[\frac{dr^2}{1-kr^2} + r^2 d\theta^2 + r^2 \sin^2\theta d\varphi^2\right], \tag{2.1}$$

where $a(t)$ is the scale factor and $k = -1, 0, 1$ for open, flat and closed spatial geometry, respectively. We will focus on the spatially flat case $(k = 0)$, for which the Friedmann and

[ii] There are some promising phantom DE models [198, 199] which are free from ghosts and gradient instabilities (see also [200]).

Raychaudhuri equations read

$$H^2 = \frac{8\pi G}{3}\rho\,, \tag{2.2}$$

$$\dot{H} = -4\pi G\left(\rho + p\right)\,. \tag{2.3}$$

Here, H is the Hubble parameter, a dot represents a derivative with respect to the cosmic time, t, G is the cosmological constant and ρ and p are the total energy density and pressure of all the matter content of the Universe. In this work, and as we will focus on the late-Universe we will consider the Universe to be filled by radiation, dust (cold DM and baryons), and DE. As such, we can decompose ρ and p as

$$\rho = \rho_{\mathsf{r}} + \rho_{\mathsf{m}} + \rho_{\mathsf{d}} \qquad \text{and} \qquad p = p_{\mathsf{r}} + p_{\mathsf{m}} + p_{\mathsf{d}}\,, \tag{2.4}$$

where ρ_{r}, ρ_{m}, and ρ_{d} correspond to the energy density of radiation, matter (cold DM and baryons) and DE. Similarly, p_{r}, p_{m}, and p_{d} are the pressure of radiation ($p_{\mathsf{r}} = 1/3\rho_{\mathsf{r}}$), matter ($p_{\mathsf{m}} = 0$), and DE ($p_{\mathsf{d}} = w_{\mathsf{d}}\rho_{\mathsf{d}}$). We will not take into account interactions between the individual matter components. Consequently, each fluid $A = \mathsf{r},\mathsf{m},\mathsf{d}$ verifies the usual conservation equation:

$$\dot{\rho}_A + 3H\left(\rho_A + p_A\right) = 0\,. \tag{2.5}$$

For latter convenience, we define the fractional energy density of the individual mater components as

$$\Omega_{\mathsf{r}} = \frac{\rho_{\mathsf{r}}}{\rho}\,, \qquad \Omega_{\mathsf{m}} = \frac{\rho_{\mathsf{m}}}{\rho}\,, \qquad \Omega_{\mathsf{d}} = \frac{\rho_{\mathsf{d}}}{\rho}\,, \tag{2.6}$$

and the individual parameters of EoS

$$w_{\mathsf{r}} = \frac{p_{\mathsf{r}}}{\rho_{\mathsf{r}}} = \frac{1}{3}\,, \qquad w_{\mathsf{m}} = \frac{p_{\mathsf{m}}}{\rho_{\mathsf{m}}} = 0\,, \qquad w_{\mathsf{d}} = \frac{p_{\mathsf{d}}}{\rho_{\mathsf{d}}}\,. \tag{2.7}$$

The DE parameter of EoS, w_{d}, will be fixed later for each individual model. From (2.4) and (2.6) we can obtain the total parameter of EoS, w, from the individual w_A as:

$$w \equiv \frac{p}{\rho} = \Omega_{\mathsf{r}} w_{\mathsf{r}} + \Omega_{\mathsf{m}} w_{\mathsf{m}} + \Omega_{\mathsf{d}} w_{\mathsf{d}}\,. \tag{2.8}$$

We have considered the case of a spatially flat Universe in agreement with observations [15]. We assume that each component is independently conserved as shown in (2.5). In consequence, the Friedman equation can be written as

$$H^2 = H_0^2\left[\Omega_{\mathsf{r}0} a^{-3(1+w_{\mathsf{r}})} + \Omega_{\mathsf{m}0} a^{-3(1+w_{\mathsf{m}})} + \Omega_{\mathsf{d}0} f_{\mathsf{j}}\left(a\right)\right] \tag{2.9}$$

where H is the Hubble parameter, a is the scale factor and the parameters $\Omega_{\mathsf{i}0}$ (i=r,m,d) are the current fractional energy densities of the components. The subindex 0 denotes the values at present time. From now on, we will adopt $a_0 = 1$. In order to avoid repetitions on the notation, the scale factor will be denoted simply by a. While the EoS parameters for radiation ($w_{\mathsf{r}} = 1/3$) and matter ($w_{\mathsf{m}} = 0$) are constant, it can be scale dependent in the case of DE. The contribution of DE to the total energy budget can be expressed by means of the dimensionless function $f_{\mathsf{j}}\left(a\right)$, where the subindex j refers to the selected model (j=A,B,C).

The set of parameters corresponding to each models are fixed, mainly, by using Planck data [13, 15]. The necessary parameters to totally describe the background models are: The current fractional energy densities of radiation and matter, $\Omega_{\mathsf{r}0}$ and $\Omega_{\mathsf{m}0}$; the current Hubble parameter, H_0. While to get the perturbations we need: The root mean square mass fluctuations amplitude in spheres of size $8\ \mathrm{h}^{-1}$Mpc, σ_8; the amplitude of the scalar for single field inflation, A_s, and the spectral index, n_s. In different works the criteria for fixing these model parameters is a little bit different, and therefore, the numerical value of those parameters is slightly different in the subsequent works. However, as the selected parameters are not very different, the expected differences are so small that we expect no large deviations on the perturbations.

We understand that the difference between background models mostly lie on the $f_{\mathsf{j}}(a)$ function, while we expect to find footprints of different DE models, (i) at present, in such a way that it could be useful to distinguish between different DE models, and (ii), in the far future, where such a deviation between DE models becomes larger and arises some features of each particular DE model.

2.2.1 BR singularity: model A

A BR singularity [28–35] can be induced by a perfect fluid whose EoS parameter, w_{d}, is constant and smaller than -1:

$$p_{\mathsf{d}} = w_{\mathsf{d}}\rho_{\mathsf{d}}, \tag{2.10}$$

Solving the conservation equation we get the expression for the corresponding $f_{\mathsf{A}}(a)$ function in (2.9)

$$f_{\mathsf{A}}(a) = a^{-3(1+w_{\mathsf{d}})}. \tag{2.11}$$

Finally, the asymptotic evolution of the scale factor is

$$a(t) \sim \left[\frac{3}{2}\left|1+w_{\mathsf{d}}\right| H_0\sqrt{\Omega_{\mathsf{d}0}}\,(t_{\mathsf{s}}-t)\right]^{\frac{2}{3(1+w_{\mathsf{dA}})}} \tag{2.12}$$

where t_s corresponds to the time where the singularity would take place. In this kind of future singularity, the scale factor, the Hubble parameter and its cosmic time derivatives blow up at a finite cosmic time $t = t_s$.

2.2.2 LR abrupt event: model B

The case of a LR [47, 55, 59, 64–67, 201] can be caused by a perfect fluid whose EoS fulfils [47, 55]

$$p_{\mathsf{d}} = -\rho_{\mathsf{d}} - \mathcal{B}\sqrt{\rho_{\mathsf{d}}}, \tag{2.13}$$

where $\mathcal{B}$ is a positive constant whose dimensions are those of an inverse squared length. This model can be understood as a deviation of the widely known ΛCDM paradigm. Notice that for a vanishing parameter $\mathcal{B}$ the ΛCDM model is recovered. Solving the conservation equation, we

get the corresponding $f_{\mathsf{B}}(a)$ function for model B [64, 201],

$$f_{\mathsf{B}}(a) = \left[1 + \frac{3}{2}\sqrt{\frac{\Omega_{\mathsf{B}}}{\Omega_{\mathsf{d}0}}}\ln(a)\right]^2, \tag{2.14}$$

where $\mathcal{B}$ is reabsorbed in the dimensionless parameter $\Omega_{\mathsf{B}} \equiv \left[(8\pi G)/\left(3H_0^2\right)\right]\mathcal{B}^2$. This class of abrupt event suffers from all the divergences present in a BR singularity but driven at an infinite cosmic time. Therefore, we consider a LR less harming than a BR. Finally, the asymptotic future evolution of the scale factor can be written as [66]

$$a(t) \sim \exp\left[\exp\left(\frac{3}{2}\sqrt{\Omega_{\mathsf{B}}}H_0 t\right)\right]. \tag{2.15}$$

In this kind of abrupt event, the scale factor, the Hubble parameter and its cosmic time derivatives blow up at an infinite cosmic time.

2.2.3 LS abrupt event: model C

The LS can be induced by a perfect fluid whose EoS deviates from that of a cosmological constant as [69, 71, 205]

$$p_{\mathsf{d}} = -\rho_{\mathsf{d}} - \frac{\mathcal{C}}{3}, \tag{2.16}$$

where $\mathcal{C}$ is a positive constant. The smaller is $\mathcal{C}$, the closer is model C to ΛCDM. Solving the conservation equation we get the corresponding expression of $f_{\mathsf{C}}(a)$ for this model [69],

$$f_{\mathsf{C}}(a) = 1 + \frac{\Omega_{\mathsf{C}}}{\Omega_{\mathsf{d}0}}\ln(a), \tag{2.17}$$

where $\mathcal{C}$ is a positive constant and whose dimensions are length to the fourth power. It can be absorbed in the new parameter $\Omega_{\mathsf{C}} \equiv \left[(8\pi G)/\left(3H_0^2\right)\right]\mathcal{C}$. Model C induces the abrupt event known as LS. In this type of abrupt event, the scale factor and the Hubble parameter blow up at infinite cosmic time. However, the cosmic time derivative of the Hubble parameter remains constant. We regard the LS as the less harming abrupt event among those induced by phantom scenarios. Finally, the future asymptotic growth of the scale factor with respect to the cosmic time can be written as [69]

$$a(t) \sim \exp\left(\frac{1}{4}\Omega_{\mathsf{C}}H_0^2 t^2\right). \tag{2.18}$$

2.2.4 Comparing these models

Aside from the definition of the BR, LR and LS given in the introduction, a few words are in order to compare the models we analyse in this thesis from a background point of view. All the models presented above can be seen as a deviation from ΛCDM which can be recovered by setting $w_d = -1$ on the first model, $\mathcal{B} = 0$ on the second model and $\mathcal{C} = 0$ on the third model. Despite this apparent similarity with ΛCDM, they are characterised by a DE EoS satisfying $w < -1$, so they correspond to phantom models whose end state is drastically different from the de Sitter behaviour of a cosmological constant dominated Universe. In all these cases, the Universe is not only accelerating but super accelerating asymptotically. This fact leads the universe unavoidably to unzip itself; i.e., all the bound structures within it will be destroyed. As can be seen from the

asymptotic expansion of the scale factor $a(t)$ in (2.15), the BR is a true singularity as it would take place at a finite cosmic time from now. In addition, the geodesics cannot be extended beyond that point [53]. On the other hand, the LR is more virulent than the LS as can be seen from (2.15) and (2.18), although both of them would happen at an infinite time from now.

In a FLRW background a phantom perfect fluid can in principle be described through a phantom scalar field, i.e., a minimally coupled scalar field with the opposite sign for its kinetic term [30]. In particular, this statement applies to the models we are considering. While a detailed study of this equivalence is not the purpose of this manuscript, in the Appendix B.7, we briefly explore the phantom scalar field model that could describe the phantom models (A), (B) and (C).

We will next analyse the behaviour of these models within the standard framework for the cosmological perturbations. As a first approach and in the rest of the work, we will disregard any anisotropic stress tensor and consider that the DE perturbations are non-adiabatic. As we will show, the second supposition is crucial to get a right description of the matter power spectrum. In addition, and as a matter of simplicity, the non-abiabaticity will be described within a phenomenological approach rather than in a more fundamental scope able to describe unequivocally and realistically the speed of sound. This issue is discussed in Section 2.3.3.

2.3 Linear cosmological perturbations

In this section, we review the theory of linear perturbations for multi-fluid components. We choose the Newtonian gauge and work with the corresponding gauge invariant perturbation quantities. For a FLRW Universe, the perturbed line element is [92, 206]

$$ds^2 = a^2 \left[-(1+2\Phi)\, d\eta^2 + (1-2\Psi)\, \delta_{ij} dx^i dx^j \right] , \tag{2.19}$$

where η is the comoving time, $d\eta = (1/a)dt$, a latin index denote purely spatial coordinates, and $\Psi(\eta, x^i)$ and $\Phi(\eta, x^i)$ are the gauge invariant Bardeen potentials [207]. The transformation rule $\dot{\{\,\}} = (1/a)\{\,\}'$, where a prime represents a derivative with respect to the conformal time, allows us to write H and $\dot{H}$ in terms of the conformal Hubble parameter, $\mathcal{H} \equiv a'/a$, and its derivative, $\mathcal{H}'$, as

$$H = \frac{1}{a}\mathcal{H} , \qquad \dot{H} = \frac{1}{a^2}\left(\mathcal{H}' - \mathcal{H}^2\right) . \tag{2.20}$$

Drawing from the line element (B.2), the inverse of the metric tensor can be obtained applying a Taylor expansion up to first order. Once we define the Christoffel symbols, we can compute the perturbation of the Ricci tensor, $\delta R_{\mu\nu}$, and of the curvature scalar, δR, in order to obtain the perturbed Einstein tensor $\delta G_{\mu\nu} \equiv \delta R_{\mu\nu} - \frac{1}{2}\delta^\mu_\nu \delta R$. In addition, the perturbed Einstein equations read

$$\delta G^\mu{}_\nu = 8\pi G \delta T^\mu{}_\nu , \tag{2.21}$$

where $\delta T^\mu{}_\nu$ is the linear perturbation of the total energy momentum tensor. The individual

components of (2.21) can be written as [92, 206]

$$\begin{aligned} 3\mathcal{H}\left(\Psi' + \Phi\mathcal{H}\right) - \nabla^2\Psi &= 4\pi G a^2 \delta T^0{}_0\,, \\ -\left(\Psi' + \mathcal{H}\Phi\right)_{,i} &= 4\pi G a^2 \delta T^0{}_i\,, \\ \Psi'' + 2\mathcal{H}\left(\Phi' + 2\Psi'\right) + 2\Phi\left(2\mathcal{H}' + \mathcal{H}^2\right)\Phi + \frac{2}{3}\nabla^2\left(\Phi - \Psi\right) &= \frac{4\pi G}{3} a^2 \delta T^i{}_i\,, \\ \left(\Phi - \Psi\right)_{,ij} &= 8\pi G a^2 \delta T^i{}_j\,, \qquad (i \neq j)\,. \end{aligned} \tag{2.22}$$

The $\delta T^{\mu}{}_{\nu}$ on the right hand side (rhs) of (2.21) is the sum of the perturbations of the energy momentum tensor of radiation, $\delta T^{\mu}_{\mathsf{r}\,\nu}$, non-relativistic matter (cold DM and baryons), $\delta T^{\mu}_{\mathsf{m}\,\nu}$, and DE, $\delta T^{\mu}_{\mathsf{d}\,\nu}$. For each fluid, we can write the individual components of $\delta T^{\mu}_{A\,\nu}$ ($A = \mathsf{r}, \mathsf{m}, \mathsf{d}$) as

$$\begin{aligned} \delta T^0_{A\,0} &= -\,\delta\rho_A\,, \\ \delta T^i_{A\,0} &= -\left(p + \rho\right)\partial^i v_A\,, \\ \delta T^0_{A\,i} &= \left(p + \rho\right)\partial_i v_A\,, \\ \delta T^i_{A\,j} &= \delta p_A\,\delta^i_j + \Pi^i_{A\,j}\,, \end{aligned} \tag{2.23}$$

where $\delta\rho_A$, δp_A, v_A, and $\Pi^i_{A\,j}$ are, respectively, the perturbation of the energy density, the perturbation of the pressure, the peculiar velocity potential and the anisotropic stress tensor of the fluid A. As a first approximation, we consider that none of the fluids introduce anisotropies at the linear level of scalar perturbations. Therefore, from this point onward we will set $\Pi^i_{A\,j} = 0$. From (2.22), we find that this implies the equality of the metric potentials $\Psi = \Phi$. Replacing this equality and (2.23) in the first three equations of (2.22), we obtain [92, 206]

$$\begin{aligned} 3\mathcal{H}\left(\mathcal{H}\Psi + \Psi'\right) - \nabla^2\Psi &= -4\pi G a^2 \delta\rho\,, \\ \nabla^2\left(\mathcal{H}\Psi + \Psi'\right) &= -4\pi G a^2\left(\rho + p\right)\nabla^2 v\,, \\ \Psi'' + 3\mathcal{H}\Psi' + \Psi\left(2\mathcal{H}' + \mathcal{H}^2\right) &= 4\pi G a^2 \delta p\,, \end{aligned} \tag{2.24}$$

where we have introduced the total energy density perturbation, $\delta\rho$, total pressure perturbation, δp, and total velocity potential, v. These can be written in terms of the individual fluid variables in (2.23) through the relations

$$\delta\rho = \sum_A \delta\rho_A\,, \qquad \delta p = \sum_A \delta p_A\,, \qquad v = \sum_A \tfrac{1+w_A}{1+w}\Omega_A v_A\,. \tag{2.25}$$

Following [16, 101], we decompose the pressure perturbation as[iii]

$$\delta p_A = c^2_{sA}\delta\rho_A - 3\mathcal{H}\left(1 + w_A\right)\left(c^2_{sA} - c^2_{aA}\right)\rho_A v_A\,, \tag{2.26}$$

where

$$c^2_{sA} = \left.\frac{\delta p_A}{\delta\rho_A}\right|_{\text{r.f.}}\,, \qquad c^2_{aA} = \frac{p'_A}{\rho'_A}\,, \tag{2.27}$$

are, respectively, the effective squared speed of sound, defined in the rest frame (r.f.), of the fluid and the adiabatic speed of sound. In the following analysis, we will replace the energy density perturbation $\delta\rho_A$ by the fractional energy density perturbation $\delta_A = \delta\rho_A/\rho_A$. The total

[iii] The re-derivation of this expression is presented in the Appendix B.5.

perturbation δ can be obtained from (2.25) and reads

$$\delta = \sum_A \frac{\rho_A}{\rho}\delta_A = \sum_A \Omega_A \delta_A \,. \tag{2.28}$$

The perturbed conservation equations of the energy-momentum tensor for each fluid read:

$$\nabla_\mu \delta T^\mu_{A\,\nu} + \delta\Gamma^\mu_{\mu\alpha} T^\alpha_{A\,\nu} - \delta\Gamma^\alpha_{\mu\nu} T^\mu_{A\,\alpha} = 0\,, \tag{2.29}$$

where $\delta\Gamma^\alpha_{\mu\nu}$ is the perturbation of the Christoffel symbol and $T^\alpha_{A\nu}$ is the background value of the energy momentum tensor. Using (2.23), (2.26), (2.27), and (2.28), we can compute the temporal and spatial components of (2.29) and obtain the evolution equations for the fractional energy density perturbation δ_A and the velocity potential v_A

$$\begin{aligned} \delta'_A &= 3\mathcal{H}\left(w_A - c^2_{sA}\right)\delta_A + (1+w_A)\left[9\mathcal{H}^2\left(c^2_{sA} - c^2_{aA}\right) - \nabla^2\right] v_A + 3\,(1+w_A)\,\Psi'\,, \\ v'_A &= \left(3c^2_{sA} - 1\right)\mathcal{H} v_A - \frac{c^2_{sA}}{1+w_A}\delta_A - \Psi\,. \end{aligned} \tag{2.30}$$

In summary, from the perturbed Einstein equation, we obtain (B.40) which relate the metric perturbations to the total perturbed matter quantities. On the other hand, from the perturbed conservation equations we obtain (2.30) which dictate the dynamics for the individual energy density and velocity perturbations. In order to study the evolution of the linear perturbations, we conveniently apply a Fourier transformation, where we decompose a given function $\psi(\eta, \mathbf{x})$ into its Fourier components $\psi_k(\eta)$ as

$$\psi(\eta, \mathbf{x}) = \frac{1}{(2\pi)^{3/2}} \int e^{-i\mathbf{k}\cdot\mathbf{x}} \psi_k(\eta)\; d^3\mathbf{k}\,. \tag{2.31}$$

Therefore, for practical purposes, we make the substitution $\nabla^2 \to -k^2$ in all the evolution equations. On the other hand for our numerical calculations, we will apply the following change of variable:

$$x \equiv \ln(a)\;, \qquad \{\}' = \{\}_x\,\mathcal{H}\,, \qquad \{\}'' = \{\}_{xx}\,\mathcal{H}^2 + \{\}_x\,\mathcal{H}'\,, \tag{2.32}$$

where the subscript x denotes a derivative with respect to x. By applying the Fourier decomposition (B.47) and the transformation (B.51) to the sets of equations (B.40) and (2.30), we obtain the evolution equations for each mode of the energy density and velocity perturbations of radiation, dust and DE

$$\begin{aligned} (\delta_{\mathsf{r}})_x &= \frac{4}{3}\left(\frac{k^2}{\mathcal{H}} v_{\mathsf{r}} + 3\Psi_x\right)\,, \\ (v_{\mathsf{r}})_x &= -\frac{1}{\mathcal{H}}\left(\frac{1}{4}\delta_{\mathsf{r}} + \Psi\right)\,, \\ (\delta_{\mathsf{m}})_x &= \left(\frac{k^2}{\mathcal{H}} v_{\mathsf{m}} + 3\Psi_x\right)\,, \\ (v_{\mathsf{m}})_x &= -\left(v_{\mathsf{m}} + \frac{\Psi}{\mathcal{H}}\right)\,, \\ (\delta_{\mathsf{d}})_x &= (1+w_{\mathsf{d}})\left\{\left[\frac{k^2}{\mathcal{H}} + 9\mathcal{H}\left(c^2_{s\mathsf{d}} - c^2_{a\mathsf{d}}\right)\right] v_{\mathsf{d}} + 3\Psi_x\right\} + 3\left(w_{\mathsf{d}} - c^2_{s\mathsf{d}}\right)\delta_{\mathsf{d}}\,, \\ (v_{\mathsf{d}})_x &= -\frac{1}{\mathcal{H}}\left(\frac{c^2_{s\mathsf{d}}}{1+w_{\mathsf{d}}}\delta_{\mathsf{d}} + \Psi\right) + \left(3c^2_{s\mathsf{d}} - 1\right) v_{\mathsf{d}}\,. \end{aligned} \tag{2.33}$$

and for the metric potential

$$\begin{aligned} \Psi_x + \Psi\left(1 + \frac{k^2}{3\mathcal{H}^2}\right) &= -\frac{1}{2}\delta\,, \\ \Psi_x + \Psi &= -\frac{3}{2}\mathcal{H}v\,(1+w)\,, \\ \Psi_{xx} + \left[3 - \frac{1}{2}\,(1+3w)\right]\Psi_x - 3w\Psi &= \frac{3}{2}\frac{\delta p}{\rho}\,. \end{aligned} \tag{2.34}$$

2.3.1 Initial conditions

Once the system of equations of the perturbed quantities is defined, we need to impose proper initial conditions in order to compute the cosmological evolution of the perturbations (cf. for example [208, 209] for a detailed discussion on the initial conditions on DE models). For this goal, we will take into account the following considerations. First, we assume that at an initial moment, $z \sim 10^6$ (which roughly corresponds to $x_{\text{ini}} \sim -14$), the Universe is completely dominated by radiation, so that all relevant quantities of the total matter fluid are those of a perfect fluid with $p = \rho/3$. Secondly, we note that at such moment the wave-length of all the relevant modes is small when compared with the comoving Hubble parameter ($k \ll \mathcal{H}$), i.e. they are outside the horizon. With these two approximations, we can combine the first and third equations of (2.34) and obtain a closed evolution equation for the metric potential in the asymptotic past [23]

$$\Psi_{xx} + 3\Psi_x \approx 0\,. \tag{2.35}$$

The dominant solution of this equation is a constant solution $\Psi_{\text{ini}} = \Psi(x_{\text{ini}})$[iv]. Applying this result to the set of equations (2.34), we find that initially

$$\begin{aligned} \Psi_{\text{ini}} &\approx -\frac{1}{2}\delta_{\text{ini}}\,, \\ \Psi_{\text{ini}} &\approx -2\mathcal{H}_{\text{ini}}v_{\text{ini}}\,. \end{aligned} \tag{2.36}$$

Assuming initial adiabatic conditions, we can relate the initial values of the individual fluid perturbed variables to the total perturbation in (B.61) through [23, 208, 209]

$$\frac{\delta_{\text{r}}}{1+w_{\text{r}}} = \frac{\delta_{\text{m}}}{1+w_{\text{m}}} = \frac{\delta_{\text{d}}}{1+w_{\text{d}}} = \frac{\delta}{1+w}\,. \tag{2.37}$$

This allows us to write the initial values of δ_A in terms of δ_{ini} as

$$\frac{3}{4}\delta_{\text{r,ini}} = \delta_{\text{m,ini}} = \frac{\delta_{\text{d,ini}}}{1+w_{\text{d,ini}}} \approx \frac{3}{4}\delta_{\text{ini}}\,, \tag{2.38}$$

By imposing the adiabatic condition (B.63) between two fluids A and B on the comoving gauge, we obtain

$$\frac{\delta_{A,\text{ini}} - 3\mathcal{H}_{\text{ini}}\,(1+w_{A,\text{ini}})\,v_{A,\text{ini}}}{1+w_{A,\text{ini}}} = \frac{\delta_{B,\text{ini}} - 3\mathcal{H}_{\text{ini}}\,(1+w_{B,\text{ini}})\,v_{B,\text{ini}}}{1+w_{B,\text{ini}}}\,, \tag{2.39}$$

[iv] For the rest of this section we will denote by X_{ini} the value of a quantity X evaluated at $x = x_{\text{ini}}$.

which then leads to the initial values of the peculiar velocities:

$$v_{\mathsf{r,ini}} = v_{\mathsf{m,ini}} = v_{\mathsf{d,ini}} \approx \frac{\delta_{\mathsf{ini}}}{4\mathcal{H}_{\mathsf{ini}}} \,. \tag{2.40}$$

We note that the conditions (B.64) and (B.66) coincide with the ones presented in [208] in the absence of neutrinos. Making use of the linearity of (2.33) and (2.34), we can first compute the evolution of the perturbation quantities using the initial conditions (B.61), (B.64) and (B.66) for $\Psi_{\mathsf{ini}} = 1$ (which implies $\delta_{\mathsf{ini}} = -2$) and then multiply all the solutions obtained by the physical value of $\delta_{\mathsf{phys}}(k)$, which we will take from the Planck observational fit to single field inflation [14]:

$$\delta_{\mathsf{phys}}(k) = \frac{8\pi}{3}\sqrt{2A_s}\left(\frac{k}{k_{\mathsf{pivot}}}\right)^{\frac{n_s-1}{2}} k^{-\frac{3}{2}} \,. \tag{2.41}$$

Here, A_s and n_s are defined as the amplitude and spectral index of the primordial inflationary power spectrum corresponding to a previously selected pivot scale $k_{\mathsf{pivot}} = 0.05$ Mpc^{-1}. We will consider $A_s = 2.143 \times 10^{-9}$, and $n_s = 0.9681$ in accordance with Planck observational data [14].

2.3.2 Matter power spectrum and the growth rate

The matter power spectrum describes how galaxies are distributed along the Universe and provides us with a method to compare theoretical predictions with the observational data. In the next chapter, we will compute the linear matter power spectrum for each model studied in section 2.2 and we will try to detect deviations from the predictions of ΛCDM. The whole framework presented in this chapter provide us the necessary tools to obtain the aimed results. Notice, however, that the correct definition of the matter power spectrum uses the fractional energy density perturbation in the comoving gauge [210, 211], while the analysis carried out in this work has been done in the Newtonian gauge. Using the variables employed in the previous sections, we can resolve this gauge difference by expressing the matter power spectrum as

$$P_{\hat{\delta}_{\mathsf{m}}} = \left|\delta_{\mathsf{m}}^{(com)}\right|^2 = \left|\delta_{\mathsf{m}} - 3\mathcal{H}v_{\mathsf{m}}\right|^2 \,. \tag{2.42}$$

Another method we will use to constrain the models presented in Section 2.2 is based in computing the growth rate of the matter perturbations for the different models. By definition, the growth rate of the matter perturbations is given by the formula [88]

$$f \equiv \frac{d\left(\ln \delta_{\mathsf{m}}\right)}{d\left(\ln a\right)} \,. \tag{2.43}$$

For DM-DE models that closely mimic ΛCDM, it was found that the growth rate at late-time can be approximated reasonably well by the formula [19, 212, 213]

$$f \simeq \Omega_{\mathsf{m}}^{\gamma} \,, \tag{2.44}$$

where $\gamma \simeq 0.55$ for ΛCDM. The next to leading order of (2.44) can be found in [18].

In this thesis, instead of using any approximated parametrisation, we opt to calculate the evolution of the growth rate f for each DE model using the full (2.33)-(2.34) and compare the results with observations. We note, however, that in most cases, the observational data refers not to

the growth rate f directly, but to the combination $f\sigma_8$, where σ_8 is the root mean square mass fluctuation amplitude in spheres of size $8\mathrm{h}^{-1}$Mpc which is used to normalise the matter power spectrum. This combination has the advantage that it avoids the degeneracy in the parameter space regarding σ_8 and the linear bias, b, between the perturbations of DM and density of galaxies [214]. We calculate the temporal evolution of σ_8 by the formula [215]

$$\sigma_8\left(z,\, k_{\sigma_8}\right) = \sigma_8\left(0,\, k_{\sigma_8}\right) \frac{\delta_{\mathsf{m}}\left(z,\, k_{\sigma_8}\right)}{\delta_{\mathsf{m}}\left(0,\, k_{\sigma_8}\right)}\,, \tag{2.45}$$

where $k_{\sigma_8} = 0.125$ h Mpc^{-1} is the wave-length of the mode corresponding to distances of 8 h^{-1}Mpc. For each of the DE models considered in this work, we will calculate the evolution of $f\sigma_8$ using the numerical solutions of (2.33)-(2.34) and the relations (2.43) and (2.45). For all the models we use $\sigma_8(0, k_{\sigma_8}) = 0.820$ [18] as the present day value of σ_8. We compare the results obtained with the available observational data [214, 216–230] to check whether the predictions of the models are within the observational constraints. Since at the background level these models are very similar to ΛCDM till the present time, we expect that the deviations from ΛCDM in the evolution of the growth rate to be small.

2.3.3 The speed of sound of DE

So far, in this thesis we have described all the individual matter components as perfect fluids with a barotropic equations of state $p_A(\rho_A)$. Since a barotropic fluid is adiabatic, its effective and adiabatic squared speeds of sound are the same (cf. (2.27)). While for radiation and matter such a representation works well, for fluids with negative EoS, in particular for fluids playing the role of DE, there might be some problems if the squared speed of sound becomes negative, as this would lead to instabilities at the perturbative level. As a matter of extra-clarification we discuss in the Appendix B.6 how instabilities at the linear level in perturbations arise in fluids with a negative adiabatic squared speed of sound. It is therefore necessary to take into account additional considerations for the DE fluid. To avoid this problem we note that the EoS presented in the previous section are effective descriptions of some unknown fundamental field. As such, the barotropic nature of the models at the background level is not necessarily inherited by the cosmological perturbations. Bearing this in mind, we fix the effective squared speed of sound of DE, as defined in (2.27), to unity, i.e., in (2.33) we set $c^2_{s\mathsf{d}} = 1$, while $c^2_{a\mathsf{d}}$ is given by (2.27). We next show the expressions for the adiabatic speed of sound corresponding to the the models A, B and C, respectively.

$$\begin{aligned}
&\mathsf{A} \qquad c_a^2 = w_{\mathsf{d}}\,,\\
&\mathsf{B} \qquad c_a^2 = -\left(1 + \frac{1}{2}\frac{\mathcal{B}}{\rho_{\mathsf{d}}^{1/2}}\right)\,,\\
&\mathsf{C} \qquad c_a^2 = -1\,.
\end{aligned} \tag{2.46}$$

This strategy can be encountered in several works in the literature [16, 101, 231] and in cosmological codes such as CAMB [232] and CLASS [233] in particular when interpreting the DE fluid as Quintessence. Here, we would like to point out that our choice of $c^2_{s\mathsf{d}} = 1$ is purely phenomenological rather than deduced from a realistic theoretical grounded model. Nevertheless, as discussed in the Appendix B.7, this choice for $c^2_{s\mathsf{d}}$ extends to first order in perturbations the possibility of mapping the phantom DE fluid to a phantom scalar field.

On the next chapter, we will solve numerically the cosmological perturbations of the three models presented in this chapter.

2.3.4 Summary

In the present thesis, we have followed the strategy shown in this chapter to compute the perturbations. In summary, we first define a background for DE components. The latter should be a well defined function in the full interval in which we pretend to compute the perturbations. This interval ranges from well inside the radiation dominated epoch till the far future. We assume that radiation, matter (Baryonic and DM) and DE are conserved separately. The model parameters are fixed using different constraint methods. In order to avoid instabilities on the DE sector, we follow the method of DE pressure decomposition on its adiabatic and non-adiabatic contributions [16, 101]. Then, we use the Fourier transforms in order to separate the spatial dependence and get a dynamical set of first order differential equations. Finally, in order to fix the initial conditions we impose the adiabatic condition in the early Universe where we assume a Universe completely dominated by radiation.

3

Perturbations in a genuine phantom Universe

I feel at home in the entire world, wherever there are clouds and birds and human tears

– Rosa Luxemburg

3.1 Introduction

In this thesis, we will analyse the cosmological perturbations of DE models that induce a BR, LR or LS[i]. While the background analysis of the phantom DE scenario has been widely analysed, this has not been the case of its cosmological perturbations [88–90, 103, 234]. In [88–90] a kinematical approach was assumed, i.e., a dependence of the scale factor as a function of the cosmic time was considered for FLRW Universes with future singularities at a finite cosmic time. Within this setup and using approximated equations for the growth of the perturbations at late-time, the authors obtained the DM and DE perturbations [89]. Furthermore, in [88, 90], DE perturbations are disregarded and only the growth rate of matter perturbations is calculated. In this chapter, we will rather assume a dynamical model, i.e., we assume a given EoS for DE. This is the approach employed in Ref [234], where the future behaviour of the linear scalar perturbations is presented for a type of model that, depending on the value of the parameters, can lead to a BR or a BF singularity [46]. In our analysis, we use the full theory of linear perturbation to study how the perturbations of DM and DE, as well as, the gravitational potential evolve for a range of different scales. Our numerical integrations start from well inside the radiation era and continue till the far future. In fact, in order to see the behaviour of the phantom DE models, we extend our numerical calculations till the Universe is roughly e^{12} times larger than at present, i.e., roughly $z \sim -1$. In the perturbative analysis carried out we (i) disregard any anisotropic stress tensor, (ii) consider the DE perturbations to be non-adiabatic and (iii) describe this non-adiabaticity within a phenomenological approach for the speed of sound. On the other hand, we disregard the contribution of neutrinos as a first approach where we do not use a more advanced Boltzman code such as CAMB [232] or CLASS [233].

The chapter is organised as follows: In Sect. 3.2 we briefly present the method to obtain a numerical value for the model parameters and some other relevant quantities as for instance, the Hubble parameter and the amplitude and spectral indexes. In Sect. 3.3 we present the numerical results for the models introduced in Sect. 2.2 (where we have made use of the equations and initial conditions presented in Sect. 2.3). We show show the evolution of different perturbed quantities related to DM and DE. We present as well the matter power spectrum for the different models. We equally constrain these models using several measurements of the growth rate function, more precisely $f\sigma_8$. Finally, in Sect. 3.4, we present our conclusions.

[i] This chapter corresponds mainly to our publication [105]

3.2 method for the model parameter fixing

For the BR model, we fix the free parameters of the model to the best fit in accordance with Planck data for wCDM model [18]: $w_{\mathsf{d}} = -1.019$, $\Omega_{\mathsf{m0}} = 0.306$ and $H_0 = 68.1$ km Mpc^{-1}s^{-1} (please, cf. page 687 of [14, 18]). For our later numerical calculations and as a guideline we fix the same values for current Hubble parameter and matter fractional energy density. However, the value of the parameter Ω_{B} and Ω_{C} are chosen such that at the start of our numerical calculations the corresponding EoS parameters is equal to the one given by the model A, i.e. $w_{\mathsf{C}}\left(a_{\mathsf{ini}}\right) = w_{\mathsf{B}}\left(a_{\mathsf{ini}}\right)) = w_{\mathsf{A}}$. This equality implies that initially the DE perturbations δ_{d} of the three models are also equal if the condition (B.64) is imposed. On the other hand, the values for the amplitude and espectral index are set to be $A_s = 2.143 \times 10^{-9}$, and $n_s = 0.9681$ in accordance with Planck observational data [14].

3.3 Results

In this section, we present and discuss the results obtained for the evolution of the cosmological perturbations in the three models discussed in Sec 2.2 that contain distinct future cosmological abrupt events: BR (model A), LR (model B) and LS (model C). For each of these models, the evolution of the matter perturbations δ_{m}, v_{m}, δ_{r}, v_{r}, δ_{d}, and v_{d} was obtained by numerically integrating the set of (2.33) after substituting Ψ and Ψ_x given in (2.34). After carrying this numerical integration, the gravitational potential Ψ and its derivative Ψ_x can be obtained from the first two equations in (2.34). The integration was performed since an initial moment deep inside the radiation epoch ($z \sim 10^6$), when all the relevant modes are outside the horizon, and till a point in the distant future ($z \sim -0.99$). At the initial moment, the values of the variables were fixed according to (B.64), (B.66) and (2.41). In addition, for each model this integration was repeated for 200 different modes with wave-numbers ranging from $k_{\mathsf{min}} \sim 3.3 \times 10^{-4}$h Mpc^{-1}, which corresponds to the mode that is exiting the Hubble horizon at the present time, to a $k_{\mathsf{max}} \sim 3.0 \times 10^{-1}$h Mpc^{-1}. Notice that for $k \gtrsim k_{\mathsf{max}}$ the validity of the linear perturbation theory breaks down as non-linear effects start to become dominant in the evolution of the perturbations. In fact, k_{max} should be at most 2.0×10^{-1}h Mpc^{-1}. On the plots we included the higher value $k_{\mathsf{max}} \sim 3.0 \times 10^{-1}$h Mpc^{-1} to amplify visually the effect and evolution on the largest modes. As we mention in section 2.2, the cosmological parameters Ω_{m0} and H_0 for all the three models studied were taken from the recent Planck mission [14]. While the value of w_d for the model (i) was fixed according to the Planck data for wCDM model [18], the parameter Ω_{B} of model B and the parameter Ω_{C} of model C were fixed so that in all models the variable δ_{d} has the same value at the initial moment[ii]. As such, the results of this section should be viewed as a first step in obtaining a description of the evolution of the cosmological perturbations in phantom DE models. A more realistic picture of the imprints of each model will be explored in a next chapter where a fit of the parameters of the models will be performed using the available cosmological data.

In figure 3.1, we illustrate the evolution of the cosmological perturbations, since the initial moment and till a point in the future evolution of the Universe. The two top panels show the evolution (top-left) of the fractional energy densities of DM, δ_{m}, and (top-right) of the gravitational potential, Ψ, which has been normalised with respect to its initial value, Ψ_{ini},

[ii]This implies that initially all the models have the same value for the DE EoS.

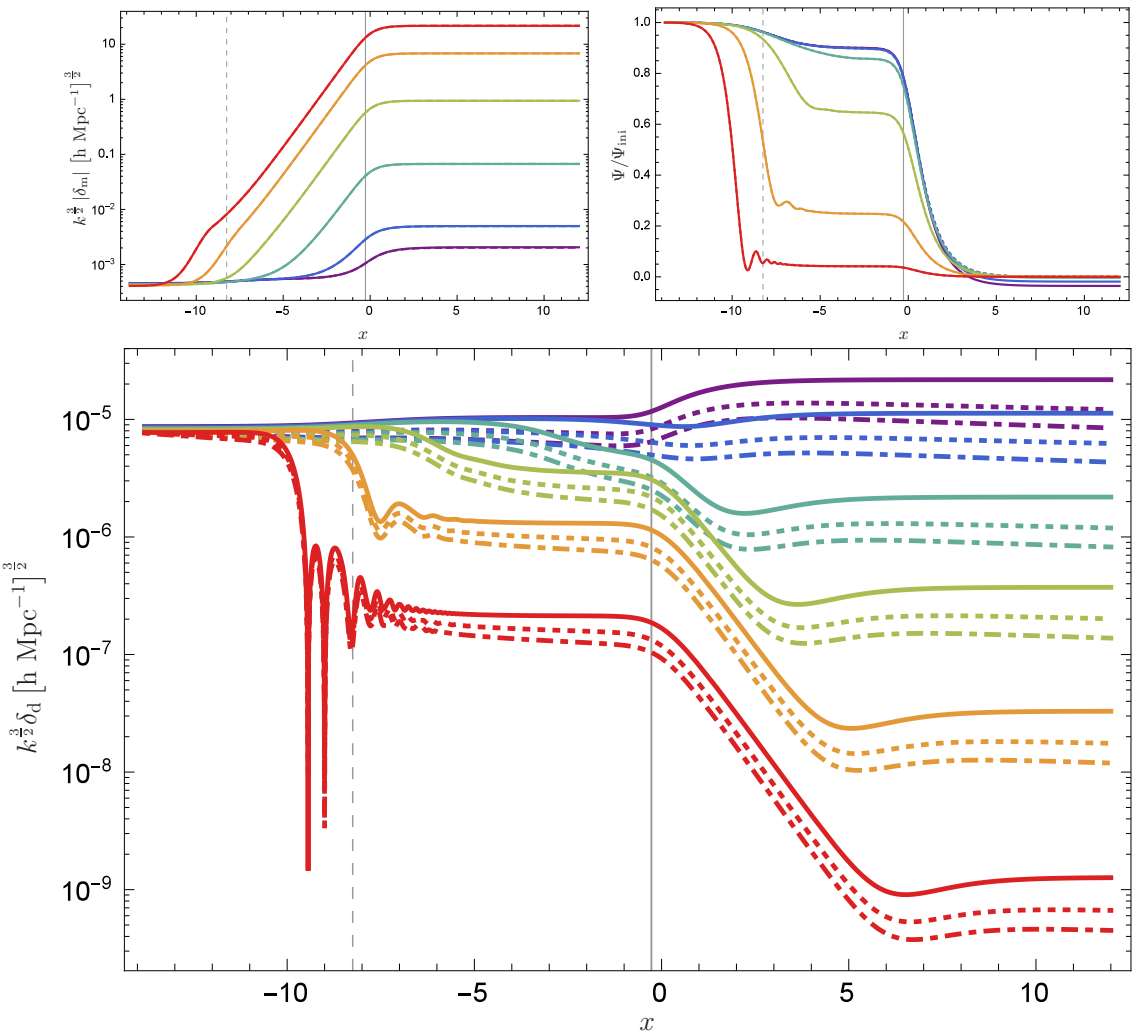

Figure 3.1: The top panels of this figure show the evolution of (top-left) the matter perturbation, δ_m, and (top-right) the gravitational potential, Ψ, the latter being normalised to its initial value Ψ_{ini}, for different modes k. All the three models considered present an almost identical behaviour that makes them indistinguishable from ΛCDM (such is the case that although we have plotted the results of $k^{3/2}\,|\delta_m|$ and Ψ/Ψ_{ini} for ΛCDM, we cannot distinguish those results from the others). The bottom panel shows the evolution of the perturbation of DE, δ_d, for the same modes. Here, the differences between the three models become more noticeable, in particular in the amplitude of the perturbations. In all panels the solid lines correspond to the model (i), the dotted lines to the model B and the dot-dashed lines to the model C. Each colour represents a different mode: $k = 3.33 \times 10^{-4}$h Mpc^{-1} (purple), $k = 7.93 \times 10^{-4}$h Mpc^{-1} (dark blue), $k = 3.50 \times 10^{-3}$h Mpc^{-1} (light blue), $k = 1.54 \times 10^{-2}$h Mpc^{-1} (green), $k = 6.80 \times 10^{-2}$h Mpc^{-1} (orange), $k = 0.30$h Mpc^{-1} (red). All perturbations are represented versus $x = \log(a/a_0)$ which varies from values well inside the radiation era ($x = -13.81$) till the far future ($x = 12$). The value $x = 0$ corresponds to the present time. The dashed vertical line corresponds to the radiation-matter equality while the solid vertical line represents the equality between DE and matter.

while the bottom panel shows the evolution of the fractional energy densities of DE, δ_d. In each panel we identify the results of the model A using solid lines, the results of the model B using dotted lines and the results of the model C using dot-dashed lines. For each of these quantities, we plot the results for 6 different wave-numbers: $k = 3.33 \times 10^{-4}$h Mpc^{-1} (purple), $k = 7.93 \times 10^{-4}$h Mpc^{-1} (dark blue), $k = 3.50 \times 10^{-3}$h Mpc^{-1} (light blue), $k = 1.54 \times 10^{-2}$h Mpc^{-1} (green), $k = 6.80 \times 10^{-2}$h Mpc^{-1} (orange), and $k = 0.30$h Mpc^{-1} (red). In terms of evolution, we can distinguish three different behaviours, according to the range of the wave-numbers:

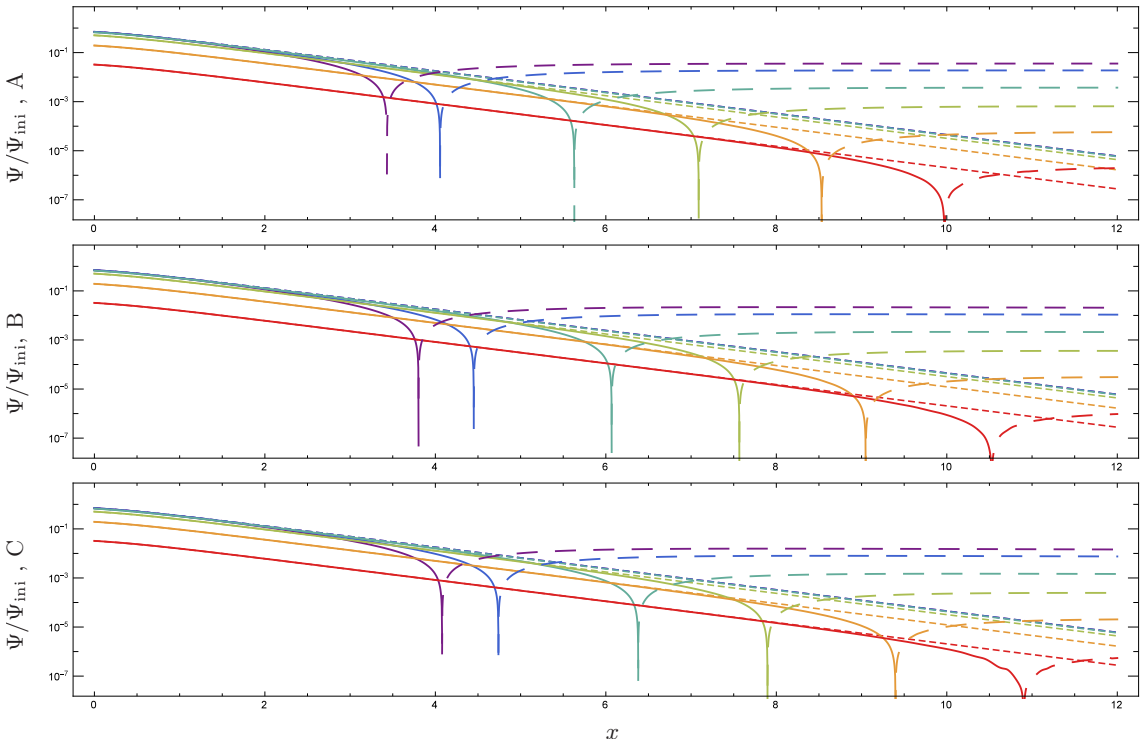

Figure 3.2: This Figure shows the evolution of the gravitational potential Ψ for the model A on the top-panel, for the model B on the middle panel, and for the model C on the bottom panel for the same modes k shown in 3.1. Positive (negative) values of Ψ are indicated with solid (dashed) lines. On all panels the corresponding behaviour in ΛCDM model is indicated by a dotted line. While within a ΛCDM model the gravitational potential decays exponentially with positive values of x until the asymptotic future, in the phantom DE models A, B and C Ψ approaches constant negative negative value in the future. The change in sign of Ψ is scale and model dependent - for a given model it happens first for the larger scales (smaller k) and for the same mode it happens first for the model A, then for the model B and then for the model C.

- large k: 0.30 hMpc^{-1} (red) and 6.80×10^{-2}hMpc^{-1} (orange).
- medium k: 1.54×10^{-2} hMpc^{-1} (green) and 3.50×10^{-3}hMpc^{-1} (light blue).
- small k: 7.93×10^{-3} hMpc^{-1} (dark blue) and 3.33×10^{-4} hMpc^{-1} (purple).

The top-left panel of figure 3.1 shows that the evolution of the matter perturbations for the different models and for ΛCDM presents an almost identical behaviour. During the initial radiation dominated epoch, each individual mode remains constant until it enters the Hubble horizon. After this point, the gravitational collapse leads to the growth of $\delta_{\rm m}$, which becomes exponential in x during the matter era (we have used however a logarithmic scale for $k^{3/2}\delta$). Once the DE starts to become dominant, the growth of the matter perturbations slows down as $\delta_{\rm m}$ seems to converge to a constant value in the asymptotic future. Notice that since the modes with larger k enter the horizon at earlier time, they correspond to the curves with higher values of $\delta_{\rm m}$ in figure 3.1.

The top-right panel of figure 3.1 presents the evolution of the gravitational potential Ψ. As in the case of $\delta_{\rm m}$, the overlap between the three models studied and ΛCDM is almost perfect and any differences until the present time are virtually undetectable. For all the ranges of k considered the perturbations start with a constant value at the radiation dominated epoch, reach a second plateau during the matter dominated era and start decaying when DE starts to

dominate. Nevertheless, we can identify some qualitative differences in the evolution of Ψ until the present time, depending on the range of k:

- large k: These modes enter the Horizon during the radiation dominated era. Around the time of horizon crossing they start to decay and can present oscillations before the moment of radiation-matter equality. Then, during the matter dominated era the oscillations are suppressed and the perturbations reach a constant value till DE gains importance.

- medium k: The gravitational potential remains constant during the radiation dominated epoch, decays around the radiation-matter equality and reaches a second plateau in the matter dominated era. The decay observed in the transition between the two epochs is scale dependent and affects mostly the modes with higher wave-number.

- small k: As in the previous case, the modes corresponding to the smallest wave-numbers show a constant behaviour during the radiation dominated and the matter dominated epochs and a decay around the radiation-matter equality. Here, however, the decay is scale independent and for all the modes the amplitude of Ψ/Ψ_{ini} during the matter era is $9/10$ of its initial value, as follows from theoretical prediction in the limit $k \to 0$ [23].

Around the matter-DE equality, we find that for all modes the amplitude of the gravitational potential starts to decay rapidly. However, after some 5 e-folds of expansion into the future, the top-right panel of figure 3.1 seems to indicate that the value of the modes of the gravitational potential stabilises at a negative value. In order to have a clearer picture of this behaviour, we plot in figure 3.2 the evolution of $|\Psi/\Psi_{\mathsf{ini}}|$ in logarithmic scale from $x = 0$ to $x = 12$ for: top panel - model A; middle panel - model B; and bottom panel - model C. Here, we see that after an initial period of exponential decay, eventually the value of Ψ changes sign and then evolves towards a negative constant (negative values of Ψ are indicated a dashed line). This behaviour is in clear contrast with the evolution in the ΛCDM model, indicated by dotted lines, where we see that the exponentially decay with respect to x continues asymptotically. Although not depicted here, it was found that for quintessence models with constant $w > -1$ the gravitational potential also evolves towards a constant but with a positive asymptotic value. Therefore, this change in sign of the gravitational potential appears as a clear indicator of a phantom evolution. Notice however that this only happens in the far future and cannot be observed at the present time. From figure 3.2 it can also be seen that this effect is scale dependent, for the same model the change in sign happens first for the larger scales and only later for the smaller ones, and model dependent, for the same value of k the change in sign happens first for the model A, then for the model B and finally for the model C.

In order to understand the effects described above, we note that once the DE dominated era begins and the modes start to exit the horizon again, the gravitational potential is initially sourced by the matter perturbations and DE perturbations. Therefore, the first equation in (2.34) can be written as

$$\Psi_x + \Psi\left(1 + \frac{k^2}{3\mathcal{H}^2}\right) \quad = -\tfrac{1}{2}\left(\Omega_{\mathsf{m}}\delta_{\mathsf{m}} + \Omega_{\mathsf{d}}\delta_{\mathsf{d}}\right) . \tag{3.1}$$

If the rhs of (3.1) evolves asymptotically to a negative constant, then the potential stabilises at a negative value. On the other hand, if the potential is to cross the $\Psi = 0$ value and stabilise at a positive value than the the rhs of (3.1) needs to evolve towards a positive constant in the far future. We now recall that Ω_{m} is decreasing exponentially with x while Ω_{d} is approaching unity,

and that is due to the adiabatic conditions 2.37 (see the (B.64) for a detailed calculation and approximations) imposed at the beginning of the integration, δ_{m} is positive-valued while for a phantom fluid δ_{d} is negative-valued. Thus, the changing of sign of the gravitational potential can happen in a phantom DE model after the equality

$$|\Omega_{\mathsf{m}}\delta_{\mathsf{m}}| = |\Omega_{\mathsf{d}}\delta_{\mathsf{d}}|\,, \tag{3.2}$$

is reached. From figure 3.1 we observe that when δ_{m} and δ_{d} become constant after matter-DE equality, $|\delta_{\mathsf{m}}|$ is larger for the modes with larger k while δ_{d} larger for the modes with smaller k. Therefore, the modes corresponding to smaller scales are the ones that see the change in the sign of Ψ first. On the other hand, for the model A the ratio $\Omega_{\mathsf{m}}/\Omega_{\mathsf{d}}$ decays faster than for the models B and C, while decaying faster for the model B than for the model C. Therefore, for the same value of k the equality (3.2) is reached first for model A, then for model B and finally for model C, as seen in figure 3.2.

The bottom panel of figure 3.1, we present the evolution of the fractional energy density of DE for different wave-numbers. In contrast with the perturbations of DM, here we observe some differences between the three models. First, we note that while the initial value of $\delta_{\mathsf{d,ini}}$ is the same for all the models, at the present time for the models B and C δ_{d} appears to be systematically suppressed on all the scales with regards to the model A. This suppression can be understood by the evolution of δ_{d} deep inside the radiation dominated and the matter dominated epochs. For model A we observe in figure 3.1 that all the modes present a constant plateau in these periods. in contrast, in the models B and C we find that similar plateaus exist in these periods but with a negative tilt, meaning that the amplitude of δ_{d} is continuously decreasing until the present time. This effect seems to be tied to how strong is the variation of w_{d} during these periods since the model C, which is the one that more rapidly converges to $w_{\mathsf{d}} \approx -1$ is the one that sees a stronger suppression of the DE perturbations.

Similarly to what happens with the DM perturbations, we can characterise the qualitative evolution of δ_{d} in terms of the range of the wave-number of the mode:

- large k: These modes are the first to enter the horizon during the radiation epoch. While initially their amplitude decreases slowly, after the horizon crossing they suffer a fast decay and we observe a damped oscillatory behaviour till the radiation-matter equality. At this point the modes present a second plateau and that lasts until the end of the matter era. Once DE starts to dominate they start to decay rapidly once more.
- medium k: In this range, the modes present a behaviour of transition. While they enter the horizon only in the matter era, and therefore present no early oscillations, we still observe the existence of a plateau during the matter dominated era. The length of the plateau depends on the horizon crossing time - for the modes with smaller k the amplitude does not have time to stabilise before the DE dominated epoch. At this point, the amplitude starts to decay but, much like what happens for modes in the small k range, it stabilises once the accelerated expansion shrinks the Hubble radius and leads the modes to exit the horizon.
- small k: These modes are outside of the horizon for most of their evolution and therefore present little to no variation in amplitude till close to the present time, when they enter the horizon. At this point we observe a difference in behaviour, with the modes

with smallest wave-numbers being amplified during the initial stages of the DE dominated epoch, while the largest modes in this range present a slight decay. Once the DE fluid completely dominates, however, the modes exit the horizon and their amplitude stabilises once more.

Despite all the differences in behaviour and amplitude between distinct modes, we always find that the amplitude of DE perturbations is extremely small when compared to DM. This validates the usual assumption of a DE smooth fluid.

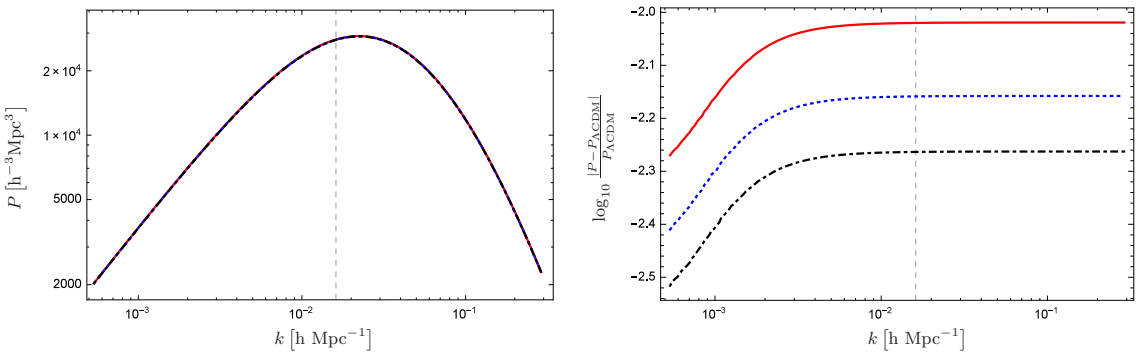

Figure 3.3: The lhs panel shows the almost perfect superposition of the matter power spectra, P_{δ_m}, of the models A, B and C with the matter power spectrum of ΛCDM. For clarity of the plot, we did not plot the case of ΛCDM as it overlaps perfectly with the other three curves. The rhs panel shows the relative deviation of each model in comparison with ΛCDM. In both panels, the red solid curve corresponds to the model A, the blue dotted curve corresponds to the model B and the black dot-dashed curve corresponds to the model C. The dashed vertical line denotes the mode that crossed the horizon at the moment of the radiation-matter equality. All the models present a small enhancement ($\lesssim 1\%$) of the amplitude of P_{δ_m}. This effect is increasingly suppressed for large scales but seems to become scale invariant for modes that are already inside the horizon during the radiation-matter equality. The model that induces a BR singularity shows the highest enhancement in the power spectrum while the model that induces a LS abrupt event presents the smallest deviation respect to the ΛCDM model.

In addition, on the left hand side (lhs) of figure 3.3, we compare theoretical matter power spectrum, P_{δ_m}, for each of the models considered in this work with the one predicted by ΛCDM. For all the cases, we find an almost perfect superposition of the spectra. This reflects the close resemblance in terms of evolution of all the models up to the present time and suggests that observables like the matter power spectrum may not be able to distinguish DE models that do not differ significantly from ΛCDM till today. In each panel we identify the results of model A using solid lines, the results of model B using dotted lines and the results of model C using dot-dashed lines.

In order to be able to make a comparison between the results of the models A, B and C, we have proceeded to plot on the rhs panel of Figure 3.3 the relative difference in the magnitude of the matter power spectrum with respect to the ΛCDM model. For all the models we find a small enhancement ($\lesssim 1\%$) in the amplitude of the matter power spectrum that is practically constant for modes that are outside of the horizon at the moment of the radiation-matter equality. At the large-scale end of the spectrum, we find that this enhancement becomes increasingly small. This effect seems to be related to how much the model in question deviates from ΛCDM until the present time: model A which is the one that deviates the most from ΛCDM is the one that sees a stronger enhancement, while model C is the one that more closely resembles ΛCDM and sees the faintest effect. These results are in conformity with figure 6 of [30] where it is shown

that in wCDM the suppression of the growth of the matter perturbations becomes smaller as $(1 + w_{\mathrm{d}})$ becomes more and more negative.

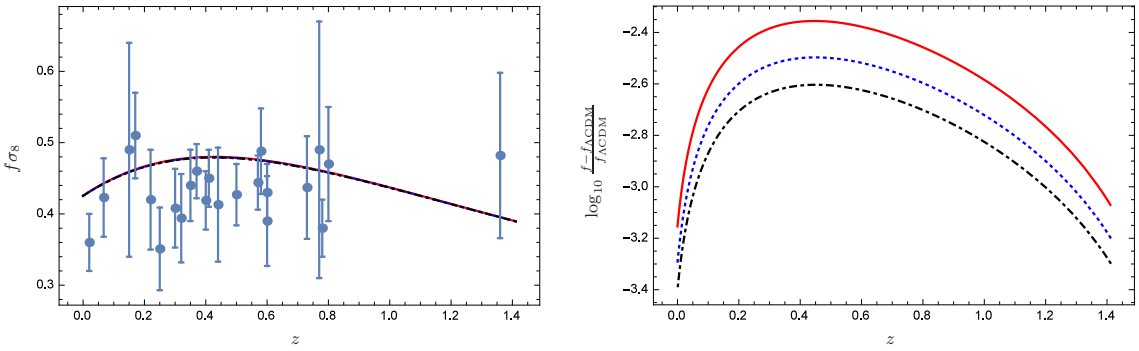

Figure 3.4: The lhs panel of this figure shows the evolution of $f\sigma_8$ in terms of the redshift against the available data points indicated in Table 4.5. The red solid curve corresponds to the model A, the blue dotted curve corresponds to the model B and the black dot-dashed curve corresponds to the model C. For clarity of the plot, we did not plot the case of ΛCDM as it overlaps with the other three curves. The rhs panel shows the relative deviation of $f\sigma_8$ with respect to ΛCDM. It can be shown that for the models there is a small enhancement of $f\sigma_8$ ($\lesssim 0.4\%$), which starts to decrease rapidly after the matter-DE equality ($z \sim 0.3 - 0.4$). The model that induces a BR singularity shows the highest enhancement in the power spectrum while the model that induces a LS abrupt event presents the smallest deviation respect to the ΛCDM model.

Finally, we present in figure 3.4 the evolution of $f\sigma_8$ (lhs panel) and the relative deviation of $f\sigma_8$ with respect to ΛCDM (rhs panel) for the three models studied and for a redshift within the range $z \in (0, 1.4)$. In each panel we identify the results of the model A using solid lines, the results of the model B using dotted lines and the results of the model C using dot-dashed lines. We find that all models are within the error bars for almost all the points (cf. Table 3.2). Nevertheless, there seems to be some tension between the theoretical predictions and the observational data, as the $f\sigma_8$ curves are systematically above most of the data points for redshifts up to $z \sim 0.8$. This tension between the theoretical predictions based on CMB data - higher values of Ω_{m} and σ_8 - and the local redshift distortion measurements - lower values of Ω_{m} and σ_8 - is already found in ΛCDM and is not a special feature of the models studied in this work. A more detailed discussion on this topic can be found in [235, 236].

On the rhs panel of figure 3.4, which presents the relative deviation of each model with regards to ΛCDM, we find the same tendency as in the case of the matter power spectrum in figure 3.3: there is an enhancement of $f\sigma_8$ for all models ($\lesssim 0.4\%$) that seems to be more intense the more the model deviates from ΛCDM, i.e., the effects are more intense for the model A, followed by the model B and finally for the model C. These results are in conformity with the increase in the growth of the matter perturbations in a phantom scenario shown in figure 6 of [30]. After the matter-DE equality at $z \sim 0.3 - 0.4$, this effect starts to vanish rapidly, with the deviations from ΛCDM being $\lesssim 0.08\%$ around the present time. This behaviour seems to be associated to the fact that in all models δ_{m} becomes constant at late-time, when DE completely dominates the energy budget of the Universe.

By simply looking at the plot on the lhs of figure 3.4, we can clearly see that the three considered models fit pretty well the observations. We can try to understand which of these three models fits better the observational data. For this we would need to make a fitting of the background models which is far beyond the current work. Therefore, we will simply "extrapolate" the

Model	N_{fp}		χ^2	
ΛCDM	2	0	1.094	1.010
A	3	0	1.202	1.063
B	3	0	1.185	1.048
C	3	0	1.176	1.040

Table 3.1: This table shows the reduced χ^2 for different values of N_{fp}. The lhs (rhs) column within the N_{fp} column corresponds to the lhs (rhs) column within the χ^2 column.

definition of the reduced χ^2:

$$\chi^2 = \frac{1}{N - N_{\text{fp}}} \sum_i^N \frac{\left[f_{obs}\left(z_i\right) - f_{th}\left(z_i\right)\right]^2}{\sigma_i^2} \,. \tag{3.3}$$

Here, $f_{obs}\left(z_i\right)$ and $f_{th}\left(z_i\right)$ are, respectively, the observational and theoretical growth rates at redshift z_i, while σ_i is the corresponding error for each measurement and N the total number of observations while N_{fp} is the number of fitted parameters. We will work out these numbers for $N_{\text{fp}} = 3$ as our model has, or $N_{\text{fp}} = 0$ as we did not fit any of them. Likewise, we will do it for the ΛCDM model. Our results are shown in table 3.1. These results seem to suggest that although all the models considered in this work provide a good fit to the observational data, this fit tends to become worse as the background evolution deviates more from ΛCDM.

3.4 Conclusions

In this chapter, we analyse the cosmological perturbations within the framework of GR, taking into full account the presence of DE at the perturbative level. The DE component is described by three different models, where each one of them behaves almost as ΛCDM model at present but induces a unique doomsday scenario in the future: model A leads to a BR; model B leads to a LR; model C leads to a LS. At late time, the parameter of EoS of DE for each of these models is very close to but slightly smaller than -1, thus corresponding to a phantom-like behaviour of DE. Despite the small variations of the parameter of the EoS for the three models, the asymptotic behaviour of the Universe is quite different from the one in ΛCDM, with the unavoidable rip of all the structure in the Universe no matter the interaction that bound them.

The cosmological parameters of the models are fixed as follows: the value of H_0 and $\Omega_{\text{m},0}$ in all the models, as well as of w_{d} in model A were fixed using the best fit in the Planck data [18]. For the models B and C we fix the respective parameters Ω_{B} and Ω_{C} so that the amplitude of the DE energy density perturbations is the same for all models in the distant past. This choice of parameters was made so as to better understand the relative effects of each model on the evolution of the perturbations. In addition, we fix the effective squared speed of sound of the DE fluid, defined as $\delta p_{\text{d}}/\delta\rho_{\text{d}}$ in the rest frame of the fluid, to unity. This choice was made to remove potential instabilities in the dark sector that would lead the DE perturbations to quickly violate observational constraints. An improved analysis would incorporate in the calculations an observationally constrained value for all the parameters , obtained by constraining the homogeneous and isotropic evolution of the model using standard candles like SNeIa. This will be done on the next chapter.

z	$f\sigma_8$	Survey	Ref.
0.02	0.36 ± 0.04		[216]
0.067	0.423 ± 0.055	6dF Galaxy Survey	[217]
0.15	0.49 ± 0.15	SDSS DR7 MGS	[218]
0.17	0.51 ± 0.06	2dF Galaxy Redshift Survey	[214, 219]
0.22	0.42 ± 0.07	WiggleZ Dark Energy Survey	[220]
0.25	0.351 ± 0.058	SDSS II LRG	[221]
0.3	0.407 ± 0.055	SDSS I/II LRG + SDSS III BOSS CMASS	[222]
0.32	0.394 ± 0.062	SDSS III BOSS DR12 LOWZ	[223]
0.35	0.440 ± 0.05	SDSS DR5 LRG	[214, 224]
0.37	0.460 ± 0.038	SDSS II LRG	[221]
0.38	0.430 ± 0.054	SDSS III BOSS DR12	[230]
0.4	0.419 ± 0.041	SDSS I/II LRG + SDSS III BOSS CMASS	[222]
0.41	0.45 ± 0.04	WiggleZ Dark Energy Survey	[220]
0.44	0.413 ± 0.080	WiggleZ Dark Energy Survey + Alcock-Paczynski distortion	[225]
0.5	0.427 ± 0.043	SDSS I/II LRG + SDSS III BOSS CMASS	[222]
0.51	0.452 ± 0.057	SDSS III BOSS DR12	[230]
0.57	0.444 ± 0.038	SDSS III BOSS DR12 CMASS	[223]
0.59	0.488 ± 0.06	SDSS III BOSS DR12 CMASS	[226]
0.60	0.43 ± 0.04	WiggleZ Dark Energy Survey	[220]
0.6	0.433 ± 0.067	SDSS I/II LRG + SDSS III BOSS CMASS	[222]
0.60	0.390 ± 0.063	WiggleZ Dark Energy Survey + Alcock-Paczynski distortion	[225]
0.61	0.457 ± 0.052	SDSS III BOSS DR12	[230]
0.73	0.437 ± 0.072	WiggleZ Dark Energy Survey + Alcock-Paczynski distortion	[225]
0.77	0.490 ± 0.18	VIMOS-VLT Deep Survey	[214, 227]
0.78	0.38 ± 0.04	WiggleZ Dark Energy Survey	[220]
0.8	0.470 ± 0.08	VIMOS Public Extragalactic Redshift Survey	[228]
1.36	0.482 ± 0.116	FastSound	[229]

Table 3.2: This table shows the available observational data points for $f\sigma_8$ at different redshifts, which are plotted in figure 3.4. For each data point we present, in order, the value of the effective redshift, the value of $f\sigma_8$ and respective error, the corresponding survey, and the reference from which the values were taken.

For each of the models studied, we analyse the evolution of the linear cosmological perturbations in absence of an anisotropic stress tensor and considering non-adiabatic contributions for the DE perturbations. In particular, we compute numerically the evolution of the matter

density contrast for the DM and DE components, together with the evolution of the gravitational potential. The integrations are performed from well inside the radiation era till the far future. The outcome, which we present in figure 3.1, shows that in all the models there is a very similar behaviour in the evolution of the perturbations. The largest difference until the present time seems to lie in the magnitude of DE perturbations: even though the initial value of δ_{d} is the same in all the models, we find that the more the background model resembles ΛCDM, the smaller δ_{d} is at the present time. This effect is observed for all the scales. On the other hand, our numerical results indicate that in the future, when the perturbations of DE are the only sources of the gravitational potential, a change of the sign of Ψ occurs on a scale-dependent order: it starts at large scales and progressively affects the smaller ones. We also find that this effect is model dependent, in the sense that it happens first in the model A, which leads the Universe to a BR singularity, then in model B which leads to a LR abrupt event, while in model C which leads to a less virulent LS abrupt event, this effect happens later. We interpret this result as a change in the behaviour of gravity, which in the far future becomes repulsive and starts to rip structures apart, an effect that was already discussed in previous works [66, 69] on the same kind of phantom DE-fuelled abrupt events.

Using the results of the numerical integrations, we obtain for each model theoretical prediction for the matter power spectrum, as observed today, and the late-time evolution of the observable combination $f\sigma_8$. In all three models the deviations to the results of ΛCDM are within the $\lesssim 1\%$ margin for the matter power spectrum (cf. figure 3.3), and within the $\lesssim 0.3\%$ margin for $f\sigma 8$ (cf. figure 3.4). Comparing the results of the three models we find that the deviations to ΛCDM, are stronger for the model A that leads the Universe to a BR and weaker in the model C that leads the Universe to a LS, while the model B that induces a LR in the future has an intermediate behaviour. This suggests that these effects become more noticeable the more the background model deviates from ΛCDM at the present time.

We compare the evolution of $f\sigma_8$ for low reshift ($z \lesssim 1.4$) with the latest observations and find that, for all the models, the curve of $f\sigma_8$ is within the error bars for most data points. We quantify the deviation from the observations by calculating the corresponding reduced χ^2, which allows us to make a preliminary comparison of the results for the three models. We find that all models are only slightly worse that ΛCDM at fitting the observational data. Here, we note that we do not perform a true statistical comparison of our models with observations, in particular we do not take into account the difference in number of parameters of the models. Nevertheless, since the three models analysed in this work have the same number of free parameters, the reduced χ^2 allows us to state that model A provides the worse fit, while model B seems to be of the three models analysed the one that best fits the observational data. We thus conclude that although the ΛCDM model gives the best fit to the observations, we cannot exclude other models like the ones analysed in this thesis.

In general, the results of this paper suggest the possibility of finding imprints of a phantom DE which can be in agreement with the current observations. Nevertheless, the effects are small and a further examination is necessary to find an indication that could more clearly differentiate each model. We also stress that since we did not make an observational fit of these models (from a homogeneous and isotropic point of view), all our results should be taken as a guideline for a more accurate study that we hope to carry in the future.

While the classical cosmological pertubations of these models at first order are well defined, as we have shown, there are still some fundamental and intrinsic problems related to phantom DE models. In fact, as discussed in [31, 237, 238], when a particle-physics description of the phantom DE is attempted, some instabilities may rise in theory due to higher order effects. In all three models presented in this work, this kind of effects can potentially become more problematic as the Universe evolves into one of the cosmological events considered, as the energy density becomes increasingly high. Though a thorough examination of these effects and the compatibility of the phantom DE models with a particle physics description is outside the scope of this thesis, we will take this question into account in a future study.

4

Constraining observationally the phantom DE models

Science, for me, gives a partial explanation for life. In so far as it goes, it is based on fact, experience and experiment

– Rosalind Franklin

4.1 introduction

It is well known that the expansion of our Universe is accelerating. This fact was observationally supported firstly in 1998 by the measurements of supernova type Ia (SNIa) [10, 11] and then, corroborated by measurements of the Cosmic Microwave Background (CMB) and Baryonic Acoustic Oscillations (BAO) [13]. On the other hand, the history of the expansion reveals that the transition to an accelerated state happened recently [14, 15]. The origin of the matter that induces the current speed up of the Universe is still unknown and it is usually dubbed DE [23, 194]. In addition, the contribution of DE to the total energy density of the Universe is roughly 70% [13, 14], so the hidden source that causes the current acceleration of the Universe covers a significant portion of the total energy budget. We do not know much about the fundamental cause of DE. However, there are phenomenological models that can describe suitably the current expansion of the Universe. Amazingly, the cosmological constant suggested by Einstein, in principle, to get a static Universe, becomes nowadays the paradigm that better fits the observational data. The model, which also takes into account the contribution of DM was coined as ΛCDM. This model is characterised by having an Equation of State (EoS) parameter for DE which is constant and equal to -1, in such a way that the asymptotic evolution leads to a de Sitter Universe. Despite that the ΛCDM model gives the best observational fit, there is no reason to exclude other models that could describe as well suitably the current acceleration, as those that we will address in the present thesis[i]. In addition, the ΛCDM model suffers from some fine tuning problems.

It can be said that the problem has become the problem of the century for cosmologist. The urge to reveal this intriguing fact has motivated a vast amount of works trying to explain the recent speed up of the Universe. In this way, several models that can induce a positive acceleration have been suggested. We can classify them in two groups: (i) quintessence models which are those that preserve the null energy condition, i.e. $0 \leq \rho + p$, in such a way that the EoS parameter is always larger than -1. (ii) phantom models where the null energy condition is violated and the EoS parameter can go below -1 [33, 239, 240]. Surprisingly, phantom models are not excluded, but even seem to be favoured by observations [15, 30, 85, 241–243].

On the other hand, the discovery of an accelerated Universe has opened the door to theorise about an infinity of possible doomsdays, where the universal acceleration is so powerful that

[i] This chapter corresponds mainly to our publication [107]

the Universe ends ripping itself in a dramatic state. Those events are named and classified as *singularities* or *abrupt events* depending if they occur at a finite or an infinite cosmic time, respectively. In particular, we will focus on three genuine phantom models, where each of them induce a specific doomsday known as BR [28–35, 244], LR [47, 55, 59, 64–67, 201, 245] and LS [69, 71, 205]. While a BR is a true singularity, we highlight that a LR and a LS are abrupt events. However, in all these models the bound structures will be ripped apart unavoidably sooner or later. In this scenario, the energy density could increase up to the Planck scale, where quantum effects are expected to be important. This has lead to carry a quantum analysis close to the cosmological singularities/abrupt events, where the classical singularity could be avoided in the quantum realm [42, 44, 48, 51, 57, 63, 70, 110, 188, 189, 202–204, 246–248] (see the recent review [61]). In this work, we allude to the models that induce these events as model A, B and C, respectively. In particular, the model A is actually the model known as wCDM, where its EoS parameter is constant and less than -1. The corresponding model parameters were observationally constrained in [14, 15, 18]. On the other hand, the model B was constrained in [66], where the authors fit observationally the model parameters and compute when different bound structures are destroyed. However, the model C has not been observationally constrained so far. All these models need to be compared and fitted with the available observational data. In addition, the cosmological perturbations have been a useful tool for cosmologist in this task, for example, they predict the matter distribution that can be compared with the observations. The predicted observables within the cosmological perturbations theory have been widely used to test several models of DE, as well as DE-DM interacting models and $f(R)$ modified gravity.

In the models studied in [88–91], it is assumed a dependence of the scale factor with cosmic time. In [88] the authors disregard DE perturbations and the predicted evolution of the growth rate is compared with observations. In [89, 90], DE and DM perturbations are considered. These models are suitable to describe the Universe from the matter dominated epoch till the present time. In addition, most of them predict future singularities or abrupt events. In [234] the authors compute the matter and DE perturbations and fit the results with the observational data. In [103] a mixture of phantom and standard fluids is studied in order to analyse the instabilities arisen at the perturbative level. Some instabilities merge when dealing with a negative EoS parameter of DE fluids. To avoid such instabilities, in [16, 101] the authors suggest a decomposition of the pressure in its adiabatic and non adiabatic contributions. In [105] this method is applied and initial conditions are imposed at the radiation dominated epoch. On the other hand, in [249] the authors analyse the effects of non adiabaticity on the growth rate for several DE models and compute the observable $f\sigma_8$.

There are other interesting models of DE that have been studied within the framework of cosmological perturbations. In [250] the authors obtain the growth rate in the framework of a scale invariant theory. The initial conditions are set at a matter dominated epoch and they compute the resulting perturbations for a range of different backgrounds. The DE-DM interacting models are useful to describe a transition to an accelerated Universe [251–253]. In [251] the authors focus on computing the anisotropies of the CMB and find a particular footprints of the model studied. In [252], models arising from the scalar-fluid theories with a derivative coupling are analysed. The authors compute the perturbations and predict particular footprints on the growth rate. On the other hand, in [253] the authors study the perturbations for a model where a DM superfluid is assumed to be responsible of the current acceleration. Such superfluid consists on a combination of the ground and excited states of DM. The obtained expansion history

and growth rate are compared with that given by ΛCDM.

A large class of modified gravity models have been studied. For example, in [196, 254] the authors consider different $f(R)$ models with a non vanishing anisotropic stress tensor. The impact of the EoS parameter in several perturbation variables is studied and the predicted anisotropies on CMB are faced against observations. In [255] the authors not only constrain observationally the background model but also compute the resulting perturbation variables such as the Bardeen potentials and $f\sigma_8$.

On the other hand, the cosmological perturbations are useful to constrain further observationally DE models. For example, in [91] the scale dependent DE perturbations are studied for different DE models where some future singularities are involved. The authors find the possibility to distinguish different DE models in the oncoming missions as DESI, *Euclid*, and *WFirst-2.4*. In [256] the authors constrain observationally a DE scalar field representation in the so called bound DE model.

The most considered observational probes of DE are SNIa, BAO and CMB. SNIa describe the expansion history of the Universe by means of luminosity distances. BAO have been also developed and provides a direct measurement of the Hubble expansion, $H(z)$, and the angular diameter distance. CMB provides distance priors which are a strong constraint on DE. In order to avoid degeneracy in the observational data, a tighter constraints on the model parameters are obtained by combining all of SNIa, CMB, BAO and measurement of $H(z)$, i.e. the Hubble expansion. In addition, since the observational data are obtained from independent cosmological probes, their total likelihood is the product of each separate likelihoods.

In this chapter, we focus in two goals. The first one consists on constraining observationally the parameters that characterise the models A, B and C using, for consistency, the same samples of data. Indeed, We compare and classify these models with respect to the ΛCDM and test their consistency to the observational data. In order to obtain the best fit parameters, their mean values and their uncertainties, we confront our DE models by means of a Markov Chain Monte Carlo (MCMC) [255] method to the observational data. We use the Pantheon compilation of SNIa dataset [257], the Planck 2018 distance priors of CMB [15, 258], the BAO data[ii] including (6dFGS+SDSS+BOSS-LOWZ+BOSS-CMASS+WiggleZ+BOSS-DR12) [260–264] and measurements of the Hubble rate [260, 265–271]. For the second goal, we will use the previous best fit parameters to compute the first order linear perturbations and analyse the distribution of matter during the different cosmological epochs. The aim is to analyse the footprints that these models could leave on the distribution of galaxies. Indeed, we compute the predicted matter power spectrum and the evolution of $f\sigma_8$ quantity at low redshift. This $f\sigma_8$ evolution is faced against a second and independent set of observations (matter power spectrum and $f\sigma_8$ data set). For consistency, aside from the models A, B and C, we compute as well the results for the ΛCDM setup, which we use as a pattern to compare with the other three models.

The chapter is organised as follows: In section 4.2, we discuss the details of the different data. In section 4.3, we show the obtained results for the model parameters with their confidence levels and contourplots. In section 4.4, we compute the evolution of the perturbation variables

[ii]The authors of [259] have regrouped in a chronological order 30 BAO non correlated data points.

and the predicted matter power spectrum and $f\sigma_8$. Finally, in section 4.5, we discuss our main conclusions.

4.2 Data description

4.2.1 SNIa data

We have used the Pantheon compilation as a SNIa dataset, they are made of 1048 spectroscopically confirmed Type Ia Supernovae distributed in the redshift interval $0.01 < z < 2.26$ [257]. The Pantheon sample is the largest compilation up to date and consists of a different supernovae surveys, including SDSS, SNLS, various low-z samples and some high-z samples from HST. The distance modulus for supernovae is given by,

$$\mu_{th} = 5\log_{10}\frac{d_L}{Mpc} + 25, \tag{4.1}$$

where $d_L = (c/H_0)\,D_L$ is the luminosity distance, H_0 is the Hubble constant, c is the speed of light,

$$D_L = (1+z_{\text{hel}})\int_0^{z_{\text{CMB}}}\frac{dz}{E(z)}, \tag{4.2}$$

where z_{hel} is the heliocentric redshift and z_{CMB} is the CMB frame redshift, $E(z) = H(z)/H_0$ is the normalised Friedmann equation which encodes DE models.

The observed apparent magnitude for the Pantheon compilation is given by $m_{obs} = \mu_{obs} + M$ [257], where μ_{obs} is the observed distance modulus and M is the absolute magnitude. To estimate the cosmological parameters, we compute the *chi-square*, χ^2. For SNIa, χ^2_{SN} is constructed as

$$\chi^{\mathbf{2}}_{\mathbf{SN}} = (\mu_{\mathbf{obs}} - \mu_{\mathbf{th}})^{\mathbf{T}}.\mathbf{C}^{\mathbf{-1}}_{\mathbf{Pantheon}}.(\mu_{\mathbf{obs}} - \mu_{\mathbf{th}}), \tag{4.3}$$

where $(\mu_{obs} - \mu_{th})$ is the difference vector between the model expectations and the observed magnitudes, where $\mathbf{C_{Pantheon}}$ is the covariance matrix of Pantheon data which is given by the sum of a statistical part and systematic part $\mathbf{C_{Pantheon}} = \mathbf{C_{stat}} + \mathbf{C_{sys}}$. In order to get rid of the nuisance parameter M, we perform an analytical marginalisation over it, by defining a new chi-square [272]

$$\chi^{\mathbf{2}}_{\mathbf{SN}} = \mathbf{A} + \ln\frac{\mathbf{C}}{2\pi} - \frac{\mathbf{B^2}}{\mathbf{C}}, \tag{4.4}$$

where $\mathbf{A} = (\mu_{\mathbf{obs}} - \mu_{\mathbf{th}})^{\mathbf{T}}.\mathbf{C}^{\mathbf{-1}}_{\mathbf{Pantheon}}.(\mu_{\mathbf{obs}} - \mu_{\mathbf{th}})$, $\mathbf{B} = (\mu_{\mathbf{obs}} - \mu_{\mathbf{th}})^{\mathbf{T}}.\mathbf{C}^{\mathbf{-1}}_{\mathbf{Pantheon}}.\mathbf{1}$ and $\mathbf{C} = \mathbf{1}^{\mathbf{T}}.\mathbf{C}^{\mathbf{-1}}_{\mathbf{Pantheon}}.\mathbf{1}$ being $\mathbf{1}$ the 1048×1048 identity matrix.

4.2.2 CMB data

The power spectrum of CMB affects crucially the physics, from the decoupling epoch till today. These effects are mainly quantified by the acoustic scale l_a and the shift parameter R given by

[17]

$$R \equiv \sqrt{\Omega_{\mathsf{m}} H_0^2}(1+z_{\mathsf{CMB}})D_A(z_{\mathsf{CMB}}), \tag{4.5}$$

$$l_a \equiv (1+z_{\mathsf{CMB}})\frac{\pi D_A(z_{\mathsf{CMB}})}{r_s(z_{\mathsf{CMB}})}. \tag{4.6}$$

where z_{CMB} is the redshift at the decoupling epoch, $D_A(z_{\mathsf{CMB}})$ is the angular diameter distance of photons in a flat FLRW Universe expressed as

$$D_A(z) = \frac{1}{H_0(1+z)}\int_0^z \frac{dz'}{E(z')}, \tag{4.7}$$

and $r_s(z)$ is the comoving sound horizon given by

$$r_s(z) = \frac{1}{H_0}\int_0^a \frac{da'}{a'E(a')\sqrt{3(1+\bar{R}_b)a'}}, \tag{4.8}$$

where $a = (1+z)^{-1}$ is the conversion rule from the redshift to the scale factor and $R_b = 31500\Omega_{\mathsf{b}}h^2(T_{\mathsf{CMB}}/2.7K)^{-4}$, with $T_{\mathsf{CMB}} = 2.275K$ [273]. The redshift at decoupling is given by the fitting formula [274]

$$z_{\mathsf{CMB}} = 1048[1+0.00124(\Omega_{\mathsf{b}}h^2)^{-0.738}][1+g_1(\Omega_{\mathsf{m}}h^2)^{g_2}], \tag{4.9}$$

where

$$g_1 = \frac{0.0783(\Omega_{\mathsf{b}}h^2)^{-0.238}}{1+39.5(\Omega_{\mathsf{b}}h^2)^{0.763}}, \tag{4.10}$$

and

$$g_2 = \frac{0.56}{1+21.1(\Omega_{\mathsf{b}}h^2)^{1.81}}. \tag{4.11}$$

The CMB covariance matrix is given by [258]

$$\mathbf{C}_{\mathsf{CMB}} = \mathbf{10^{-8}} \times \begin{pmatrix} 1598.9554 & 17112.007 & -36.311179 \\ 17112.007 & 811208.45 & -494.79813 \\ -36.311179 & -494.79813 & 2.1242182 \end{pmatrix}. \tag{4.12}$$

Finally, the CMB contribution to the total χ^2 is

$$\chi^{\mathbf{2}}_{\mathsf{CMB}} = \mathbf{X}^{\mathbf{T}}_{\mathsf{CMB}}.\mathbf{C}^{\mathbf{-1}}_{\mathsf{CMB}}.\mathbf{X}_{\mathsf{CMB}}, \tag{4.13}$$

where X_{CMB} is the CMB parameters vector based on Planck 2018 release, as derived by [258]

$$\mathbf{X}_{\mathsf{CMB}} = \begin{pmatrix} R-1.74963 \\ l_a - 301.80845 \\ \Omega_{\mathsf{b}}h^2 - 0.02237 \end{pmatrix}. \tag{4.14}$$

4.2.3 BAO data

The baryon acoustic oscillation is an important observational data currently used to constrain the cosmological parameters more efficiently in combination with other probes such as the CMB. The information taken from the BAO peaks present in the matter power spectrum can be used to determine the Hubble parameter $H(z)$ and the angular diameter distance $D_A(z)$ which allows us to calculate DE parameters. The combination of the angular-diameter distance and the Hubble parameter, $D_V(z)$, is given by [275]

$$D_V(z) \equiv \left[(1+z)^2 D_A^2(z)\frac{z}{H(z)}\right]^{1/3}, \tag{4.15}$$

where the redshift at the drag epoch, z_{d}, is given by the fitting formula [276]

$$z_{\mathsf{d}} = \frac{1291(\Omega_{\mathsf{m}}h^2)^{0.251}}{1+0.659(\Omega_{\mathsf{m}}h^2)^{0.828}}[1+b_1(\Omega_{\mathsf{b}}h^2)^{b_2}], \tag{4.16}$$

where

$$b_1 = 0.313(\Omega_{\mathsf{m}}h^2)^{-0.419}[1+0.607(\Omega_{\mathsf{m}}h^2)^{0.674}], \tag{4.17}$$

and

$$b_2 = 0.238(\Omega_{\mathsf{m}}h^2)^{0.223}. \tag{4.18}$$

To infer the cosmological parameters, BAO data can be used as constraints beside other surveys such as SNIa and CMB, in general the χ^2 statistics is used for that purpose, and BAO contribution takes the from

$$\chi^2_{\mathsf{BAO}} = \mathbf{X}^{\mathbf{T}}_{\mathsf{BAO}}.\mathbf{C}^{-\mathbf{1}}_{\mathsf{BAO}}.\mathbf{X}_{\mathsf{BAO}}, \tag{4.19}$$

where $\mathbf{X}_{\mathsf{BAO}}$ is the difference vector between theoretical predictions (the third column of the tabe 4.1) and observational measurements (the fourth column of the same table) and C_{BAO} is the covariance matrix given for the correlated data.

We should mention that WiggleZ and BOSS-DR12 data are correlated, and their covariance matrices are given respectively [263, 264]

$$\mathbf{C}_{\mathsf{WiggleZ}} = \mathbf{10^{-4}} \times \begin{pmatrix} 2.17898878 & -1.11633321 & 0.46982851 \\ & 1.70712004 & -0.71847155 \\ & & 1.65283175 \end{pmatrix}, \tag{4.20}$$

$$\mathbf{C}_{\mathsf{BOSS\text{-}DR12}} = \begin{pmatrix} 624.707 & 23.729 & 325.332 & 8.34963 & 157.386 & 3.57778 \\ & 5.60873 & 11.6429 & 2.33996 & 6.39263 & 0.968056 \\ & & 905.777 & 29.3392 & 515.271 & 14.1013 \\ & & & 5.42327 & 16.1422 & 2.85334 \\ & & & & 1375.12 & 40.4327 \\ & & & & & 6.25936 \end{pmatrix}. \tag{4.21}$$

BAO name	z	BAO expression	BAO measurement	$\sigma_{\mathbf{BAO}}$	$\mathbf{r_s^{fid}}$	Ref
6dFGS	0.106	$\frac{r_s}{D_V}$	0.327	0.015	–	[261]
SDSS DR7 MGS	0.15	$D_V \frac{r_s^{fid}}{r_s}$	4.47	0.16	148.69	[262]
BOSS-LOWZ	0.32	$D_V \frac{r_s^{fid}}{r_s}$	8.47	0.17	149.28	[260]
BOSS-CMASS	0.57	$D_V \frac{r_s^{fid}}{r_s}$	13.77	0.13	149.28	[260]
WiggleZ	0.44	$D_V \frac{r_s^{fid}}{r_s}$	1716	83	148.6	[263]
	0.60		2221	101		
	0.73		2516	86		
BOSS-DR12	0.38	$D_A(1+z)\frac{r_s^{fid}}{r_s}$	1512.39	25.00	147.78	[264]
		$H\frac{r_s^{fid}}{r_s}$	81.2087	2.3683		
	0.51	$D_A(1+z)\frac{r_s^{fid}}{r_s}$	1975.22	30.10		
		$H\frac{r_s^{fid}}{r_s}$	90.9029	2.3288		
	0.61	$D_A(1+z)\frac{r_s^{fid}}{r_s}$	2306.68	37.08		
		$H\frac{r_s^{fid}}{r_s}$	98.9647	2.5019		

Table 4.1: Summary of the Baryon Acoustic Oscillations data used in the current work.

The total $\chi^2_{\mathbf{BAO}}$ can be expressed as:

$$\begin{aligned}\chi^2_{\mathsf{BAO}} &= \chi^2_{\mathsf{6dFGS}} + \chi^2_{\mathsf{SDSS}} + \chi^2_{\mathsf{BOSS\text{-}LOWZ}} + \\ &\quad \chi^2_{\mathsf{BOSS\text{-}CMASS}} + \chi^2_{\mathsf{WiggleZ}} + \chi^2_{\mathsf{BOSS\text{-}DR12}}.\end{aligned} \tag{4.22}$$

4.2.4 The $H(z)$ measurements

In our analysis we have induced the Hubble expansion rate data to have a tighter constraints on our DE models, in general the $H(z)$ data can be derived either by the clustering of galaxies and quasars by measuring the BAO in the radial direction [277] or by the differential age method by expressing the Hubble parameter as

$$H(z) = -\frac{1}{(1+z)}\frac{dz}{dt} \tag{4.23}$$

and inferring dz/dt from $\Delta z/\Delta t$ [278], where Δz and Δt are respectively the redshift difference and the age difference between two passively evolving galaxies. In the current analysis we used a compilation of 36 data points of the Hubble parameter shown in table 4.2 where each data point is given with its corresponding reference. While the Hubble parameter data points are not correlated, the $\chi^2_{H(z)}$ function can be written as

$$\chi^2_{H(z)} = \sum_{i=1}^{36}\left[\frac{H_{obs,i} - H(z_i)}{\sigma_{H,i}}\right]^2, \tag{4.24}$$

where $H_{obs,i}$ is the observational value of the Hubble parameter given for each redshift z_i in the table 4.2 and $H(z)$ is the theoretical prediction of the Hubble parameter.

z	$H(z)$	σ_H	Ref.	z	$H(z)$	σ_H	Ref.
0.07	69.0	19.6	[265]	0.48	97.0	62.0	[266]
0.09	69.0	12.0	[266]	0.57	96.8	3.4	[260]
0.12	68.6	26.2	[265]	0.593	104.0	13.0	[267]
0.17	83.0	8.0	[266]	0.60	87.9	6.1	[266]
0.179	75.0	4.0	[267]	0.68	92.0	8.0	[267]
0.199	75.0	5.0	[267]	0.73	97.3	7.0	[266]
0.2	72.9	29.6	[265]	0.781	105.0	12.0	[267]
0.27	77.01	14.0	[266]	0.875	125.0	17.0	[267]
0.28	88.8	36.6	[265]	0.88	90.0	40.0	[266]
0.35	82.7	8.4	[268]	0.9	117.0	23.0	[266]
0.352	83.0	14.0	[267]	1.037	154.0	20.0	[267]
0.3802	83.0	13.5	[270]	1.3	168.0	17.0	[266]
0.4	95.0	17.0	[266]	1.363	160.0	33.6	[269]
0.4004	77.0	10.2	[270]	1.43	177.0	18.0	[266]
0.4247	87.1	11.2	[270]	1.53	140.0	14.0	[266]
0.44	82.6	7.8	[225]	1.75	202.0	40.0	[266]
0.44497	92.8	12.9	[270]	1.965	186.5	50.4	[269]
0.4783	80.9	9.0	[270]	2.34	222.0	7.0	[271]

Table 4.2: This table shows the measurements of the Hubble expansion.$H(z)$ data used in the current analysis are in the unit of km s^{-1} Mpc^{-1}.

Finally, the χ^2_{tot} is the sum of all the χ^2 previously defined:

$$\chi^{\mathbf{2}}_{\mathbf{tot}} = \chi^{\mathbf{2}}_{\mathbf{SN}} + \chi^{\mathbf{2}}_{\mathbf{CMB}} + \chi^{\mathbf{2}}_{\mathbf{BAO}} + \chi^{\mathbf{2}}_{\mathbf{H(z)}}. \tag{4.25}$$

4.3 background results

In this section, we present the obtained results for the observational fit. The figure 4.1, 4.2 and 4.3 show the contour plots of the model parameters corresponding to the model A, B and C, respectively. The numerical results are all gathered in Table 4.3.

The criteria methods used in the literature to compare between models are mainly the χ^{red}_{min} and the corrected Akaike Information Criterion (AIC_c) defined as [279–281]

$$AIC_c = -2\ln\mathcal{L}_{max} + 2N_p + \frac{2N_p(N_p+1)}{N_d - N_p - 1}, \tag{4.26}$$

where N_p denotes the number of parameters and N_d denotes the number of data. In the case of Gaussian errors, $\chi^2_{min} = -2\ln\mathcal{L}_{max}$ and

$$AIC_c = \chi^2_{min} + 2N_p + \frac{2N_p(N_p+1)}{N_d - N_p - 1}. \tag{4.27}$$

Model	Par	Best fit	Mean	χ^2_{tot}	$\chi^{2\ red}_{tot}$	AIC_c	ΔAIC_c
ΛCDM	Ω_m	$0.318349^{+0.00248001}_{-0.00248001}$	$0.31834^{+0.00248987}_{-0.00248987}$	1047.42	0.957422	1053.441953	0
	h	$0.69814^{+0.0480814}_{-0.0480814}$	$0.698602^{+0.0481787}_{-0.0481787}$				
	$\Omega_b h^2$	$0.022218^{+0.000120872}_{-0.000120872}$	$0.0222202^{+0.000122619}_{-0.000122619}$				
A	Ω_m	$0.317173^{+0.00318473}_{-0.00318473}$	$0.317327^{+0.0031808}_{-0.0031808}$	1047.51	0.958380	1055.54663	2.104677
	w_d	$-1.02758^{+0.0240102}_{-0.0240102}$	$-1.02874^{+0.0239306}_{-0.0239306}$				
	h	$0.691013^{+0.0507771}_{-0.0507771}$	$0.691523^{+0.0507536}_{-0.0507536}$				
	$\Omega_b h^2$	$0.0221218^{+0.000170789}_{-0.000170789}$	$0.022123^{+0.000170538}_{-0.000170538}$				
B	Ω_m	$0.317198^{+0.00276851}_{-0.00276851}$	$0.317705^{+0.00280131}_{-0.00280131}$	1047.53	0.958398	1055.56663	2.124677
	Ω_B	$0.000445721^{+0.000416159}_{-0.000416159}$	$0.000763824^{+0.000416359}_{-0.000416359}$				
	h	$0.694604^{+0.0494111}_{-0.0494111}$	$0.688584^{+0.0493315}_{-0.0493315}$				
	$\Omega_b h^2$	$0.0221295^{+0.000130585}_{-0.000130585}$	$0.0221028^{+0.000132755}_{-0.000132755}$				
C	Ω_m	$0.317115^{+0.00253975}_{-0.00253975}$	$0.316144^{+0.00253899}_{-0.00253899}$	1047.56	0.958426	1055.59663	2.154677
	Ω_C	$0.0500261^{+0.0130141}_{-0.0130141}$	$0.0299424^{+0.0133398}_{-0.0133398}$				
	h	$0.695705^{+0.0481201}_{-0.0481201}$	$0.701962^{+0.0481465}_{-0.0481465}$				
	$\Omega_b h^2$	$0.022138^{+0.000121724}_{-0.000121724}$	$0.0221928^{+0.000121811}_{-0.000121811}$				

Table 4.3: Summary of the best fit and the mean values of the cosmological parameters.

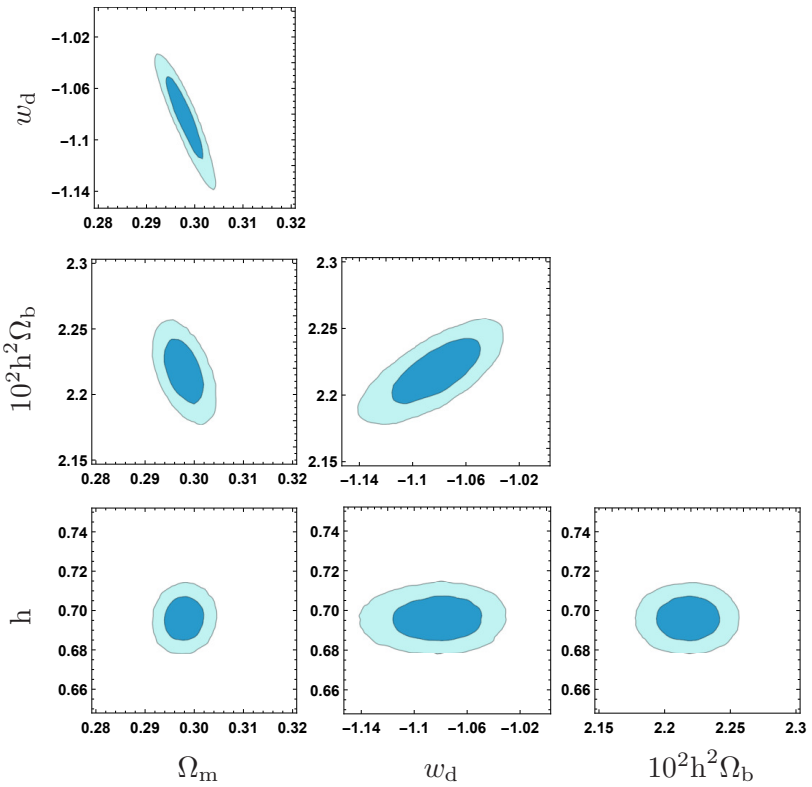

Figure 4.1: These figures correspond to 1σ and 2σ confidence contours obtained from SNIa+CMB+BAO+H(z) data for the model A.

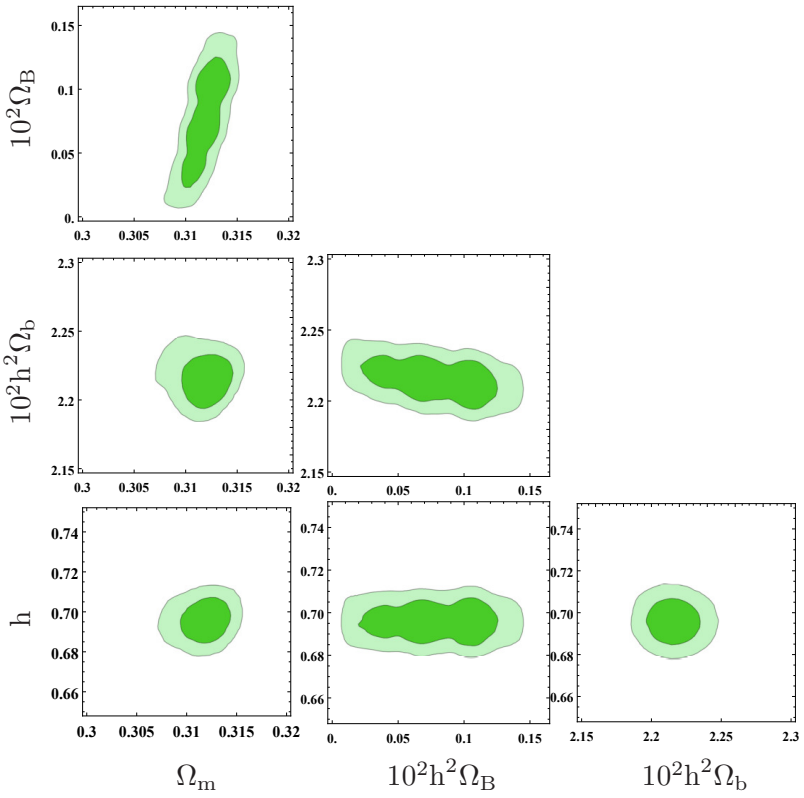

Figure 4.2: These figures correspond to 1σ and 2σ confidence contours obtained from SNIa+CMB+BAO+H(z) data for the model B.

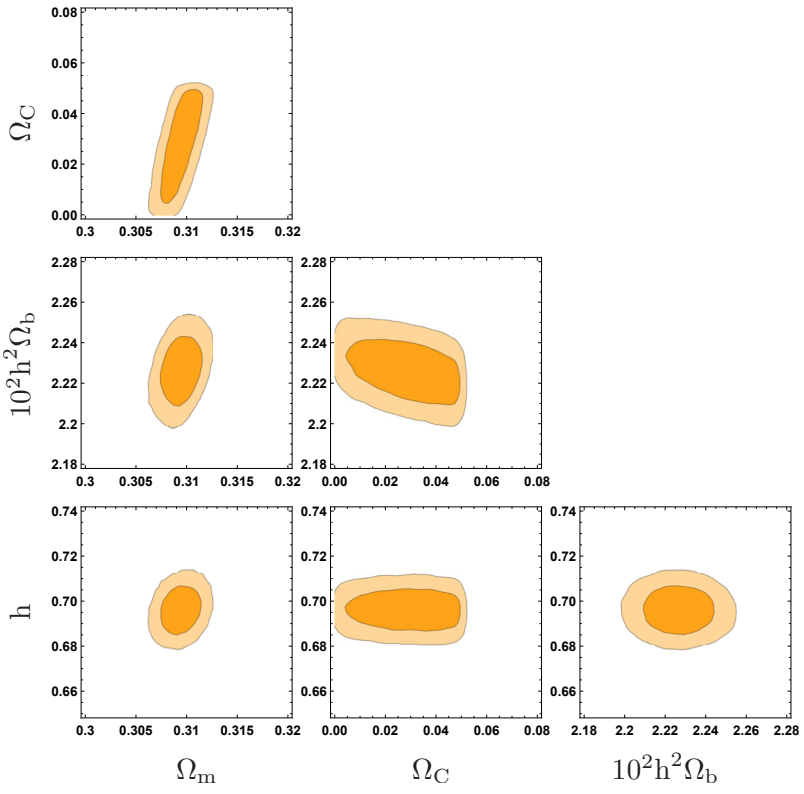

Figure 4.3: These figures correspond to 1σ and 2σ confidence contours obtained from SNIa+CMB+BAO+H(z) data for the model C.

In practice, we do not care about AIC_c value itself in model comparisons. Actually we are interested to calculate the ΔAIC_c between models, i.e, $\Delta AIC_c = AIC_{c,model} - AIC_{c,min}$. The model with a minimal value of AIC_c is more favoured by data and it is chosen as a reference model. Roughly speaking, the models with $0 < \Delta\text{AIC}_c < 2$ have substantial support, those with $4 < \Delta\text{AIC}_c < 7$ have considerably less support, and models with $\Delta\text{AIC}_c > 10$ have essentially no support, with respect to the reference model. Finally, ΛCDM model is also favoured by the χ^{red}_{min} selection.

In table 4.3, we show the best fit and the mean values of the parameters. The free parameter vectors when assuming a flat Universe for ΛCDM, A, B, and C models are respectively $\theta_{\Lambda CDM} = (\Omega_m, h, \Omega_b h^2)$, $\theta_A = (\Omega_m, \omega_{\mathsf{d}}, h, \Omega_b h^2)$, $\theta_B = (\Omega_m, \Omega_{\mathsf{B}}, h, \Omega_b h^2)$ and $\theta_C = (\Omega_m, \Omega_{\mathsf{C}}, h, \Omega_b h^2)$. The χ^2_{tot} and $\chi^{2\ red}_{tot}$ are also given in the same table. In order to study the statistical significance of our constraints, we compute AIC_c and ΔAIC_c with $N_d = 1097$, $N_p = 3$ for ΛCDM and $N_p = 4$ for the rest of the models. The values of ΔAIC_c are 2.104677, 2.124677 and 2.154677 for the models A, B and C respectively, and are given for the purpose of models comparison. Given that all the ΔAIC_c values are close to ~ 2, it makes the three models A, B and C competitive and supported by the data. But still the strongly favoured model is the ΛCDM.

4.4 Perturbation Results

Before tackling the cosmological perturbations of the models introduced in chapter 2, we show how the EoS parameter evolves in time for the models A, B and C. The reason for highlighting w_{d} for these models, is the important role they play for the initial condition of DE perturbations (cf. (3.20) and (3.21) of [105]).

In order to get figure 4.4, we use the best fit parameters values obtained in section 8.45 which are shown in table 4.3. In this figure, the black line corresponds to ΛCDM, the red line to model A; i.e. a constant EoS and smaller than -1, and leading to a BR, the green line to model B; i.e. the one leading to a LR, and the purple line to model C; i.e. the one leading to a LS.

We next show our results for the evolution of the cosmological perturbations of radiation, DM and DE. We have computed these perturbations for six relevant modes which run from roughly a mode corresponding to the current Hubble horizon $k_1 = 3.33 \times 10^{-4}$h Mpc^{-1} to the largest mode where the linear regime is still valid, $k_6 = 0.1$ h Mpc^{-1}. The six modes are equidistant in a logarithmic scale as follows

$$k_j = k_1 \left(\frac{k_6}{k_1}\right)^{\frac{j-1}{5}}, \tag{4.28}$$

where i runs from 1 to 6. Therefore, the numerical value of the six modes are

$$k_1 = 3.33 \times 10^{-4}\text{h Mpc}^{-1}, \qquad k_4 = 1.02 \times 10^{-2}\text{h Mpc}^{-1}, \tag{4.29}$$

$$k_2 = 1.04 \times 10^{-4}\text{h Mpc}^{-1}, \qquad k_5 = 3.19 \times 10^{-2}\text{h Mpc}^{-1}, \tag{4.30}$$

$$k_3 = 3.26 \times 10^{-3}\text{h Mpc}^{-1}, \qquad k_6 = 1.00 \times 10^{-1}\text{h Mpc}^{-1}. \tag{4.31}$$

As mentioned on the previous section, the evolution of the perturbations are computed from

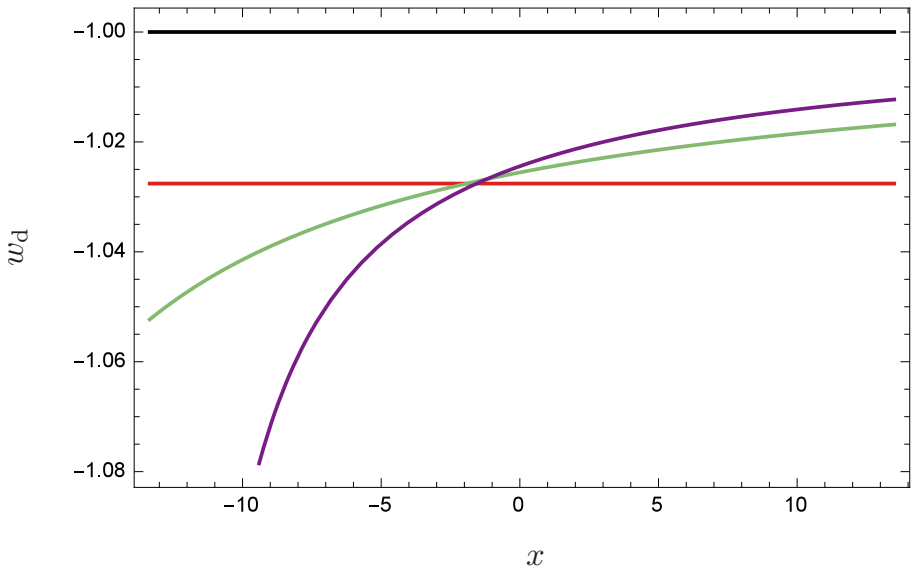

Figure 4.4: This figure shows the evolution of the EoS parameter of DE, $w_{\rm d}$, versus $x \equiv \ln(a)$ for the model parameters given by the best fit in table 4.3. The model A corresponds with the red line describing a constant EoS. The model B is represented by the green line while the model C is shown in purple. The ΛCDM model is presented as a black line at $w_{\rm d} = -1$.

well inside the radiation dominated epoch, $x_{\rm i} = -13.8$, till the distant future, $x_{\rm f} = 13$, where the DE completely dominates the dynamics of the Universe. We consider $x_{\rm f}$ large enough to detect relative deviations between the studied models. We next present the main results. The left panel of figure 4.5 shows the evolution of the matter density contrast of models A, B and C together with ΛCDM. As can be seen, there is no significant deviation since all the modes show almost identical evolution. As expected, the matter density contrast of each mode grows linearly when the mode enters the horizon and reaches it maximum value when DE starts dominating.

The right panel of figure 4.5 shows the evolution of the gravitational potential, Ψ, divided by its initial value, Ψ_*. The results of the models A, B, C and ΛCDM are plotted together in the figure. Once again, the overlap is almost perfect, except for the small deviations presented by all the modes at very large scales, we will discuss this feature later on.

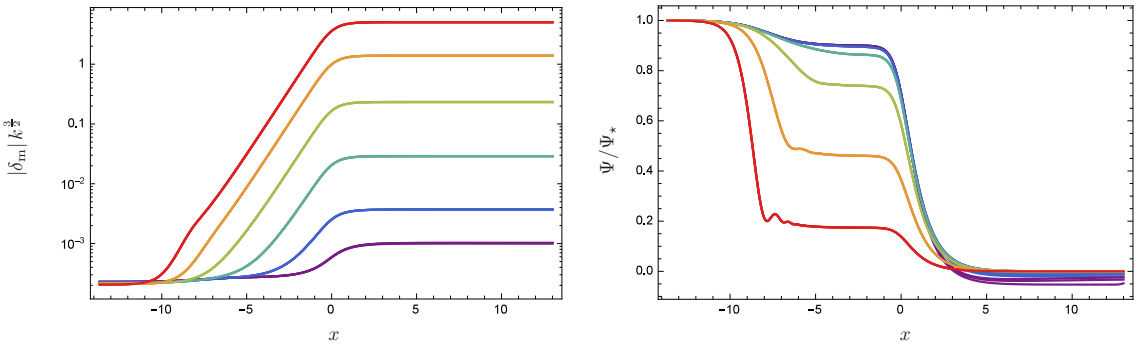

Figure 4.5: The left panel of this figure shows the evolution of the mater density contrast while the right panel shows the evolution of the gravitational potential divided by its initial value. Both panels show a perfect overlapping of the results corresponding to the models A, B, C and ΛCDM. The results corresponding to a given mode are represented by a particular color as follows: k_1 (purple), k_2 (dark blue), k_3 (light blue), k_4 (green), k_5 (orange) and k_6 (red).

The left panel of figure 4.6 shows the predicted current matter power spectrum of models A, B, C and ΛCDM. The black curve corresponds to the ΛCDM model while the models A, B and C are shown overlapped in a single red curve. The overlap is almost perfect being impossible to distinguish any footprints between these models and ΛCDM. In general, the main behaviour is in accordance with that found in the literature and gives a suitable description of the current matter power spectrum.

The right panel of figure 4.6 shows the evolution of $f\sigma_8$. The results of the models A, B and C are overlapped and appear as purple curve, while the results corresponding to ΛCDM are in black. There are no significant deviations between models A, B and C. However, there is some deviation with regards to ΛCDM for $z \sim 0.3$ to $z \sim 0.6$. This result implies that $f\sigma_8$ is larger for phantom DE models as compared with ΛCDM. This result is in agreement with [105, 106].

As can be seen from figures 4.5 and 4.6, it is very difficult to distinguish the models A, B and C as no significant deviation is observed on the matter density contrast and gravitational potential. In view of this, we find convenient to compute relative deviations with respect to ΛCDM.

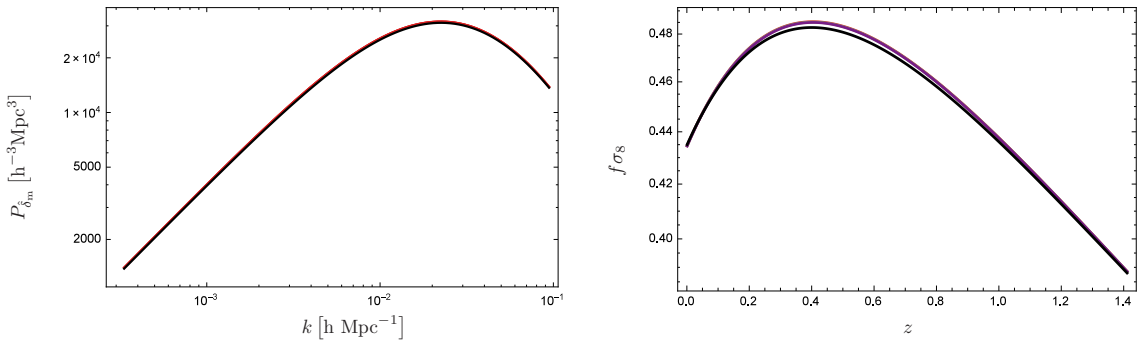

Figure 4.6: The left panel of this figure shows the matter power spectrum when using the model parameters given table 4.3. The result corresponding to the models A, B and C are shown overlapped in red, while the black color corresponds to the ΛCDM model. As can be seen, both results are almost indistinguishable. On the other hand, the right panel of this figure shows the evolution of the $f\sigma_8$. The evolution corresponding to the ΛCDM model is shown in black color, while the results given by the models A, B and C are gathered in a single purple curve.

The left panel of figure 4.7 shows the relative difference for the models A, B and C with respect to ΛCDM of the matter power spectrum. As can be seen, all the models show a very similar behaviour. The deviation is positive for all the modes, reaching a maximum at $k \simeq 5\times10^{-3}$h Mpc^{-1} where the largest deviation is around a 2%. The right panel of Figure 4.7 shows the relative difference of $f\sigma_8$ for the models A, B and C with respect to ΛCDM. Such deviations show a maximum at $z \simeq 0.5$ with a value around 0.5%. The deviation of $f\sigma_8$ with respect to ΛCDM is positive for all the redshift range except for the lowest values. In fact, a transition to a negative difference is observed around redshift $z \simeq 0.05$. This later deviation increases as we approach the present. Once again, we obtain very similar plots when comparing the results obtained for the models A, B and C. We find that the largest deviations correspond to the model A and the smallest one to the model C.

Figure 4.8 shows the evolution of DE density contrast, where each panel corresponds to a given

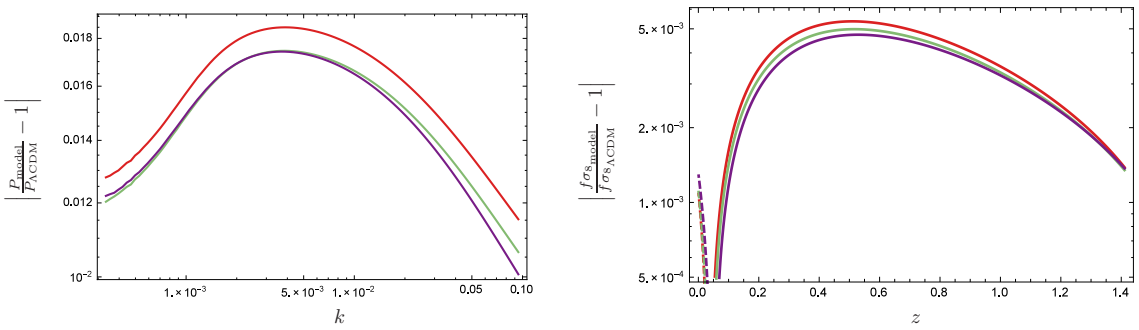

Figure 4.7: The left and right panels of this figure show the relative deviation of the matter power spectrum and $f\sigma_8$ with respect to ΛCDM, respectively. The colors red, green and purple have been used to plot results corresponding to the models A, B and C, respectively. Both plots are drawn in a logarithmic scale, where the dashed line is used to denote negative values and the solid line to denote positive values.

mode. As the perturbations of DE into the ΛCDM model vanishes, we do not compare them with the result of our models. The initial values of the perturbations $\delta_{\rm d}$ are not significantly affected for different modes, i.e. k. However, they depend on the specific model because the EoS of DE is model dependent, in particular at $x = x_{\rm i}$ where we start our numerical integrations. Moreover, given that the EoS parameter for the model C is closer to -1 and it shows the highest density contrast for DE at earlier time (cf. (B.64)). The model A presents the opposite behaviour, while the model B shows an intermediate behaviour. This hierarchical behaviour is inverted in the future, where $\delta_{\rm d}$ gets larger values for the model A and smaller values for the model C. This transition occurs at very low redshifts which brings difficulties in distinguishing the different DE models analysed.

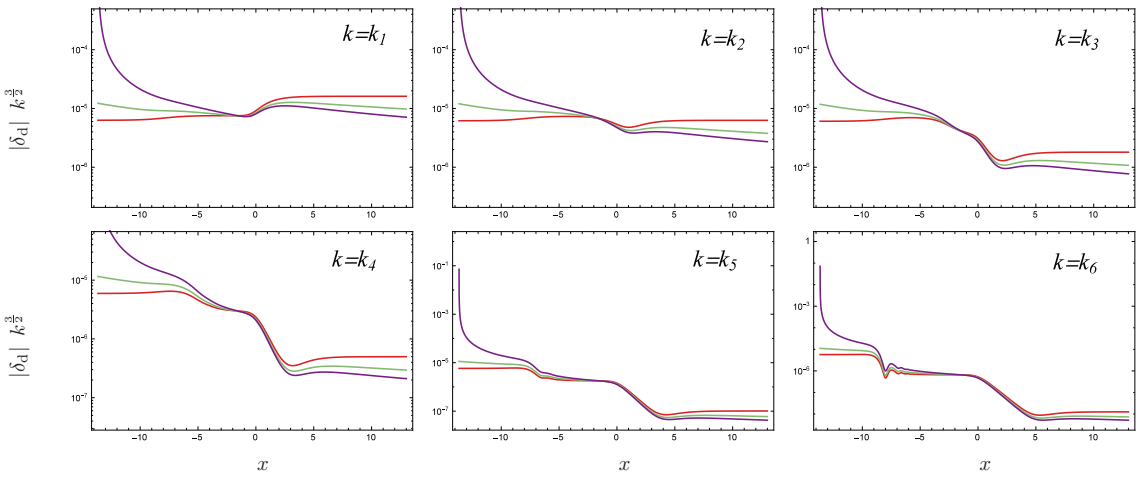

Figure 4.8: This figure shows the DE density contrast for the models A (red), B (green) and C (purple). Each panel corresponds to a specific wave-number k.

We have seen that the difference between models are very small. However, we know very well that each model induces a different and unique abrupt event in the far future. Therefore, we have focused on the evolution of the gravitational potential at very large scale factors. Figure 4.9 shows the evolution of the gravitational potential, Ψ, from the present cosmic time to the far future for different modes. As can be seen, at present the gravitational potential of all the models are very close to ΛCDM. However, at some point in the future, the gravitational potential flips its sign and evolves towards a constant negative value. Within these asymptotic evolutions, model A introduces the highest deviation while model C introduces the smallest one.

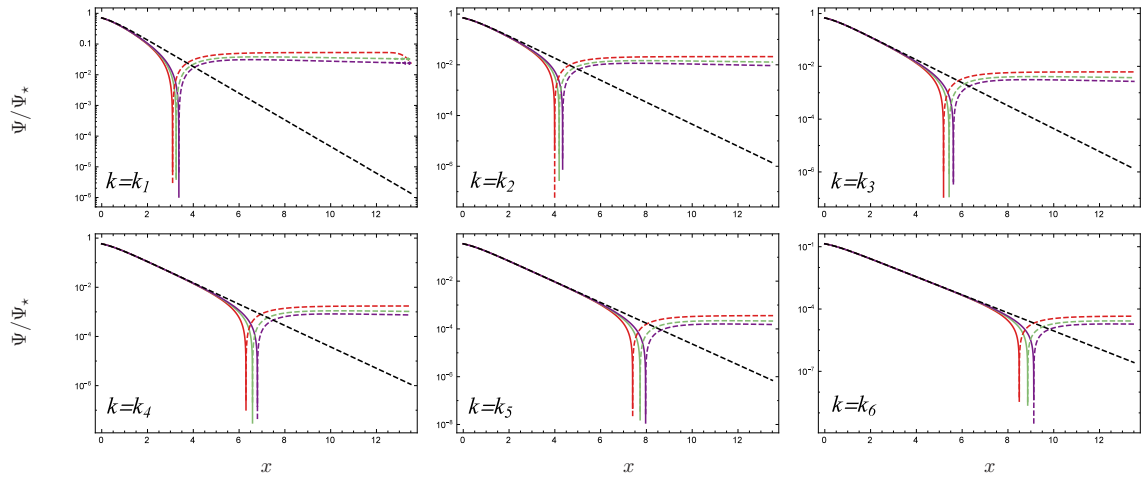

Figure 4.9: This figure shows the evolution of the gravitational potential, Ψ, divided by its initial value, $\Psi_\star$. As done in the previous figures, each panel corresponds to a given value of wave-number while each color represents a particular model (model A red, model B green and model C purple). The dashed lines denote negative values while solid lines represent positive values. The black dashed lines correspond to the ΛCDM model.

The flip on the sign of Ψ occurs sooner in the model A, then in the model B and finally in the model C, independently of the mode. On the other hand, the smallest is the mode the sooner occurs the sign flip on the gravitational potential.

Finally, and based on the best parameters of table 4.3, we have computed the reduced χ^2 for the $f\sigma_8$ analysis in order to have a numerical value that could quantify the difference between models. Note that we do not run a different chain taking into account such $f\sigma_8$ data. We rather perform a simple analysis in order to get some preliminary results involving background and perturbative observations. Here, we have used the "Gold 2017" data [282]. This data provides a set of the latest measurements of $f\sigma_8$ values[iii] (ranging from a redshift $z \sim 0$ to $z \sim 1.4$) where all samples are considered as independent. The obtained results are shown in table 4.4. As can be seen, the model A is the model that more deviates from ΛCDM, followed by the model B and finally by the model C. The best value is still given by the ΛCDM model, however, among the studied phantom models in this work, the model C is observationally preferred. We notice that the background classification of the models A, B and C, table 4.3, is not in agreement with that based on the measurement of $f\sigma_8$. In a future work, we will carry a full Monte Carlo Markov Chain which takes into account the background and the perturbative quantities.

Model	Event	χ^2
ΛCDM	De Sitter	1.13498
A	BR	1.16163
B	LR	1.15919
C	LS	1.15680

Table 4.4: This table presents the values of the reduced χ^2 for each model. These results have been obtained using a data collection of independent survey known as "Gold 2017" growth dataset, which values are shown in table 4.5.

Figure 4.10 shows the evolution of $f\sigma_8$. The ΛCDM model is plotted in black dashed line while

[iii] An extension of the Gold 2017 compilation is given by [283].

z	$f\sigma_8$	Survey	Ref.
0.02	0.314 ± 0.048	2MASS	[284]
0.02	0.398 ± 0.065	SNIa + IRAS	[285]
0.02	0.428 ± 0.046	6dF Galaxy Survey + SNIa	[286]
0.10	0.370 ± 0.130	SDSS-veloc	[287]
0.15	0.49 ± 0.15	SDSS DR7 MGS	[218]
0.17	0.51 ± 0.06	2dF Galaxy Redshift Survey	[214, 219]
0.18	0.360 ± 0.090	GAMA	[288]
0.25	0.351 ± 0.058	SDSS II LRG	[221]
0.32	0.384 ± 0.095	BOSS LOWZ	[289]
0.37	0.460 ± 0.038	SDSS II LRG	[221]
0.38	0.440 ± 0.060	GAMA	[288]
0.44	0.413 ± 0.080	WiggleZ Dark Energy Survey + Alcock-Paczynski distortion	[225]
0.59	0.488 ± 0.06	SDSS III BOSS DR12 CMASS	[226]
0.60	0.390 ± 0.063	WiggleZ Dark Energy Survey + Alcock-Paczynski distortion	[225]
0.60	0.550 ± 0.120	Vipers PDR-2	[290]
0.73	0.437 ± 0.072	WiggleZ Dark Energy Survey + Alcock-Paczynski distortion	[225]
0.86	0.400 ± 0.110	Vipers PDR-2	[290]
1.40	0.482 ± 0.116	FastSound	[229]

Table 4.5: This table shows $f\sigma_8$ measurements from independent surveys. The first column denotes the redshift while in the second column the corresponding value of $f\sigma_8$ and its error. In the third column, we show the name of survey and in the final column the reference.

models A, B and C are plotted in red.

4.5 Conclusions

In this chapter we have analysed three genuine phantom models. We call those models as A, B and C, where each of them induces a particular future cosmological event known as a BR, a LR and a LS, respectively. These models are characterised by having a particular EoS, which can be understood as deviations from the widely accepted ΛCDM model and therefore, suitable models to describe the current Universe. We use SNIa, CMB, BAO and $H(z)$ data and the Markov Chain Monte Carlo method to estimate the cosmological parameters of models A, B and C. We remark that the model C has not been constrained previously. In the case of the model A, the corresponding model parameter consists on the EoS parameter of DE. This value has been observationally constrained, for example, in [14, 18], where the result given, $w_{\rm d} = -1.019$, is very close to the one we have found, $w_{\rm d} = -1.02758$. Similarly, the result obtained for the model B is of the same order of magnitude to that found in [66] where the relative difference is less than a 6%, this can be understood as an indicative of the reliability of the obtained

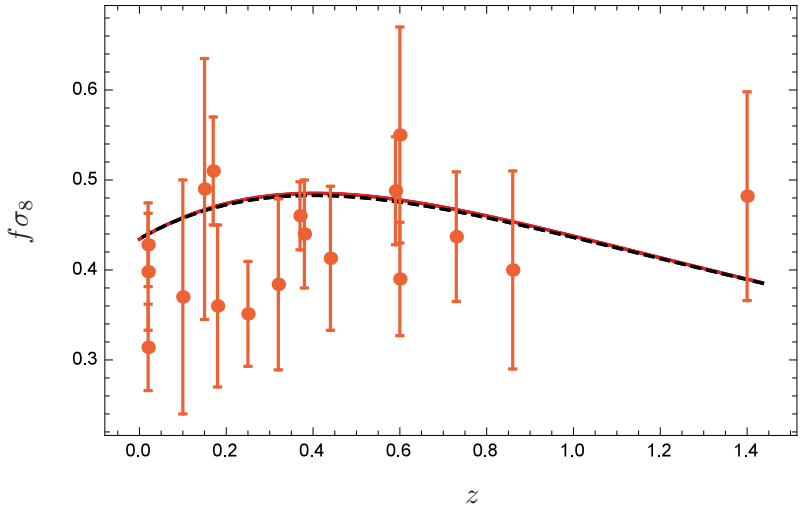

Figure 4.10: This figure shows the evolution of the predicted $f\sigma_8$ observable versus the redshift, z. The results given by the models A, B and C are plotted in red color where the overlap is almost perfect. The result given by the ΛCDM model is plotted in black dashed line. We have included the survey data given in table 4.5 with the corresponding error.

results. In addition, we have computed the results of the ΛCDM model as well, in order to make a comparison with the models A, B and C.

Once we have fitted observationally the parameters of the models, we have computed numerically linear cosmological perturbations since the radiation dominated epoch. Therefore, we have not only considered perturbations of DM and DE but also those of radiation. The numerical calculations have been performed till the far future. In particular, we have obtained the density contrast of DM and DE and evaluated as well the matter power spectrum of DM and the corresponding evolution of $f\sigma_8$. We have as well computed the evolution of the Bardeen gravitational potential. We have confirmed that indeed in phantom DE models, it is expected that the Bardeen gravitational potential will flip its sign in the future [105, 106]. This is in accordance with the fact that all the structures will be destroyed in phantom DE models.

Using the values of the best fit (shown in the third column of table 4.3), the matter power spectrum given by models A, B and C are so similar that it is almost impossible to distinguish them. Something similar happens when comparing the results of $f\sigma_8$. In order to give an account of small differences, we compute the relative deviation with respect to ΛCDM and found that the largest differences are around a 2% for the matter power spectrum and $f\sigma_8$. The models show a very similar phenomenology till the present time and future cosmic times. We notice that there are no significant differences that could allow us to find a characteristic footprint of each model with enough accuracy.

In view of this, we compare the predicted $f\sigma_8$ evolution against the observational data and compute the reduced χ^2. We conclude that the ΛCDM model gives the best fit. The models A, B and C have similar behaviour with respect to the ΛCDM. When performing the χ^2 analysis at $f\sigma_8$ level, what we found is that the model C is the one which less deviates from ΛCDM while the model A is the one with larger deviations. However, this is not enough to conclude that the model C is observationally preferred. We conclude as well that there is a disagreement between

the background and the perturbation analysis. This discordance will be a subject of a future work.

5

What if gravity becomes really repulsive in the future?

We know what we are, but know not what we may be

– William Shakespeare

5.1 Introduction

Hubble's discovery was crucial for our understanding of the Universe. He showed that the Universe was evolving and not static as it was believed at that time [3]. His discovery was based on observing that the spectrum of far away galaxies was red-shifted which implied that those galaxies were moving away from us. He even measured the galaxies radial outward velocities and realised that it followed a rule: (i) the velocities were proportional to the distances at which the galaxies were located from us and (ii) the proportionality factor was a constant, the Hubble constant. About 70 years later, two independent teams [11, 12] realised that by measuring further objects, SNeIa, the Hubble constant was not quite constant as was already expected. The issue was that the deviation from the constancy was not on the anticipated direction. It was no longer enough to invoke only matter to explain those observations. A new component had to be invoked adjectivated dark, as it interacts as far as we know only gravitationally, and named energy. This component started recently fuelling a second inflationary era of the visible Universe. Of course, all these observations, and subsequent ones, are telling us how gravity behaves at cosmological scales through the kinematic expansion of our Universe [14, 197, 217, 219, 220, 230].

This kinematic description is linked to the dynamical expansion through the gravitational laws of Einstein theory. To a very good approximation, we can assume that our Universe is homogeneous and isotropic on large scales and it is filled with matter (standard and dark) and DE, where their relative fractional energy densities are $\Omega_{\mathsf{m}} = 0.309$ and $\Omega_{\mathsf{d}} = 0.691$, respectively, at present. In addition, the current Hubble parameter is of the order of $H_0 = 67.74$ km s^{-1} Mpc^{-1}. We have fixed those values by using the latest Planck data [14] but please notice that our conclusions in this chapter[i] are unaltered by choosing other values for these physical quantities. In what refers to EoS parameter, w, to be constant; i.e. we will be considering wCDM model as a natural candidate to describe our Universe. As it is well known (i) for $w < -1$ the Universe would face a BR singularity [28–30], i.e., the Universe would unzip itself in a finite time from now, (ii) for $w = -1$ the Universe would be asymptotically de Sitter and finally (iii) if $w > -1$ the Universe would be asymptotically flat locally; i.e. the scalar curvature and the Ricci tensor would vanish for large scale factors. As we next show this pattern is shown as well on the behaviour of the gravitational potential.

[i] This chapter corresponds mainly to our publication [106]

The chapter is organised as follows: in section 5.2, we review briefly the models to be considered and compare them using a cosmographic/statefinder analysis. In section 5.3, we present the cosmological perturbations of the models focusing on the asymptotic behaviour of the gravitational potential. Finally, in section 5.4, we conclude. In the A.1, we include some formulas useful to section 5.2.

5.2 Background Approach

In this work, we adopt three different values for w: $\{-0.99,\, -1,\, -1.01\}$, in order to obtain three qualitatively different types of late-time behaviour for DE: quintessence ($w \gtrsim -1$), cosmological constant ($w = -1$) and phantom behaviour ($w \lesssim -1$). In a cosmographic approach [196, 291-293], the scale factor is Taylor expanded around its present day value $a_0 := a(t_0)$ as

$$\frac{a\,(t)}{a_0} = 1 + \sum_{n=1}^{\infty} \frac{A_n\,(t_0)}{n!}\left[H_0\,(t - t_0)\right]^n \,. \tag{5.1}$$

Here, H_0 is the present day value of the Hubble rate $H := \dot{a}/a$, where a dot represents a derivative with respect to the cosmic time, and the cosmographic parameters A_n are defined as $A_n := a^{(n)}/(a\,H^n)$, $n \in \mathbb{N}$, where $a^{(n)}$ is the n^{th}-derivative of the scale factor with respect to the cosmic time[ii]. Based on the cosmographic expansion (5.1), the statefinder hierarchy was developed as a tool to distinguish different DE models [294-297]. In fact, the statefinder parameters are defined as specific combinations of the cosmographic parameters:

$$S_3^{(1)} = A_3\,, \tag{5.2}$$
$$S_4^{(1)} = A_4 + 3\,(1 - A_2)\,, \tag{5.3}$$
$$S_5^{(1)} = A_5 - 2\,(4 - 3A_2)\,(1 - A_2)\,, \tag{5.4}$$

such that, by construction, $S_n^{(1)}|_{\Lambda\text{CDM}} = 1$, i.e., the statefinder hierarchy defines a null diagnostic for the ΛCDM model [296]. It is also convenient to introduce the statefinder parameter s defined in [294] as

$$s = \frac{1 - S_3^{(1)}}{3\left(A_2 + \frac{1}{2}\right)}. \tag{5.5}$$

For the case of a wCDM model with a radiation component, such as the models considered in this chapter, we present in A.1 the full expressions of the statefinder parameters as functions of the scale factor a/a_0 and the cosmological parameters $\{\Omega_{\text{i,0}},\, w\}$. In the limit $a \to +\infty$ the expressions found reduce to

$$S_3^{(1)}|_{w\text{CDM}} = 1 + \frac{9}{2}w\,(1 + w)\,, \tag{5.6}$$
$$S_4^{(1)}|_{w\text{CDM}} = 1 - \frac{9}{4}w\,(1 + w)\,(7 + 9w)\,, \tag{5.7}$$
$$S_5^{(1)}|_{w\text{CDM}} = 1 + \frac{9}{4}w\,(1 + w)\left(41 + 87w + 54w^2\right)\,, \tag{5.8}$$
$$s|_{w\text{CDM}} = 1 + w\,. \tag{5.9}$$

[ii]The parameters A_2, A_3, A_4, A_5 are also known as the deceleration parameter $q = -A_2$, the jerk $j = A_3$, the snap $s = A_4$ and the lerk $l = A_5$, respectively [291].

We thus find that as w deviates from the nominal value -1 the asymptotic values of the statefinder parameters $S_i^{(1)}$ run away from unity. In fact, for small deviations $\Delta w := |w+1| \ll 1$ the statefinder parameters depend linearly on Δw and we find that $S_n^{(1)} < 1$ for quintessence models and $S_n^{(1)} > 1$ in the case of phantom behaviour. On the other hand, it can be shown that asymptotically s vanishes for ΛCDM, and it gets negative for $w < -1$ and positive for $-1 < w$. We have assumed on all our conclusions the presence of radiation no matter its tiniest contribution.

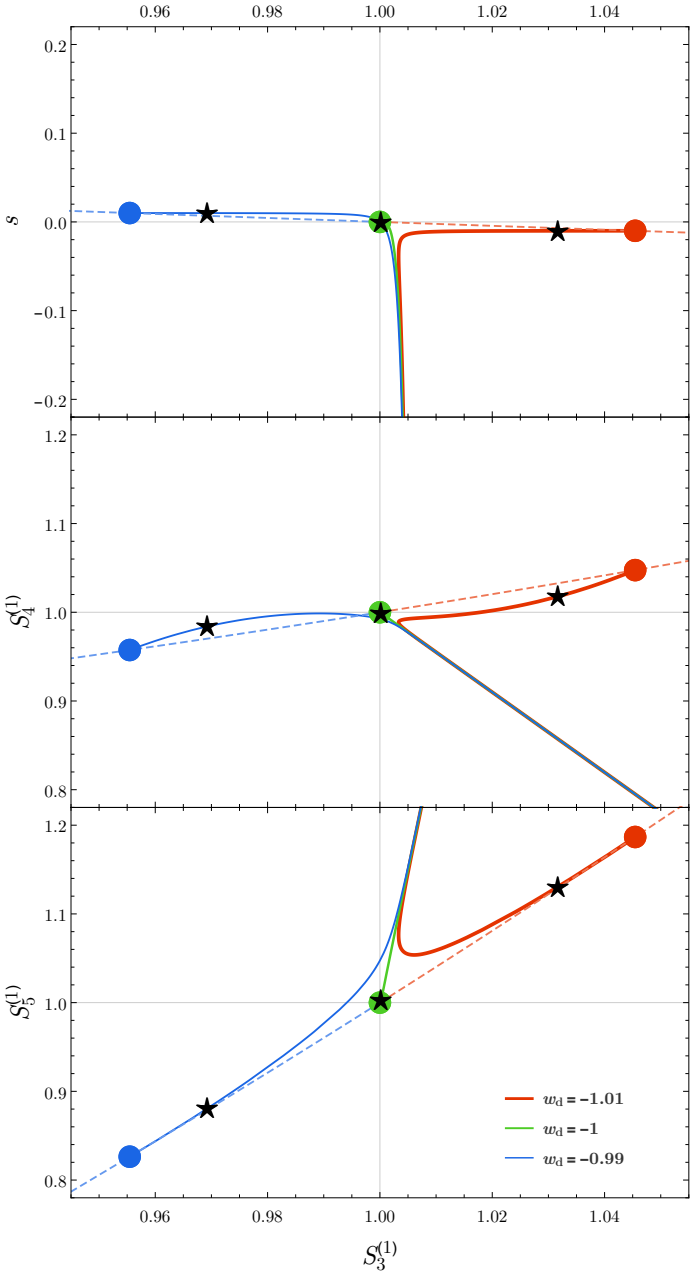

Figure 5.1: This figure shows the trajectory of the three models considered in this work in the planes $\{S_3^{(1)}, s\}$, $\{S_3^{(1)}, S_4^{(1)}\}$ and $\{S_3^{(1)}, S_5^{(1)}\}$ that characterise the statefinder hierarchy. The coloured points indicate the asymptotic values of the statefinder parameters as presented in (5.6)-(5.8). The dependence of these points on the deviation of w from the ΛCDM value -1 is illustrated by the dashed lines. The black stars indicate the present day values of the statefinder parameters for each of the models.

On figure 5.1, we present the evolution of the statefinder hierarchy $\{S_3^{(1)}, s\}$ (top panel),

$\{S_3^{(1)}, S_4^{(1)}\}$ (middle panel) and $\{S_3^{(1)}, S_5^{(1)}\}$ (bottom panel) for the three models considered: $w = -0.99$ (blue), $w = -1$ (green) and $w = -1.01$ (red). When the Universe is dominated by radiation and matter the three models are indistinguishable and can be seen following the same straight line trajectory in the planes $\{S_3^{(1)}, s\}$, $\{S_3^{(1)}, S_4^{(1)}\}$ and $\{S_3^{(1)}, S_5^{(1)}\}$. However, as DE starts to dominate at late-time the differences between the three models become apparent. The trajectory $\{S_3^{(1)}, s\}$ evolves towards the point (1, 0) for the ΛCDM model, then for a quintessence model that trajectory evolves towards the second quadrant in the plane $\{S_3^{(1)}, s\}$, i.e. $S_3^{(1)} < 1$ and $0 < s$, and, finally, for a phantom scenario the trajectory $\{S_3^{(1)}, s\}$ heads towards the fourth quadrant, i.e. $1 < S_3^{(1)}$ and $s < 0$. For the second group of trajectories $\Big(\{S_3^{(1)}, S_4^{(1)}\}$ and $\{S_3^{(1)}, S_5^{(1)}\}\Big)$, while the trajectories of the model with $w = -1$ evolve towards the point (1, 1) that characterises ΛCDM, in the quintessence model the trajectories evolve towards the third quadrant in both panels ($S_n^{(1)} < 1$ for $n = 3, 4, 5$). In contrast, for the model with phantom behaviour the trajectories evolve towards the first quadrant in the planes $\{S_3^{(1)}, S_4^{(1)}\}$ and $\{S_3^{(1)}, S_5^{(1)}\}$ characterised by $S_n^{(1)} > 1$ for $n = 3, 4, 5$. Finally, by looking at figure 5.1, it seems that the pair $\{S_3^{(1)}, S_5^{(1)}\}$ are better to distinguish the model with $w < -1$ from $-1 < w$.

5.3 Cosmological Perturbations: from gravity to DM and DE

In order to tackle the cosmological perturbations of a perfect fluid with a negative and constant EoS some care has to be taken into account [105]. In fact, unless non-adiabatic perturbations are taken into account a blow up on the cosmological perturbations quickly appears even at scales we have already observed. Please notice that this is so even for non-phantom fluids, i.e., for $w \geq -1$. This will be our first assumption and therefore non-adiabatic perturbations will be considered. The non-adiabaticity implies the existence of two distinctive speed of sounds for the DE fluid: (i) its quadratic adiabatic speed of sound $c_a^2 = w$ (in our case) and (ii) its effective quadratic speed of sound, c_s^2, whose deviation from $c_a^2 = w$ measures the non-adiabaticity in the evolution of the fluid [101]. For simplicity, we will set the latter to one which fits perfectly the case of a scalar field, no matter if it is a canonical scalar field of standard or phantom nature[iii]. In addition, we will solve the gravitational equations describing the cosmological perturbations at first order using the same methodology we presented in [105]. The initial conditions are fully fixed by the Planck observational fit to single inflation [14] as follows from equations (2.41) and (B.61):

The behaviour of the gravitational potential and the perturbations is shown in the top panel of figure 5.2 for a given scale. We choose as an example $k = 10^{-3}$ Mpc^{-1}. As it must be, the gravitational potential is constant during the matter era and start decreasing as soon as DE *goes on stage*. This behaviour is independent of the considered DE model. However, shortly afterwards; i.e., in our *near future*, the gravitational potential will depend on the specifically chosen EoS for DE. In fact, (i) it will decrease until reaching a positive non-vanishing value at infinity for $w > -1$, (ii) it will vanish asymptotically for $w = -1$ and amazingly (iii) it will vanish and become negative for $w < -1$!!! This is in full agreement with the fact that close to the BR the different structures in our Universe will be destroyed no matter their sizes or bounding energies.

[iii] As long as the speed of sound c_s^2 is not too close to zero and $w \simeq -1$, the value of c_s^2 will not affect so much the perturbations of DM. A full discussion on the effect of the speed of sound of DE on the perturbations of the late Universe can be found in [16, 209, 298]. Therefore, our choice $c_s^2 = 1$ is not crucial in our study, it was taken just for simplicity and because it is common to use it in codes like CAMB and CLASS though there is no fundamental reason for such a choice.

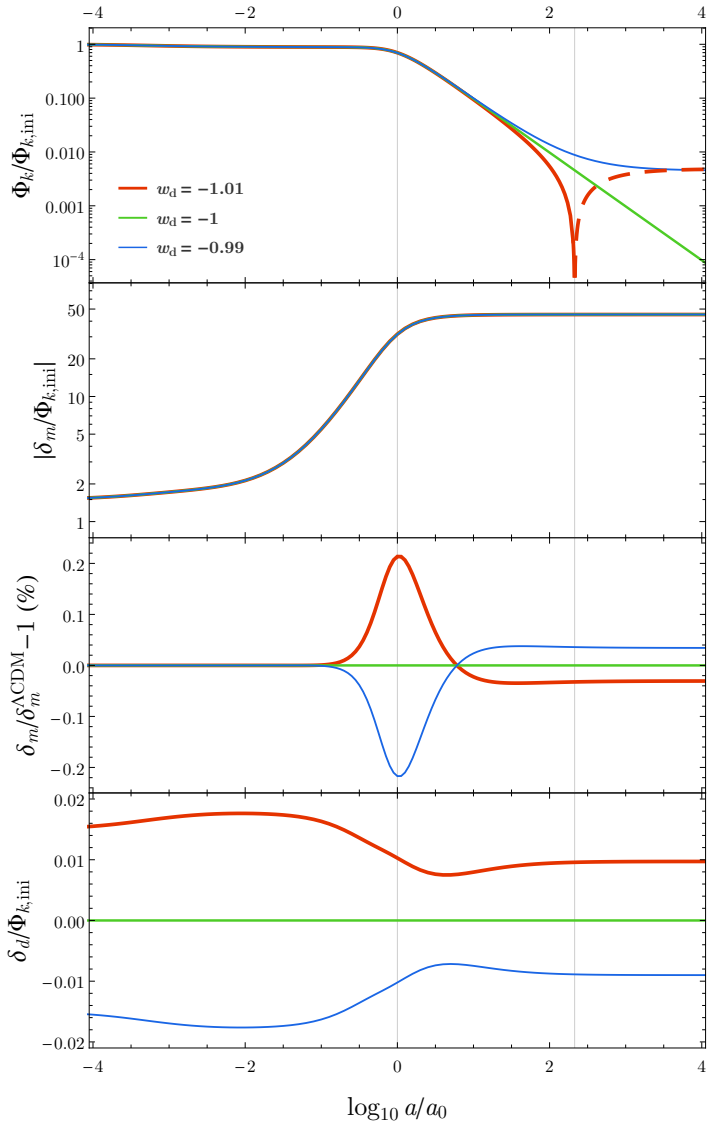

Figure 5.2: The evolution of the Fourier mode of the gravitational potential Φ_k (top panel), the DM perturbation δ_m (middle panels) and the DE perturbation (bottom panel), from the matter era to the far future for the mode $k = 10^{-3}$ Mpc^{-1} and for three DE models: (blue) $w = -0.99$, (green) $w = -1$ and (red) $w = -1.01$. For the quintessence model (blue) the gravitational potential evolves towards a constant in the far future without changing sign, while for ΛCDM (green) Φ_k vanishes asymptotically. In the phantom model (red), Φ_k also evolves towards a constant in the far future but a change of sign occurs roughly at $\log_{10} a/a_0 \simeq 2.33$, corresponding to 8.84×10^{10} years in the future. A dashed line indicates negative values of Φ_k.

When could the gravitational potential vanishes and flip its sign? Of course, the answer is model and scale dependent [105]. For the model we have considered, the gravitational potential for the mode $k = 10^{-3}$ Mpc^{-1} will vanish in 8.84×10^{10} years from the present time or equivalently when the Universe is roughly 213 times its current size. Furthermore, numerical results show that the smaller the scale that is considered (larger k) the later the gravitational potential will flip sign [105].

In addition to the gravitational potential, we present in the second and third panels of figure 5.2 the behaviour of the density contrast of DM. We observe that the growth of the linear perturba-

tions is very similar in all models, with differences of $\lesssim 0.2\%$ with regards to ΛCDM. However, when comparing the phantom DE model with ΛCDM we find that until the present time there is an excess in the growth of the linear perturbations of DM in the phantom DE case. In the case of quintessence the opposite behaviour is observed: until the present time $\delta_{\rm m}$ is smaller in the quintessence case when compared with ΛCDM. This effect, which depends on the qualitative behaviour of DE, was first noted in [30]. Surprisingly, these deviations peak around the present time and their sign reverses in the near future. On the bottom panel of figure 5.2 we present the evolution of $\delta_{\rm DE}$ for the different models. Of course, for the ΛCDM case the perturbations remain at 0 as the cosmological constant does not cluster. In good agreement with observations, for the quintessence and phantom DE models we find that the DE perturbations remain small, with small variations of the initial value, throughout the whole evolution of the Universe.

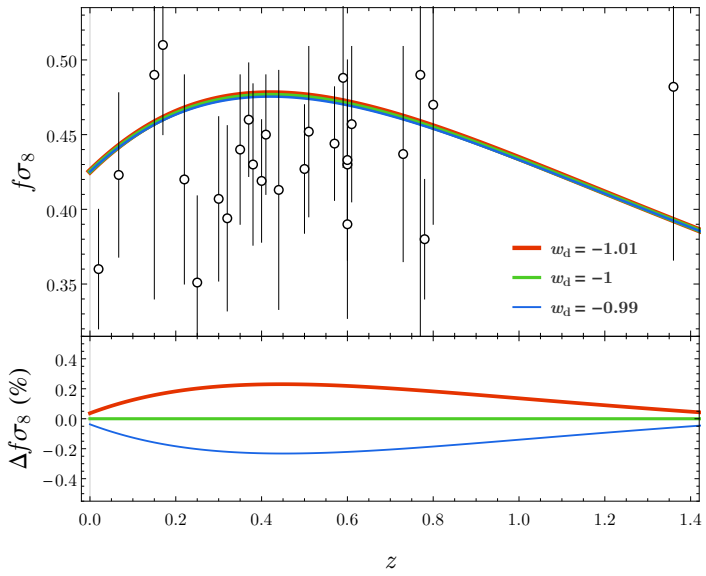

Figure 5.3: (Top panel) evolution of $f\sigma_8$ for low red-shift $z \in (0, 1.4)$ for three DE models: (blue) $w = -0.99$, (green) $w = -1$ and (red) $w = -1.01$. White circles and vertical bars indicate the available data points and corresponding error bars (cf. Table I of [105]). (Bottom panel) evolution of the relative differences of $f\sigma_8$ for each model with regards to ΛCDM ($w = -1$). $\Delta f\sigma_8$ is positive in the phantom case and negative in the quintessence case. For all the models, it was considered that σ_8 evolves linearly with $\delta_{\rm m}$ and that $\sigma_8 = 0.816$ at the present time [14].

Finally, and most importantly, all these models are in full agreement with observations. In figure 5.3, we show the evolution of the observable $f\sigma_8$ for the three models mentioned above. This combination of f, the relative growth of the linear matter perturbations, and σ_8, the root-mean-square mass fluctuation in spheres with radius 8 h^{-1}Mpc, was proposed in [214] as a discriminant for different models of late-time acceleration that is independent of local galaxy density bias. On the top-panel of figure 5.3, we contrast the $f\sigma_8$ curves of the three models with the available observational data (cf. Table I of [105]). All the three curves, which are practically indistinguishable at the naked eye, are within the error bars of nearly all the points. On the bottom panel of figure 5.3, we present the relative difference, $\Delta f\sigma_8$, of the results of each model with regards to ΛCDM.[iv] Despite the small values found in terms of amplitudes, the behaviour observed suggests that the sign of $\Delta f\sigma_8$ can distinguish between a phantom (positive $\Delta f\sigma_8$) and a quintessence model (negative $\Delta f\sigma_8$). As a consequence of this difference in sign, the growth of the linear matter perturbations is stronger in a phantom scenario as opposed to

[iv] $\Delta f\sigma_8^{(\rm model)}(\%) := 100[(f\sigma_8^{(\rm model)})/(f\sigma_8^{\Lambda\rm CDM}) - 1]$.

ΛCDM and quintessence. This is in full agreement with the results presented in [30] where the decay of the growth suppression factor of the linear matter perturbations is found to be faster in quintessence models and slower in phantom models.

5.4 Concluding remarks

Summarising, what we have shown is that after all gravity might behave the other way around in the future and rather than the apple falling from the tree, the apple may fly from the earth surface to the branches of the tree, if DE is repulsive enough, as could already be indicated by current observations[v].

To illustrate these observations, we have considered three models where DE is characterised by a constant parameter of EoS w with values $w = -0.99, -1, -1.01$. After comparing the present and future behaviour at the background level by using a statefinder approach, as illustrated in figure 5.1, we have considered the cosmological perturbations of these models. We have shown that for models with $w < -1$ the gravitational potential changes its sign in the future (cf. figure 5.2). We have as well analysed the behaviour of the DM and DE perturbations as shown for example in figure 5.2. Finally, we have proven that no matter the future behaviour of the gravitational potential depicted in figure 5.2, the three models discussed above are in full agreement with the latest observations of $f\sigma_8$ (cf. figure 5.3).

Before concluding, we would like to remind that on this work, we have considered the existence of phantom matter, however it might be possible that Nature presents rather a phantom-like behaviour as happens in brane world-models [244, 300] where no BR takes place and where the perturbations can be stable. In addition, even the presence of phantom matter might not be a problem at a cosmological quantum level where the BR or other kind of singularities can be washed away [42, 48, 51].

[v] Repulsive gravity could happen as well if the effective gravitational constant changes sign. This could happen, for example, in scalar-tensor theories, in particular, for a non-minimally coupled scalar field [299]. However, an anisotropic curvature singularity arises generically at the moment of this transition.

6

The Speed of sound in phantom DE models

We have peered into a new world and have seen that it is more mysterious and more complex than we had imagined. Still more mysteries of the Universe remain hidden. Their discovery awaits the adventurous scientists of the future. I like it this way

– Vera Rubin

6.1 Introduction

During the last two decades Cosmology has experienced a great improvement in the theoretical and observational scopes. The discovery of an accelerated Universe, a fact supported by several observations [10, 11], has developed a flourishing of new ideas that deal with the intriguing speed up. The simplest explanation consists into invoking a new component in the Universe named DE as the responsible of the current acceleration [23]. Among the vast amount of DE models, those where the null energy condition is violated are coined as phantom [28, 30, 33, 239]. In these class of models, the DE EoS parameter stays always below -1. Despite some energy conditions are not satisfied, phantom DE models seem to be favoured by observations [15].

It is known that most phantom DE models predict future singularities. As we have already mentioned in the introduction chapter, we focus on three genuine phantom models[i] where each of them induce a particular future doomsday known as BR, LR, and LS (see [28–35], [47, 55, 59, 64–67, 201], [69, 71, 205] for a detailed description of the respective model). We recall that no matters if a true singularity or an abrupt event takes place, all the bound structures in the Universe are torn away and destroyed.

All the models mentioned above can be understood as alternatives from the widely accepted ΛCDM paradigm, and therefore, good models to describe suitably the current Universe. An appropriate fitting of the parameters involved will made these models indistinguishable among them at the background level. Therefore, it becomes necessary to address the cosmological perturbations.

Observables as for example, the matter power spectrum and the growth rate provide useful data about the distribution of matter. Unfortunately, in most of the cases the imprints of different DE models on such observables are insignificant. Therefore, important efforts have been made to improve the accuracy of the observations, particularly, focusing on scrutinising the DE sector as it is the case of Euclid mission [99, 100].

The squared speed of sound parameter, $\tilde{c}_s^2$, is another important variable that plays a key role on cosmological perturbations. It is well known that DE models with a negative $\tilde{c}_s^2$ parameter

[i] This chapter is based on a work in progress to be submitted soon.

induce instabilities at the perturbation level. To avoid those instabilities, in [16, 101] the authors consider a non-adiabatic contribution on the pressure perturbations. This method lead to separate the adiabatic speed of sound, c_a; which depends on the EoS, and the effective speed of sound, c_s; which is regarded as a free parameter[ii]. For example, in [301] the authors analyse the implications of a varying effective speed of sound parameter on the matter perturbations. In [302], the authors consider a DE model with a constant EoS parameter and estimate the corrections on the growth index when ranging c_s^2. On the other hand, in [303] it is considered a DE model with an affine EoS. Then, the results obtained when fixing $c_s^2 = 0$ and $c_s^2 = 1$ are compared. A further analysis on the effective speed of sound parameter is performed in [209], where the authors consider the contribution of matter (Baryonic and DM), photons and neutrinos to get, for example, a probability distribution for the c_s^2 value. In [304], a new class of DM-DE interacting models is identified. The authors study the implications of a varying effective speed of sound on the CMB and the matter power spectrum. An interesting model with viscosity parameter is suggested in [305], where the effects of such viscosity on the CMB and matter power spectrum are compared against the effects that a non-vanishing effective speed of sound could induce.

Several models have been observationally constrained in order to fit a value for c_s^2. For example, in [16, 298] the authors use the temperature fluctuations of the CMB dataset to set the value of the speed of sound. In [306] the authors study the structure formation and constrain a CPL model with a free effective speed of sound parameter. In view of the upcoming Euclid mission, several works forecast the necessary accuracy in order to discriminate between different DE models. For instance, in [104] the authors compute the sensitivity of the photometric and spectroscopic surveys for measuring the speed of sound and viscosity parameters.

In this chapter, we consider a Universe filled with radiation, matter and DE components, where the latter is described by three different phantom models. We address the scalar cosmological perturbations following the method of pressure decomposition for DE [16, 101]. We set the initial conditions as done in [105, 196] where the physical value of the total matter density contrast, $\delta_{\rm phys.}(k)$, for a single field inflation is taken from Planck data 2018 [18]. After imposing adiabatical conditions for scales larger than the horizon at the beginning, the physical value of $\delta_{\rm phys.}(k)$ is the last condition needed to ultimately fix all the initial numerical values. We analyse the phenomenological effects of changing the effective speed of sound on the perturbations. In addition, we compute the relative differences on observables by evaluating the matter power spectrum and $f\sigma_8$ growth rate. Finally, we study the behaviour of the gravitational potential on large scales.

The chapter is organised as follows, In section 6.2 we present the obtained results and in section 6.3, we present the main conclusions.

6.2 Results: The effect of the speed of sound

In the following, we present the results obtained for the cosmological perturbations evolution and for the three models addressed in this thesis. We remind that in order to set the model pa-

[ii] In the case of a scalar field representation, the effective speed of sound parameter coincides with unity, i.e. $c_s^2 = 1$ (c.f please [16, 101] for a detailed explanation).

rameters we have used those obtained in our work [107]. We compute the evolution of the matter density contrast and peculiar velocities, from well inside the radiation dominated epoch[iii], $a \sim 2.65 \times 10^{-6}$, till the far future, $a \sim 1.62 \times 10^{5}$. We perform the integrations for the following six particular modes

- small k (large distances): $k_1 = 3.33 \times 10^{-4}$h Mpc^{-1} and $k_2 = 1.04 \times 10^{-4}$h Mpc^{-1}.
- medium k (intermediate distances): $k_3 = 3.26 \times 10^{-3}$h Mpc^{-1} and $k_4 = 1.02 \times 10^{-2}$h Mpc^{-1}.
- large k (short distances): $k_5 = 3.19 \times 10^{-2}$h Mpc^{-1} and $k_6 = 1.00 \times 10^{-1}$h Mpc^{-1}.

The minimum mode, k_1, coincides with the current Hubble horizon, i.e. no smaller mode can be detected. On the other hand, we consider as maximum mode, k_6, where the linear approximation breaks down and the non-linear contributions become important.

6.2.1 Matter power spectrum and f$_{\sigma_8}$

We have computed the current matter power spectrum and the growth rate $f\sigma_8$, testing the effective squared speed of sound from 0 to 1 in steps of 0.2. In this process, the numerical integration was repeated for 200 modes ranged from k_1 to k_6.

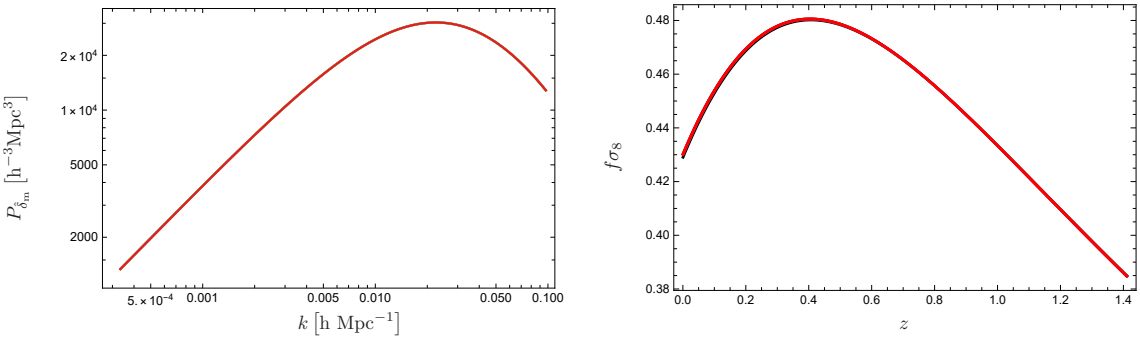

Figure 6.1: The left panel of this figure represents the matter power spectrum while the right panel shows the evolution of $f\sigma_8$ in terms of the redshift z. All models with different values of c^2_{sd} give an almost identical result, so the curves appear completely overlapped and their differences are negligible.

Figure 6.1 shows the current matter power spectrum and the evolution of $f\sigma_8$ predicted by the models. These results are in agreement with observations but does not allow to distinguish any deviation for different models. In addition, the effects of a varying speed of sound turn out to be almost undetectable since the results appear totally overlapped. Therefore, in order to give an account of the contrast, we compute the relative deviation with respect to $c^2_{\text{sd}} = 1$.

As it is shown in the left column of figure 6.2, the relative differences (with respect to $c^2_{\text{sd}} = 1$) on the matter power spectrum are negative for the smallest modes and positive for the largest ones. The transition occurs in a narrow interval around the wave number $k \sim 1.8 \times 10^{-3}$h Mpc^{-1}. The separation obtained for a vanishing speed of sound parameter is remarkable. First, looking at small modes, the deviations are constant, the larger is the deviation from $c^2_{\text{sd}} = 1$ the larger is such a constant. Secondly, looking at the large modes, the deviation is constant for vanishing c^2_{sd} parameters while such deviation vanishes for non vanishing c^2_{sd} parameters.

[iii] The scale factor for this epoch represents a moment in the early Universe where its energy content consists in 1% of matter against 99% of radiation.

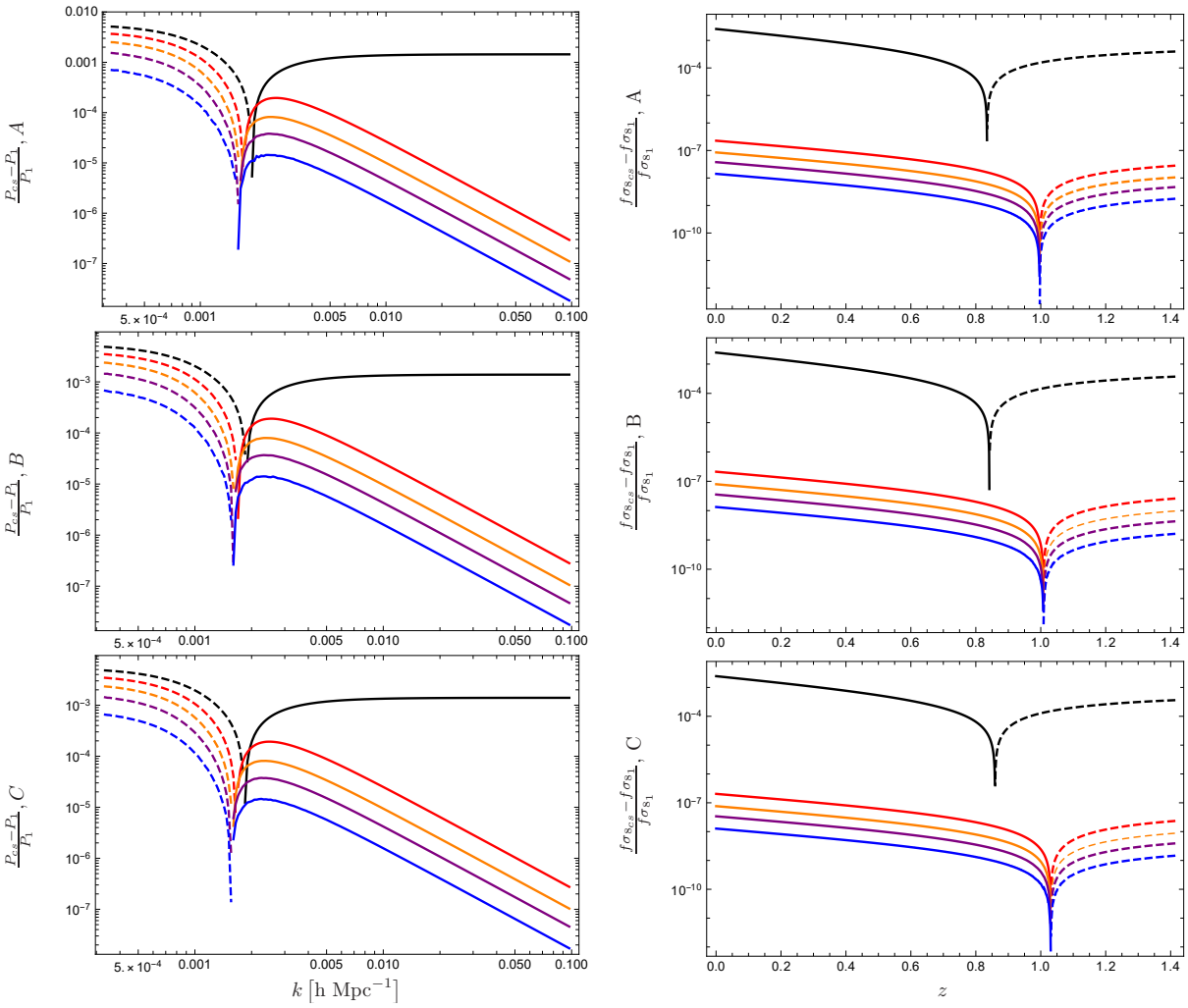

Figure 6.2: This figure presents the relative deviation with respect to the result given when $c_{sd}^2 = 1$. The top, middle and bottom panels correspond with the models A, B and C, respectively. The left panels show the results for the matter power spectrum as a function of the mode. The right panels show the results for $f\sigma_8$ in terms of redshift, z. Different values of c_{sd}^2 are coloured as; $c_{sd}^2 = 0$ (black), $c_{sd}^2 = 0.2$ (red), $c_{sd}^2 = 0.4$ (orange), $c_{sd}^2 = 0.6$ (purple) and $c_{sd}^2 = 0.8$ (blue). The plots are represented in a logarithmic scale, in such a way that dashed lines corresponds with negative values while solid lines represents positive values.

Something similar happen for $f\sigma_8$ results. As it is shown on the right column of figure 6.2, the relative difference for a vanishing effective speed of sound parameter show an important separation with respect to the results given for a non-vanishing c_{sd}^2 parameter. Conversely, the deviation is positive for the smallest redshifts and negative for the largest ones. The transition occurs at $z \sim 0.85$ for a vanishing c_{sd}^2 and at $z \sim 1$ for non-vanishing c_{sd}^2. Such transition point is slightly affected depending which DE model is considered. In addition, contrary to what happens for the matter power spectrum, in $f\sigma_8$ the deviations goes to a constant for both large and small modes. As expected, such a constant is larger the larger is the deviation from $c_{sd}^2 = 1$.

The largest deviations are of the order 10^{-3} in both, the matter power spectrum and $f\sigma_8$ evolution. So we conclude that no significant footprints appear on the matter distribution when changing the effective speed of sound. In fact, the most relevant effects of a varying effective speed of sound are clearly manifested in the DE sector.

6.2.2 DE perturbations

Figure 6.3 shows the evolution of the matter density contrast of DE for different models and ranges of c^2_{sd}. We remind that due to the phantom nature of DE models, the adiabatic condition imposed at the early Universe implies that the DE perturbations are negative [105, 106].

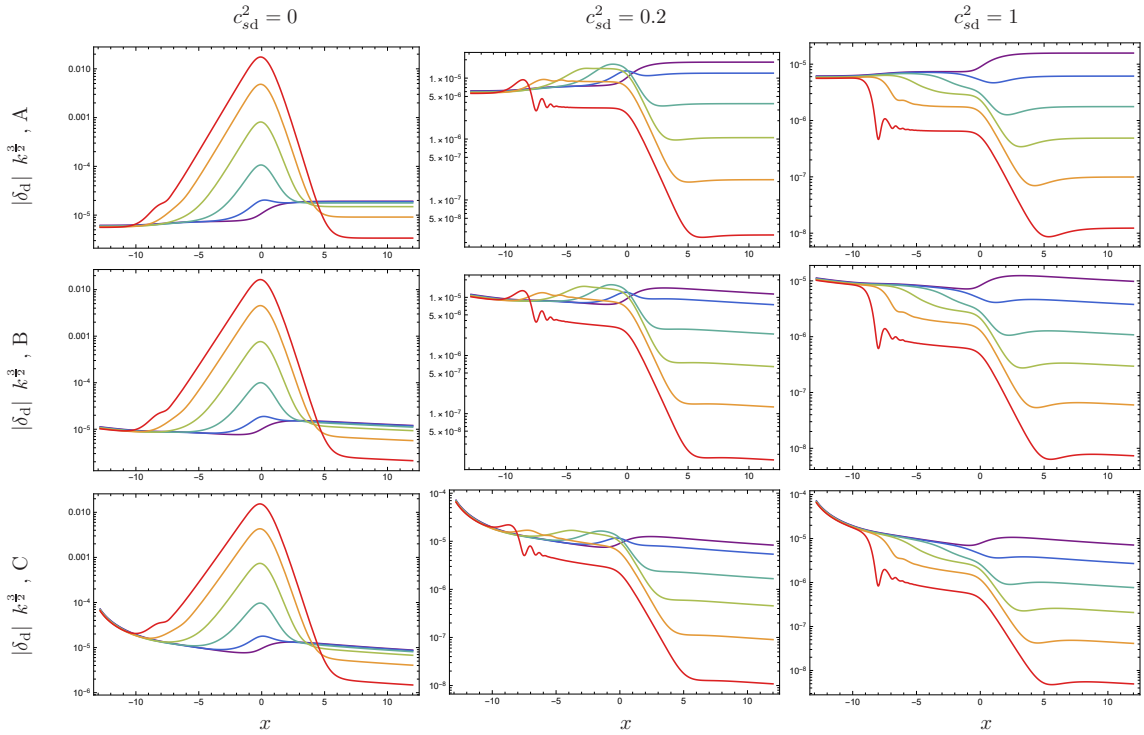

Figure 6.3: This figure shows the evolution of DE density contrast for different models and different values of c^2_{sd}. The panels of the first, second and third row correspond with the model A, B and C, respectively. The panels of the first, second and third columns correspond, respectively, to the values of the squared speed of sound $c^2_{sd} = 0$, $c^2_{sd} = 0.2$ and $c^2_{sd} = 1$. The plot is drawn as a function of $x = \ln(a)$ which goes from well inside the radiation dominated epoch, $x^\star = -12.84$, to the far future, $x = 12$. Each colour corresponds to a particular value of the wave-number k: $k_1 = 3.33\times10^{-4}$h Mpc^{-1} (purple), $k_2 = 1.04\times10^{-4}$h Mpc^{-1} (dark blue), $k_3 = 3.26\times10^{-3}$h Mpc^{-1} (light blue), $k_4 = 1.02\times10^{-2}$h Mpc^{-1} (green), $k_5 = 3.19\times10^{-2}$h Mpc^{-1} (orange) and $k_6 = 1.00\times10^{-1}$h Mpc^{-1} (red).

Figure 6.3 shows the evolution of DE density contrast for different models and values of c^2_{sd}. We realise that the effect of varying c^2_{sd} is minimal for values larger than 0.2, i.e., inside the interval $[0.2, 1]$. Hence, we just show the results for $c^2_{sd} = 0$, $c^2_{sd} = 0.2$ and $c^2_{sd} = 1$. As can be seen in the first column of Figure 6.3 (i.e. for a vanishing c^2_{sd} parameter), once the modes enters the horizon, the perturbations increase up to three orders of magnitude in the case of the largest mode and around two orders of magnitude for the medium size modes. All the growing modes reach a maximum at present time and decay during the DE domination era. That is; once the modes enters the horizon they grow, and then, when they exit the horizon, the perturbations decay evolving towards a negative constant[iv]. This is not the case of the smallest modes, we should bear in mind that such small modes have recently entered the horizon and are the first exiting it, so the smallest modes do not experience important deviations.

[iv]We remind that phantom DE perturbations are considered to be negative at the beginning of the numerical integration, as it is the case of the gravitational potential. On the other hand, standard matter perturbations are considered to be positive.

For a $c^2_{s\mathsf{d}} = 0.2$, the growth of DE perturbations is strongly suppressed in the matter domination era. During this epoch, the largest modes (k_5 and k_6) decay and reach a plateau while the medium sized modes (k_3 and k_4) experience a small growth. When DE starts dominating, the perturbations decrease up to three orders of magnitude for the largest modes and one order of magnitude for the medium sized modes. The smallest modes (k_1 and k_2) do not show to be significantly affected.

For a value of $c^2_{s\mathsf{d}} = 1$, the resulting plot is very similar to the one when $c^2_{s\mathsf{d}} = 0.2$. The main difference consists on the total suppression of the growing perturbations during the matter dominated epoch. Once again, the perturbations decay when the corresponding mode enters the horizon and evolve to a negative constant after exiting the horizon.

In summary, DE perturbation are strongly affected near vanishing values of $c^2_{s\mathsf{d}}$ parameter and mostly, for large modes. On the contrary, small modes do not show significant deviations. We should bear in mind that due to the change of the acceleration of the Universe (from a negative to a positive acceleration stage) the smallest modes are the last entering the horizon and the first exiting it, therefore, such modes have not enough time to be significantly affected.

On the other hand, it is possible to find important deviations between the different models, mostly, in the early Universe where radiation dominates over the other components. We set the initial value of DE matter density contrast, $\delta^\star_{\mathsf{d}}$ (where the script * denotes the initial value) through the adiabatic conditions written in (2.37) [23]. Taking into account that we have used in all the models the same value of the current radiation fractional energy, $\Omega_{\mathrm{r}0}$, and that the current matter fractional energy is almost the same in the three paradigms analysed, $\Omega_{\mathsf{m}0} \simeq 0.3$, it is worthy to point out the next approximation relating the initial DE perturbations of the different models

$$\frac{\delta^\star_{\mathsf{d,A}}}{1+w^\star_{\mathsf{d,A}}} \simeq \frac{\delta^\star_{\mathsf{d,B}}}{1+w^\star_{\mathsf{d,B}}} \simeq \frac{\delta^\star_{\mathsf{d,C}}}{1+w^\star_{\mathsf{d,C}}}. \tag{6.1}$$

Given the model parameters used in this chapter [107], the EoS parameters at the beginning (deep inside the radiation era) read

$$w^\star_{\mathsf{d,A}} = -1.027, \qquad w^\star_{\mathsf{d,B}} = -1.050, \qquad w^\star_{\mathsf{d,C}} = -1.320. \tag{6.2}$$

Therefore, the relation of the initial DE perturbation between the different models is roughly

$$12\delta^\star_{\mathsf{d,A}} \simeq \tfrac{13}{2}\delta^\star_{\mathsf{d,B}} \simeq \delta^\star_{\mathsf{d,C}}. \tag{6.3}$$

As can be seen the larger is the deviation from -1 of the initial EoS parameter, the larger is the initial DE density contrast. This explains the large initial amplitude for model C. Similarly, in the case of model B it can be observed a weak decay, while in model A, on the contrary, it is almost constant. Despite the large deviation given by these DE models in the early Universe, the amplitudes are strongly suppressed during the late-radiation dominated epoch and matter domination era, in such a way that different models predict very similar results at present time, and therefore, no significant deviations should be expected at a future cosmic time.

6.2.3 Evolution of the gravitational potential

Aside from DE perturbations, we found some deviations on the evolution of the gravitational potential. We remind that in our phantom models the gravitational potential evolves asymptotically to a positive constant, which is not the case of a ΛCDM or standard DE models, where the gravitational potential evolves towards a vanishing or a negative constant [106]. Since no relevant differences are observed for the different models, we just present the results corresponding to model A. The left panel of figure 6.4 shows the gravitational potential evolution for a vanishing effective speed of sound parameter. As can be seen, at a particular scale factor the gravitational potential flips the sign. We can notice that the gravitational potential evolution is almost unaffected by changing $c^2_{s\mathsf{d}}$ from the early time till present. However, in the far future some differences merge.

The left panel of figure 6.4 shows the evolution of the gravitational potential, Ψ, divided by its initial value, $\Psi_\star$ for the six relevant modes previously chosen. As can be seen, the gravitational potential almost vanishes for the largest modes, while it evolves to a positive constant for small modes. We remind once again that the gravitational potential is negative at the beginning of the computations, which confers the attractive nature of gravity. Therefore, a positive sign on the gravitational potentials is understood as a repulsive effect.

The right panel of figure 6.4 shows the asymptotic value of the gravitational potential divide by the initial value, $\Psi_\star$. The plot is done to highlight how such a constant is affected by the different values of the modes and $c^2_{s\mathsf{d}}$ parameter. As can be seen, for large modes the gravitational potential vanishes with independence of the chosen $c^2_{s\mathsf{d}}$ parameter, while for the smallest modes such a constant is set to be around -0.065. Bear in mind that the initial value of the gravitational potential is negative while asymptotically it approximates to the constant Ψ_{fin}, which is a positive value.

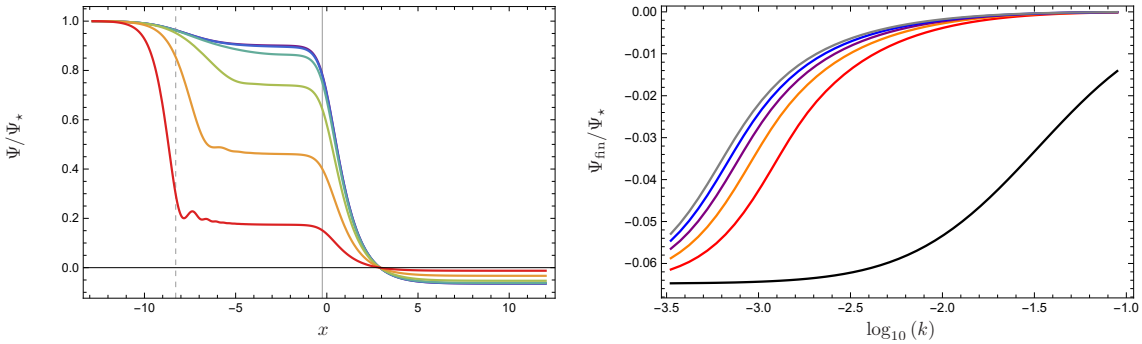

Figure 6.4: The left panel of the above figure presents the evolution of the gravitational potential divided by its initial value, $\Psi^\star$. These results corresponds to model A and choosing a vanishing effective speed of sound $c^2_{s\mathsf{d}} = 0$. The vertical dashed line corresponds to radiation-matter equality, $x \sim -8.24$, while the solid gray vertical line denotes the matter-DE equality, $x \sim -0.27$. The range and the numerical value of the modes for different colours are the same as those used in figure 6.3. The right panel shows the asymptotic value of the gravitational potential in terms of $\log(k)$ for five different values of the effective speed of sound parameter: $c^2_{s\mathsf{d}} = 0$ (black), $c^2_{s\mathsf{d}} = 0.2$ (red), $c^2_{s\mathsf{d}} = 0.4$ (orange), $c^2_{s\mathsf{d}} = 0.6$ (purple), $c^2_{s\mathsf{d}} = 0.8$ (blue) and $c^2_{s\mathsf{d}} = 1$ (gray).

We find interesting to focus on the evolution of the gravitational potential in the far future, mainly, where it flips its sign. For instance, figure 6.5 shows the evolution of the gravitational potential from the present time till the distant future. As can be seen, for a vanishing effective

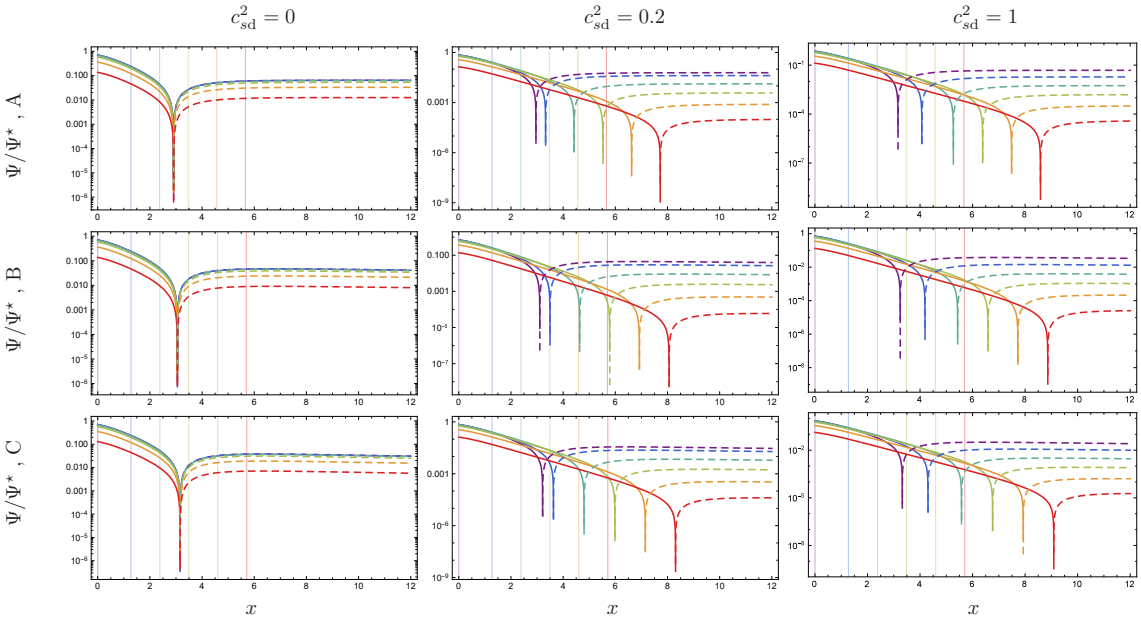

Figure 6.5: This figure presents the evolution of the gravitational potential, Ψ, with respect to its initial value, $\Psi^\star$, in a logarithmic scale and from the present to the far future. The solid lines represent the positive values while the dashed lines represent negative values. We apply the same criteria as the ones used in figure 6.3 to represent the different modes. The coloured vertical lines represent the moment of horizon exit for the corresponding mode.

speed of sound parameter the gravitational potential flip of sign occurs, for all the modes, at the same time ($x \sim 3$). In addition, such flip occurs before some of the modes have exited the horizon. This is not the case of a non-vanishing c^2_{sd} parameter (second and third column of figure 6.5, for $c^2_{sd} = 0.2$ and $c^2_{sd} = 1$, respectively). As can be seen, the smallest modes switch the sign earlier than the largest modes do, however, all the relevant modes have exited the horizon when those flips occur. In addition, we found that that the more abrupt is the cosmic event induced by the model, the sooner occurs the sign flip. This difference is more pronounced the larger are the k modes and c^2_{sd} values.

With the aim to better understand the asymptotic evolution of the metric perturbation, we solve the second order differential equation for the gravitational potential. By incorporating the decomposition of the pressure[v] in (2.34) we get

$$\Psi_{xx} + \frac{1}{2}\left[5 - 3w + 6c^2_{ad}\right]\Psi_x + \left[3\left(c^2_{ad} - w\right) + \frac{c^2_{sd}k^2}{\mathcal{H}^2}\right]\Psi = 0 \tag{6.4}$$

Let us consider a constant EoS parameter where [vi] $c^2_{ad} = w_d$. Therefore, in a phantom DE dominated Universe the Eq (6.4) can be approximated as [vii]

$$\Psi_{xx} + \frac{1}{2}\left(5 + 3w_d\right)\Psi_x + \left(\frac{c^2_{sd}k^2}{\Omega_{d0}k_0^2}\right)e^{(3w_d+1)x}\,\Psi = 0, \tag{6.5}$$

[v] see B.5) for detailed calculations on decomposing the DE pressure in its adiabatic and non-adiabatic contributions.

[vi] The differential equations for models B and C are not the same. However, after solving by numerical analysis these cases, we have not found significant deviations

[vii] In the case of the models B and C, this assumption is not correct since the differential equation (6.4) is different. However, we do not observe significant changes between the results given by the different models. So we focus on model A since its differential equation becomes analytically solvable.

whose solutions are given by

$$\Psi_{\left[c_{s\mathsf{d}}^2=0\right]} = C_1 + \frac{C_2}{\beta} e^{-\beta x}, \tag{6.6}$$

$$\Psi_{\left[c_{s\mathsf{d}}^2\neq 0\right]} = e^{-\frac{\beta}{2}x}\left\{D_1 J_\nu\left[A\left(k\right)e^{-\gamma x}\right] - D_2 Y_\nu\left[A\left(k\right)e^{-\gamma x}\right]\right\}, \tag{6.7}$$

$$\sim \frac{D_1}{\Gamma\left(\nu+1\right)}\left[\frac{A\left(k\right)}{2}\right]^{\nu} + \frac{D_2\Gamma\left(-\nu\right)}{\pi}\left[\frac{A\left(k\right)}{2}\right]^{-\nu} e^{-\beta x} \qquad \text{for } 0 \ll x, \tag{6.8}$$

where J_ν and Y_ν are the first kind Bessel functions with order ν, Γ is the Gamma function, while C_1, C_2, D_1 and D_2 are integration constants. The remaining parameters are defined as

$$\beta \equiv \frac{1}{2}\left(5+3w_{\mathsf{d}}\right), \qquad \gamma \equiv -\frac{1}{2}\left(1+3w_{\mathsf{d}}\right), \qquad \nu \equiv -\frac{\beta}{2\gamma}, \qquad A\left(k\right) \equiv \frac{1}{\gamma}\sqrt{\frac{c_{s\mathsf{d}}^2}{\Omega_{\mathsf{d}0}}}\frac{k}{k_0} \tag{6.9}$$

Since Ψ is linear, a particular solution multiplied by a constant factor is still a solution. Therefore, the total result can be written as

$$\Psi_{\mathsf{tot}}\left(x\right) = \Psi\left(x\right)F\left(k, c_{s\mathsf{d}}\right), \tag{6.10}$$

where $F\left(k, c_{s\mathsf{d}}\right)$ can be fixed (with an appropriate choice for C_1, and D_1) by analysing the asymptotic behaviour of the gravitational potential shown on the right panel plot of figure 6.4.

As can be seen, the asymptotic behaviour for large scale factors given in [viii] Eq (6.8), coincides with the solution for a vanishing $c_{s\mathsf{d}}^2$, Eq (6.6). However, instead of having just the constants terms C_1, and C_2, the solutions for non-vanishing $c_{s\mathsf{d}}^2 \neq 0$ parameter keep some information of the modes through the function $A(k)$ and modulated by the constants D_1, and D_2. Note that the dominant solution for $x \to \infty$ is constant as long as the coefficient β is positive, i.e. $-5/3 < w_{\mathsf{d}}$ which is indeed our case.

Finally, in order to obtain the point where the gravitational potential flip of sign occurs, we just solve $\Psi = 0$ for the couple of equations (6.6) and (6.7). Therefore, we get

$$x_{\mathsf{crit}} = -\frac{1}{\beta}\ln\left[-\alpha_1\beta\right], \tag{6.11}$$

$$x_{\mathsf{flip}} = -\frac{1}{\beta}\ln\left[\alpha_2\sin\left(\pi\nu\right)\right] + \frac{1}{\gamma}\ln\left[\frac{1}{2}\sqrt{\frac{c_{s\mathsf{d}}^2}{\Omega_{\mathsf{d}0}}}\right] + \frac{1}{\gamma}\ln\left[\frac{k}{k_0}\right]. \tag{6.12}$$

where we have defined a proportionality between the integration constants, i.e. $C_1/C_2 \equiv \alpha_1$ and $D_1/D_2 \equiv \alpha_2$. Given that $C_1, D_1 < 0$ and $0 < C_2, D_2$, α_1 and α_2 are negative constants.

On the one hand, x_{crit} is the lower value for which the gravitational potential can switch its sign and corresponds to a vanishing effective speed of sound parameter. Bear in mind that the differential equation (6.5) remains invariant by choosing different k and $c_{s\mathsf{d}}^2$ as long as the product $k^2c_{s\mathsf{d}}^2$ is fixed. Therefore, the solution for the limit $k \to 0$ corresponds to the solution for a vanishing $c_{s\mathsf{d}}^2$. On the other hand, for non-vanishing values of the product $k^2c_{s\mathsf{d}}^2$, the moment at which the gravitational potential flips its sign is given by (6.12) (which is valid as long as

[viii] Notice that the coefficient γ is positive, therefore, the argument of Bessel function vanishes when $x \to \infty$. We have obtained the expression for small arguments making use of (9.1.7) and (9.1.9) of reference [307])

$x_{\text{crit}} < x_{\text{flip}}$).

Therefore, we could define a second horizon whose size is the distance where the gravitational potential becomes positive. In addition, we notice that such a second horizon changes with time as fast as the true horizon does, i.e. $\ln(k/k_0) \sim \gamma x$. So this could be understood as two horizons, the true one; i.e. that enclose the observable Universe, and a second one; i.e. where the gravitational potential becomes positive, keeping the relative distance as constant at the far future.

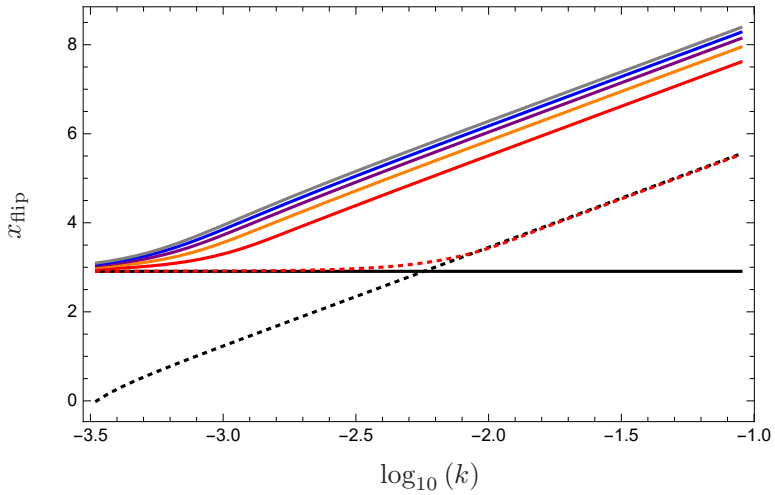

Figure 6.6: This figure shows the moment where the gravitational potential switches its sign, x_{flip}, in terms of $\log_{10}(k)$. Each curve corresponds to a given value of the speed of sound parameter; $c^2_{s\text{d}} = 0$ (solid black), $c^2_{s\text{d}} = 0.2$ (red), $c^2_{s\text{d}} = 0.4$ (orange), $c^2_{s\text{d}} = 0.6$ (purple),$c^2_{s\text{d}} = 0.8$ (blue) and $c^2_{s\text{d}} = 1$ (gray). The red dashed curve corresponds to $c^2_{s\text{d}} = 2.09 \times 10^{-3}$ while the black-dotted line represent the value of x where modes exit the horizon.

Figure 6.6 shows a plot of x_{flip} vs $\log_{10}(k)$. Since no relevant differences are found between models, we again only present the result given for the model A. We should keep in mind that the differential equation that lead to the analytical solution will be different instead we choose model B or C. However, at a perturbation level all the models give similar numerical solutions.

As it is shown in Figure 6.6, for a vanishing $c^2_{s\text{d}}$ parameter (solid black line) the flip of sign occurs at the same time for all the modes. The plots given by non-vanishing $c^2_{s\text{d}}$ parameters (coloured solid lines) becomes parallel, at large modes, with respect to the horizon exiting line (black dotted line). This means that there is an upper bound on $c^2_{s\text{d}}$ that will ensure sign-flipped modes inside the horizon, while values larger than such an upper bound would stand beyond the observable Universe. We have estimated such an upper bound roughly to be the order of $c^2_{s\text{d}} \lesssim 2 \times 10^{-3}$ (represented by the red dotted curve).

6.3 Conclusions

In this work, we have analysed the cosmological perturbations of three genuine phantom DE models with a varying effective speed of sound parameter. These models, named in the present thesis as model A, B and C, induce a particular future event known as BR, LR and LS, respectively. In these future events the Universe reach a scenario where all the bound structures are ripped

apart. We have addressed the computation of the linear cosmological perturbations following the method of decomposing the DE pressure perturbation in its adiabatic and non adiabatic contributions [16, 101], which leaves a dynamical set of equations free of instabilities. In this way, the effective speed of sound parameter of DE, $c^2_{s\mathsf{d}}$, is regarded as a free parameter.

We have considered a Universe filled with radiation, matter and DE, where the latter is described by the aforementioned models. We have computed the perturbations since the radiation dominated epoch, ($a_{\mathsf{ini}} \sim 2.6 \times 10^{-6}$), till a far future ($a_{\mathsf{fin}} \sim 1.6 \times 10^{5}$), where the DE completely dominates. On the one hand, the model parameters where fixed by using the observational constraints obtained in [107]. On the other hand, the physical values as the initial conditions for a single field inflation, spectral amplitude and spectral index were fixed using Planck data [18]. Then, we obtain the predicted current matter power spectrum and evolution of $f\sigma_8$ growth rate. Finally, we study the effect of changing $c^2_{s\mathsf{d}}$ from 0 to 1.

We find that different values of the $c^2_{s\mathsf{d}}$ parameter does not affect significantly the matter perturbations. Consequently, the matter power spectrum and $f\sigma_8$ evolution do not show any relevant footprint. However, we have found interesting footprints in the DE density contrast when changing $c^2_{s\mathsf{d}}$. Those changes are amplified when $c^2_{s\mathsf{d}}$ is set very small. Despite the different three models are almost indistinguishable at present, there are significant deviations in the early Universe, which strongly depend on the initial EoS parameter of DE due to the adiabatic conditions imposed at the beginning (see (6.1) and (6.3)).

We conclude that the possibility of a vanishing speed of sound parameter does not seem to be favoured by two reasons: (i) the DE density contrast grows too much during the matter dominated epoch, and this would lead to a DE clustering, something that has not been detected so far, (ii) the gravitational potential sign flip occurs at the same time for all the modes, such unexpected and sudden event does not seem physical. This is not the case of a non-vanishing effective speed of sound parameter, where the Bardeen potential becomes progressively negative from very large distances to smaller ones. Such distances decrease with time as fast as the horizon does. Therefore, there is a particular value of $c^2_{s\mathsf{d}}$ where the gravitational potential switches the sign precisely at the horizon. We have found that this value is close to $c^2_{s\mathsf{d}} \sim 2 \times 10^{-3}$. We stress that the effect of a gravitational potential sign flip occurs due to the negative sign of DE perturbations.

Despite the fact that the DE perturbations have not been observed so far, we strongly believe that they hide revealing footprints that could allow us to distinguish different DE models if ever detected. We hope that upcoming missions such as Euclid will provide crucial information about the dark sector of the Universe, granting us a useful tool to favouring or discriminating among DE models as those addressed in the present thesis.

7

WDW equation in QC

If you wish to make an apple pie from scratch, you must first invent the Universe
– Carl Sagan

7.1 introduction

The WDW equation can be introduced in the canonical quantisation of gravity in the so called quantum geometrodynamics approach. From the Einstein–Hilbert gravitational action functional, the Einstein (Euler–Lagrange) equations can be obtained and used to deduce the Hamiltonian equations describing the dynamical evolution. It turns out that this is a constrained dynamical system, in which the constraints correspond to the invariance of the model with respect to space-time diffeomorphisms. There are two types of constraints: the momenta constraints (space diffeomorphisms) and the Hamiltonian constraint (time diffeomorphisms) [151, 152]. The canonical formulation of general relativity leads to four local constraints. If quantisation is performed in the Dirac sense, they turn into the WDW equation and the quantum diffeomorphism constraints [151]. Therefore, the WDW equation can be understood as the analogous to the Schrödinger equation in QM where the Universe is taken as a whole; i.e. as the full system to be analysed [151, 152]. In order to deduce the WDW equation, the first step is to obtain the classical Hamiltonian from the usual Hilbert-Einstein action (in our case we restrict to a FLRW metric). Then the quantum operators are introduced according to the canonical quantisation procedure leading to the WDW equation [151, 152]. The gravitational action depends upon the chosen metric, in particular for a FLRW space-time, the Hilbert-Einstein action is given by

$$S_{HE} = \frac{1}{16\pi G}\left[\int d^4x\sqrt{-g}\,(R-2\Lambda) - 2\int d^3x\sqrt{-h}K\right]. \tag{7.1}$$

The second term on the right hand side of the previous equation contains the extrinsic curvature K and is a compulsory boundary term to have a well-defined variational problem. The extrinsic curvature and its trace read [151, 152]

$$K_{ab} = \frac{1}{2N}\frac{\partial h_{ab}}{\partial t}, \tag{7.2}$$

$$K = K_{ab}h^{ab}, \tag{7.3}$$

where $N(t)$ is the lapse function and h_{ab} is the induced spatial metric [151, 152]

$$h_{ab} = a^2(t)\left(\frac{dr^2}{1-kr^2} + r^2d\theta^2 + r^2\sin^2\theta d\varphi\right). \tag{7.4}$$

The Lambda function introduced in the action corresponds to $\Lambda = 8\pi G\rho$; i.e. the matter Lagrangian of the Universe is described by $\Lambda(a)$. From the Hilbert-Einstein action, we obtain the

following Lagrangian density (after performing an integral)

$$L = N\left[\frac{3\pi}{4G}\left(-\frac{a\dot{a}^2}{N^2} + ka - \Lambda(a)\frac{a^3}{3}\right)\right]. \tag{7.5}$$

Defining the momentum p_a as

$$p_a \equiv \frac{\partial L}{\partial \dot{a}} = -\frac{3\pi}{2G}\left(\frac{a\dot{a}}{N}\right), \tag{7.6}$$

we get the Hamiltonian corresponding to the action (7.1)

$$\mathcal{H} = N\left[-\frac{G}{3\pi}\frac{p_a^2}{a} + \frac{\pi}{4G}\Lambda\left(a\right)a^3\right], \tag{7.7}$$

where p_a is the canonical momentum corresponding to the scale factor. Notice that the canonical momentum associated with the lapse function does not appear because it corresponds to a primary constraint [152]. Therefore, the scale factor is the only variable in this particular cosmological problem. The curvature term is reabsorbed in the $\Lambda(a)$ function which can be understood as an effective potential. Depending on the features of the model inducing the abrupt event, such a potential is described, in general, by a growing function of the scale factor, for example: by a power law, by an exponential function or by a product of both.

A perfect fluid description, where the scale factor is the single degree of freedom, shows interesting features and have been analised in the present thesis, but it turns out that it describes a simple one dimensional problem where the roles of the scale factor and time are not very clear. By mapping the fluid to a scalar field adds an additional variable, in consequence, the wave function can be spread over a larger number of variable while the scale factor could be understood as playing the role of time. Choosing, in addition, a perfect fluid and a set of minimally coupled scalar fields, the total action consisting of the Einstein-Hilbert action and the matter action reduces to [42, 44, 51, 70, 151, 152]

$$\mathsf{S} = \int \mathcal{L}\ dt, \qquad \mathcal{L} = \frac{\mathcal{V}_0}{2\pi}\left[-\frac{3\pi}{4GN}\dot{a}^2 a - 2\pi^2 N a^3\left(\rho - \frac{1}{2N^2}\sum_i l_i \dot{\phi_i}^2 + V\left(\phi_1, ..\phi_n\right)\right)\right], \tag{7.8}$$

The energy density ρ could represents a mixture of those perfect fluids while ϕ_i represents the scalar field where $l = 1, (-1)$ for a standard (phantom) scalar field. The constant $\mathcal{V}_0$ stands for the volume of the three-dimensional spatial sections for $a = 1$. As we are dealing with spatially flat sections, it is implicitly assumed that we either choose a torus compactification with the correct volume or we leave the volume open, that is, choose a reference volume $\mathcal{V}_0$ [i]. We can work out both options without loss of generality. Bear in mind that this choice leads only to a constant factor multiplying the Lagrangian and, therefore, will not affect the results presented below, after all, the Hamiltonian is obtained from a Legendre transformation and the classical constraint $\mathcal{H} = 0$ becomes after quantisation [151, 152]

$$\hat{\mathcal{H}}\Psi = 0. \tag{7.9}$$

This equation enables an appropriate quantum approach where the wave function of the Uni-

[i] For non-vanishing spatial curvature, the total action can be written as [151, 152], $S = \frac{3\pi}{4G}\int\left[-\dot{a}^2 a + ka\right]dt - \pi^2\int a^3\left[\dot{\phi}^2 + 2V(\phi)\right]dt$, where the lapse function is taken as unity, $N = 1$.

verse Ψ depends on the degrees of freedom used to describe the physical system under study, that is, the configuration space. We will address quantisation by means of: (i) a single degree of freedom corresponding to the scale factor, where the matter content is given by a perfect fluid (with a known EoS corresponding to the chosen model (see chapter 2), and (ii) two degrees of freedom corresponding to the scale factor and a scalar field (which portrays the matter content).

In the first approach, the scale factor is the only independent variable. This is certainly a very simple model, but it is interesting enough to study the behavior of the wave function near the singularities. In the absence of a full quantum gravity framework it is, of course, an open question what the correct criterion of singularity avoidance is. A useful heuristic criterion is the one introduced by DeWitt in 1967 [176] ; it states that the wave function should vanish at the place of the classical singularity. This criterion was successfully applied to a variety of cosmological models, see [151, 152, 308] and [44, 48, 63, 70, 309].

In the second approach, an approximation describing the matter content by a scalar field yields a suitable framework with an additional degree of freedom. We move from the classical trajectory, $\phi = \phi(a)$, to the corresponding quantum analog where the wave function is defined over the configuration space (a, ϕ). In this way, the quantum nature arises and gains significance close to the singularity, once the quantum effects become important. Here, again, the DW criterion is useful as a heuristic device.

7.2 Quantisation procedures: Factor ordering

The passage to the quantum description is done by promoting all the degrees of freedom and canonically conjugate momenta to operators acting on some Hilbert space. The usual approach is to consider the so called minisuperspace, the space of all 3-dimensional totally symmetric (FLRW) metrics and all matter-energy configurations. It is analogous to the configuration space in the classical analysis. The wave function of the Universe (in the Schrödinger representation) will live on this space and each point on it represents a FLRW Universe with a certain value of the scale factor and certain well defined values for all the matter-energy degrees of freedom. The WDW equation governs precisely the distribution of the wave function in this (quantum) configuration space. It corresponds to the Hamiltonian constraint (time diffeomorphism invariance) previously mentioned, where the Hamiltonian operator acting on the wave function gives zero. In fact, the classical Hamiltonian constraint $\mathcal{H} = 0$ corresponds to the Friedmann equation. Therefore, time is absent in this quantum description and the wave function in the Born interpretation is expected to provide a stationary probability (amplitude) distribution in minisuperspace [151]. As mentioned in the introduction, in the canonical quantisation procedure we have to take into account that there are different "factor-orderings" in obtaining the WDW equation.

A reasonable model is one in which the decoherence of the general superposition of quantum states is absent in those regions of minisuperspace corresponding to a classically behaving Universe [151]. This requirement is analogous to the correspondence principle in usual QM where the classical regime is re-obtained for large quantum numbers. Here, coherence presupposes the possibility for confined wave packet solutions, effectively reproducing the classical tra-

jectory in configuration space. However, in the vicinity of classical singularities, where the quantum cosmology can have important non-classical effects, decoherence might be present and the quantum results can differ from the classical description [42]. Therefore, for any FLRW model with singularities (or abrupt events such as the LR and the LS), one should check if the distribution of the wave function in minisuperspace is such that these (classical) cosmic events can be effectively avoided with the quantum approach. That is, it is necessary to check the DW boundary condition verifying whether among the obtained solutions exists a wave function which effectively vanishes at the vicinity of the abrupt event. Unfortunately, we have not yet a complete quantum theory and there is some inconsistency as the factor ordering choice, i.e. different factor orderings lead to different wave function of the Universe. Therefore, every result is taken rigorously as a hint rather than a proof of singularity avoidance.

One of the factor ordering chosen in the present work is the corresponding to the covariant generalisation of the LB operator. This method has the attribute of waranting a kinetic term invariant under phase-space transformations as it happens with the Schrödinger equation in QM [151]. The corresponding WDW equation $\hat{\mathcal{H}}\psi(\alpha,\phi)=0$, for flat spatial geometry is [42]

$$\frac{\hbar^2}{2}\left[\frac{\kappa^2}{6}\frac{\partial^2}{\partial\alpha^2}+\frac{\partial^2}{\partial\phi^2}\right]\psi(\alpha,\phi)+a_0^6e^{6\alpha}V(\phi)\psi(\alpha,\phi)=0, \tag{7.10}$$

where $\alpha\equiv\ln(a/a_0)$, $\kappa^2\equiv 8\pi G$ and $V(\phi)$ represents the potential of the scalar field. Bear in mind that the above quantisation in terms of LB operator corresponds to the minusuperspace of variables considering both metric and the scalar field. In the case of a single degree of freedom the term p_a^2/a in the classical Hamiltonian given in (7.7) becomes in the quantum version something proportional to $\partial^2/\partial u^2$, where $u\equiv(3/2)a^{3/2}$.

On the other hand, some others factors orderings are considered in the present work. Bear in mind that the classical Hamiltonian results in a vanishing outcome, so it is always possible to multiply by an arbitrary function[ii]. In general, this function could depend on both variable, the scale factor and the scalar field. For simplicity, we assume that such a function depends only on the scale factor. The goal is to see that our results do not depend on the factor ordering.

Then, once the factor ordering is selected, it comes the diagonalisation of the operator. This step is performed by a change of the gravitational variable, usually the scale factor or a function of it. This becomes a differential equation in a double derivative over the new gravitational variable, as well as, over the scalar field if it is present, and plus an effective potential. The latter is a product of separated functions depending on the gravitational variable and the scalar field for those cases where two variables are involved. The resulting differential equation could be difficult to solve, therefore, we apply some methods as the well known BO approximation (see C.3 in the appendix for a detailed analysis).

When solving the WDW equation some comments are in order. The quantum description based on the WDW equation will be limited to a subset of the minisuperspace corresponding to DE dominance, ($\rho_{\rm tot}\approx\rho_{\rm de}=\rho$ in (2.2)). In the second place, α and ϕ are not independent classically. Naively, this could seem to imply that to check the fulfilment of the DW criterium we

[ii]Of course, as long as such a function is not divided by zero, which would imply an indetermination to be solved.

should search for solutions $\psi(\alpha,\phi)$ that decay along that line $\phi=\phi^{\rm class}(\alpha)$, $\psi(\alpha,\phi^{\rm class}(\alpha))\to 0$, when the scale factor goes to infinity. Nevertheless, when the energy density approaches a certain quantum gravity threshold, the quantum effects should become important breaking the classical constraint $\phi=\phi^{\rm class}(\alpha)$. Indeed, although the potential is classically obtained, α and ϕ are independent in the quantum description. Therefore, we must investigate the evolution of the wave function $\psi(\alpha,\phi)$ for $\alpha\to\infty$ and arbitrary values of ϕ. Finally, for a compatible link between the quantum solutions and the classical behaviour, far from the quantum effects dominance, the wave function should be described by wave-packets centered in each point of the classical trajectory $\phi=\phi^{class}(\alpha)$ [151]. We will not consider this issue in the present work.

7.3 WDW equation in EiBI theories

The WDW equation derived in the previous section comes from the fundamental action which consists on the Hilbert-Einstein action minimally coupled to a matter field. Then, we move from the classical to the quantum real by promoting the Hamiltonian constraints and the conjugate momenta as operators acting over the wave function. Therefore, this step is always doable as far as it exists a physically motivated Hamiltonian. So, in order to analyse the possible factor orderings that changes the resulting wave function, we go beyond and ask *what if the action that leads to the classical Hamiltonian is different?* One of the most appealing suggestion is the EiBI modified gravity. On the one hand, it has shown to be effective to address the issue of cosmological singularities. The merging of an auxiliary (or equivalent) space-time metric "absorbs" the physical singularity leading to a harmless scenario. On the other hand, it is interesting from the application of the WDW equation, since it could provide an original Hamiltonian giving rise to different mechanics deviated from those addressed in the previous sections, where our starting point to obtain the WDW equation lied on the usual Hilbert-Einstein action.

The EiBI theory is inspired on the Eddington's functional [121], where the connection is considered as the main field. We will focus on the EiBI action proposed in [122]

$$\mathcal{S}_{EiBI}=\frac{2}{\kappa}\int d^4x\Big[\sqrt{|g_{\mu\nu}+\kappa R_{\mu\nu}(\Gamma)|}-\lambda\sqrt{-g}\Big]+S_m(g), \tag{7.11}$$

where $|g_{\mu\nu}+\kappa R_{\mu\nu}|$ is the determinant of the tensor $g_{\mu\nu}+\kappa R_{\mu\nu}$. From now on, we assume $8\pi G=c=1$.

The theory is assumed to contain only the symmetric part of the Ricci tensor $R_{(\mu\nu)}$ and the curvature is constructed by the affine connection Γ, which is independent of $g_{\mu\nu}$. Within this setup, the theory respects the projective gauge symmetry and the torsion field, if it exists, can be removed by simply choosing a gauge. On the other hand, the dimensionless constant λ quantifies the effective cosmological constant at the low curvature limit. Moreover, on the action (7.11) $|g_{\mu\nu}+\kappa R_{(\mu\nu)}|$ stands for the absolute value of the determinant of the rank two tensor $g_{\mu\nu}+\kappa R_{(\mu\nu)}$. Finally, κ characterises the theory and has inverse dimensions to that of a cosmological constant. In addition, this parameter is assumed to be positive to avoid the imaginary effective sound speed instabilities usually associated with a negative[iii] κ [142].

[iii] However, within the quantum study we will perform later on in the chapter 13 both cases, $<\kappa$ and $\kappa<0$, will be considered.

The EiBI theory is equivalent to GR in vacuum, while it could deviate from GR when matter fields are included. In the early Universe, the theory has been shown to be free of the big bang singularity. Furthermore, it should be stressed that the equations of motion of the theory contain derivatives of the metric up to only second order because of the Palatini structure of the theory. To be more precise, one can define an auxiliary metric $\lambda q_{\mu\nu} = g_{\mu\nu} + \kappa R_{(\mu\nu)}$ such that $q_{\mu\nu}$ is compatible with the connection. One of the two field equations relates algebraically the matter field with the two metrics, and the other equation corresponds to a second order differential equation of $q_{\mu\nu}$. It can be seen that when the curvature vanishes, the two metrics are identical up to a *constant* conformal rescaling, rendering the equivalence of the EiBI theory and GR in the zero curvature regime.

Considering a homogeneous and isotropic spacetime which can be described by the following metric ansatz:

$$ds_g^2 = -N(t)^2 dt^2 + a(t)^2 \delta_{ij} dx^i dx^j \,, \qquad ds_q^2 = -M(t)^2 dt^2 + b(t)^2 \delta_{ij} dx^i dx^j \,, \tag{7.12}$$

where $N(t)$ and $a(t)$ are the lapse function and the scale factor of the physical metric $g_{\mu\nu}$, while $M(t)$ and $b(t)$ are the lapse function and the scale factor of the auxiliary metric $q_{\mu\nu}$. In this metric ansatz, these four quantities can be expressed as functions of the cosmic time t and their evolutions in time are determined by the Euler-Lagrange equations of motion. The field equations are obtained by varying (7.11) with respect to $g_{\mu\nu}$ and the connection Γ. Therefore, in a flat, homogeneous and isotropic (FLRW) Universe filled with a perfect fluid. The Friedmann equations of the physical metric $g_{\mu\nu}$ and of the auxiliary metric compatible with Γ are [130]

$$\begin{aligned} \kappa H^2 &= \frac{8}{3}\Big[\bar{\rho} + 3\bar{p} - 2 + 2\sqrt{(1+\bar{\rho})(1-\bar{p})^3}\Big] \\ &\quad \times \frac{(1+\bar{\rho})(1-\bar{p})^2}{[(1-\bar{p})(4+\bar{\rho}-3\bar{p}) + 3\frac{d\bar{p}}{d\bar{\rho}}(1+\bar{\rho})(\bar{\rho}+\bar{p})]^2}, \end{aligned} \tag{7.13}$$

and

$$\kappa H_q^2 = \kappa\Big(\frac{1}{b}\frac{db}{d\tilde{t}}\Big)^2 = \frac{1}{3} + \frac{\bar{\rho} + 3\bar{p} - 2}{6\sqrt{(1+\bar{\rho})(1-\bar{p})^3}}, \tag{7.14}$$

where[iv] $\bar{\rho} \equiv \kappa\rho$ and $\bar{p} \equiv \kappa p$. On the above equations a and b are the scale factor of the physical and auxiliary metrics, respectively. $\tilde{t}$ is a rescaled time such that the auxiliary metric can be written in a FLRW form.

The deduction of the WDW equation of the EiBI model is based on the construction of a classical Hamiltonian that is promoted to a quantum operator. As shown in [203], this can be achieved more straightforwardly by considering an alternative action which is dynamically equivalent to

[iv] Notice that we are dealing with Palatini type of models which are also known as affine models. On these types of theories (c.f. the action (7.11)) there is a metric $g_{\mu\nu}$ and a connection Γ which does not correspond to the Christoffel symbols of the metric. However, it is always possible to define a metric compatible with that connection [310] and this is the metric that we are referring to as the auxiliary metric. The same applies to the action (7.15) where we denote the auxiliary metric as $q_{\mu\nu}$ and the physical metric $g_{\mu\nu}$. This is the standard and usual nomenclature in Palatini/affine theories.

the EiBI action (7.11):

$$\mathcal{S}_a = \lambda \int d^4x\sqrt{-q}\Big[R(q) - \frac{2\lambda}{\kappa} + \frac{1}{\kappa}\Big(q^{\alpha\beta}g_{\alpha\beta} - 2\sqrt{\frac{g}{q}}\Big)\Big] + S_m(g). \tag{7.15}$$

On the above action (7.15), the fundamental variables are $g_{\mu\nu}$ and the auxiliary metric $q_{\mu\nu}$. It can be proven that the equations of motion derived from the original action (7.11) can be obtained unambiguously by varying the action (7.15) with respect to $g_{\mu\nu}$ and $q_{\mu\nu}$. In [126] it has been shown that the field equations obtained by varying the action (7.15) with respect to $g_{\mu\nu}$ and the auxiliary metric $q_{\mu\nu}$ are the same to those derived from the action (7.11).

We will use this alternative action (7.15) to deduce the classical Hamiltonian and the corresponding WDW equation in the EiBI gravity. It turns out that the construction of the WDW equation is much more straightforward because of the absence of the square root structure of the curvature present in the original action (7.11). For the sake of later convenience, we use the following changes of variables

$$X \equiv \frac{N}{M}\,, \qquad Y \equiv \frac{a}{b}\,, \tag{7.16}$$

to replace N and a with X and Y, respectively. Using the alternative action (7.15) and assuming that the matter sector is described by a perfect fluid with energy density ρ and pressure p, the reduced Lagrangian associated with the action (7.15) can be written as

$$\mathcal{L} = \lambda M b^3\left[-\frac{6\dot{b}^2}{M^2b^2} - \frac{2\lambda}{\kappa} + \frac{1}{\kappa}\left(X^2 + 3Y^2 - 2XY^3\right)\right] - 2\rho\left[(bY)\right]Mb^3XY^3\,, \tag{7.17}$$

where ρ is a function of a where the relation $a = bY$ has been imposed, i.e., $\rho = \rho(bY)$. In the present work, the energy density will be fixed by the selected DE model. Note that for large scale factors DE dominates the dynamics of the Universe, in such a way that the Universe is considered to be filled by a single DE component neglecting the contribution of the matter content.

According to the definition of conjugate momenta, we have three primary constraints:

$$p_X = \frac{\partial\mathcal{L}}{\partial\dot{X}} \sim 0\,, \qquad p_Y = \frac{\partial\mathcal{L}}{\partial\dot{Y}} \sim 0\,, \qquad p_M = \frac{\partial\mathcal{L}}{\partial\dot{M}} \sim 0\,, \tag{7.18}$$

where $\sim$ denotes a weak equality, i.e., an equality on the constraint surface. The total Hamiltonian is defined as follows

$$\begin{aligned}\mathcal{H}_T &= M\left[-\frac{p_b^2}{24\lambda b} + \frac{2\lambda^2b^3}{\kappa} - \frac{\lambda}{\kappa}b^3X^2 - \frac{3\lambda}{\kappa}b^3Y^2 + \frac{2XY^3b^3}{\kappa}\left(\lambda + \kappa\rho\right)\right] \\ &\quad + \lambda_X p_X + \lambda_Y p_Y + \lambda_M p_M,\end{aligned} \tag{7.19}$$

where p_b is the conjugate momentum of the phase space variable b. In the last few terms, λ_X, λ_Y, and λ_M are Lagrange multipliers associated with each primary constraint. Note that the primary constraints are obtained directly from the definition of the conjugate momenta. These constraints should be satisfied throughout time and this would lead to the so called secondary constraints. To derive these secondary constraints requires the use of the equations of motion: $\dot{p}_M = [p_M, \mathcal{H}_T] \sim 0$, $\dot{p}_X = [p_X, \mathcal{H}_T] \sim 0$, and $\dot{p}_Y = [p_Y, \mathcal{H}_T] \sim 0$. We call these requirements con-

sistent conditions of the corresponding constraints and the consistent conditions of the primary constraints lead to the following secondary constraints [311, 312]:

$$C_X \equiv \lambda X - Y^3(\lambda + \kappa\rho) \sim 0, \tag{7.20}$$

$$C_Y \equiv 3\lambda - 3XY(\lambda + \kappa\rho) - XY^2 b\kappa\rho' \sim 0, \tag{7.21}$$

$$C_M \equiv \frac{p_b^2}{24\lambda b} - \frac{2\lambda^2 b^3}{\kappa} + \frac{\lambda}{\kappa}b^3X^2 + \frac{3\lambda}{\kappa}b^3Y^2 - \frac{2XY^3b^3}{\kappa}(\lambda + \kappa\rho) \sim 0. \tag{7.22}$$

The prime denotes the derivative with respect to $a = bY$. Furthermore, it can be shown that the total Hamiltonian is a constraint of the system:

$$\mathcal{H}_T = -MC_M + \lambda_X p_X + \lambda_Y p_Y + \lambda_M p_M \sim 0. \tag{7.23}$$

Because the Poisson brackets of the total Hamiltonian with all the constraints should vanish weakly by definition, $\mathcal{H}_T$ is a first class constraint and we will use it to construct the modified WDW equation.

This system has six independent constraints: p_X, p_Y, p_M, C_X, C_Y, and C_M. After calculating their Poisson brackets with each other, we find that except for p_M, which is a first class constraint, the other five constraints are second class [311, 312]. The existence of the first class constraint p_M implies a gauge degree of freedom in the system and one can add a gauge fixing condition into the system to make the constraint second class. An appropriate choice of the gauge fixing condition is $M =$ constant and after fixing the gauge, the conservation in time of this gauge fixing condition, i.e., $[M, \mathcal{H}_T] = 0$, implies $\lambda_M = 0$.

Within the EiBI framework, the scale factor plays the role of a parameter while the true variable corresponds to the auxiliary scale factor denoted by b. As done in the previous section, the content given by a perfect fluid can be mapped to a scalar field, in such a way that the system has a further degree of freedom. The resulting reduced Lagrangian constructed from the action, $S_a = v_0 \int dt\mathcal{L}$, can be rewritten as

$$\mathcal{L} = \lambda M b^3\Big[-\frac{6\dot{b}^2}{M^2b^2} - \frac{2\lambda}{\kappa} + \frac{1}{\kappa}\Big(\frac{N^2}{M^2} + 3\frac{a^2}{b^2} - 2\frac{Na^3}{Mb^3}\Big)\Big] + Na^3\Big(l\frac{\dot{\phi}^2}{N^2} - 2V(\phi)\Big), \tag{7.24}$$

where v_0 corresponds to the spatial volume after a proper compactification for spatially flat sections. On the above equation $l = \pm 1$ denotes the ordinary scalar field ($+1$) and phantom scalar field (-1), respectively. After applying the change of variables (7.16) in (7.11), the Lagrangian then becomes

$$\mathcal{L} = \lambda M b^3\Big[-\frac{6\dot{b}^2}{M^2b^2} - \frac{2\lambda}{\kappa} + \frac{1}{\kappa}(X^2 + 3Y^2 - 2XY^3)\Big] + MXb^3Y^3\Big(l\frac{\dot{\phi}^2}{M^2X^2} - 2V(\phi)\Big). \tag{7.25}$$

The conjugate momenta of this system are

$$p_b = -\tfrac{12\lambda b}{M}\dot{b}\,, \qquad p_\phi = \tfrac{2b^3Y^3}{MX}l\dot{\phi}\,, \tag{7.26}$$

$$p_X = 0\,, \quad p_Y = 0\,, \quad p_M = 0\,. \tag{7.27}$$

It can be seen that the variables $\dot{X}$, $\dot{Y}$, and $\dot{M}$ cannot be inverted to be functions of canonical variables and their conjugate momenta, so the system is a constrained system and it has the same three primary constraints as given in (7.18) [312]. Provided the existence of the primary

constraints, the corresponding Hamiltonian for a content described by a scalar field is defined as follows [312]

$$\begin{aligned}\mathcal{H}_T = \; & -\tfrac{M}{24\lambda b}p_b^2 + \tfrac{MX}{4b^3Y^3}lp_\phi^2 - \tfrac{\lambda M b^3}{\kappa}(X^2+3Y^2-2XY^3-2\lambda) \\ & +2MXb^3Y^3V(\phi) + \lambda_M p_M + \lambda_X p_X + \lambda_Y p_Y .\end{aligned} \tag{7.28}$$

Therefore, the secondary constraints when describing the content by scalar field read as follows [139]

$$C_X \equiv \frac{\lambda X}{Y^3} - \lambda - \kappa\Big(\frac{lp_\phi^2}{8b^6Y^6} + V(\phi)\Big) \sim 0\,, \tag{7.29}$$

$$C_Y \equiv \frac{\lambda}{XY} - \lambda + \kappa\Big(\frac{lp_\phi^2}{8b^6Y^6} - V(\phi)\Big) \sim 0\,, \tag{7.30}$$

$$C_M \equiv \frac{p_b^2}{24\lambda b} - \frac{X}{4b^3Y^3}lp_\phi^2 + \frac{\lambda b^3}{\kappa}(X^2+3Y^2-2XY^3-2\lambda) - 2Xb^3Y^3V(\phi) \sim 0\,. \tag{7.31}$$

Moreover, the consistent conditions of these secondary constraints do not generate new constraints anymore. Once again, we have six constraints in this system, where p_M is a first class constraint, i.e. its Poisson brackets with other constraints are zero weakly, while p_X, p_Y, C_X, C_Y and C_M are second class constraints because they have at least one non-vanishing Poisson bracket with the other constraints on shell. Therefore, mapping the perfect fluid into a scalar field does not change the underlying feature of the first and second class constraints and the Hamiltonian is within both descriptions a first class constraint since it can be written as a linear combination of the constraints as follows

$$\mathcal{H}_T = -MC_M + \lambda_M p_M + \lambda_X p_X + \lambda_Y p_Y, \tag{7.32}$$

and therefore, its Poisson brackets with all the constraints vanish weakly by definition. In the following subsection, we will use the Hamiltonian to write down the WDW equation, i.e., $\hat{\mathcal{H}}_T|\Psi\rangle = 0$.

7.3.1 Quantisation with Dirac brackets

The system that we are dealing with contains several second class constraints. According to [312], it was suggested that to quantise such a system, one needs to use the Dirac bracket, instead of the Poisson bracket, to define the commutation relations and promote the phase space functions to quantum operators. The Dirac bracket is basically constructed by calculating the Poisson brackets among all independent second class constraints of the system. The notion of *independent* second class constraints means that one cannot obtain any other first class constraints by taking linear combinations of these second class constraints. The independent second class constraints in our system (after choosing the gauge) are $\chi_i = \{M, p_M, p_X, p_Y, C_X, C_Y\}$. Note that the Hamiltonian (7.32) is a first class constraint and it can be written as a linear combination containing C_M. That is the reason why we have excluded C_M when defining χ_i.

The Dirac bracket of two phase space functions F and G is defined by [312]

$$[F,G]_D = [F,G] - [F,\chi_i]\Delta_{ij}[\chi_j,G], \tag{7.33}$$

We remind that the existence of the matrix Δ_{ij} is proven in Dirac's lecture [312] while Poisson

bracket is defined as

$$[F,G]=\frac{\partial F}{\partial q_i}\frac{\partial G}{\partial p_i}-\frac{\partial F}{\partial p_i}\frac{\partial G}{\partial q_i}, \tag{7.34}$$

where q_i are the variables and p_i their conjugate momenta and Δ_{ij} is a matrix satisfying

$$\Delta_{ij}[\chi_j,\chi_k]=\delta_{ik}, \tag{7.35}$$

where the repeating suffices denote the summation. According to [312], the second class constraints can be treated as zero operators after promoting them to quantum operators as long as the Dirac brackets are used to construct the commutation relations:

$$[\hat{F},\hat{G}]=i\hbar[F,G]_{D,\ (F=\hat{F},\,G=\hat{G})}. \tag{7.36}$$

This is due to the fact that the Dirac brackets of the constraints χ_i with any phase space function vanish strongly (they vanish without inserting any constraint). Considering a perfect fluid description, the Dirac brackets between the fundamental variables take the forms

$$\begin{aligned}
[b,p_b]_D &= [b,p_b]=1,\\
[b,X]_D &= 0,\\
[b,Y]_D &= 0,\\
[X,Y]_D &= 0,\\
[X,p_b]_D &= f_1(X,Y,b)=f_1(b),\\
[Y,p_b]_D &= f_2(X,Y,b)=f_2(b),
\end{aligned} \tag{7.37}$$

where f_1 and f_2 are two non-vanishing functions. Notice that f_1 and f_2 can be written as functions of b because it is legitimate to insert the constraints C_X and C_Y to replace X and Y with b when calculating the Dirac brackets. One of the important properties of the Dirac bracket is that the Dirac bracket of a second class constraint with any phase space function is zero strongly, i.e., $[\chi_i,G]_D=0$. This means that after promoting the phase space functions to quantum operators via the Dirac bracket, the second class constraints χ_i can be treated as zero operators and the Hamiltonian can be significantly simplified. Therefore, when describing the content by a scalar field and considering the constraints C_X and C_Y, the Hamiltonian operator $\hat{\mathcal{H}}_T$ only contains $\hat{b}$, $\hat{p}_b$, $\hat{\phi}$, and $\hat{p}_\phi$. The Dirac brackets of the fundamental variables corresponding to these operators are

$$\begin{aligned}
[b,\phi]_D &= [b,p_\phi]_D=[\phi,p_b]_D=[p_b,p_\phi]_D=0,\\
[b,p_b]_D &= [\phi,p_\phi]_D=1.
\end{aligned} \tag{7.38}$$

This means that the standard commutation relations are still valid. In the next analysis done in the present thesis (see chapters 11, 12 and 13) we will make use of the second class constraints χ_i to derive an explicit form of the WDW equation.

7.4 conclusions

In the current chapter we have disclosed the method used to move from the classical description to the quantum realm. Such a quantisation is carried via the WDW equation, where the classical Hamiltonian is derived from the fundamental action given by: (i) the Hilbert-Einstein action, and (ii), within the context of EiBI theory. That is, we consider the Eddington's functional provided with a Born-Infeld like structure. On the other hand, the DE content could be given by: (i) a perfect fluid, and (ii), a phantom scalar field. The conjugate momenta of the metric and scalar field are promoted as operators acting on a wave function. Such a function, in principle, should be defined within a Hilbert space with well defined eigenvalues and eigenfunctions. However, as aforementioned, we have not yet a fundamental theory of gravity that allows a particular way to perform the transitions from classical GR to its quantum analogous. This becomes obvious when dealing with different factor orderings. However, different approaches have shown to be viable in order to avoid the cosmological singularities prevalent in the classical theory of gravity. That is, the obtained wave function effectively vanishes when approaching cosmic to the doomsday. We stress that this result is not meant as a proof of singularity avoidance in QC, it should be rather understood as a hint of singularity avoidance. If a fundamental theory able to handle QM and GR simultaneously exists, it should, in principle, avoid those singularities present in the classical theory. In such a way that the subsequent wave functions obtained by different approaches are just the results of a more fundamental theory holding all the underlying approaches as those performed in the present thesis.

8

The BR singularity in a HRDE model

To the dumb question "Why me?" the cosmos barely bothers to return the reply: Why not?

– Christopher-Hitchens

8.1 Introduction

The late-time observed acceleration of the Universe has promoted several scenarios that try to describe this recent speed up of the Universe. In fact, it is well known that a Universe filled only with matter and radiation (for open, flat or closed spatial geometries) cannot expand with positive acceleration. Therefore, it is necessary to find other mechanisms/matters that could explain this feature. The simplest phenomenological approach consists in invoking another kind of energy density responsible for the current acceleration of the Universe which is usually dubbed DE being the cosmological constant the simplest option [23]. The common way to describe DE is via its equation of state (EoS) parameter, which is usually denoted by ω_{d}. This cosmological parameter is the ratio between the pressure and the energy density of DE. It can be constant or time-dependent. By definition, DE EoS must fulfil $\omega_{\mathsf{d}} < -1/3$ at late-time to be able to describe the current speed up of the Universe. In fact, observations suggest $\omega_{\mathsf{d}} \approx -1$ at present (see for example [14]).

Within the above framework, the ΛCDM model is the best fit to the observational data [14]. This model assumes besides ordinary matter, the presence of non-baryonic matter corresponding to DM and a cosmological constant Λ. In fact, the EoS of Λ is just $\omega_\Lambda = -1$ and remains unchanged in time [313]. In this Universe, the expansion is accelerated at late-time reaching an infinite scale factor in an infinite cosmic time where the Universe geometry is described by a de Sitter spacetime. Planck latest results when combined with other cosmological measurements provides $\omega_{\mathsf{d}} \approx -1.006 \pm 0.045$ for a DE constant equation of state [14]. Even though this value is very close to minus one, a slight deviation from it is crucial for the asymptotic future behaviour of the Universe. In fact, if ω_Λ is slightly larger than -1, the Universe will continue expanding eternally, but if this value is slightly smaller than -1, and no matter how tiny is such a deviation, the Universe could end up in a doomsday. For example, it could happen that the energy density becomes infinite at a finite cosmic time [28–30, 32, 45–47, 59, 60].

Although the ΛCDM model gives the best observational fit to explain our current Universe, there are other ways that have gained great attention [23]. One of them is the holographic DE scenario [40, 314] which is inspired on the holographic principle rooted in quantum gravity. We next explain[i] briefly the ideas behind the HRDE.

[i] This chapter corresponds mainly to our publication [44]

As it is well known, the entropy of a given closed system with finite volume L^3 has an upper bound which is not proportional to its volume, but to its surface area, L^2 [315, 316]. On the other hand, for an effective quantum field theory with a given ultra-violet (UV) cutoff, M_{UV}, the entropy of the same system is scaled as $L^3 M_{\mathsf{UV}}^3$. Therefore, there is always a scale or a length where the quantum field theory with UV cutoff is expected to fail. This will happen for large volumes or lengths. To overcome this problem a link between UV and infrared (IR) cutoffs was proposed in [317]:

$$L^3 M_{\mathsf{UV}}^4 \lesssim L M_p^2. \tag{8.1}$$

This proposal ensures the validity of the quantum field theory within this regime. When the inequality is saturated, we can define an energy density which is inversely proportional to the square of the characteristic length of the system. Applying these ideas to the universe give rise to the holographic DE scenario [40].

Now, the next task would be to find a suitable holographic energy density able to speed up the current Universe. This issue has been tackled in different works. For example, taking as a characteristic length the inverse of the Hubble parameter, $l_{\mathsf{H}} = H^{-1}$, it was found that the effective EoS for DE is equal to zero and therefore is not a suitable proposal to describe the current Universe because it would imply an eternally decelerating Universe [40]. Later on, the particle horizon was suggested as a characteristic length for the universe within the holographic approach $l_{\mathsf{PH}} = a \int_0^t dt/a$ [318]. In this case, it turns out that the effective EoS is larger than -1/3, therefore this choice is equally unsuitable to describe our present Universe [40, 318]. Contrary to the previous proposals, the future event horizon $l_{\mathsf{EH}} = a \int_t^{t_f} dt/a$ is phenomelogically viable as it fits the current observations [40, 319], however, it has a drawback with causality; the future event horizon should not affect the current or past physical evolution of our Universe [320]. There is a further possibility to define an holographic DE model which consists in taking as the square of the length characterising the Universe, the inverse of the Ricci scalar curvature [321]. This model was named the Holographic Ricci Dark Energy scenario (HRDE) for further generalization of the holographic DE model see [39, 102, 322–325].

While the HRDE is suitable to describe the current acceleration of the universe as shown in [321, 326–329], it might induce a BR singularity [321]; i.e., the scale factor, the Hubble parameter and its first cosmic time derivate blow up in a finite future cosmological time [28–30]. This model has been observationally constrained in [330]. For more updated observational constraints on the HRDE we refer to [329], where even interaction between DM and the HRDE is considered, and again, a BR is favoured observationally.

When the Universe approach the BR regime, we expect quantum effects to be important, therefore, it is necessary to do a quantum analysis. The field of cosmological singularities has been extensively studied in quantum cosmology [151, 152] (see [204] for a review on this topic). Quantum Cosmology consists in applying the quantum theory to the Universe as a whole [331]. A consistent theory of quantum gravity should in principle avoid the classical singularities prevalent in the classical theory of general relativity [42, 48, 51]. Indeed, it has been shown that in some specific models, most DE related singularities can be avoided in the analogous quantum version [42, 48, 51, 63].

In the present chapter, we address the quantisation of the HRDE model. We use the WDW formalism for a homogenous, isotropic and spatially flat universe. The solutions to the WDW equation must obey the DW boundary conditions [151, 152], which implies that the wave function of the Universe has to vanish close to the singularities, ensuring that the classical singularity is avoided through the quantisation procedure. We extend our analysis to the primordial Universe where a Big Bang is expected to take place from a classical point of view and where again a quantum analysis is required.

The chapter is outlined as follows. In the next section, we make a brief review of the HRDE model. In section III, we present the WDW equation for a standard fluid and present the solutions for the HRDE model. Finally, in section IV we discuss the overall conclusions. In the appendix C.1, we include a brief explanation of the WKB method that was used to solve the WDW equation for some periods of the expansion of the Universe.

8.2 The HRDE: a short review

We start reviewing the HRDE model. The Universe on its largest scale can be described by a FLRW Universe. On the other hand, we consider an energy density proportional to the Ricci scalar, i.e. [321]

$$\rho_R = 6\tilde{\beta}\left(\dot{H} + 2H^2 + \frac{k}{a^2}\right), \tag{8.2}$$

where $\tilde{\beta}$ is a proportionality constant and dot stands for derivates with respect to the cosmic time t. Defining a dimensionless quantity $\beta \equiv 16\pi G\tilde{\beta}$, and solving the Friedmann equation, the expression for the Ricci DE density is found to be [321]

$$\rho_R = \frac{3H_0^2}{8\pi G}\left[\left(\frac{\beta}{2-\beta}\right)\Omega_{\mathrm{m0}}\left(\frac{a}{a_0}\right)^{-3} + \Omega_{\mathrm{p0}}\left(\frac{a}{a_0}\right)^{-2\left(2-\frac{1}{\beta}\right)}\right], \tag{8.3}$$

where Ω_{p0} is an integration constant which will quantify the effective amount of DE in the HRDE model [321]. Notice that the presence of radiation and spatial curvature in the Universe do not modify the previous result. The Ricci DE has one part that behaves as matter and another part which depends on the value of β and plays the role of DE. The asymptotic future behaviour of the Universe depends on the values acquired by β, more precisely:

1. If $1 < \beta$, the cosmic acceleration is negative. We disregard this case as it cannot describe the present Universe.

2. If $1/2 < \beta < 1$, the Universe enters in an accelerating state when the HRDE dominates. The Universe is asymptotically flat in the future.

3. If $\beta = 1/2$, the model is equivalent to the existence of a cosmological constant plus the matter contributions. We will disregard this case as it reduces to ΛCDM model.

4. If $0 < \beta < 1/2$, the Universe not only enters in an accelerated state, but also super accelerates ($\dot{H} > 0$) in the future hitting a BR; i.e. the Universe hit a singularity at a finite cosmic time.

The observational constraints of the HRDE model favour the last case, i.e $0 < \beta < 1/2$ [329, 330], so the Universe would reach a future singularity in a finite time. In this framework, classical Einstein theory is no longer valid and it is necessary to make a quantum treatment.

8.3 Quantisation of the HRDE

For a HRDE model we follow the one dimensional description where the action (7.1) leads to the Lagrangian given in Eq (7.5). Therefore, the total matter content is absorbed in the $\Lambda(a)$ function which reads

$$\Lambda\left(a\right)=3H_{0}^{2}\left[\Omega_{\mathsf{r}0}\left(\frac{a}{a_{0}}\right)^{-4}+\left(\frac{2}{2-\beta}\right)\Omega_{\mathsf{m}0}\left(\frac{a}{a_{0}}\right)^{-3}+\Omega_{\mathsf{k}0}\left(\frac{a}{a_{0}}\right)^{-2}+\Omega_{\mathsf{p}0}\left(\frac{a}{a_{0}}\right)^{-2\left(2-\frac{1}{\beta}\right)}\right]. \tag{8.4}$$

Here, Ω_{k0} is the dimensionless energy density parameter for curvature at present. On the other hand, we follow the quantisation procedure where the term p_a^2/a generates the operator

$$\frac{p_{a}^{2}}{a}=-\hbar^{2}\left[a^{-\frac{1}{2}}\partial_{a}\right]\left[a^{-\frac{1}{2}}\partial_{a}\right], \tag{8.5}$$

in the quantum framework where we have choosen a factor ordering corresponding to the covariant generalization of the LB operator [151] (for alternative choices see for example [332–334]). It is useful to apply the following change of variable to remove the first order derivate from the quantum Hamiltonian operator

$$x=\left(\frac{a}{a_{0}}\right)^{\frac{3}{2}}. \tag{8.6}$$

Therefore, the quantum Hamiltonian operator can be written as

$$\hat{\mathcal{H}}=N\left\{\frac{3G\hbar^{2}}{4\pi a_{0}^{3}}\partial_{x}^{2}+\frac{3\pi H_{0}^{2}a_{0}^{3}}{4G}\left[\Omega_{\mathsf{r}0}x^{-\frac{2}{3}}+\left(\frac{2}{2-\beta}\right)\Omega_{\mathsf{m}0}+\Omega_{k0}x^{\frac{2}{3}}+\Omega_{\mathsf{p}0}x^{-\frac{2}{3}\left(1-\frac{2}{\beta}\right)}\right]\right\}. \tag{8.7}$$

As the variation of the Hamiltonian with respect to the lapse function N produces the Hamiltonian constraint, the WDW equation reads $\hat{\mathcal{H}}\Psi\left(x\right)=0$. We will take the case of a spatially flat universe ($\Omega_{\mathsf{k}0}=0$) for simplicity and in accordance with the current observations [14]. Therefore the WDW equation reduces to

$$\left\{\partial_{x}^{2}+\gamma\left[\Omega_{\mathsf{r}0}x^{-\frac{2}{3}}+\left(\frac{2}{2-\beta}\right)\Omega_{\mathsf{m}0}+\Omega_{\mathsf{p}0}x^{-\frac{2}{3}\left(1-\frac{2}{\beta}\right)}\right]\right\}\Psi\left(x\right)=0, \tag{8.8}$$

where we have introduced the following dimensionless constant:

$$\gamma\equiv\left(\pi H_{0}a_{0}^{3}/G\hbar\right)^{2}. \tag{8.9}$$

Due to the complexity of the equation (8.8), we will divide the evolution of the Universe thereof in three regimes corresponding to the domination eras of radiation, matter and DE, respectively. The first one, has an exact solution, for the others two cases we will make a WKB approximation (up to first order). In the radiation dominated era the WDW is

$$\left\{\partial_{x}^{2}+\gamma\Omega_{\mathsf{r}0}x^{-\frac{2}{3}}\right\}\Psi\left(x\right)=0, \tag{8.10}$$

whose exact solution reads [307]

$$\Psi_1(x) = (\Omega_{\mathsf{r}0}\gamma)^{\frac{3}{8}}\sqrt{x}\left[C_1 J_{\frac{3}{4}}\left(\frac{3}{2}\sqrt{\Omega_{\mathsf{r}0}\gamma}x^{\frac{2}{3}}\right) + C_2 Y_{\frac{3}{4}}\left(\frac{3}{2}\sqrt{\Omega_{\mathsf{r}0}\gamma}x^{\frac{2}{3}}\right)\right], \tag{8.11}$$

where C_1 and C_2 are constants. The functions $J_{3/4}$ and $Y_{3/4}$ correspond to the first and second kind Bessel functions of order $3/4$, respectively. We choose $C_2 = 0$ to ensure that the wave function vanishes when $a \to 0$, according with the DW boundary condition [151, 330]. For the matter dominated era the WDW is

$$\left\{\partial_x^2 + \gamma g_2(x)\right\}\Psi(x) = 0, \tag{8.12}$$

where the function $g_2(x)$ is defined as

$$g_2(x) = \left[\Omega_{\mathsf{r}0}x^{-\frac{2}{3}} + \left(\frac{2}{2-\beta}\right)\Omega_{\mathsf{m}0}\right]. \tag{8.13}$$

The first order WKB solution gives

$$\Psi_2(x) \approx \left[-\gamma g_2(x)\right]^{-\frac{1}{4}}\left[\alpha_1 e^{ih_2(x)} + \alpha_2 e^{-ih_2(x)}\right], \tag{8.14}$$

where α_1 and α_2 are constants and the function $h_2(x)$ is given by

$$h_2(x) = \sqrt{\gamma\left(\frac{2}{2-\beta}\right)\Omega_{\mathsf{m}0}}\left[x^{\frac{2}{3}} + \left(\frac{2-\beta}{2}\right)\frac{\Omega_{\mathsf{r}0}}{\Omega_{\mathsf{m}0}}\right]^{\frac{3}{2}}. \tag{8.15}$$

Finally, during the DE dominated era the WDW is

$$\left\{\partial_x^2 + \gamma g_3(x)\right\}\Psi(x) = 0, \tag{8.16}$$

where the function $g_3(x)$ is defined as

$$g_3(x) = \left[\left(\frac{2}{2-\beta}\right)\Omega_{\mathsf{m}0} + \Omega_{\mathsf{p}0}x^s\right]. \tag{8.17}$$

The first order WKB approximation gives the solution

$$\Psi_3(x) \approx \left[-\gamma g_3(x)\right]^{-\frac{1}{4}}\left[\delta_1 e^{ih_3(x)} + \delta_2 e^{-ih_3(x)}\right], \tag{8.18}$$

where δ_1 and δ_2 are constants. The function $h_3(x)$ reads

$$h_3(x) = \frac{\sqrt{\gamma}}{2+s}x\left\{2\sqrt{g_3(x)} + s\sqrt{\left(\frac{2}{2-\beta}\right)\Omega_{\mathsf{m}0}}\ {}_2F_1\left[\frac{1}{2}, \frac{1}{s}; 1+\frac{1}{s}; \left(\frac{\beta-2}{2}\right)\frac{\Omega_{\mathsf{p}0}}{\Omega_{\mathsf{m}0}}x^s\right]\right\}, \tag{8.19}$$

where $s \equiv -2/3(1-2/\beta)$. Notice that (i) the hypergeometric function defined in (8.19) is not well defined as a series but it is well defined as an integral [307] and (ii) the parameter s is positive, in fact it is larger than 2 for $0 < \beta < 1/2$. The function $h_3(x)$ is always real, on the other hand, the function $g_3(x)$ is positive and an increasing function of x; in fact, it blows up for large values of x. Therefore, the wave-function (8.18) which corresponds to an Universe dominated by DE vanishes at large scales and the DW condition is fullfilled authomatically for Ψ_3.

Now, it is necessary to connect continuously the solutions among them. Taking the arbitrary constant $C_1 = 1$ (for convenience, this election will not modify the fundamental behaviour of the wave function), the conditions for a smooth wave-function give the values of $\alpha_1, \alpha_2, \delta_1, \delta_2$. These conditions are just the continuity conditions of the wave function and its first derivate on a first connecting point (x_1) and on a second connecting point (x_2), which can be read as

$$\Psi_1(x_1) = \Psi_2(x_1), \Psi_1\prime(x_1) = \Psi_2\prime(x_1), \Psi_2(x_2) = \Psi_3(x_2), \Psi_2\prime(x_2) = \Psi_3\prime(x_2), \tag{8.20}$$

where prime stands for a derivative with respect to x.

We choose the first connecting point (x_1) in which the matter component is subdominant with respect to the radiation component (for example $\rho_m \sim 10^{-4}\rho_r$), the second connecting point (x_2) is just where the radiation and the phantom contribution in equation (8.8) are subdominant with respect to DM (for example when they are equal). The connecting points then read

$$x_1 = 10^{-6}\left[\left(\frac{2}{2-\beta}\right)\frac{\Omega_{\mathrm{m0}}}{\Omega_{\mathrm{r0}}}\right]^{-\frac{3}{2}}, \tag{8.21}$$

$$x_2 = \left(\frac{\Omega_{\mathrm{r0}}}{\Omega_{\mathrm{p0}}}\right)^{\frac{3\beta}{4}}. \tag{8.22}$$

Using the Cramer method to solve the algebraic system, the constants $\alpha_1, \alpha_2, \delta_1, \delta_2$ can be written as follows

$$\alpha_1 = -\frac{1}{2}\left[-\gamma g_2(x_1)\right]^{\frac{3}{4}}\begin{vmatrix} y_1 & a_{12} \\ y_2 & a_{22} \end{vmatrix}, \tag{8.23}$$

$$\alpha_2 = -\frac{1}{2}\left[-\gamma g_2(x_1)\right]^{\frac{3}{4}}\begin{vmatrix} a_{11} & y_1 \\ a_{21} & y_2 \end{vmatrix}, \tag{8.24}$$

$$\delta_1 = -\frac{1}{2}\left[-\gamma g_3(x_2)\right]^{\frac{3}{4}}\begin{vmatrix} z_1 & b_{12} \\ z_2 & b_{22} \end{vmatrix}, \tag{8.25}$$

$$\delta_2 = -\frac{1}{2}\left[-\gamma g_3(x_2)\right]^{\frac{3}{4}}\begin{vmatrix} b_{11} & z_1 \\ b_{21} & z_2 \end{vmatrix}, \tag{8.26}$$

where we define

$$a_{11} \equiv \left[-\gamma g_2(x_1)\right]^{-\frac{1}{4}} e^{ih_2(x_1)}, \tag{8.27}$$

$$a_{12} \equiv \left[-\gamma g_2(x_1)\right]^{-\frac{1}{4}} e^{-ih_2(x_1)}, \tag{8.28}$$

$$a_{21} \equiv \left\{-\frac{\gamma^{-\frac{1}{4}}}{4}\left[-g_2(x_1)\right]^{-\frac{5}{4}}\left(\frac{2}{3}\Omega_{\mathrm{r0}}x_1^{-\frac{5}{3}}\right) - i\left[\gamma g_2(x_1)\right]^{-\frac{1}{2}}\right\} e^{ih_2(x_1)}, \tag{8.29}$$

$$a_{22} \equiv \left\{ -\frac{\gamma^{-\frac{1}{4}}}{4} \left[-g_2 \left(x_1 \right) \right]^{-\frac{5}{4}} \left(\frac{2}{3} \Omega_{\mathsf{r}0} x_1^{-\frac{5}{3}} \right) + i \left[\gamma g_2 \left(x_1 \right) \right]^{-\frac{1}{2}} \right\} e^{-i h_2(x_1)}, \tag{8.30}$$

$$y_1 \equiv \left(\Omega_{\mathsf{r}0} \gamma \right)^{\frac{3}{8}} \sqrt{x_1} J_{\frac{3}{4}} \left(\frac{3}{2} \sqrt{\Omega_{\mathsf{r}0} \gamma} x_1^{\frac{2}{3}} \right), \tag{8.31}$$

$$y_2 \equiv \left(\Omega_{\mathsf{r}0} \gamma \right)^{\frac{3}{8}} \frac{1}{2\sqrt{x_1}} \left[J_{\frac{3}{4}} \left(\frac{3}{2} \sqrt{\Omega_{\mathsf{r}0} \gamma} x_1^{\frac{2}{3}} \right) - 2 \left(\Omega_{\mathsf{r}0} \gamma \right)^{\frac{1}{2}} x_1^{-\frac{1}{3}} J_{\frac{7}{4}} \left(\frac{3}{2} \sqrt{\Omega_{\mathsf{r}0} \gamma} x_1^{\frac{2}{3}} \right) + 1 \right], \tag{8.32}$$

$$b_{11} \equiv \left[-\gamma g_3 \left(x_2 \right) \right]^{-\frac{1}{4}} e^{i h_3(x_2)}, \tag{8.33}$$

$$b_{12} \equiv \left[-\gamma g_3 \left(x_2 \right) \right]^{-\frac{1}{4}} e^{-i h_3(x_2)}, \tag{8.34}$$

$$b_{21} \equiv \left\{ \frac{\gamma^{-\frac{1}{4}}}{4} \left[-g_3 \left(x_2 \right) \right]^{-\frac{5}{4}} \left(s \Omega_{\mathsf{p}0} x_2^{s-1} \right) - i \left[\gamma g_3 \left(x_2 \right) \right]^{-\frac{1}{2}} \right\} e^{i h_3(x_2)}, \tag{8.35}$$

$$b_{22} \equiv \left\{ \frac{\gamma^{-\frac{1}{4}}}{4} \left[-g_3 \left(x_2 \right) \right]^{-\frac{5}{4}} \left(s \Omega_{\mathsf{p}0} x_2^{s-1} \right) + i \left[\gamma g_3 \left(x_2 \right) \right]^{-\frac{1}{2}} \right\} e^{-i h_3(x_2)}, \tag{8.36}$$

$$z_1 \equiv \left[-\gamma g_2 \left(x_2 \right) \right]^{-\frac{1}{4}} \left[\alpha_1 e^{i h_2(x_2)} + \alpha_2 e^{-i h_2(x_2)} \right], \tag{8.37}$$

$$z_2 \equiv \alpha_1 \left\{ -\frac{\gamma^{-\frac{1}{4}}}{4} \left[-g_2 \left(x_2 \right) \right]^{-\frac{5}{4}} \left(\frac{2}{3} \Omega_{\mathsf{r}0} x_2^{-\frac{5}{3}} \right) - i \left[\gamma g_2 \left(x_2 \right) \right]^{-\frac{1}{2}} \right\} e^{i h_2(x_2)} \tag{8.38}$$

$$-\alpha_2 \left\{ \frac{\gamma^{-\frac{1}{4}}}{4} \left[-g_2 \left(x_2 \right) \right]^{-\frac{5}{4}} \left(\frac{2}{3} \Omega_{\mathsf{r}0} x_2^{-\frac{5}{3}} \right) + i \left[\gamma g_2 \left(x_2 \right) \right]^{-\frac{1}{2}} \right\} e^{-i h_2(x_2)}. \tag{8.39}$$

With the aim to show a numerical result, we use the constraints $\beta = 0.3823$, $\Omega_{\mathsf{r}0} = 8 \cdot 10^{-5}, \Omega_{\mathsf{m}0} = 0.2927, \Omega_{\mathsf{p}0} = 0.6380$ in accordance with the best fit of the current Universe within the HRDE model [330]. Therefore, the connecting points are

$$x_1 = 3.287 \cdot 10^{-12}, \; x_2 = 0.07608, \tag{8.40}$$

and the constants can be written as

$$\alpha_1 = u_\alpha + v_\alpha i, \tag{8.41}$$

$$\alpha_2 = v_\alpha + u_\alpha i, \tag{8.42}$$

$$\delta_1 = u_\delta + v_\delta i, \tag{8.43}$$

$$\delta_2 = v_\delta + u_\delta i. \tag{8.44}$$

We next show an example of these constants. We choose $\gamma = 10^{20}$, sufficiently large to ensure the validity of the WKB approximation for the connecting first point; i.e. well inside the radiation dominated epoch where matter is subdominant. Notice that if the WKB approximation is

fulfilled for the first connecting point it is well defined for the second connecting point. Then we obtain $q(x_1) = 0.035$ (see (C.7)). Finally, using the above introduced constraints and for the selected γ we find:

$$u_\alpha = 80274.39, \tag{8.45}$$

$$v_\alpha = -288039.58, \tag{8.46}$$

$$u_\delta = -298682.24, \tag{8.47}$$

$$v_\delta = 14131.34. \tag{8.48}$$

In principle, γ is much larger, in fact, taking $a_0 = 1$ gives the value $\gamma = 8.072 \cdot 10^{87}$. If in addition, we take into account the whole number of e-folds since the radiation dominated epoch, the parameter γ would be much larger. We choose the previous value of γ; i.e. $\gamma = 10^{20}$, to be able to get numerically the values of the constants defined in (8.41).

8.4 Conclusions and outlook

The HRDE is a suitable proposal to describe the late Universe. The best fit of the model provides a value for the proportionality constant β inside the interval $0 < \beta < 1/2$ [330]. This means that the Universe is not only accelerating but will also face a future BR singularity. This classical singularity is analysed within a quantum treatment where the quantisation is realised in the framework of the WDW equation for a flat FLRW universe and imposing the DW boundary condition. We have shown that the BR singularity as a consequence of the phantom like behaviour of the HRDE could be avoidable and would be harmless within the quantum approach used in this work. This might not be the case within a classical approach [335]. The DW condition can be regarded as a guidance in the nowadays incomplete theory of quantum cosmology. In fact, the disappearance of the probability distribution at singularities should arise in the theory in a natural way as a dynamical consequence of some other requirements, such as the normalizability of the wave function, and should not be postulated. Given that we lack of a complete and consistent quantum gravity theory, we will stick to the DW condition as our guidance for singularity avoidance.

Despite the quantum analysis presented in this work about the avoidance of the Big Bang and BR singularities, this fact cannot be interpreted as an exact and thorough evidence of singularities avoidance in quantum cosmology, but rather an indication that a consistent and complete quantum theory of gravity should be free of these singularities.

To solve the WDW equation we carry two types of approximations: (i) we divide the evolution of the universe in three different epoch corresponding to radiation, matter and DE dominance as explained in the previous section, (ii) for the last two periods we use a WKB approximation where it is enough to go to first order in the WKB approximation to ensure the DW boundary condition for large scale factors where the wave function is asymptotically decreasing and vanishing.

During the radiation dominated epoch, we obtain the exact wave function, fulfilling the DW condition, which can be matched with the WKB approximation for the second period (matter+radiation). The larger is the value of γ, defined in (8.9), the sooner, i.e. for smaller scale factors, we can carry the matching between the two wave functions. In fact, the asymp-

totic behaviour of the wave function during the radiation dominated epoch matches smoothly and naturally with the WKB approximated solution corresponding to the matter and radiation epochs.

The quantisation is necessary to describe the Universe close to singularities. However, outside of these singularities the Universe can be described classically. In this regime, the square of the modulus of the wave function can be interpreted as the classical probability density distribution. We can see this clearly when the value of γ is very large and therefore, the wave function carries out a significant number of oscillations within a short interval of the chosen variable. In fact, these oscillations are modulated by the classical probability density distribution, which is defined as the time average of the scale factor.

In an analogy with the classical picture, a slight deviation of the resulted wave function from the classical probability density distribution is expected. This is due to the performed first type of approximation, which disregards the contribution of DE for small scales and the contribution of radiation for large scales. Therefore, this deviation is more significant in the matter dominated epoch.

Next, we would like to stress that our model has only one degree of freedom described through the scale factor which in fact can play the role of the classical time. On the other hand, gravity is a reparametrisation invariant theory with first class constraints. Therefore, there is always a gauge fixing condition which reduces the number of physical variables and in our case we would be left without any degree of freedom after the gauge fixing. However, our current work can be regraded as a first approach in quantising the HRDE model, in fact a toy model, and we expect to present in a different work a more elaborated scenario for the quantisation of the HRDE with two physical variables and a genuine degree of freedom [70, 188, 189, 202]. In fact, to get at least one degree of freedom with physical meaning, we can map the matter content given by a perfect fluid to one or more scalar fields that could mimic the different components of the universe. This method was carried out for example in [57] for a minimally coupled scalar field or a tachyon scalar field.

In addition, we have been mainly focussing on the wave function of the universe while in fact the important thing is the probabilistic interpretation of it. This requires the definition of a Hilbert space with a proper scalar product and measure. In the interesting review [181], this non trivial problem is discussed and several potential solutions are presented while in [183, 204] those procedures are applied to different cosmological models. We hope to implement those methods for the HRDE in a future work.

The aforementioned interpretation has some conceptual drawbacks: first, this picture corresponds with the description of an “external observer”, who lives in a reality outside from the quantum system under study. This is certainly not the case for a cosmological system where the observer is part of the system [181]. In fact, we would need to apply a quantum theory of closed systems or the many-worlds interpretation of QM to our universe but this is beyond the scope of our current work (see [181] for more details on this subject).

We have restricted our analysis to a homogeneous and isotropic configuration. However, it is well known that the inhomogeneities and anisotropies can be quite important close to singularities,

for example through the creation of particle and gravitons (see for example [52, 336]). We leave this interesting issue for a future work.

9

Classical and quantum cosmology of the LR abrupt event

> *The universe we observe has precisely the properties we should expect if there is, at bottom, no design, no purpose, no evil, no good, nothing but blind, pitiless indifference*
>
> – Richard Dawkins

9.1 introduction

One of the most challenging problems in theoretical physics is the formulation of a consistent quantum theory of gravity [151, 152]. Such a theory is needed not only for conceptual reasons, but also for understanding the origin of the Universe and the structure of black holes. In this chapter[i], we shall deal with quantum cosmology, that is, the application of quantum theory to the Universe as a whole. For this purpose, we shall use the conservative framework called quantum geometrodynamics, with the WDW equation as its central equation. This framework is straightforwardly obtained by constructing quantum wave equations from which the Einstein equations can be recovered in the semiclassical (WKB) limit [337].

Besides these fundamental issues, we also encounter the problem to explaining the observed acceleration of the Universe. Phenomenologically, this is done by adding an ingredient called DE [23]. Some of the models describing DE predict the occurrence of singularities beyond big bang (or big crunch), occurring for example in the finite future. Aside from DE singularities, there are also DE abrupt events like the LR [47, 55, 59, 64–67, 201]. We name them abrupt events rather than singularities because they occur at an infinite future cosmic time. Some of these models are in accordance with current data [85]. Since the presence of singularities and abrupt events in a theoretical framework is an indication of its breakdown, we expect quantum effects to be important there, too. A central question is then whether those future singularities and abrupt events can be avoided in quantum cosmology or not [308]. This question will be also addressed (and answered) for the models discussed in this chapter. Naively, we would expect that at cosmological scales quantum effects are important only in the early Universe, that is, on time scales of the order of the Planck time, t_{P}, and for distances related to the Planck length l_{P}. This naive belief is based on the fact that quantum theory is usually important for small systems such as atoms or molecules. Assuming the universality of the superposition principle, quantum effects can occur at any scale, whenever decoherence is negligible. This can happen even for the Universe as a whole, for example, in the case of a classically recollapsing Universe [338], or in cases where singularities or abrupt events are present in the classical theory, as is the case here.

[i] This chapter corresponds mainly to our publication [202]

Before proceeding further, we should clarify that among all DE singularities and abrupt events, only three of them are intrinsic to phantom DE, that is, within a relativistic model they happen if and only if suitable phantom matter is present. These are the BR, the LR, and the LS. Consequently, if we want to address the question: *can quantum cosmology smoothen or avoid divergent behaviors caused by phantom matter*, we need to quantise models that induce in the classical picture a BR, a LR, or a LS. These questions have been partially addressed in the quantum theory of cosmological models with a BR [42, 44] or a LS [70]. In this paper, we will complete the answer to these questions by quantising a classical model for the LR.

This chapter is organised as follows In section 9.2 and for later convenience, we introduce as well a scalar field suitable to describe the nowadays late-time acceleration of the universe and are simultaneously able to induce a LR asymptotically in the presence and absence of DM. In Section 9.3, we present and solve the WDW equation for the model B. Here, the DE is described by a perfect fluid and we have made use of two different factor orderings. In Section 9.4 we address the same model B but with a DE content mapped to a scalar field. We assume a variable separation ansatz and apply some approximations to get a separable differential equation. We show in all the analysed cases the existence of solutions to the WDW equation that avoid the LR. Finally, in 9.5 we present our conclusions. In addition, a detailed analysis for the WKB approximation performed in this chapter can be found in C.1.2, in which we prove the validity of the approximations used in section 9.3. Finally, in the appendix section C.5, the Symanzik scaling behavior is presented as an alternative method to analyse the scalar field eigenstates.

9.2 The LR as induced by a scalar field

For later convenience, we map the perfect fluid with EoS (2.13) to a scalar field, ϕ. As the constant $\mathcal{B}$ must be positive to induce a LR, the mapping to a scalar field entails a phantom character for the field. Consequently, we can write the kinetic energy and potential of the scalar field as

$$\dot{\phi}^2 = -(\rho + p), \tag{9.1}$$

$$V = \frac{1}{2}(\rho - p). \tag{9.2}$$

Making use of (2.13) and (2.14) in (9.1), we get

$$\dot{\phi}^2 = \mathcal{B}\rho_d^{\frac{1}{2}} = \left| \frac{3\mathcal{B}^2}{2} \ln\left(\frac{a}{a_0}\right) + \mathcal{B}\sqrt{\rho_{d0}} \right|. \tag{9.3}$$

Introducing the new variable

$$x \equiv \ln\left(\frac{a}{a_0}\right), \tag{9.4}$$

we can express $\dot{\phi}$ as

$$\dot{\phi} = \frac{d\phi}{dx} H. \tag{9.5}$$

We now treat in separate subsections the cases without and with DM.

9.2.1 Disregarding DM

Using (9.3) and (2.2), we can write

$$d\phi = \frac{\dot{\phi}}{H}dx = \pm\frac{\sqrt{3}}{\kappa}\left(\frac{\Omega_{\mathsf{B}}}{\Omega_{d0}}\right)^{\frac{1}{4}}\frac{dx}{\left|\frac{3}{2}\sqrt{\frac{\Omega_{\mathsf{B}}}{\Omega_{d0}}}x+1\right|^{\frac{1}{2}}}, \tag{9.6}$$

where $\kappa^2 \equiv 8\pi G$ and $\Omega_{\mathsf{B}} \equiv \left(\mathcal{B}\kappa/\sqrt{3}H_0\right)^2 \equiv \rho_{\mathsf{B}}/\rho_{\mathrm{c}}$. The latter denotes a critical energy density fraction which is related with the model parameter $\mathcal{B}$ and quantifies the deviation of a DE model based on (2.13) from the standard ΛCDM model, that is, the smaller is Ω_{B}, the closer we are to the ΛCDM model. Notice that the expression (9.6) is only valid asymptotically, for we have disregarded the contribution of DM which will red-shift quickly in the future and thus become negligible compared to DE. Finally, from integrating (9.6) we find (for $\Omega_{\mathsf{B}} \neq 0$)

$$\phi(x) = \pm\frac{4}{\sqrt{3}\kappa}\left(\frac{\Omega_{d0}}{\Omega_{\mathsf{B}}}\right)^{\frac{1}{4}}\left|\frac{3}{2}\sqrt{\frac{\Omega_{\mathsf{B}}}{\Omega_{d0}}}x+1\right|^{\frac{1}{2}}\mathsf{sign}\left(\frac{3}{2}\sqrt{\frac{\Omega_{\mathsf{B}}}{\Omega_{d0}}}x+1\right). \tag{9.7}$$

We have chosen the integrations constants, ϕ_* and x_* such that

$$\phi_* = \pm\frac{4}{\sqrt{3}\kappa}\left(\frac{\Omega_{d0}}{\Omega_{\mathsf{B}}}\right)^{\frac{1}{4}}\left|\frac{3}{2}\sqrt{\frac{\Omega_{\mathsf{B}}}{\Omega_{d0}}}x_*+1\right|^{\frac{1}{2}}\mathsf{sign}\left(\frac{3}{2}\sqrt{\frac{\Omega_{\mathsf{B}}}{\Omega_{d0}}}x_*+1\right). \tag{9.8}$$

In addition, we have selected x_* to be large enough to ensure the validity of the approximation made in (9.6); that is, we are far enough in the future such that the DM component can be ignored in the Friedmann equation. For practical purpose, we select $x_* = 1.17$, where the matter energy density is two orders of magnitude smaller than the DE density. Therefore, x_* is large enough for the Universe to be in an almost total DE domination phase. This numerical value is not crucial for this subsection, but it has to be fixed in the next subsection where numerical calculations are required and therefore a fixed value of x_* is needed. In addition, our results do not change by imposing larger values of x_*. Finally, the function $\mathsf{sign}\,(x)$ is the sign function, that is

$$\mathsf{sign}\,(x) = \begin{cases} -1 & \mathsf{if} \quad x<0 \\ 0 & \mathsf{if} \quad x=0 \\ 1 & \mathsf{if} \quad x>0 \end{cases}. \tag{9.9}$$

As mentioned before, the EoS shown in (2.13) describes a deviation from the standard ΛCDM model through the parameter A. Therefore, for a vanishing parameter A, the expected classical trajectory, $\phi\,(x)$, is characterised by a constant, i.e. $d\phi = 0$. This result can be recovered by taking the limit $\Omega_{\mathsf{B}} \to 0$ in (9.6), however, after the integration done in (9.7) the outcome is not well defined for the limit $\Omega_{\mathsf{B}} \to 0$ (notice that ϕ_* could blows up in this case). To get a suitable expression for small values of Ω_{B}, we perform a Taylor expansion up to first order of the general integral of (9.6), which reads

$$\phi(x) - \tilde{\phi}_* \simeq \pm\frac{\sqrt{3}}{\kappa}\left(\frac{\Omega_{\mathsf{B}}}{\Omega_{d0}}\right)^{\frac{1}{4}}(x-\tilde{x}_*), \tag{9.10}$$

where in this case, we have chosen $\tilde{\phi}_*$ and $\tilde{x}_*$ in such way that:

$$\tilde{\phi}_* = \pm\frac{\sqrt{3}}{\kappa}\left(\frac{\Omega_{\mathsf{B}}}{\Omega_{d0}}\right)^{\frac{1}{4}}\tilde{x}_*. \tag{9.11}$$

This result will be used later to determine the potential $V(\phi)$. In the LR not only the scale factor gets very large, but also the scalar field ϕ, see figure 9.1. From now on we will focus on this regime.

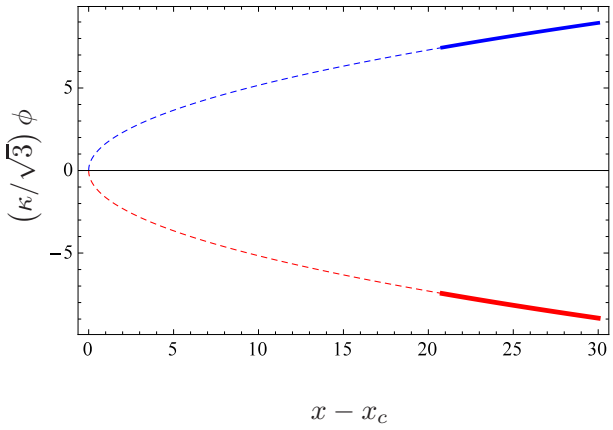

Figure 9.1: Plot of the scalar field, ϕ, versus $x \equiv \ln(a/a_0)$ where $x_c = -2\sqrt{\Omega_{d0}}/3\sqrt{\Omega_{\mathsf{B}}}$. This plot is valid for $\Omega_{\mathsf{B}} \neq 0$ since x_c is not well defined for a vanishing Ω_{B}, i.e. a vanishing $\mathcal{B}$. The solution (9.7) gives two branches, one above $\phi = 0$ (blue color) and another below $\phi = 0$ (red color) The dashed curve describes a realm where the neglected DM contribution is important, while the solid lines describes a regime where we assume a complete DE domination. We disregard the solutions for $x < x_c$ as our approximation breaks down there. Therefore, only the solid lines are physically relevant for our purpose.

For the case of $\Omega_{\mathsf{B}} \neq 0$, since the function (9.7) is invertible, we can consequently write $x = x(\phi)$,

$$x = \frac{\kappa^2}{8}\phi^2 - \frac{2}{3}\sqrt{\frac{\Omega_{d0}}{\Omega_{\mathsf{B}}}}, \qquad \text{for} \qquad 0 < \frac{3}{2}\sqrt{\frac{\Omega_{\mathsf{B}}}{\Omega_{d0}}}x + 1, \tag{9.12}$$

$$x = -\frac{\kappa^2}{8}\phi^2 - \frac{2}{3}\sqrt{\frac{\Omega_{d0}}{\Omega_{\mathsf{B}}}}, \qquad \text{for} \qquad \frac{3}{2}\sqrt{\frac{\Omega_{\mathsf{B}}}{\Omega_{d0}}}x + 1 < 0. \tag{9.13}$$

Once we have the relation between the potential and the energy density, (9.2), we can write the potential in terms of x, that is

$$V(x) = \rho_{d0}\left[\frac{3}{2}\sqrt{\frac{\Omega_{\mathsf{B}}}{\Omega_{d0}}}x + 1\right]^2 + \frac{3H_0^2}{2\kappa^2}\sqrt{\Omega_{d0}\Omega_{\mathsf{B}}}\left|\frac{3}{2}\sqrt{\frac{\Omega_{\mathsf{B}}}{\Omega_{d0}}}x + 1\right|. \tag{9.14}$$

As can be seen, for a vanishing Ω_{B}, the potential becomes constant as expected within the ΛCDM paradigm, i.e. $V = \rho_{d0}$. Using (9.12) in the later expression, the potential shows a quadratic dependence on the scalar field:

$$V(\phi) = b_1\phi^4 + b_2\phi^2, \tag{9.15}$$

where the constants b_1 and b_2 are defined as

$$b_1 \equiv \frac{27}{256}\kappa^2 H_0^2\Omega_{\mathsf{B}}, \qquad b_2 \equiv \frac{9}{32}H_0^2\Omega_{\mathsf{B}}. \tag{9.16}$$

On the one hand, notice that b_1 has physical dimension of an inverse mass times length (and is thus dimensionless in natural units where $\hbar = 1$ and $c = 1$), while b_2 has dimension of an inverse length squared (mass squared in natural units). As was mentioned above, (9.7) does not take into account the contribution of DM; therefore, the result shown in figure 9.1 is only valid for very large values of the scale factor.

On the other hand, for a vanishing parameter A the potential given in (9.15) cannot show the expected constant value. This is not surprising as (9.15) was deduced using (9.7) which is not valid for $A = 0$. To recover this solution it is necessary to replace in (9.14) the expression obtained in (9.10) for small values of Ω_{B}. In fact, on that case, we obtain

$$V(\phi) \simeq \rho_{d0}\left[\frac{\sqrt{3}\kappa}{2}\left(\frac{\Omega_{\mathsf{B}}}{\Omega_{d0}}\right)^{\frac{1}{4}}\phi + 1\right]^2 + \frac{3H_0^2}{2\kappa^2}\sqrt{\Omega_{d0}\Omega_{\mathsf{B}}}\left|\frac{\sqrt{3}\kappa}{2}\left(\frac{\Omega_{\mathsf{B}}}{\Omega_{d0}}\right)^{\frac{1}{4}}\phi + 1\right|. \tag{9.17}$$

As can be seen from the previous expression when $A \to 0$, $V(\phi)$ approaches a constant; i.e. the model in this case behaves as ΛCDM.

9.2.2 Including DM

Just for completeness and to get an accurate solution also for small values of x (but still large enough to be in a matter domination epoch after the radiation dominated epoch), it is necessary to incorporate the DM contribution to the energy density budget of the Universe. Following the same approach we used before, (9.5) can be written as

$$d\phi = \pm\frac{\dot{\phi}}{H}dx = \left\{\frac{|p_d(x) + \rho_d(x)|}{H^2}\right\}^{\frac{1}{2}}dx. \tag{9.18}$$

The contribution of DM is here included in the Hubble parameter. The equation for $\phi(x)$ is now given by

$$\phi(x) = \pm\frac{\sqrt{3}}{\kappa}\int_{x_*}^{x}\left\{\frac{\sqrt{\Omega_{\mathsf{B}}\Omega_{d0}}\left|\frac{3}{2}\sqrt{\frac{\Omega_{\mathsf{B}}}{\Omega_{d0}}}x + 1\right|}{\Omega_{m0}e^{-3x} + \Omega_{d0}\left(\frac{3}{2}\sqrt{\frac{\Omega_{\mathsf{B}}}{\Omega_{d0}}}x + 1\right)^2}\right\}^{\frac{1}{2}}dx + \phi_*. \tag{9.19}$$

The integral in (9.19) cannot be solved analytically; therefore, we have performed a numerical integration in which the integration constant ϕ_* was fixed as after (9.7) to the value imposed in (9.8). In this way, we ensure that the approximated model and the numerical solution are equal at the point x_* as long as x_* is large enough. For practical purpose, we select $x_* = 1.17$, where the matter energy density is two orders of magnitude smaller than the DE density. Therefore, x_* is large enough for the Universe to be in an almost total DE domination phase. Figure 9.17 shows $\phi(x)$.

Once we have obtained the solution for the scalar field, we get the numerical solution for the potential $V(\phi)$, which also takes into account the DM contribution. We compare the obtained potential with the approximated potential (which neglects DM) in figure 9.3.

Because DM is completely negligible at late times, the quantum analysis of the LR is unaffected by it. We will thus neglect DM from now on.

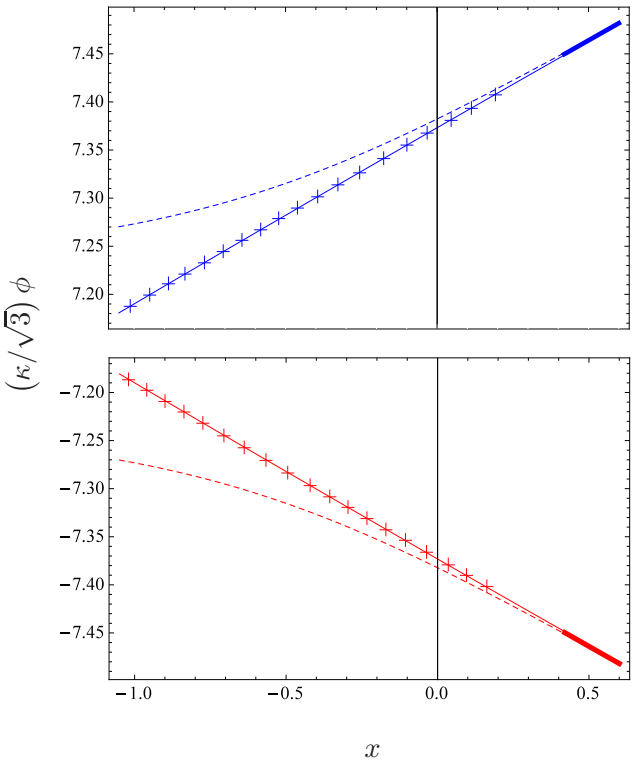

Figure 9.2: Plot of the rescaled scalar field, $(\kappa/\sqrt{3})\,\phi$, versus x, the logarithmic scale factor. The solution (9.19) has two branches which we have drawn as dashed linesin bottom (red) and upper (blue) panels. These lines take into account DM contribution. The solid blue and red lines correspond to the solution (9.7) where DM is neglected. All the plots have been obtained for $x_* = 1.17$. For practical purpose, we see that for values larger than $x = 0.42$ (i.e. the energy density of DM is 10 times smaller than that of DE), the difference between the two solutions (inclusion of DM and exclusion of DM) is almost negligible. For values of x smaller than $x = 0.42$, the approximated solution starts to show a relevant deviation from the exact solution and we have drawn in this case the approximated solution as a curve with crosses. In addition, we have fixed the other constants as $H_0 = 70.1$ km s^{-1}Mpc^{-1}, $\Omega_{m0} = 0.274$, and $\mathcal{B}\kappa = 3.46 \cdot 10^{-3}$Gyr^{-1} according to the best fit obtained in [66].

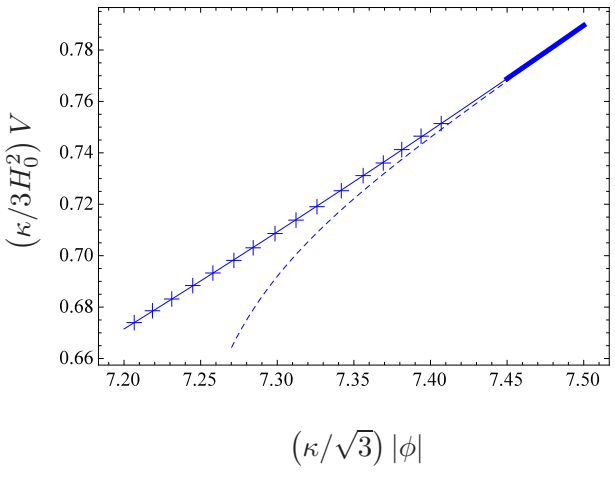

Figure 9.3: Plot of the dimensionless potential, $(\kappa/3H_0^2)\,V$, versus the absolute value of the scaled scalar field, $(\kappa/\sqrt{3})\,|\phi|$. The dashed curve takes into account the presence of DM, while the solid line neglects it. In consistency with the other plots, we take $x_* = 1.17$. The deviation becomes significant when $(\kappa/\sqrt{3})\,|\phi| < 7.45$ (drawn as thin curve with crosses), that is, $x < 0.42$, corresponding to the energy density of DM being 10 times smaller than that of DE.

9.3 WDW equation with a perfect fluid

In this subsection, we will implement the quantisation in the simplest way, which consists in describing the matter content as a perfect fluid with a given EoS. Therefore, the energy density can be written in terms of the scale factor, which is the single variable within this analysis. The Lagrangian for this model reads [44, 151, 152, 333]

$$\mathcal{L} = -\frac{3\pi}{4GN}\dot{a}^2 a - 2N\pi^2 a^3 \rho\left(a\right). \tag{9.20}$$

The conjugate momentum is

$$\pi_a \equiv \frac{\partial \mathcal{L}}{\partial \dot{a}} = -\frac{3\pi}{2G} N a \dot{a}, \tag{9.21}$$

and the Hamiltonian reads

$$\mathcal{H} = -N\frac{G}{3\pi}\frac{\pi_a^2}{a} + 2\pi^2 N a^3 \rho\left(a\right). \tag{9.22}$$

For the sake of simplicity, we introduce the new constants

$$\eta \equiv \frac{\pi a_0^3 H_0}{G\hbar}, \qquad b \equiv \frac{3}{2}\sqrt{\frac{\Omega_{\mathsf{B}}}{6\Omega_{d0}}}. \tag{9.23}$$

The exact form of the WDW equation depends on the chosen factor ordering. We shall employ two different such orderings in order to study its influence.

9.3.1 First quantisation procedure: $a\hat{\mathcal{H}}(a,\hat{\pi}_a)\psi(a) = 0$

We choose here [42]

$$\hat{\pi}_a^2 = -\hbar^2 \partial_a^2. \tag{9.24}$$

Employing this in the quantum version of (10.5) and multiplying the result by $\left[3\pi a/G\hbar^2 N\right]$, we get

$$\frac{3\pi}{G\hbar^2}\frac{a}{N}\hat{\mathcal{H}} = \partial_a^2 + \frac{6\pi^3}{\hbar^2 G} a^4 \rho\left(\frac{a}{a_0}\right). \tag{9.25}$$

In order to get a dimensionless WDW equation, we will rescale the scale factor and its partial derivative as

$$u \equiv \frac{a}{a_0}, \qquad \partial_u^2 \equiv a_0^2 \partial_a^2. \tag{9.26}$$

After carrying the change of variable introduced above and using (2.14) for the energy density, the WDW equation (7.9) can be written as

$$\left\{\partial_u^2 + \left(\frac{3}{2}\eta\right)^2 \Omega_{d0} u^4 \left[1 + \sqrt{6} b \ln\left(u\right)\right]^2\right\} \Psi_1\left(u\right) = 0, \tag{9.27}$$

where we have used the definitions given in (9.23). The approximated WKB solution up to first order reads (see, for example, the method used in [44, 70, 339] and Appendix A)

$$\Psi_1(u) \approx \Omega_{d0}^{-\frac{1}{4}} \sqrt{\frac{2}{3\eta}} \frac{1}{u} \left[1+\sqrt{6}b\ln(u)\right]^{-\frac{1}{2}} \left\{D_1 e^{i\frac{3\eta}{2}S_0(u)} + D_2 e^{-i\frac{3\eta}{2}S_0(u)}\right\}, \tag{9.28}$$

where D_1 and D_2 are constants and

$$\begin{aligned} S_0(u) &= \sqrt{\Omega_{d0}} \int_{u_1}^{u} y^2 \left[1+\sqrt{6}b\ln(y)\right] dy \\ &= \frac{\sqrt{\Omega_{d0}}}{3} u^3 \left\{1+\sqrt{6}b\left[\ln(u)-\frac{1}{3}\right]\right\} - \frac{\sqrt{\Omega_{d0}}}{3} u_1^3 \left\{1+\sqrt{6}b\left[\ln(u_1)-\frac{1}{3}\right]\right\}. \end{aligned} \tag{9.29}$$

In addition, u_1 is a large enough constant to ensure not only a positive value of the above integral, but also to guarantee that the system is well inside the DE domination regime, that is, $\ln(u_1) \gg -1/(b\sqrt{6})$. Note that in the quantum treatment, we disregard the contribution of DM by assuming a single component through which the energy density is expressed. This is in full agreement with the fact that by the time the classical abrupt event is approached, DM contribution is negligible, see section 9.2.2.

From the inspection of (9.28), we see that the wave function vanishes for large values of u. This is exactly the region where in the classical model the LR takes place. The DW criterion is fulfilled, and the LR is avoided. It is interesting to note that this criterion is here equivalent to the boundary condition that $\Psi_1 \to 0$ for $a \to \infty$ in analogy with the boundary condition usually imposed on the Schrödinger equation for bounded systems.

9.3.2 Second quantisation procedure (LB factor ordering): $\hat{\mathcal{H}}(a,\hat{\pi}_a)\psi(a)=0$

This quantisation procedure is based on the LB operator which is the covariant generalisation of the Laplacian operator in minisuperspace [151]. The corresponding operator is different depending on the involved degrees of freedom. For the case of a single component described by a perfect fluid, it is written as (cf. for example [44])

$$\frac{\hat{\pi}_a^2}{a} = -\hbar^2 \left[a^{-\frac{1}{2}}\frac{d}{da}\right]\left[a^{-\frac{1}{2}}\frac{d}{da}\right]. \tag{9.30}$$

To diagonalise the operator, we suggest the following change of variable

$$z \equiv \left(\frac{a}{a_0}\right)^{\frac{3}{2}} \qquad , \qquad \frac{\hat{\pi}_a^2}{a} = -\frac{9}{4}\frac{\hbar^2}{a_0^3}\frac{d^2}{dz^2}. \tag{9.31}$$

Using this operator in the quantum version of (7.7) and multiplying by $\left[4\pi a_0^3/3G\hbar^2 N\right]$, we get the following dimensionless expression,

$$\frac{4\pi a_0^3}{3G\hbar^2 N}\hat{\mathcal{H}} = \partial_z^2 + \frac{8\pi^3 a_0^6}{3G\hbar^2} z^2 \rho(z). \tag{9.32}$$

Using (2.13) for the energy density, the fundamental WDW equation given in (7.9) reduces to

$$\left\{\partial_z^2 + \eta^2\Omega_{d0}z^2\left[1+\sqrt{\frac{8}{3}}b\ln(z)\right]^2\right\}\Psi_2(z) = 0, \tag{9.33}$$

where the constants η and b are defined in (9.23). The approximated WKB solution up to first order reads (see, for example, [44, 339]; for a summary, see also Appendix A)

$$\Psi_2(a) \approx \Omega_{d0}^{-\frac{1}{4}} \sqrt{\frac{1}{\eta}} z^{-\frac{1}{2}} \left[1 + \sqrt{\frac{8}{3}} b \ln(z)\right]^{-\frac{1}{2}} \left\{C_1 e^{i\eta Q_0(z)} + C_2 e^{-i\eta Q_0(z)}\right\}, \tag{9.34}$$

where C_1 and C_2 are constants and

$$\begin{aligned} Q_0(z) =& \sqrt{\Omega_{d0}} \int_{z_1}^{z} y \left[1 + \sqrt{\frac{8}{3}} b \ln(y)\right] dy, \\ =& \frac{\sqrt{\Omega_{d0}}}{2} z^2 \left\{1 + \sqrt{\frac{8}{3}} b \left[\ln(z) - \frac{1}{2}\right]\right\} - \frac{\sqrt{\Omega_{d0}}}{2} z_1^2 \left\{1 + \sqrt{\frac{8}{3}} b \left[\ln(z_1) - \frac{1}{2}\right]\right\}. \end{aligned} \tag{9.35}$$

Like in the first quantisation procedure, we assume that z_1 is large enough to ensure a positive value of the above integral; in fact, it corresponds to the same scale factor u_1 that we used in the previous quantisation.

As can be seen, the wave function vanishes for large values of z, where the LR takes place. Therefore, the DW criterion is again fulfilled; this can be seen as an indication that our results do not depend on the chosen factor ordering.

Before concluding, we would like to highlight that both WKB solutions at first order can be related by

$$\frac{|\Psi_1(u)|^2}{|\Psi_2(z)|^2} = \frac{du}{dz}, \qquad \text{where} \qquad z = u^{\frac{3}{2}}, \tag{9.36}$$

where the equalities $D_1 = C_1$ and $D_2 = C_2$ have been assumed. At zero order, the two WKB solutions coincide as $(3/2)\, S_0(u) = Q_0(z)$.

9.4 WDW equation with a phantom scalar field

For a system with a single (phantom) scalar field and a given potential, the quantum Hamiltonian is written as [42, 51, 70, 151, 152]

$$\hat{\mathcal{H}} = N a_0^{-3} e^{-3x} \left\{\frac{\hbar^2}{4\pi^2}\left[\frac{\kappa^2}{6}\partial_x^2 + \partial_\phi^2\right] + 2\pi^2 a_0^6 e^{6x} V(\phi)\right\}. \tag{9.37}$$

Close to the LR we can approximate the potential as $V(\phi) \simeq b_1 \phi^4$. Since $\hat{\mathcal{H}}\Psi(x,\phi) = 0$, we have

$$\left\{\frac{\hbar^2}{4\pi^2}\left[\frac{\kappa^2}{6}\partial_x^2 + \partial_\phi^2\right] + \sigma e^{6x}\phi^4\right\}\Psi(x,\phi) = 0, \tag{9.38}$$

where we have gathered all parameters in a single one called σ which reads[ii]

$$\sigma \equiv 2\pi^2 a_0^6 b_1 = \frac{27}{128}\pi^2 a_0^6 \kappa^2 H_0^2 \Omega_{\mathrm{B}}. \tag{9.39}$$

[ii] This WDW equation can be solved following the method introduced in [35-37] and, in particular, invoking the Symanzik scaling law. We briefly summarise this method in Appendix. We thank the referee of our paper [202] for pointing out this method to us.

We next apply the following change of variables:

$$\phi = r\left(z\right)\varphi, \quad x = z, \tag{9.40}$$

where $r = r(z)$ is a function that only depends on the new variable z. Consequently, we have

$$\begin{aligned}\partial_{\phi}^{2} =& r^{-2}\partial_{\varphi}^{2},\\ \partial_{x}^{2} =& \left(\frac{r'}{r}\right)^{2}\left[\varphi^{2}\partial_{\varphi}^{2} + \varphi\partial_{\varphi}\right] - 2\frac{r'}{r}\varphi\partial_{\varphi}\partial_{z} + \left[\left(\frac{r'}{r}\right)^{2} - \frac{r''}{r}\right]\varphi\partial_{\varphi} + \partial_{z}^{2},\end{aligned} \tag{9.41}$$

where primes stands for derivatives with respect to z. Applying this change of variable and multiplying (9.38) by r^2, we get

$$\begin{aligned}&\left\{\frac{\hbar^{2}\kappa^{2}}{24\pi^{2}}r^{2}\left[\left(\frac{r'}{r}\right)^{2}\left[\varphi^{2}\partial_{\varphi}^{2} + \varphi\partial_{\varphi}\right] - 2\frac{r'}{r}\varphi\partial_{\varphi}\partial_{z} + \left[\left(\frac{r'}{r}\right)^{2} - \frac{r''}{r}\right]\varphi\partial_{\varphi} + \partial_{z}^{2}\right]\right.\\ &\left. + \frac{\hbar^{2}}{4\pi^{2}}\partial_{\varphi}^{2} + \sigma e^{6z}r^{6}\varphi^{4}\right\}\Psi(z,\varphi) = 0.\end{aligned} \tag{9.42}$$

Now, we choose $r\left(z\right) = e^{-z}$ with the aim to leave the potential term with a single dependence on the variable φ.

$$\left\{\frac{\hbar^{2}\kappa^{2}}{24\pi^{2}}e^{-2z}\left[\varphi^{2}\partial_{\varphi}^{2} + \varphi\partial_{\varphi} + 2\varphi\partial_{\varphi}\partial_{z} + \partial_{z}^{2}\right] + \frac{\hbar^{2}}{4\pi^{2}}\partial_{\varphi}^{2} + \sigma\varphi^{4}\right\}\Psi(z,\varphi) = 0. \tag{9.43}$$

We next assume that in (9.43) some terms can be neglected under the presumption

$$\begin{aligned}&\frac{\hbar^{2}\kappa^{2}}{24\pi^{2}}e^{-2z}\left[\varphi^{2}\partial_{\varphi}^{2} + \varphi\partial_{\varphi} + 2\varphi\partial_{\varphi}\partial_{z}\right]\Psi(z,\varphi) \ll \frac{\hbar^{2}\kappa^{2}}{24\pi^{2}}e^{-2z}\partial_{z}^{2}\Psi(z,\varphi), \frac{\hbar^{2}}{4\pi^{2}}\partial_{\varphi}^{2}\Psi(z,\varphi),\\ &\frac{\hbar^{2}\kappa^{2}}{24\pi^{2}}e^{-2z}\left[\varphi^{2}\partial_{\varphi}^{2} + \varphi\partial_{\varphi} + 2\varphi\partial_{\varphi}\partial_{z}\right]\Psi(z,\varphi) \ll \sigma\varphi^{4}\Psi(z,\varphi),\end{aligned} \tag{9.44}$$

for large values of z and φ which is the regime where we want to solve the partial differential equation (9.43). This approximation must be justified after obtaining the solutions for $\Psi(z,\varphi)$ (see appendix C.4 for details). As can be seen, after disregarding these elements in (9.43) we have two terms whereby each of them depends on a single variable. Therefore, we can employ a separation ansatz, and the wave function can be written as a sum over products of two functions,

$$\Psi\left(z,\varphi\right) = \sum_{k} U_{k}\left(\varphi\right)C_{k}\left(z\right)q_{k}, \tag{9.45}$$

where q_k denotes the amplitude for each solution and k is a constant related to the "energy" of the system which characterises the states described through the functions $C_k\left(z\right)$ and $U_k\left(\varphi\right)$. These functions, in turn, are the solutions of the following differential equations

$$\left\{\frac{\hbar^{2}\kappa^{2}}{24\pi^{2}}\partial_{z}^{2} + ke^{2z}\right\}C_{k}(z) = 0, \tag{9.46}$$

$$\left\{\frac{\hbar^{2}}{4\pi^{2}}\partial_{\varphi}^{2} + \sigma\varphi^{4} - k\right\}U_{k}(\varphi) = 0. \tag{9.47}$$

Equation (9.47) corresponds to the inverted anharmonic oscillator in QM; see, for example, [340]. For $C_k(z)$, we get exact solutions corresponding to Bessel functions with vanishing order:

- For $k > 0$

$$C_k(z) = C_{k1} J_0\left[\frac{2\pi}{\hbar\kappa}\sqrt{6k}\; e^z\right] + C_{k2} Y_0\left[\frac{2\pi}{\hbar\kappa}\sqrt{6k}\; e^z\right], \tag{9.48}$$

- For $k < 0$

$$C_k(z) = \tilde{C}_{k1} I_0\left[\frac{2\pi}{\hbar\kappa}\sqrt{6|k|}\; e^z\right] + \tilde{C}_{k2} K_0\left[\frac{2\pi}{\hbar\kappa}\sqrt{6|k|}\; e^z\right], \tag{9.49}$$

where C_{k1}, C_{k2} $\tilde{C}_{k1}$ and $\tilde{C}_{k2}$ are constants. Since the functions $I_0(z)$ diverge for $z \to \infty$ [307], we choose $\tilde{C}_{k1} = 0$ to ensure that the wave function vanishes close to the LR. For large values of z, we then get

- For $k > 0$

$$C_k(z) \sim \left[\frac{\hbar^2\kappa^2}{6\pi^4 k}\right]^{\frac{1}{4}} e^{-\frac{z}{2}}\left[C_{k1}\cos\left(\frac{2\pi}{\hbar\kappa}\sqrt{6|k|}\; e^z - \frac{\pi}{4}\right) + C_{k2}\sin\left(\frac{2\pi}{\hbar\kappa}\sqrt{6|k|}\; e^z - \frac{\pi}{4}\right)\right], \tag{9.50}$$

- For $k < 0$

$$C_k(z) \sim \tilde{C}_{k2}\left[\frac{\hbar^2\kappa^2}{96k}\right]^{\frac{1}{4}} e^{-\frac{z}{2}}. \tag{9.51}$$

The second order differential equation for $U_k(\varphi)$ is more difficult to solve. Disregarding the constant term k in (9.47), which is equivalent to finding the solution for $k = 0$, it can be written as (see the appendix A)[iii]

$$U(\varphi) = \sqrt{\varphi}\left\{U_1 J_{\frac{1}{6}}\left[\frac{2\pi\sqrt{\sigma}}{3\hbar}\varphi^3\right] + U_2 J_{-\frac{1}{6}}\left[\frac{2\pi\sqrt{\sigma}}{3\hbar}\varphi^3\right]\right\}, \tag{9.52}$$

where U_1 and U_2 are integration constants. For large values of φ, we have

$$U(\varphi) \sim \sqrt{\frac{6\hbar}{2\pi^2\sigma^{\frac{1}{2}}}}\frac{1}{\varphi}\left\{U_1\cos\left(\frac{2\pi\sqrt{\sigma}}{3\hbar}\varphi^3 - \frac{\pi}{3}\right) + U_2\sin\left(\frac{2\pi\sqrt{\sigma}}{3\hbar}\varphi^3 - \frac{\pi}{3}\right)\right\}, \tag{9.53}$$

and the wave function vanishes asymptotically. It is worth notice that for small values of the argument $(2\pi\sqrt{\sigma}/3\hbar)\,\varphi^3$ in (9.53) we have

$$U(\varphi) \sim U_1\left(\frac{\pi\sqrt{\sigma}}{3\hbar}\right)^{\frac{1}{6}}\frac{\varphi}{\Gamma\left(\frac{7}{6}\right)} - U_2\left(\frac{\pi\sqrt{\sigma}}{3\hbar}\right)^{-\frac{1}{6}}\frac{\Gamma\left(\frac{1}{6}\right)}{\pi}. \tag{9.54}$$

This limit seems to correspond to a regime where σ (which is proportional to the parameter Ω_{B}, i.e. quadratic in A^2) is small enough to ensure infinitesimal values of the argument in (9.52) even for large values of φ. It turns out that the term proportional to U_2 in (9.54) is not well defined when σ or A vanishes. This might indicate that the wave function for the ΛCDM universe is not well defined. However, this is not the case because when σ or A approaches zero $V(\phi)$ should be the one given in (9.17) rather than we used and defined in (9.15). In addition, the

[iii] Naively, we expect k to be irrelevant close to the LR where φ gets very large values; see below for a rigorous justification of this observation.

solution (9.54) was obtained after disregarding the term k in (9.47) which cannot be ignored in the case of small $\sigma\varphi^4$.

After performing the approximation ($k \ll [4\pi^2\sigma/\hbar^2]\varphi^4$) in (9.47), we can find an exact solution, but in return, we lose the information of k in $U_k(\varphi)$. A simple way to obtain an approximated wave function keeping the contribution of k is via the WKB approximation, the expression for the approximated wave function up to first order is given by

$$U(\varphi) \simeq \left[\frac{4\pi^2}{\hbar^2}\left(\sigma\varphi^4 - k\right)\right]^{-\frac{1}{4}} \left\{U_{k1}e^{iS_0(\varphi)} + U_{k2}e^{-iS_0(\varphi)}\right\}, \tag{9.55}$$

where U_{k1} and U_{k2} are constants and

$$S_0(\varphi) = \frac{2\pi}{\hbar}\int_{\varphi_1}^{\varphi} \sqrt{\sigma y^4 - k}\, dy\ , \tag{9.56}$$

where φ_1 is large enough to ensure a purely real solution even for positive values of k ($0 < \sigma\varphi_1^4 - k$). The latter integral can be expressed as follows (see pages 128 and 129 of [341])

- for $0 < k$

$$\int_{\varphi_1}^{\varphi} \sqrt{\sigma y^4 - k}\, dy = \frac{2\pi}{3\hbar}\left\{y\left(\sigma y^4 - k\right)^{\frac{1}{2}} - \sqrt{2}\frac{k^{\frac{3}{2}}}{\sigma^{\frac{1}{4}}}F\left[\arccos\left(\frac{k^{\frac{1}{4}}}{\sigma^{\frac{1}{4}}y}\right), \frac{1}{\sqrt{2}}\right]\right\}\Bigg|_{\varphi_1}^{\varphi}, \tag{9.57}$$

- for $k < 0$

$$\int_{\varphi_1}^{\varphi} \sqrt{\sigma y^4 - k}\, dy = \frac{2\pi}{3\hbar}\left\{y\left(\sigma y^4 + |k|\right)^{\frac{1}{2}} + \frac{|k|^{\frac{3}{2}}}{\sigma^{\frac{1}{4}}}F\left[\arccos\left(\frac{\sqrt{|k|} - \sqrt{\sigma}y^2}{\sqrt{|k|} + \sqrt{\sigma}y^2}\right), \frac{1}{\sqrt{2}}\right]\right\}\Bigg|_{\varphi_1}^{\varphi} \tag{9.58}$$

where the function $F\left[h(y), d\right]$ is an elliptic integral of the first kind with argument $h(y)$ and elliptic modulus d. Note that for $k = 0$ we recover the asymptotic solution given by the Bessel functions (9.52). For large values of φ the performed WKB approximation and the found Bessel functions has the same asymptotic behavior, in this limit, no matter what is the value of k. Therefore, for very large values of φ we can write

$$\Psi\left(z, \varphi\right) \simeq U\left(\varphi\right)\sum_k C_k\left(z\right) q_k, \tag{9.59}$$

In any case, the resulting wave function has two oscillatory terms modulated by a function which goes to zero for large values. Returning to the initial variables, for $z \to \infty$ and $\varphi \to \infty$ limits the wave function decrease as

$$\Psi(x, \phi) \sim \left[\phi e^{\frac{3}{2}x}\right]^{-1}. \tag{9.60}$$

Therefore, the wave function vanishes close to the LR, fulfilling the DW boundary condition.

9.5 Conclusions

A central issue in any theory of quantum gravity is the avoidance of classical singularities. At the present state of the field, this cannot be done in any sense close to the rigour of the classical

singularity theorems. The hope is thus to get some insight from suitable models for which concrete results can be obtained. As a heuristic sufficient (though not necessary) criterion of singularity avoidance, one can employ the DW criterion of vanishing wave function. The applicability of this criterion has already been studied for a wide class of classical singularities. In the present chapter, we have completed the discussion by studying the situation of the LR, which is strictly speaking not a singularity, like it is the case of a BR, but an abrupt event, though it shares some features with it. We have studied the two situations of a perfect fluid and of a phantom scalar field, the first being a phenomenological, the second a more fundamental dynamical model. A phantom field (field with negative kinetic energy) is needed in order to implement the EoS leading to a LR. We have found that the DW criterion can indeed be applied in both cases and that the LR can thus be avoided. We should emphasise that models such as these, although looking purely academic at first glance, are supported by data [85]. If indeed true, the future of the Universe would end in a full quantum era (without classical observers), in full analogy to its quantum beginning.

Some words about the applicability of the DW criterion (cf. (6.31) in [176]) are in order. It is based on the heuristic extrapolation of the quantum mechanical probability interpretation (based on the Schrödinger inner product) to quantum cosmology. But since the WDW equation is of hyperbolic nature (with and without matter), and thus resembles a Klein-Gordon equation, one might think that a Klein-Gordon inner product would be more appropriate. This is, however, not the case, because it was proven that one cannot separate positive and negative frequencies in the WDW equation, and thus one is faced with the problem of negative probabilites; see, for example, [151], Sec. 5.2.2 for a discussion and references. This problem can perhaps be avoided by going to "third quantisation", but this is a framework different from the present one. Our point of view here is that an inner product of the Schrödinger type can be used in quantum cosmology, even if the situation in the full theory is unclear[iv] and even if this poses the danger of not allowing normalisable solutions. At least in the models hitherto considered, this inner product can be implemented and the DW criterion can be applied.

In this chapter, we have restricted ourselves to the minisuperspace approximation. The real Universe is, however, not homogeneous, so one possible extension of our work is the inclusion of (scalar and tensor) perturbations and solving the WDW equation near and at the region of the LR. The full quantum state then describes an entanglement between the minisuperspace part and the perturbations. Tracing out the perturbation part from the full state leads to a density matrix ρ for the minisuperspace part. If the interaction with the perturbations leads to a suppression of the off-diagonal elements in ρ, one can interpret this as an effective quantum-to-classical transition or decoherence for the background. Decoherence in quantum cosmology was discussed in detail for many situations; see, for example, [342] and the references therein. One might expect that close to the LR region, decoherence stops and quantum interferences become important, enabling the DW criterion to be fulfilled there, as discussed in this chapter. Genuine quantum effects have also shown to be important near the turning point of a classically recollapsing universe [338]. We hope to address these and other issues in future publications.

[iv] The formalism of full loop quantum gravity, for example, employs a Schrödinger inner product.

10

The Quantum realm of the LS abrupt event

Knowledge and error flow from the same mental sources; only success can tell one from the other

– Ernst Mach

10.1 Introduction

From the early thinkers that devoted their reasoning to the nature of motion and the related conceptions of space and time, to modern theories of gravitation, geometry has always been an essential aspect of the epistemological bridge between observations and theory. General relativity (GR) opened the door for a dynamical role of space-time geometry in physics. GR was the main theoretical foundation for the development of relativistic astrophysics and modern cosmology. Accordingly, the evolution of black hole research inspired the formulation of the singularity theorems of Hawking and Penrose [343] (together with the cosmic censorship conjecture, excluding the possibility of naked singularities [344]). These efforts contemplated past and future singularities. The first, associated with the Big Bang, were supposed to obey the Weyl curvature hypothesis, following thermodynamical motivations [344], whereas future singularities in that time were of two types: astrophysical (gravitational collapse of a star into a black hole) and cosmological (big crunch scenarios). On the other hand, the remarkable evolution of research in cosmology, both theoretically and observationally, led to the most accepted paradigm of (ΛCDM) cosmology (with inflation), which still contains the unresolved puzzles of DM and DE [25, 193, 313, 345–347]. The empirical data supporting a present accelerated expansion (see for example [14]), motivated the re-appearance of the cosmological constant [190, 193, 313, 346]. Nevertheless, the absence for a corresponding physical theory (or an inconsistency with the quantum field predictions for the vacuum energy) remains. Moreover, a constant DE density gives the so called coincidence problem, i.e. the same order of magnitude at present time for the DM and DE densities. These issues inspired alternative descriptions. Dynamical DE models based on scalar fields were widely investigated and the research is still active.

From the point of view of physical ontology[i], the ideal study would follow from a fundamental theory describing the form of the equation of state for a DE fluid, based on the understanding of its origin and constituents. In fact, different cosmological evolutions can be explored depending on the nature of the energy-momentum tensor and on the equation of state (satisfying or transgressing some energy conditions). Until the present date, the nature of DE remains unclear, therefore cosmologists have been somewhat limited to testing different equations of state (and different potentials for the hypothetical scalar fields), and compute the resulting cosmic dynamics. In this context, dynamical DE models based on scalar fields have many applications. Some models try to unify DM and DE as in the case of the generalised Chaplygin gas [20, 41, 348]

[i] This chapter corresponds mainly to our publication [70]

and also early-time and late-time acceleration, see for example [102]. Other models assume an interaction between the DM and DE components (see [349] and [350] for recent observational constraints). But most importantly, was the discovery that dynamical DE models known as phantom energy (which might have a negative kinetic term) could give rise to a new type of singularity, the BR [28–35], in which the scale factor, the Hubble parameter and its cosmic time derivative diverge in a finite cosmic time. It was the beginning of the study of late-time or future singularities, or more generally, of cosmic singularities related to DE. Other types of singularities were discovered such as, Sudden singularity [47, 49, 54, 54], BF [45–47, 47, 60], type IV [45–47, 47, 58, 60, 62, 351], LR[55, 64–67, 201] and the recently investigated LS [69].

Future cosmic singularities or abrupt events are fascinating new areas of cosmology. Can these events be absent when the classical theory is quantised? Some works have applied the methods of quantum cosmology to the classical models leading to these DE related singularities [42–44, 48, 51, 52, 63, 247, 351–353]. In fact, dynamical DE models based on scalar fields (quintessence or phantom) provide a very interesting and suitable scenario to explore the quantum gravity challenge. Accordingly, in quantum cosmology the restriction to an isotropic and homogeneous Universe, simplifies substantially the general theory. The approach is done in the line of quantum geometrodynamics where a canonical quantisation of gravity (metric functions and conjugate momenta) is performed [151, 152]. The main purpose is to solve the WDW equation and apply appropriate boundary conditions, in order to get the wave function of the Universe [151, 152, 179]. In [42] it was shown that after solving the WDW equation with phantom DE with a corresponding exponential potential, the quantum effects dominate the region of the classical BR singularity, where classically the scale factor, the Hubble rate and it cosmic time derivative blow up at a finite future cosmic time. These authors found wave packets solutions that follow the classical trajectory and disperse in the genuinely quantum region. These quantum effects occur at large scales and since the solutions are regular the BR singularity is considered to be effectively avoided in the quantum analysis. The quantum cosmology of the classical Big Brake singularity was analysed in [51]. This is a type of Sudden future singularity where the Hubble rate reaches zero and the deceleration approaches infinity leading to an abrupt brake of the expansion[ii]. It was found that under reasonable assumptions, the DW criterium is satisfied, i.e. the wave function vanishes in the region of the classical singularity. The *Big Démarrage*, another kind of Sudden singularity, and the BF , the later can be seen as a BR happening at a finite scale factor, were also investigated in the quantum approach based on the WDW equation [48]. These singularities can result from a DE fluid with an appropriate generalised Chaplygin gas equation of state [60]. In the last mentioned cases (including type IV singularity), the DW criterium for singularity avoidance is satisfied, pointing to a possible avoidance of the singularities [48, 51, 63]. An essential result from all these works is that singularity avoidance in quantum cosmology necessarily predict quantum effects at scales much larger than the Planck length.

The heart of quantum cosmology is to apply the quantum theory to the Universe as a whole. This contrasts with the approach in which there is a classical theory with quantum effects (corrections) in certain phases of the evolution. Therefore, quantum cosmology must be based on

[ii] In fact, a Sudden singularity occurs at a finite scale factor where the Hubble rate is finite but its cosmic time derivative diverges. Depending on the parameters of the equation of state, this singularity can happen in the future as a Big Brake [51] or in the past. This second case, it what we named the *Big Démarrage*, it results from a phantom fluid leading to a cosmic expansion that starts with infinite acceleration [48].

a quantum theory of gravity. Three major promising approaches are String theory, Loop Quantum Gravity and Quantum Geometrodynamics, where the last two are different developments of Canonical Quantum Gravity [151, 152]. Independently of the correct theory of quantum gravity, the quantum cosmology based on the WDW equation should remain valid at least on energies below the Planck scale (if not on all scales) [151]. The two main challenges of quantum cosmology consist in i) finding a description of the dynamical evolution and ii) in finding the quantum state of the Universe with the appropriate initial or boundary conditions. These issues are interrelated although we do not have a robust theory for the boundary conditions or the initial quantum state [151, 152, 179]. Nevertheless, the WDW equation is crucial for the topic of boundary conditions in quantum cosmology. A relevant feature of the WDW equation is the fact that, for usual scalar fields, it is locally hyperbolic (taking the form of a wave equation) such that it has a well posed initial value problem. This fact is related to the indefinite sign of the kinetic term, which is directly linked to the attractive nature of gravity for usual matter [151]. The presence of a phantom field changes the structure of this equation, for example, if there is "phantom dominance", the WDW equation becomes elliptic (or parabolic), which changes the imposition of the boundary conditions. This is of extreme relevance since while the solutions of hyperbolic equations are "wave-like", a perturbation of the initial (or boundary) data of an elliptic (or parabolic) equation is felt "at once" by essentially all points in the domain. Another important aspect is related to the problem of time: the WDW equation is independent of an external time parameter. On the other hand, the origin of the arrow of time can in principle be related to the structure of this equation [42, 151].

In summary, the quantum cosmology of DE models leading to classical singularities, is showing very clearly that quantum effects are predicted at scales much larger than the Planck length and that it is possible to find solutions to the WDW equation that could effectively avoid the classical singularity. Many open questions remain, such as the appropriate boundary conditions, the classical-quantum correspondence, the problem of time and the interpretation of the wave function.

In this chapter, we apply the methods of quantum cosmology to the LS [69]. The quantisation of the classical model presented in [69] will be carried within the geometrodynamical approach given by WDW equation. We consider the case where the LS is induced by a perfect fluid, in which the scale factor is the single degree of freedom, and also the case where the LS is induced by a scalar field with phantom character; therefore in a cosmological model with two degrees of freedom. In the canonical quantisation we have $[\hat{a}, \hat{\pi_a}] \neq 0$, where $\hat{\pi}_a$ is the canonically conjugate momentum of the scale factor a, therefore in principle one can choose different "factor-ordering" in the derivation of the WDW equation [151]. Accordingly, for the case with a perfect fluid we will solve the WDW equation within a WKB approximation, for two different factor ordering choices. For the phantom scalar field case, we solve the WDW equation within the LB factor-ordering [151], with two degrees of freedom: the scale factor and a scalar field, which classically describe the geometry and the matter content respectively. The solutions are obtained using a Born–Oppenheimer (BO) approximation. In all the approaches, we impose the DW condition and find that it can be verified which might be an indication that the classical LS event can be avoided in the quantum description. As will be pointed in the conclusions, the DW condition on the wave function might not be sufficient to guarantee that all the relevant quantities which diverge in the classical model become finite in the quantum description. One should compute the corresponding expectation values and/or probability amplitudes of the physically

relevant quantities to have a complete analysis. In this work, we simply check if the DW condition can be verified. The calculation of the expectation values and the probability amplitudes requires further investigation since it is intimately linked to various open questions in quantum cosmology regarding the Hilbert space structure of the solutions and the classical-quantum correspondence.

The structure of the chapter is as follows: in section 10.2, we review the basic aspects of the classical model analysed in [69] and introduce a phantom scalar field which could induce a classical LS. Section 10.3 includes the quantum analysis for the case of a perfect fluid where the scale factor is the only degree of freedom; i.e. the LS is induced by a perfect fluid which can be fully determined through the scale factor which equally defines the geometry. We review the WDW equation, find its solutions using the WKB approximation and verify the DW condition using two different factor ordering. In section 10.4 we solve the WDW equation for the phantom scalar field case, using a BO approximation and evaluate the asymptotic behaviour of the corresponding solutions to see if the DW condition can be satisfied. Finally, in section V we present the conclusions. Three appendixes are also included: Appendix A contains some mathematical details of the WKB approximation used in section 10.3 and also the validity of this method. Some detailed calculations related to the Parabolic Cylinder functions appearing in section 10.4 are relegated to appendix C.3. Finally, in appendix C.3.1 we present the conditions for the validity of the BO approximation used in section 10.4.

10.2 The LS event driven by a scalar field

The dynamics of the perfect fluid previously described in 2.2.3 can be represented by a scalar field with a phantom character as given by Eqs (9.1) and (9.2). Using the equation of state (2.16) we get

$$\frac{d\phi}{da} = \pm\sqrt{\frac{\mathcal{C}}{3}}\frac{1}{aH(a)}, \qquad V(a) = \Lambda + \frac{\mathcal{C}}{6}\left[1 + 6\ln\left(\frac{a}{a_0}\right)\right], \tag{10.1}$$

and considering the (asymptotic) Friedmann equation (2.2), we get two sets of general solutions for the classical trajectory in configuration space:

$$\phi(a) = \pm\frac{1}{\sqrt{2\pi G}}\sqrt{\frac{\Lambda}{\mathcal{C}} + \ln\left(\frac{a}{a_0}\right)} + \phi_1, \tag{10.2}$$

where ϕ_1 is an integration constant fixed as

$$\phi_1 = \phi(a_0) \mp \frac{1}{\sqrt{2\pi G}}\sqrt{\frac{\Lambda}{\mathcal{C}}}. \tag{10.3}$$

The evolution of the scalar field in terms of $\alpha = \ln\left(\frac{a}{a_0}\right)$ is depicted in Fig. 10.1. Finally, equation (10.2) can be inverted and through (10.1) we get a uni-parametric family of quadratic potentials $V(\phi)$

$$V(\phi) = \frac{\mathcal{C}}{6} + 2\pi\mathcal{C}G\left(\phi - \phi_1\right)^2, \tag{10.4}$$

which is shown in Fig. 10.2.

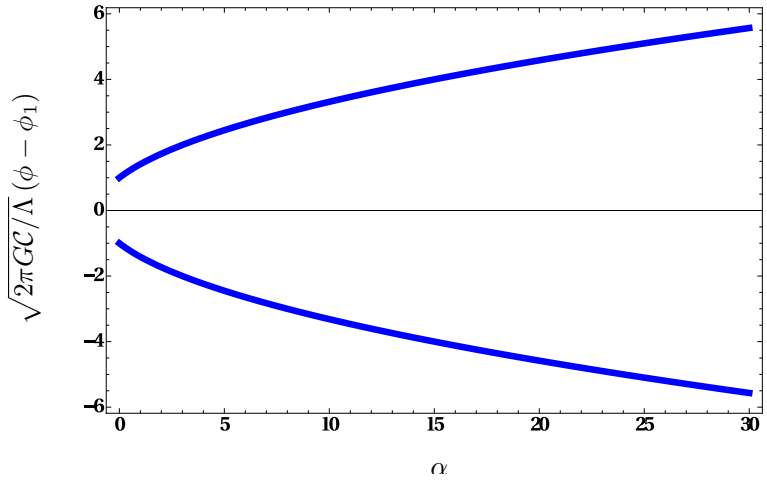

Figure 10.1: Plot of the scalar field versus the logarithmic scale factor, $\alpha = \ln(a/a_0)$, as given by the expression (10.2). The LS is located at large values of α.

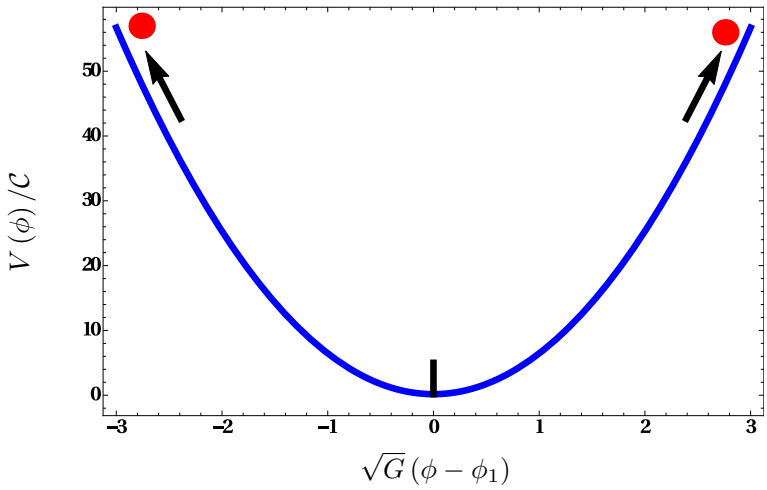

Figure 10.2: Plot of the potential (10.4). The small vertical line close to the origin corresponds to the initial value ϕ_1. The abrupt LS happens at large values as shown by the black arrows. The circles indicated schematically the occurrence of the LS.

10.3 WDW equation with a perfect fluid - WKB approximation

We start by considering the simplest case within the WDW equation where the matter content is given by a perfect fluid with a given equation of state, therefore whose energy density is specified by the scale factor. The scale factor a is then the only canonical variable, in consequence, the corresponding constraint $\mathcal{H} = 0$ is given by

$$-\frac{G}{3\pi}\frac{\pi_a^2}{a} - \frac{3\pi}{4G}ka + 2\pi^2 a^3\rho = 0. \tag{10.5}$$

This equation can be simplified, yielding precisely the Friedmann equation (2.2). As for the quantum model, depending on the factor ordering, we will get different equations. We will verify if the DW condition [151, 152], i.e the vanishing of the wave function when the scale factor goes to infinity for a ρ can be satisfied and if it depends on the factor ordering choice.

10.3.1 First quantisation procedure ($a\hat{\mathcal{H}}(a,\hat{\pi}_a)\psi(a)=0$)

The simplest way to obtain the WDW equation with the scale factor as the single degree of freedom is to multiply the Hamiltonian constraint, (10.5), by a and make the substitution $\pi_a \to \hat{\pi}_a = -i\hbar\frac{d}{da}$. The corresponding WDW equation is

$$\left[\hbar^2 \frac{G}{3\pi}\frac{d^2}{da^2} + V(a)\right]\psi(a) = 0, \tag{10.6}$$

where

$$V(a) = -\frac{3\pi}{4G}ka^2 + 2\pi^2 a^4 \rho(a). \tag{10.7}$$

For the case of a DE fluid obeying the equation of state (2.16), the wave function of the Universe obeys the following differential equation

$$\left\{\hbar^2 \frac{G}{3\pi}\frac{d^2}{da^2} - \frac{3\pi}{4G}ka^2 + 2\pi^2 a^4\left[\Lambda + \mathcal{C}\ln\left(\frac{a}{a_0}\right)\right]\right\}\psi(a) = 0, \tag{10.8}$$

and for $k=0$, it reduces to

$$\left\{\frac{d^2}{da^2} + \frac{6\pi^3}{\hbar^2 G}a^4\left[\Lambda + \mathcal{C}\ln\left(\frac{a}{a_0}\right)\right]\right\}\psi(a) = 0. \tag{10.9}$$

We perform the following changes to achieve a dimensionless WDW equation,

$$u \equiv \frac{a}{a_0}, \quad \Omega_\Lambda \equiv \frac{8\pi G}{3H_0^2}\Lambda, \quad \Omega_{\mathsf{C}} \equiv \frac{8\pi G}{3H_0^2}\mathcal{C}, \quad \eta \equiv \frac{\pi a_0^3 H_0}{G\hbar}. \tag{10.10}$$

Therefore, the equation (10.9) becomes

$$\left\{\frac{d^2}{du^2} + \left(\frac{3}{2}\eta\right)^2 u^4\left[\Omega_\Lambda + \Omega_{\mathsf{C}}\ln(u)\right]\right\}\psi(u) = 0. \tag{10.11}$$

Using the WKB (Wentzel, Kramers, Brillouin) approximation method at first order, which is enough to ensure that the DW condition is satisfied; i.e. $\Psi(u)$ vanishes for $u \to \infty$, the wave function of the Universe can be described by [44, 339]

$$\psi(u) \approx \sqrt{\frac{2}{3\eta}\frac{1}{u^2}}\left[\Omega_\Lambda + \Omega_{\mathsf{C}}\ln(u)\right]^{-\frac{1}{4}}\left\{C_1 e^{iS_0(u)} + C_2 e^{-iS_0(u)}\right\}, \tag{10.12}$$

where C_1 and C_2 are constants and the function $S_0(u)$ can be written according to (C.17) as

$$S_0(u) \approx \eta\frac{u^3}{2}\left[\Omega_\Lambda + \Omega_{\mathsf{C}}\ln(u)\right]^{\frac{1}{2}}. \tag{10.13}$$

10.3.2 Second quantisation procedure ($\hat{\mathcal{H}}(a,\hat{\pi}_a)\psi(a)=0$) LB factor ordering

The LB factor ordering is perhaps better motivated for two or higher dimensional WDW equations; i.e. with two or more physical degrees of freedom, since it is based on a covariant generalisation of the Laplacian operator in minisuperspace [151]. The starting point for the LB factor ordering for the case of a perfect fluid specified by the scale factor is to consider the wave equation obtained from the classical Hamiltonian constraint, (10.5), without multiplying

by a (c.f. also, for example, [44]). Therefore,

$$\left[-\frac{G}{3\pi}\frac{\hat{\pi}_a^2}{a}+2\pi^2 a^3\rho\right]\psi(a)=0, \tag{10.14}$$

here we are already restricting the analysis to a flat geometry ($k=0$). Introducing the change of variable

$$x\equiv\left(\frac{a}{a_0}\right)^{\frac{3}{2}}, \tag{10.15}$$

such that

$$\frac{\hat{\pi}_a^2}{a}=-\hbar^2\left[a^{-\frac{1}{2}}\frac{d}{da}\right]\left[a^{-\frac{1}{2}}\frac{d}{da}\right]=-\frac{9}{4}\frac{\hbar^2}{a_0^3}\frac{d^2}{dx^2}, \tag{10.16}$$

the expression (10.14) can be rewritten as

$$\left[\frac{d^2}{dx^2}+\tilde{V}(x)\right]\psi(a)=0. \tag{10.17}$$

Using the definitions of the parameters realised in (10.10), the effective potential $\tilde{V}(x)$ is the following

$$\tilde{V}(x)\equiv\eta^2x^2\left[\Omega_\Lambda+\frac{2}{3}\Omega_A\ln(x)\right]. \tag{10.18}$$

The general solution in the WKB, first order approximation, in this case also verifies the DW condition

$$\psi(x)\approx\frac{1}{\sqrt{\eta}}\left\{x^2\left[\Omega_\Lambda+\frac{2}{3}\Omega_A\ln(x)\right]\right\}^{-\frac{1}{4}}\left\{\tilde{C}_1e^{i\tilde{S}_0(x)}+\tilde{C}_2e^{-i\tilde{S}_0(x)}\right\}, \tag{10.19}$$

where $\tilde{C}_1$ and $\tilde{C}_2$ are constants and the function $\tilde{S}_0(x)$ can be written according to (C.17) as

$$\tilde{S}_0(x)\approx\eta\frac{x^2}{2}\left[\Omega_\Lambda+\Omega_A\ln(x)\right]^{\frac{1}{2}}. \tag{10.20}$$

10.4 Quantum study with a phantom scalar field: The BO approximation

In this section, we study the quantum behaviour of the LS using an approach based on considering a phantom scalar field. We consider the Born–Oppenheimer (BO) approximation for the the WDW equation and, as in the previous section, we check the fulfilment of the DW criterium as an indication of singularity avoidance.

To solve the WDW equation (7.10) we will now adopt the BO approximation which considers that the wave function can be factorised into two parts, corresponding to the geometric and matter parts. This is

$$\psi_k(\alpha,\phi)=\varphi_k(\alpha,\phi)C_k(\alpha). \tag{10.21}$$

The matter part $\varphi(\alpha,\phi)$ is assumed to satisfy the hypothesis of adiabatic dependence with the scale factor, such that the terms containing its derivatives with respect to α can be neglected. The consideration of the BO ansatz (10.21) in the WDW equation (7.10) leads to two differential equations, one for the geometric part of the wave function and the other for the matter part. Those are

$$\frac{\hbar^2}{2}\frac{\partial^2\varphi_k(\alpha,\phi)}{\partial\phi^2}+\left[a_0^6e^{6\alpha}V(\phi)-E_k(\alpha)\right]\varphi_k(\alpha,\phi)=0, \tag{10.22}$$

$$\frac{\kappa^2}{6}\frac{\partial^2C_k(\alpha)}{\partial\alpha^2}+k^2(\alpha)C_k(\alpha)=0, \tag{10.23}$$

where $k^2(\alpha)\equiv\frac{2}{\hbar^2}E_k(\alpha)$. In this approximation, the matter part of the wave function has no backreaction in the geometric part. The two equations become decoupled and the matter part has only an indirect influence on the geometric part through the eigenvalues $E_k(\alpha)$. The validity of this Born-Oppenheimer approximation is discussed in appendix C.3.

10.4.1 Solving the matter part

Substituting the potential given by (10.4), in the matter part of the WDW equation, (10.22), we obtain

$$\frac{\hbar^2}{2}\frac{\partial^2\varphi_k(\alpha,\phi)}{\partial\phi^2}+\left\{a_0^6e^{6\alpha}\left[\frac{\mathcal{C}}{6}+2\pi G\mathcal{C}\left(\phi-\phi_1\right)^2\right]-E_k(\alpha)\right\}\varphi_k(\alpha,\phi)=0. \tag{10.24}$$

This equation is not analogous to the quantum harmonic oscillator but is similar to a repulsor instead. This is a consequence of considering a phantom scalar field and rather than a usual (quintessence) scalar field. Therefore, the spectrum is continuous in this case and we can consider that $E_k(\alpha)=E_k$ and $k^2(\alpha)\equiv k^2$ are continuous parameters independent of α, where k is not restricted to real values. The solutions of (10.24) are (see appendix C.2 for details)

$$\varphi_k^{(1,2)}(\alpha,\phi)=W\left(\beta,\,\pm z\right), \tag{10.25}$$

$$\varphi_k^{(3)}(\alpha,\phi)=K^{-1/2}W\left(\beta,\,z\right)+iK^{1/2}W\left(\beta,\,-z\right), \tag{10.26}$$

and

$$\varphi_k^{(4)}(\alpha,\phi)=K^{-1/2}W\left(\beta,\,z\right)-iK^{1/2}W\left(\beta,\,-z\right), \tag{10.27}$$

where $W\left(\beta,\,z\right)$ is a parabolic cylinder function [307], $K=\sqrt{1+e^{2\pi\beta}}-e^{\pi\beta}$,

$$\beta=-\frac{1}{2\hbar(\pi G)^{1/2}}\left[\frac{\mathcal{C}^{1/2}a_0^3e^{3\alpha}}{6}-\frac{E_k}{\mathcal{C}^{1/2}a_0^3e^{3\alpha}}\right], \tag{10.28}$$

and

$$z=\frac{2a_0^{3/2}e^{3\alpha/2}(\pi GA)^{1/4}}{\hbar^{1/2}}(\phi-\phi_1). \tag{10.29}$$

Thus, the matter part of the wave function is a combination of these solutions [307]

$$\varphi_k(\alpha,\phi) = c_1\varphi_k^{(1)}(\alpha,\phi) + c_2\varphi_k^{(2)}(\alpha,\phi) + c_3\varphi_k^{(3)}(\alpha,\phi) + c_4\varphi_k^{(4)}(\alpha,\phi), \tag{10.30}$$

with c_i's constants. As we are dealing with a second order differential equation only at most two of the previous functions are linearly independent.

As shown in appendix C.2, in the limit $\alpha \to \infty$ these parabolic cylinder functions go as

$$W(\beta,\, z) \sim e^{-3\alpha/4}\cos(e^{3\alpha}), \tag{10.31}$$

and

$$W(\beta,\, -z) \sim e^{-3\alpha/4}\sin(e^{3\alpha}). \tag{10.32}$$

Therefore, the matter part of the wave function tend to zero when $\alpha \to \infty$ for arbitrary c_i's. This imply that the DW condition is satisfied if the geometric part of the wave function stays finite in this limit.

10.4.2 Solutions to the geometric part

The solutions of equation (10.23) are oscillatory for $E_k > 0$,

$$C_k(\alpha) = a_1 e^{i\frac{\sqrt{12E_k}}{\kappa\hbar}\alpha} + a_2 e^{-i\frac{\sqrt{12E_k}}{\kappa\hbar}\alpha}, \tag{10.33}$$

and have an exponential behaviour for $E_k < 0$

$$C_k(\alpha) = b_1 e^{\frac{\sqrt{12|E_k|}}{\kappa\hbar}\alpha} + b_2 e^{-\frac{\sqrt{12|E_k|}}{\kappa\hbar}\alpha}, \tag{10.34}$$

where a_1, a_2, b_1, b_2 are constants. Therefore, to make sure that DW criterion for singularity avoidance is fulfilled we impose $b_1 = 0$.

10.5 Conclusions and Outlook

The main purpose of the present work was to analyse the behaviour of the Universe when approaching a LS [69] within the framework of quantum cosmology [151, 152]. We have obtained the WDW equation in the context of quantum geometrodynamics for two cases: i) a perfect fluid with the equation of state (2.16) and ii) a dominant scalar field of phantom character whose potential is given in (10.4). We applied the DW criterium for singularity avoidance, namely the condition that the wave function should vanish in the region of the classical singularity. In the first case, the DW condition is satisfied, independently of the two factor ordering considered. This can easily be verified by the solutions obtained in the WKB approximation (10.12) and (10.19). For two degrees of freedom, we have also shown that it is possible to find solutions obeying the DW condition for any fixed value of the phantom field ϕ or even along the classical trajectory, c.f. the expressions (13.42), (10.26), and (10.27). These results might point to a possible resolution of the LS in the quantum description.

For the scalar field case, we used a BO approximation leading to two separate equations, one for the geometric part of the wave function and the other for the matter part. In this approximation, the matter part of the wave function has no backreaction in the geometric part. The two equations become decoupled and the matter part has only an indirect influence on the geometric part through the eigenvalues E_k. The solutions for the geometric part can be divergent (which we disregard) and convergent exponentials or oscillatory for $E_k < 0$ or $E_k > 0$, respectively. Due to the phantom character of the scalar field, the equation for the matter part is analogous to a quantum harmonic repulsor. The solutions of this equation are Parabolic Cylinder functions [307]. As it is shown in appendix C.2 in detail, these solutions vanish in the limit of arbitrarily large scale factor. Therefore, the DW condition is asymptotically satisfied.

The fundamental starting point for the classical model with the LS is the equation of state (2.16), slightly different from that of a cosmological constant. For the case of a perfect fluid, this relation, which is implicit in the energy density, is directly inserted in the WDW equation in the matter component. Since in this case the matter component has no implicit degrees of freedom, one can say that the traces of the LS equation of state are fully encapsulated in the geometric part of the WDW. On the other hand, for the phantom scalar field case, the WDW is two-dimensional and the LS signature can be inserted on the phantom part via the scalar field potential.

As mentioned in the introduction, the issue of boundary or initial conditions for the wave function is of extreme relevance in quantum cosmology and it still is in some sense an open question [151, 152]. The no-boundary wave function, the Tunnelling wave functions, were essentially motivated by the application of quantum cosmology to the very early Universe (see [179] and references therein). The no-boundary proposal was in some sense unique since it tried to bring together the dynamics and the problem of the initial state. Nevertheless, so far there is no unified theory of boundary conditions and dynamics from which that relation can be derived [179]. A more general suggestion, the one we used in this work, was first given by Bryce DeWitt, in what has been named the DW condition. It is a general condition imposed on the wave function saying that it should be zero in the regions corresponding to the classical singularities. Again, at the present moment there is no fundamental proof based on quantum gravity that the solutions to the WDW equation should obey this condition [179]. If this is found then one could say that the theory excludes the (geometric) singularity problems without any ambiguity.

For genuinely quantum regions, the correspondence between the classical and quantum predictions should in principle break down and these are expected to occur at the vicinity of classical singularities. Now, as pointed in the introduction, one way for this to happen is to get wave packets solutions (following the classical trajectory) that become smeared out in the classical singularity region, effectively avoiding it [42, 151] and another way is to have a decaying wave function in those regions, satisfying the DW condition [151]. The DW condition, taken as a criterium to avoid the classical singularities is based on the existence of square integral functions, and therefore on a consistent probability interpretation for the wave function. Accordingly the probability amplitudes for wave packets should vanish in the limit when the variables (of the representation) go to infinity. The problem is the fact that these square integral functions require an appropriate Hilbert space and it is not obvious that this can always be done in the quantum cosmology based on the WDW equation (c.f. for example the references [57, 181, 183, 204] for cases where this is doable).

The LS is an event happening in the limit when the scale factor goes to infinity, leading to the divergence of the Ricci parameter, the Hubble parameter and of course the dominant DE density. Can we avoid, with the quantum treatment, the region of configuration space corresponding to the divergent scale factor? As mentioned, in this chapter we tried to impose the DW condition on the solutions to the WDW equation in order to achieve this goal. What about the other quantities mentioned: how to compute them in the quantum geometrodynamics approach? In the quantum description, cosmological quantities such as the scale factor, the Hubble parameter (and its derivatives), or the Ricci curvature are represented by operators. Therefore, in principle if we have a normalised wave function in minisuperspace we can evaluate the expectation values and probability densities for these observables. Again, we emphasise the fact that the interpretation of the results for the expectation values in the quantum cosmology based on the WDW equation depends crucially on a consistent probability interpretation for the wave function and therefore on a minisuperspace with a proper Hilbert space nature, which remains an open question. Strictly speaking, the DW condition on the wave function is not sufficient to guarantee that all the relevant quantities which diverge in the classical model become finite in the quantum description. One should compute the corresponding expectation values and/or probability amplitudes to have a complete analysis. In this chapter, we simply checked if the DW condition could be verified. The calculation of expectation values and probability amplitudes requires further investigation since it is intimately linked to various open questions in quantum cosmology regarding a Hilbert space structure and the classical-quantum correspondence.

Nevertheless, it can be shown for the case with the scale factor as the single degree of freedom, for solutions (10.12) and (10.19) obtained in the WKB method, that the energy density expectation value is finite. If the effective Friedmann equation, obtained by replacing the classical quantities by the corresponding expectation values, remains valid, it would then imply that the Hubble rate expectation value is also finite in the quantum description. Nevertheless, this is not completely clear and requires further investigation, first of all because the calculation of the expectation value of the Hubble parameter depends on the factor ordering and second, because this effective Friedmann equation might be only valid for the classical regime. In fact, the standard quantum cosmology implied here, based on the WDW equation, is strictly speaking a canonical quantisation of the classical theory of GR. In the genuine quantum regions mentioned the classical gravitational theory of GR is expected to break and we might need a different theory of quantum gravity, although as it was mentioned in the introduction, many results regarding the WDW analysis of late time cosmology are expected to hold [42]. Does the (effective) Friedman equation $< \psi \left| \hat{H}^2(\hat{a}, \hat{\pi}_a) \right| \psi >= \frac{8\pi G}{3} < \psi \left| \hat{\rho}(\hat{a}) \right| \psi >$, using the solution to the WDW equation, correspond exactly to the classical one? If not, is there any region in minisuperspace in which it is valid, in accordance with the correspondence principle? Notice that the above expression contrasts with the semi-classical approach in which no quantisation is done in the geometric side of the Einstein equations, $R_{\mu\nu} - \frac{1}{2} g_{\mu\nu} R = \kappa^2 < \Psi \left| \hat{T}_{\mu\nu} \right| \Psi >$ (c.f. for example [354]). Historically this approach has been comparatively more explored, in which the energy momentum is replaced by the expectation value computed from the quantum state describing the matter, where Ψ is the wave function representing the degrees of freedom of some quantum field theory in the fixed background of curved space-time. These issues regarding the calculation of cosmological quantities in the quantum description and their relation to the classical model require further investigation.

Regarding the topic of future cosmic singularities, there are many open questions. First of all, what kind of observational predictions could distinguish between the different models with late-time acceleration and DE related singularities? Another interesting aspect implicit at least in some of these models is the possibility of matter-energy transgressing most or even all of the classical energy conditions. This lead to the idea that these conditions can be refined through semi-classical or purely quantum arguments [355–357]. A new door on the physics of phase transitions might be open if these non-linear quantum energy conditions (and their interpretations) are profoundly explored.

11

Doomsdays in a modified theory of gravity

If you know you are on the right track, if you have this inner knowledge, then nobody can turn you off… no matter what they say

– Barbara McClintock

11.1 Introduction

The scrutiny of extensions on GR is a well motivated topic in cosmology. Some phenomena, such as the current accelerating expansion of the Universe or gravitational singularities like the big bang, would presage extensions of GR in the infra-red as well as in the ultra-violet limits. Among these extensions, the EiBI theory [122], which is constructed on a Palatini formalism, is an appealing model in the sense that it is inspired by the Born-Infeld electrodynamics [123] and the big bang singularity can be removed through a regular stage with a finite physical curvature [122]. Various important issues of the EiBI theory have been addressed such as cosmological solutions [126, 129–133, 358], compact objects [125, 127, 140, 144–146], cosmological perturbations [134–136], parameter constraints [141–143], and the quantisation of the theory [203, 359]. However, some possible drawbacks of the theory were discovered in [128]. Finally, some interesting generalisations of the theory were proposed in [360–363].

As is known, the cause of the late time accelerating expansion of the Universe can be resorted to phantom DE, which violates the null energy condition (at least from a phenomenological point of view) while remains consistent with observations so far. Nonetheless, the phantom energy may induce more cosmological singularities in GR (curvature singularities). In particular there are three kinds of behaviors intrinsic to phantom models, which can be characterised by the behaviors of the scale factor a, the Hubble rate $H = \dot{a}/a$, and its cosmic derivatives $\dot{H}$ near the singular points: (a) The BR happens at a finite cosmic time t when $a \to \infty$, $H \to \infty$, and $\dot{H} \to \infty$ [28–35, 44, 364], (b) the LR happens at $t \to \infty$ when $a \to \infty$, $H \to \infty$ and $\dot{H} \to \infty$ [47, 55, 59, 64–67, 201, 202], (c) the LS happens at $t \to \infty$ when $a \to \infty$, $H \to \infty$, while $\dot{H} \to$ constant [69, 70, 205]. All these three scenarios would lead to the Universe to rip itself as all the structures in the Universe would be destroyed no matter what kind of binding energy is involved.

Interestingly, even though the EiBI theory can cure the big bang, in [129, 130] it was found that the BR and LR are unavoidable in the EiBI setup, hinting that the EiBI theory is still not complete and some quantum treatments near these singular events may be necessary. In this chapter[i], we will extend the investigations in [203] where we showed that the BR in the EiBI phantom model is expected to be cured in the context of quantum geometrodynamics. We will carry an analysis to encompass the rest of truly phantom DE abrupt events; i.e. the LR and LS.

[i] This chapter corresponds mainly to our publication [188]

11.2 The EiBI model: The LR and LS

In GR, the LR and LS can be driven (separately) by two phantom energy models as follows [66, 69]

$$p_{LR} = -\rho_{LR} - A_{LR}\sqrt{\rho_{LR}}\,, \qquad p_{LS} = -\rho_{LS} - A_{LS}\,, \tag{11.1}$$

where A_{LR} and A_{LS} are positive constants. Therefore,

$$\frac{\rho_{LR}}{\rho_0} = \Big(\frac{3A_{LR}}{2\sqrt{\rho_0}}\ln(a/a_0) + 1\Big)^2, \tag{11.2}$$

$$\rho_{LS} = 3A_{LS}\ln(a/a_0) + \rho_0\,, \tag{11.3}$$

where we take $\rho_{LR} = \rho_{LS} = \rho_0$ when $a = a_0$ [66, 69]. The abrupt events happen at an infinite future where a and ρ diverge. Inserting these phantom energy contents into the EiBI model, i.e., equations (7.13) and (7.14), and considering the large a limit (for ρ given in (11.3)), we have

$$\kappa H^2 \approx \frac{\bar{\rho}}{3} \to \infty\,, \qquad \kappa H_q^2 \approx \frac{1}{3}\,, \tag{11.4}$$

and

$$\dot{H} \approx \begin{cases} \frac{A_{LR}}{2}\sqrt{\rho_{LR}}\,, & \text{LR} \\ \frac{A_{LS}}{2}\,, & \text{LS} \end{cases} \tag{11.5}$$

for these two phantom energy models. Therefore, the LR and LS of the physical metric are unavoidable within the EiBI model while the auxiliary metric behaves as a dS phase at late time.

11.2.1 Quantisation of the system

The system described by the Lagrangian $\mathcal{L}$ is a constrained system. The conjugate momenta can be obtained as follows:

$$p_b \equiv \frac{\partial\mathcal{L}}{\partial\dot{b}} = -\frac{12\lambda b\dot{b}}{M}, \tag{11.6}$$

$$p_X \equiv \frac{\partial\mathcal{L}}{\partial\dot{X}} = 0, \tag{11.7}$$

$$p_Y \equiv \frac{\partial\mathcal{L}}{\partial\dot{Y}} = 0, \tag{11.8}$$

$$p_M \equiv \frac{\partial\mathcal{L}}{\partial\dot{M}} = 0. \tag{11.9}$$

Therefore, the system has the same three primary constraints as expressed in (7.18) in section 7.3, i.e. $p_X \sim 0$, $p_Y \sim 0$, $p_M \sim 0$ [311, 312]. Therefore, the secondary constraints coincide with those given in (7.20), (7.21), and (7.22). In consequence, the total Hamiltonian is a first class constraint of the system since the Poisson bracket of the total Hamiltonian with any constraint vanishes weakly by definition [311, 312]

$$\mathcal{H}_T = -MC_M + \lambda_X p_X + \lambda_Y p_Y + \lambda_M p_M \sim 0. \tag{11.10}$$

We remind that in this chapter we will focus on solving the WDW equation for a system when the DE content is described by a perfect fluid. Therefore, the auxiliary scale factor, b, is the true dynamical variable where the scale factor, a, plays the role of a parameter (it has no kinetic term). To construct the WDW equation, we impose the first class constraint $\mathcal{H}_T$ as a restriction

on the Hilbert space where the wave function of the Universe $|\Psi\rangle$ is defined, $\hat{\mathcal{H}}_T\,|\Psi\rangle = 0$. The hat denotes the operator. The remaining constraints $\chi_i = \{M,\, p_M,\, p_X,\, p_Y,\, C_X,\, C_Y\}$ are all second class constraints and we need to consider the Dirac brackets to construct the commutation relations and promote the phase space functions to operators [312]. Note that C_M can be used to construct the first class constraint $\mathcal{H}_T$, i.e., (11.10), so it is excluded from the set χ_i.

We follow the method introduced in section 7.3.1. Making use of the Dirac brackets defined by the set of equations (7.37) and selecting the XYb basis, we could define

$$\begin{aligned}
\langle XYb|\hat{b}|\Psi\rangle =& b\langle XYb|\Psi\rangle,\\
\langle XYb|\hat{X}|\Psi\rangle =& X\langle XYb|\Psi\rangle,\\
\langle XYb|\hat{Y}|\Psi\rangle =& Y\langle XYb|\Psi\rangle,\\
\langle XYb|\hat{p_b}|\Psi\rangle =& -i\hbar\frac{\partial}{\partial b}\langle XYb|\Psi\rangle\\
=& -f_1\frac{\partial}{\partial X}\langle XYb|\Psi\rangle - f_2\frac{\partial}{\partial Y}\langle XYb|\Psi\rangle,
\end{aligned} \tag{11.11}$$

it can be shown that the resulting commutation relations satisfy (7.36) and (7.37). Furthermore, the momentum operator $\hat{p_b}$ can be written as

$$\langle\xi\zeta b|\hat{p_b}|\Psi\rangle = -i\hbar\frac{\partial}{\partial b}\langle\xi\zeta b|\Psi\rangle, \tag{11.12}$$

after an appropriate redefinition of the wave functions: $\langle XYb| \rightarrow \langle\xi(X,Y,b),\zeta(X,Y,b),b|$. Therefore, in the new $\xi\zeta b$ basis, the modified WDW equation $\langle\xi\zeta b|\hat{\mathcal{H}}_T|\Psi\rangle = 0$ can be written as

$$\frac{-1}{24\lambda}\langle\xi\zeta b|\frac{\hat{p_b}^2}{b}|\Psi\rangle + V(b)\langle\xi\zeta b|\Psi\rangle = 0, \tag{11.13}$$

where the term containing $\hat{p_b}^2$ is determined by (11.12) and its explicit form depends on the factor orderings. Note that the eigenvalues X and Y can be written as functions of b according to the constraints C_X and C_Y, hence it leads to the potential $V(b)$ as follows

$$V(b) = \frac{2\lambda^2 b^3}{\kappa} + \frac{\lambda}{\kappa}b^3X(b)^2 - \frac{3\lambda}{\kappa}b^3Y(b)^2. \tag{11.14}$$

11.2.2 WDW equation: factor ordering 1

In order to prove that our results are independent of the factor ordering, we make two choices of it. First, we consider $\langle\xi\zeta b|b^3\hat{\mathcal{H}}_T|\Psi\rangle = 0$ and choose the following factor ordering:

$$b^2\hat{p_b}^2 = -\hbar^2\Big(b\frac{\partial}{\partial b}\Big)\Big(b\frac{\partial}{\partial b}\Big) = -\hbar^2\Big(\frac{\partial}{\partial x}\Big)\Big(\frac{\partial}{\partial x}\Big), \tag{11.15}$$

where $x = \ln(\sqrt{\lambda}b)$. Near the LR singular event, the energy density ρ behaves as $\rho \propto (\ln a)^2$. On that regime, the dependence between the auxiliary scale factor b and a is $b \propto a\ln a$. On the other hand, near the LS event the energy density behaves as $\rho \propto \ln a$ and b behaves as $b \propto a\sqrt{\ln a}$. For both cases, the WDW equation can be written as

$$\Big(\frac{d^2}{dx^2} + \frac{48}{\kappa\hbar^2}\mathsf{e}^{6x}\Big)\Psi(x) = 0, \tag{11.16}$$

when x and a go to infinity. Note that we have replaced the partial derivatives with ordinary derivatives and $\Psi(x) \equiv \langle \xi\zeta b|\Psi\rangle$. The wave function reads [307]

$$\Psi(x) = C_1 J_0(A_1 \mathrm{e}^{3x}) + C_2 Y_0(A_1 \mathrm{e}^{3x}), \tag{11.17}$$

and consequently when $x \to \infty$, its asymptotic behavior reads [307]

$$\Psi(x) \approx \sqrt{\frac{2}{\pi A_1}} \mathrm{e}^{-3x/2} \Big[C_1 \cos\Big(A_1 \mathrm{e}^{3x} - \frac{\pi}{4}\Big) + C_2 \sin\Big(A_1 \mathrm{e}^{3x} - \frac{\pi}{4}\Big)\Big], \tag{11.18}$$

where

$$A_1 \equiv \frac{4}{\sqrt{3\kappa\hbar^2}}. \tag{11.19}$$

Here $J_\nu(x)$ and $Y_\nu(x)$ are Bessel function of the first kind and second kind, respectively. It can be seen that the wave function vanishes when a and x go to infinity.

11.2.3 WDW equation: factor ordering 2

From the WDW equation (11.13), we can as well derive a quantum Hamiltonian by choosing another factor ordering

$$\frac{\hat{p_b}^2}{b} = -\hbar^2 \Big(\frac{1}{\sqrt{b}}\frac{\partial}{\partial b}\Big)\Big(\frac{1}{\sqrt{b}}\frac{\partial}{\partial b}\Big). \tag{11.20}$$

Before proceeding further, we highlight that this quantisation is based on the LB operator which is the Laplacian operator in minisuperspace [151]. This operator depends on the number of degrees of freedom involved. For the case of a single degree of freedom, it can be written as in (11.20). Under this factor ordering and after introducing a new variable $y \equiv (\sqrt{\lambda}b)^{3/2}$, in both cases (LR and LS) the WDW equation can be written as

$$\Big(\frac{d^2}{dy^2} + \frac{64}{3\kappa\hbar^2} y^2\Big)\Psi(y) = 0, \tag{11.21}$$

when a and y approach infinity. The solution of the previous equation reads [307]

$$\Psi(y) = C_1\sqrt{y} J_{1/4}(A_1 y^2) + C_2\sqrt{y} Y_{1/4}(A_1 y^2), \tag{11.22}$$

and when $y \to \infty$, therefore, [307]

$$\Psi(y) \approx \sqrt{\frac{2}{\pi A_1 y}} \Big[C_1 \cos\Big(A_1 y^2 - \frac{3\pi}{8}\Big) + C_2 \sin\Big(A_1 y^2 - \frac{3\pi}{8}\Big)\Big]. \tag{11.23}$$

Consequently, the wave functions approach zero when a goes to infinity. According to the DW criterium for singularity avoidance [176], the LR and LS is expected to be avoided independently of the factor orderings considered in this work.

11.2.4 Expected values

We have shown that the DW criterium of singularity avoidance is fulfilled hinting that the Universe would escape the LR and LS in the EiBI model once the quantum effects are important. We next estimate the expected value of the scale factor of the Universe a by estimating the

expected value of b. The reason we have to resort to the expected value of b rather than a is that in the classical theory [126] that we have quantised the dynamics is only endowed to the scale factor b. We remind at this regard that when approaching the LR and LS, $b \propto a \ln a$ and $b \propto a\sqrt{\ln a}$, respectively, at least within the classical framework. Therefore if the expected value of b, which we will denote as **b**, is finite, then we expect that the expected value of a; i.e. **a** would be finite as well. Therefore, non of the cosmological and geometrical divergences present at the LR and LS would take place.

We next present a rough estimation for an upper limit of **b** for the two quantisation procedures presented on the previous subsection.

- Factor ordering I:

  The expected value of b at late-time can be estimated as follows:

  $$\mathbf{b} = \int_{x_1}^{\infty} \Psi^* (x) \frac{e^x}{\sqrt{\lambda}} \Psi (x) \, dx, \tag{11.24}$$

  where x_1 is large enough to ensure the validity of the approximated potential in (11.16). In this limit, we can use the asymptotic behavior for the wave function c.f. (11.18). Then, it can be shown that the approximated value of **b** is bounded as

  $$\int_{x_1}^{\infty} \Psi^* (x) \frac{e^x}{\sqrt{\lambda}} \Psi (x) \, dx < \frac{|C_1|^2 + |C_2|^2}{\pi A_1 \sqrt{\lambda}} e^{-2x_1}. \tag{11.25}$$

  Therefore, we can conclude that **b** has an upper finite limit. Consequently, the LR and LS are avoided.

- Factor ordering II:

  In this case the expected value of b can be written as

  $$\mathbf{b} = \int_{y_1}^{\infty} \Psi^* (y) \frac{y^{\frac{2}{3}}}{\sqrt{\lambda}} \Psi (y) \, f (y) \, dy, \tag{11.26}$$

  where y_1 is large enough to ensure the validity of the approximated potential in (11.21). In addition, we have introduced a phenomenological weight $f (y)$ such that the norm of the wave function is well defined and finite for large y [57, 181, 183]. In fact, we could as well choose $f (y) = y^{-\alpha}$ with $2/3 < \alpha$. After some simple algebra, we obtain

  $$\mathbf{b} < \frac{2 \left(|C_1|^2 + |C_2|^2 \right)}{\pi A_1 \sqrt{\lambda}} \int_{y_1}^{\infty} y^{-\frac{1}{3}} f (y) \, . \tag{11.27}$$

  Consequently, we get

  $$\mathbf{b} < \frac{2 \left(|C_1|^2 + |C_2|^2 \right)}{\pi A_1 \sqrt{\lambda} \, (\alpha - 2/3)} y_1^{\frac{2}{3} - \alpha}. \tag{11.28}$$

  Once again, we reach the conclusion that **b** is finite. Therefore, the LR and LS are avoided.

11.3 Conclusions

Singularities seem inevitable in most theories of gravity. It is therefore natural to ask whether by including quantum effects would the singularities be removed. In the case of the EiBI scenario, while the big bang singularity can be removed, the intrinsic phantom DE doomsdays remain inevitable [130]. We solved the modified WDW equation of the EiBI model for a homogeneous and isotropic Universe whose matter content corresponds to two kinds of perfect fluid. Those fluids within a classical Universe would unavoidably induce LR or LS. We show that within the quantum approach we invoked, the DW criterion is fulfilled and it leads toward the potential avoidance of the LR and LS. Our conclusion appears unaffected by the choice of factor ordering.

12

Quantum cosmology of EiBI gravity fed by a scalar field: the BR event

Science is organised knowledge. Wisdom is organised life

– Immanuel Kant

12.1 Introduction

It is well known that Einstein's GR predicts the existence of spacetime singularities in several physical configurations. In [343, 365, 366], it has been proven that spacetime singularities, which are accompanied with an abrupt termination of timelike (lightlike) geodesics, exist as long as the matter fields satisfy the strong (null) energy condition. This is the definition of spacetime singularity based on the notion of the geodesic incompleteness. In this regard, the *attractive forces* between matter fields ensure the convergence of the geodesic congruence. At a certain spacetime point, the geodesics cannot be further extended and this is where the spacetime singularity is formally defined. For instance, GR predicts the existence of black hole singularities as well as the big bang singularity at the very beginning of the Universe.

Moreover, one should be aware that spacetime singularities are not restricted to small scales, they could in fact exist at large scales as well. In order to explain the late time accelerating expansion of the Universe, one may consider a Universe filled with some kinds of DE violating not only the strong energy condition, but also the null energy condition. This particular DE is called phantom DE and it could result in several cosmic curvature singularities in the future of the Universe [47]. The most famous cosmic singularity associated with phantom DE is the BR singularity [22, 28–35, 41, 46]. The size as well as the curvature of the Universe diverge at the singularity and in a finite cosmic time. Before the Universe reaches the singularity where the spacetime would be destroyed, all bound structures would be ripped asunder by the strong Hubble flow. In addition to the BR singularity, there exist several cosmic singularities and abrupt events that can be driven by phantom DE [54, 59, 60, 62, 65–67, 69].

In order to ameliorate the aforementioned spacetime singularities, one may resort to some quantum effects expected near the classical singularities[i]. One of the promising approaches to address this issue is based on the quantum geometrodynamics in which the WDW equation describes the quantum state of the Universe as a whole [151]. The WDW equation in GR is derived from the Hamiltonian constraint defined by Einstein equation. If the solution to the WDW equation satisfies the DW boundary condition [176], that is, it vanishes at the configuration corresponding to the classical singularity, one may claim that the singularity is then expected to be avoidable when quantum effects are taken into account. Following this direction, it has been shown in [42, 110] that the BR singularity in GR can be removed by quantum effects. The

[i]This chapter corresponds mainly to our publication [189]

quantum behaviors of other cosmological singularities, such as the SS [51], the BF singularity [48], the type IV singularity [63], the LR [202], and the LS [70], have also been discussed in the literature. It should be noticed that in some particular cases as shown in [57, 181, 183], a vanishing wave function at the classical singularity does not imply a vanishing probability because the measure used to define the probability diverges in those cases.

On the other hand, one can also address the spacetime singularities from a somewhat phenomenological point of view. Since a well-constructed and complete quantum theory of gravity is still lacking, one can consider some extended theories of gravity which not only reduce to GR in some proper limits, but also ameliorate spacetime singularities to some extent [367]. These theories of gravity can also be regarded as effective theories of an unknown quantum theory of gravity under some cutoff energy scales. Within this scope an interesting theory is the Eddington-inspired-Born-Infeld (EiBI) gravity [122]. This theory contains higher order correction terms of curvature as compared with GR and it removes the big bang singularity [132, 358, 368]. In addition, the EiBI cosmology [126, 133–136, 369], the astrophysical configurations [127, 144–146, 370–374], constraints of the parameters in the theory [141–143, 375, 376], and some generalisations of the EiBI theory [137, 360–363, 377–380] have been widely investigated in the literature (see [381] for a nice review of the EiBI gravity).

Even though the big bang singularity can be avoided in the EiBI theory, in our previous works [129, 130] we have shown that the BR singularity still exists in the classical theory. It is then natural to ask whether the BR singularity in the EiBI theory can be alleviated by quantum effects. In [203, 246], we considered a quantum geometrodynamical approach to address this issue by modeling the phantom DE as a perfect fluid. We have proven the existence of wave functions satisfying the DW boundary condition near the configuration of the BR and have therefore shown the possibility that the singularity can be avoided by quantum effects. In addition, some future abrupt events driven by phantom DE, such as the LR and the LS, have also been found avoidable under quantum effects in the EiBI model [188]. For another quantum treatment for the EiBI gravity, we refer to the scrutiny about the quantum tunneling effects of the singular instanton [359] and the regular instanton [382]. One of the important results is the formation of a Lorentzian wormhole during bubble materialisation shown in [382].

In this chapter[ii], we consider a more general matter content than the phantom perfect fluid to study the quantum avoidance of the BR singularity within the EiBI model. Specifically, we introduce a proper degree of freedom related to the matter sector described by a (phantom) scalar field ϕ minimally coupled to EiBI gravity to see whether a wave function satisfying the DW condition is attainable. In a homogeneous and isotropic Universe, there are two dynamical degrees of freedom in the system, one from the geometry side and the other from the matter side. We will start obtaining, for the first time, a consistent WDW equation for a Universe filled with a minimally coupled scalar field within the EiBI setup. We will prove that under a suitable BO approximation, a wave function satisfying the DW condition can be obtained. Therefore, the BR singularity is expected to be avoided by quantum effects.

This chapter is outlined as follows. In section 12.2, we concisely review the classical EiBI phantom model and exhibit how a BR singularity would occur by adding a phantom scalar field with

[ii] This chapter corresponds mainly to our publication [189]

a proper potential. In section 12.3, we construct the modified WDW equation by considering an alternative action in Einstein frame. The model corresponds to a constrained system and a thorough Hamiltonian analysis as well as the quantisation with the Dirac brackets are performed. In section 12.4, we solve the WDW equation by applying a BO approximation and show that the BR singularity is hinted to be avoided according to the DW criterion. We finally present our conclusions in section 12.5.

12.2 The EiBI model with a phantom scalar field: the BR singularity

In [129, 130], we have demonstrated that in the EiBI gravity, if the Universe is dominated by a phantom DE with a constant EoS parameter, $w < -1$, the Universe would end up at a BR singularity. In fact, making use of equation (7.13) the asymptotic behavior of the Hubble rate (defined through the physical metric) near the singularity can be expressed as

$$\frac{1}{N^2}H^2 \equiv \frac{1}{N^2}\Big(\frac{\dot{a}}{a}\Big)^2 \approx \frac{4\sqrt{|w|^3}}{3(3w+1)^2}\rho_0 a^{-3(1+w)}, \tag{12.1}$$

when a goes to infinity, where ρ_0 is the energy density of the phantom DE at present time. The dot denotes the cosmic time derivative. Therefore, H blows up which can be shown to be at finite cosmic time form now. Besides, the cosmic time derivative of H diverges as well when approaching the BR.

If the phantom DE considered in this setup is governed by a phantom scalar field ϕ and its potential $V(\phi)$, the energy density and pressure of this phantom scalar field can be written as[iii]

$$\rho_\phi = -\tfrac{\dot{\phi}^2}{2N^2} + V(\phi)\,, \tag{12.2}$$

$$p_\phi = -\tfrac{\dot{\phi}^2}{2N^2} - V(\phi)\,. \tag{12.3}$$

When the Universe is approaching the BR singularity, the energy density and pressure can be approximated as $\rho_\phi \approx \rho_0 a^{-3(1+w)}$ and $p_\phi \approx w\rho_0 a^{-3(1+w)}$. Combining (12.1), (12.2) and (12.3), one can obtain the asymptotic form of the scalar field as a function of a:

$$\phi(a) = \pm\sqrt{\frac{3|w+1|(3w+1)^2}{4\sqrt{|w|^3}}}\ln a, \tag{12.4}$$

and the scalar field potential

$$V(\phi) = A\boldsymbol{e}^{B|\phi|}, \tag{12.5}$$

where

$$A = \frac{\rho_0}{2}(1-w)\,, \qquad B = \sqrt{\frac{12|w+1|\sqrt{|w|^3}}{(3w+1)^2}}\,. \tag{12.6}$$

[iii] We will not consider DM on our approach because its effect is negligible in the asymptotic regime when the BR singularity is reached. Furthermore, we will only consider the case where κ is positive because of the instability problems usually present if $\kappa < 0$ [142, 143].

It can be seen that the BR singularity is accompanied by a divergence of the scalar field, i.e., $|\phi| \to \infty$ and its potential.

12.3 The WDW equation with a scalar field

As mentioned previously in section 7.3.1, we can use the second class constraints χ_i to simplify the Hamiltonian then derive the WDW equation. If we combine the constraints (7.29) and (7.30), we have

$$\lambda\Big(\frac{X}{Y^3}+\frac{1}{XY}\Big)=2\Big(\lambda+\kappa V(\phi)\Big). \tag{12.7}$$

After inserting this equation into (7.29), the Hamiltonian $\mathcal{H}_T$ can be simplified as follows

$$\mathcal{H}_T=M\Big(-\frac{p_b^2}{24\lambda b}+\frac{X}{Y^3}\frac{lp_\phi^2}{4b^3}+\frac{2\lambda b^3}{\kappa}(\lambda-Y^2)\Big)+\lambda_X p_X+\lambda_Y p_Y. \tag{12.8}$$

Note that $\lambda_M=0$ after the gauge fixing. Next, we will use the asymptotic behaviors of the constraints (7.29) and (7.30) near the singularity to replace X and Y in (12.8). Near the BR singularity, (7.29) and (7.30) can be approximated as ($l=-1$ for a phantom scalar field)

$$\frac{X}{Y^3}\approx\frac{\kappa}{\lambda}\rho_0 a^{-3(1+w)}\approx c_1 V(\phi), \tag{12.9}$$

and

$$Y^2\approx\frac{\lambda a^{3(1+w)}}{\sqrt{|w|}\kappa\rho_0}\approx\frac{c_2}{V(\phi)}, \tag{12.10}$$

where c_1 and c_2 are two positive constants defined as

$$c_1\equiv\frac{2\kappa}{(1+|w|)\lambda}\,,\qquad c_2\equiv(\sqrt{|w|}c_1)^{-1}. \tag{12.11}$$

Note that along the classical trajectory, we have $V(\phi(a))\approx Aa^{-3(1+w)}$ when approaching the singularity. The Hamiltonian can be written as

$$\mathcal{H}_T=M\Big[-\frac{p_b^2}{24\lambda b}-c_1V(\phi)\frac{p_\phi^2}{4b^3}+\frac{2\lambda b^3}{\kappa}\Big(\lambda-\frac{c_2}{V(\phi)}\Big)\Big]+\lambda_X p_X+\lambda_Y p_Y, \tag{12.12}$$

where the potential $V(\phi)$ is given by (13.34).

We construct the WDW equation as follows

$$\langle b\phi|b^3\hat{\mathcal{H}}_T|\Psi\rangle=0, \tag{12.13}$$

and choose, for simplicity, the following factor ordering

$$b^2\hat{p}_b^2 \qquad =-\hbar^2\Big(b\tfrac{\partial}{\partial b}\Big)\Big(b\tfrac{\partial}{\partial b}\Big)=-\hbar^2\Big(\tfrac{\partial}{\partial x}\Big)\Big(\tfrac{\partial}{\partial x}\Big), \tag{12.14}$$

$$e^{B|\phi|}\hat{p}_\phi^2 \;=-\hbar^2\Big(e^{B|\phi|/2}\tfrac{\partial}{\partial\phi}\Big)\Big(e^{B|\phi|/2}\tfrac{\partial}{\partial\phi}\Big)=-\hbar^2\Big(\tfrac{\partial}{\partial\tilde{\phi}}\Big)\Big(\tfrac{\partial}{\partial\tilde{\phi}}\Big). \tag{12.15}$$

Note that we have defined two new variables

$$x = \ln\left(\sqrt{\lambda}b\right), \qquad \tilde{\phi} = \mp\frac{2}{B}e^{-\frac{B}{2}|\phi|}, \tag{12.16}$$

where the minus (plus) sign in $\tilde{\phi}$ corresponds to a positive (negative) ϕ. Note as well that $\tilde{\phi} \to 0$ when $|\phi| \to \infty$, i.e., close to the BR singularity (on the classical trajectory, the relation between the two scale factors a and b is given in the footnote iv). Finally, the WDW equation becomes

$$\left[\frac{\hbar^2}{24}\partial_x^2 + \frac{\hbar^2}{4}\kappa\rho_0\partial_{\tilde{\phi}}^2 + \frac{2e^{6x}}{\kappa}\left(1 - c_3\tilde{\phi}^2\right)\right]\Psi(x,\tilde{\phi}) = 0, \tag{12.17}$$

where

$$c_3 \equiv \frac{f(w)}{\kappa\rho_0} \qquad \text{and} \qquad f(w) \equiv \frac{3|w(w+1)|}{(3w+1)^2}. \tag{12.18}$$

The absence of p_X and p_Y is due to the fact that they can be treated as zero operators at the quantum level.

12.4 The fulfillment of the DW condition

To solve the WDW equation (13.30), we apply a BO approximation. This method gives an approximated solution where the total wave function can be written as

$$\Psi(x,\tilde{\phi}) = \sum_k C_k(x)\varphi_k(x,\tilde{\phi}). \tag{12.19}$$

The BO approximation is valid as far as the derivatives of $\varphi_k(x,\tilde{\phi})$ with respect to x are negligible [see appendix C.3]. Within this assumption, the WDW equation given in (13.30) can be separated into the following two differential equations:

$$\left[\tfrac{\hbar^2}{24}\partial_x^2 + \tfrac{2e^{6x}}{\kappa} - E_k\right]C_k(x) = 0, \tag{12.20}$$

$$\left[\tfrac{\hbar^2}{4}\kappa\rho_0\partial_{\tilde{\phi}}^2 - \tfrac{2c_3}{\kappa}e^{6x}\tilde{\phi}^2 + E_k\right]\varphi_k(x,\tilde{\phi}) = 0, \tag{12.21}$$

where $C_k(x)$ is the solution to the gravitational part and $\varphi_k(x,\tilde{\phi})$ is the solution to the matter part. The decoupling constant between $C_k(x)$ and $\varphi_k(x,\tilde{\phi})$ is represented by the parameter E_k. We remind that the validity of the BO approximation should be justified once the solutions to the previous differential equations are obtained (we address this issue in the appendix C.3).

Let us start with the gravitational part. The solutions to the differential equation (12.20) are given by (cf. Eq 9.1.54 of [307])

$$C_k(x) = F_1 J_\mu\left[\alpha e^{3x}\right] + F_2 Y_\mu\left[\alpha e^{3x}\right], \tag{12.22}$$

where F_1 and F_2 are constants. On the other hand, $J_\mu\left[\alpha e^{3x}\right]$ and $Y_\mu\left[\alpha e^{3x}\right]$ are respectively, the first and the second kind Bessel functions of order μ and argument αe^{3x}. The values of the parameters μ and α are

$$\mu \equiv \frac{2\sqrt{6E_k}}{3\hbar} \qquad , \qquad \alpha \equiv \frac{4\sqrt{3}}{3\hbar\kappa^{\frac{1}{2}}}. \tag{12.23}$$

The asymptotic expressions for large arguments are given by (cf. Eqs. 9.2.1 and 9.2.2 of [307])

$$J_\mu\left[\alpha e^{3x}\right] \approx \sqrt{\frac{2}{\pi\alpha}} e^{-\frac{3}{2}x} \cos\left[\alpha e^{3x} - \frac{\pi}{4}(2\mu+1)\right], \tag{12.24}$$

$$Y_\mu\left[\alpha e^{3x}\right] \approx \sqrt{\frac{2}{\pi\alpha}} e^{-\frac{3}{2}x} \sin\left[\alpha e^{3x} - \frac{\pi}{4}(2\mu+1)\right]. \tag{12.25}$$

As can be seen, both kinds of Bessel functions vanish at large scale factors. As the total wave function is a product of the gravitational and matter part solutions (cf (12.19)), it is possible to ensure the compliance of the DW boundary condition for an arbitrary $\tilde{\phi}$ as long as the matter part solution is bounded with respect to the metric variable x when x gets very large.

Let us solve the differential equation corresponding to the matter part. Notice that (12.21) is the analogous to a Schrödinger equation for a harmonic oscillator. However, in the present case, there are some remarkable differences: $i)$ Due to the phantom nature of the scalar field, the sign in the kinetic operator is switched, i.e., it becomes positive, while the potential is negative. However, the relative sign between them is the same. $ii)$ The field $\tilde{\phi}$ can be positive or negative when reaching the BR at $|\tilde{\phi}| \to 0$. The solutions to (12.21) can be written as (cf. [383] chapters 16.5 and 16.51, pp .347-348)

$$\varphi_k(x,\tilde{\phi}) = C_1 D_\nu\left[r(x)\tilde{\phi}\right] + C_2 D_{-\nu-1}\left[ir(x)\tilde{\phi}\right], \tag{12.26}$$

where C_1 and C_2 are constants and $D_\nu[r(x)\tilde{\phi}]$ represents the parabolic cylinder function of order ν and argument $r(x)\tilde{\phi}$. The order and the argument of the parabolic cylinder function depend on the scale factor of the auxiliary metric through the variable x. Moreover, the parameter ν and the function $r(x)$ can be written as

$$\nu = \pm\frac{\kappa^{\frac{1}{2}} E_k}{\sqrt{2f(w)}\hbar} e^{-3x} - \frac{1}{2}, \tag{12.27}$$

$$r(x) = \beta e^{\frac{3}{2}x}, \qquad \text{where} \qquad \beta \equiv \left[\frac{32 f(w)}{\hbar^2 \rho_0^2 \kappa^3}\right]^{\frac{1}{4}}. \tag{12.28}$$

The DW condition is applied close to the singularity, i.e. at very large values of the scale factor[iv] a. Therefore, we focus on the limit $x \to \infty$. We will first consider the region where the argument $r(x)\tilde{\phi}$ is large. The reason of this priority is based on the classical trajectory. In fact, the classical trajectory is defined as

$$\tilde{\phi}(x) = \mp\frac{2}{B}\left[\sqrt{|w|}\kappa\rho_0\right]^{-\frac{h(w)}{2}} e^{h(w)x} \qquad \text{where} \qquad h(w) = -\frac{3(w+1)}{3w+1}. \tag{12.29}$$

Since the value of the EoS parameter is smaller than -1, the value of the exponent $h(w)$ is therefore negative. As expected, the classical limit of $\tilde{\phi}(x)$ tends to zero at large scale factors.

[iv] Recall that at the vicinity of the classical configuration corresponding to a BR singularity, the auxiliary scale factor b (or x) diverges because it can be related to the scale factor a via (12.10)

$$Y^2 = \frac{a^2}{b^2} \approx \frac{c_2}{V(\phi)}, \qquad \Longrightarrow \qquad c_2 b^2 \approx a^2 V(\phi) \to \infty,$$

when $a \to \infty$ and $V(\phi) \to \infty$.

Furthermore, the argument $r(x)\tilde{\phi}$ diverges classically since we have

$$r(x)\tilde{\phi} \approx \exp\left\{\left[\frac{3}{2}+h(w)\right]x\right\} = \exp\left[\left(\frac{3w}{3w+1}\right)x\right], \tag{12.30}$$

and $3w/(3w+1)$ is positive for $w<-1$. Hence, we will first focus on analysing the asymptotic behavior of (12.26) at large arguments, i.e., $r(x)\tilde{\phi}\gg 1$. This also corresponds to a region in the parameter space where the metric variable x is very large and $\tilde{\phi}$ is non-vanishing. Under this assumption, the order of the parabolic cylinder functions goes as $\nu\to -1/2$ while the argument diverges, i.e. $r(x)\tilde{\phi}\to\infty$. Therefore, the asymptotic behaviors of the solutions to the matter part read [383]

$$D_{-\frac{1}{2}}\left[r(x)\tilde{\phi}\right] \approx \quad e^{-\frac{\left[r(x)\tilde{\phi}\right]^2}{4}}\left[r(x)\tilde{\phi}\right]^{-\frac{1}{2}}, \tag{12.31}$$

$$D_{-\frac{1}{2}}\left[ir(x)\tilde{\phi}\right] \approx \quad e^{\frac{\left[r(x)\tilde{\phi}\right]^2}{4}}\left[r(x)\tilde{\phi}\right]^{-\frac{1}{2}}. \tag{12.32}$$

As the solution in (12.32) diverges very fast with respect to x, we select $C_2=0$ in order to ensure the compliance of the DW boundary condition. In addition, notice that for an order $\nu=-1/2$, the dependence on the decoupling constant E_k disappears and the solution to the matter part simply reads

$$\varphi_k(x,\tilde{\phi}) = \frac{C_1}{\sqrt{\beta e^{\frac{3}{2}x}\tilde{\phi}}}\exp\left[-\frac{\beta^2 e^{3x}\tilde{\phi}^2}{4}\right]. \tag{12.33}$$

Finally, the total wave function can be written as

$$\Psi_k(x,\tilde{\phi}) = C_k(x)\varphi_k(x,\tilde{\phi}) = \left\{\tilde{C}_1 J_\mu\left[\alpha e^{3x}\right]+\tilde{C}_2 Y_\mu\left[\alpha e^{3x}\right]\right\} D_\nu\left[r(x)\tilde{\phi}\right], \tag{12.34}$$

where $\tilde{C}_1$ and $\tilde{C}_2$ are constants and the asymptotic expression reads

$$\begin{aligned}\Psi_k(x,\tilde{\phi}) \approx & \sqrt{\frac{2}{\pi\alpha\beta\tilde{\phi}}}\exp\left[-\frac{9}{4}x-\frac{\beta^2}{4}(e^{3x}\tilde{\phi}^2)\right] \\ & \times\left\{\tilde{C}_1\cos\left[\alpha e^{3x}-\frac{\pi}{4}(2\mu+1)\right]+\tilde{C}_2\sin\left[\alpha e^{3x}-\frac{\pi}{4}(2\mu+1)\right]\right\}.\end{aligned} \tag{12.35}$$

As we have found vanishing solutions at large scale factors for both the gravitational and the matter parts, we can conclude that the total wave function vanishes at large scale factors and thus fulfills the DW boundary condition.

On the other hand, we bear in mind that at the quantum level the classical relation $\tilde{\phi}(x)$ given in (12.29) is meaningless and it just describes a curve where we expect to find confined the wave packet when approaching the semi-classical regime. There are regions in the parameter space, far away from the classical trajectory, where $\tilde{\phi}$ is small enough in such a way that the argument $r(x)\tilde{\phi}$ vanishes. For a vanishing argument $r(x)\tilde{\phi}$, the solution to the matter part given in (12.26) tends to a finite constant [307]. However, the total wave function is a product of the matter and the gravitational solutions, where the latter vanishes at large scale factors. Therefore, once the divergent solution on the matter part, (12.32), has been eliminated, it can be proven that for an arbitrary $\tilde{\phi}$ the total wave function vanishes at large scale factors.

12.5 conclusion

In this chapter, we have analysed the quantum avoidance of the BR singularity in the EiBI phantom model by using a quantum geometrodynamical approach. A complementary scrutiny has been carried out in our previous works [188, 203, 246] in which the phantom DE was described by a perfect fluid for the sake of simplicity. In this chapter, we consider a more general case in which the phantom DE is described by a phantom scalar field ϕ which adds an additional degree of freedom aside from the geometrical degree of freedom described by the scale factor of the Universe.

In the quantum geometrodynamics, the WDW equation plays a very important role since it essentially describes the quantum behavior of the whole Universe including the accompanied matter constituents. In order to obtain the WDW equation of this system, a correct and self-consistent Hamiltonian should be constructed at the classical level. One of the difficulties in the analysis of the model is from the affine structure of the EiBI theory since there are several additional auxiliary fields appearing in the system as compared with the GR case. However, in the end these additional auxiliary fields turn out to be reducible because of the corresponding second class constraints. We have identified all the first class and second class constraints in the system. More explicitly, one of the first class constraints p_M actually corresponds to a gauge degree of freedom and it can be fixed by adding an additional constraint. The other first class constraint is, not surprisingly, the Hamiltonian and it has been used to construct the WDW equation. The existence of second class constraints requires a more careful treatment. In practice, one needs to use the Dirac bracket to promote the canonical variables of a system with second class constraints to quantum operators. It turns out that the WDW equation can be significantly simplified and it becomes a second order partial differential equation with two dynamical variables x and $\tilde{\phi}$, as shown in (13.30).

To solve the WDW equation, obtained for the first time here for a minimally coupled scalar field in the EiBI theory of gravity, we impose a BO approximation on the wave function in the sense that the wave function can be decomposed into a gravitational part and a matter part. In the configuration where the classical BR singularity is approached (large value of the scale factor x), we have proven that there exist solutions whose total wave function always satisfies the DW boundary condition, no matter how the scalar field degree of freedom behaves. Therefore, the wave function vanishes near the configuration corresponding to the classical BR singularity and the BR singularity is thus hinted to be avoidable by quantum effects.

13

Eddington-inspired-Born-Infeld tensorial instabilities neutralized in a quantum approach

Life is really simple, but we insist on making it complicated

– Confucius

13.1 Introduction

It is commonly recognised that Einstein's GR, though very successful in describing our Universe, nonetheless suffers from several fundamental puzzles. On the very early stage of the Universe where the energy scale and the curvature scale were huge, say, close to the Planck scale, a purely classical description of gravity based on GR would not be sufficient. Actually, it is expected that a fundamental quantum theory of gravity is necessary such that some pathologies of GR at high energy scales can be resolved, such as the non-renormalizability of the theory and the issue regarding spacetime singularities. Whereas, it is still not clear so far how such a fundamental quantum gravity theory should be built in a self-consistent way. The development of a complete quantum theory of gravity is still an open question and it is certainly one of the most active research directions in modern theoretical physics[i].

From a more conservative point of view, to escape from the aforementioned theoretical swamp, one may resort to other modified theories beyond GR and regard them as effective theories of the unknown quantum theory of gravity [367]. It is likely that such extended theories of gravity, even presumably not complete, are already able to ameliorate the UV problems in GR. Among the plethora of extended theories of gravity, the Eddington-inspired-Born-Infeld gravity (EiBI) proposed in [122] is appealing in several theoretical aspects. First, it reduces exactly to GR in vacuum and deviates from it when matter fields are included. Second, due to the square root structure in the gravitational action, the curvature scale and the energy scale seem to be bounded from above and the big bang singularity is naturally avoided in the EiBI gravity. Third, the theory is simple in the sense that it only contains one free additional parameter, the Born-Infeld constant κ compared with GR. Fourth, it is free of ghost instabilities because the theory is constructed through the Palatini rather than the metric variational principle. Actually, the idea of including the Born-Infeld structure into the gravitational theory was proposed in [124]. However, the theory is built with the metric variational principle and it has ghost because of the higher order derivative terms in the field equations. The EiBI theory, on the contrary, is formulated via the Palatini variational principle. The field equations only contain second order derivatives and therefore no ghost is present in the theory. The applications and several properties of the EiBI gravity have been studied widely in the literature [126, 127, 129, 130, 132–138, 141–146, 358, 360–363, 368–379, 384, 385]. Some attempts to quantise the EiBI gravity have been proposed in [188, 189, 203, 246, 359, 382]. See also [381] for a nice review on the

[i]This chapter corresponds mainly to our publication [139]

EiBI gravity and other interesting Born-Infeld inspired theories of gravity. A further motivation to consider the EiBI theory is that the Born-Infeld type of theories, of which EiBI gravity is a subclass, have intrinsic Noether symmetries as shown in [386]. This is not surprising as the same happens in other modified theories of gravity [387]. For an interesting review on Noether symmetry, please see [388].

In this chapter, we will highlight an important issue regarding the viability of the EiBI theory. In the EiBI gravity, the big bang singularity in the physical metric is avoided by hiding the divergences of quantities in the second spacetime structure defined by the affine connection. The physical metric $g_{\mu\nu}$ is non-singular while the other metric, which we will call the auxiliary metric $q_{\mu\nu}$ later, turns out to be singular. Since the matter field is assumed to be coupled only to the physical metric, the singularity in the auxiliary metric seems to be unharmful for a physical observer. However, it has been proven in [134, 135] that the metric perturbations, especially the tensor perturbations, are actually unstable for the non-singular solutions in the EiBI gravity, jeopardising the validity of the theory. A more careful analysis in [138] reveals that the propagation of gravitational waves does see the structure of the auxiliary metric and it is the singularity in the auxiliary metric that gives rise to the linear instabilities of the theory. It should be noted that the problem of tensor instabilities mentioned above can be ameliorated for a positive Born-Infeld coupling constant if a time-dependent EoS parameter is considered [132].

In order to resolve this problem, we will suggest a quantum treatment to the EiBI gravity in the framework of quantum geometrodynamics. In this approach, the construction of the WDW equation is crucial since the WDW equation describes the quantum evolution of the Universe as a whole [151]. The derivation of the WDW equation stems from a self-consistent classical Hamiltonian, which and all the phase space functions are then promoted to quantum operators. The Hamiltonian, being a first class constraint of the system, turns out to be a restriction on the Hilbert space which is exactly the WDW equation. The strategy is to see whether the wave function would vanish near the configuration of the singularity in the auxiliary metric, satisfying the DW boundary condition [176]. If the answer is yes, it is then expected that the singularity can be avoided in the quantum world and the linear instabilities, which result from this singularity, can be naturally resolved. For the sake of completeness, we will consider two kinds of matter descriptions, one is the perfect fluid description and the other is the scalar field description. For the perfect fluid description, the matter field is governed by a perfect fluid with a constant EoS parameter. The system contains only one degree of freedom corresponding to the scale factor of the metric. As for the scalar field description, a scalar field degree of freedom is included into the system and the WDW equation turns out to be a partial differential equation with two independent variables. For each description and each non-singular solution, we will solve the corresponding WDW equation and we will exhibit that the DW condition can always be satisfied, indicating the resolution of the singularity in the auxiliary metric as well as the instabilities via quantum effects.

This chapter is outlined as follows. In section 13.2, we briefly review the non-singular cosmological solutions in the EiBI gravity, depending on different signs of the Born-Infeld parameter κ. We will also exhibit how the tensor instabilities are related to the singularity of the auxiliary metric. In section 13.3, we use the perfect fluid description and derive the WDW equations of the non-singular solutions with regard the physical metric for each sign of κ. The WDW equations

κ	Physical metric $g_{\mu\nu}$	Auxiliary metric $q_{\mu\nu}$
Positive	Loitering effects	Big Bang singularity
Negative	Bounce	Big Bang singularity

Table 13.1: This table summarises how the EiBI theory of gravity cures the big bang singularity in a radiation dominated Universe. If $\kappa > 0$, the big bang singularity in the physical metric is replaced with a loitering stage in which the Universe gets its minimum size in the infinite past. If $\kappa < 0$, the physical metric is described by a bouncing scenario in the past. However, there is still a big bang singularity in the auxiliary metric for both cases.

within the scalar field description are obtained in section 13.4. After deriving the WDW equation, we will obtain the wave function and see whether the solution satisfies the DW boundary condition near the singularity of the auxiliary metric. For the perfect fluid description and the scalar field description, the WDW equations will be solved, respectively, in sections 13.5 and 13.6. We finally conclude in section 13.7.

13.2 The classical Universe: big bang in the auxiliary metric

We start by considering EiBI gravity formulated by the action given in (7.11). It is well known that the EiBI gravity reduces to Einstein GR when matter fields are absent. However, the theory could have significant differences from GR when, say, the curvature and the energy density of the matter field take large values. Essentially, that is how the big bang singularity is removed in the EiBI gravity. The existence of the affine structure and its corresponding auxiliary metric actually plays a crucial role in the avoidance of singularities. The divergences of the physical metric at the singularity are *transferred* to the auxiliary spacetime, leaving the physical metric $g_{\mu\nu}$ non-singular. Since the matter field only sees the spacetime structure of the physical metric, the *hidden* singularity in the auxiliary metric seems unharmful for physical observers. Depending on the sign of the parameter κ, the big bang singularity can be replaced with a bouncing solution in the physical metric when $\kappa < 0$, or can be replaced with a *loitering stage* in which the Universe acquires its minimum size in the asymptotic past when $\kappa > 0$. Table 13.1 briefly summarises how the EiBI gravity cures the big bang singularity in the physical metric, and also points out the singularity appearing in the auxiliary metric.

In the following subsections, we will briefly review how the big bang singularity is avoided in the EiBI gravity with different signs of κ, and we shall point out the fact that the big bang singularity actually migrates to the *auxiliary* spacetime, i.e., the curvature invariants defined by the auxiliary metric diverge and the scale factor of the auxiliary metric is zero. We will illustrate it by considering a homogeneous and isotropic Universe filled with a perfect fluid with a constant and positive EoS parameter, $w > 0$. Then, we will mention how the instability issues in the physical metric arise alongside the auxiliary singularity, which motivates us for the quantum analysis in this work.

13.2.1 The big bang singularity in the auxiliary metric with $\kappa < 0$

If the Universe is dominated by a perfect fluid with energy density ρ and pressure $p = w\rho$, the equations of motion obtained from varying the action with respect to $g_{\mu\nu}$ relate algebraically

the two metrics to the matter sector as follows

$$\frac{\lambda X}{Y^3} = \lambda + \kappa\rho\,, \qquad \frac{\lambda}{XY} = \lambda - \kappa p = \lambda - \kappa w\rho\,. \tag{13.1}$$

From the above equations (13.1), one can see that when $\kappa < 0$ the energy density of the perfect fluid ρ is bounded from above by

$$\lambda + \kappa\rho \geq 0\,, \qquad \Longrightarrow \qquad |\kappa|\rho \leq \lambda\,. \tag{13.2}$$

Since the energy density $\rho \propto a^{-3(1+w)}$ is bounded from above, the physical scale factor has a minimum value a_{m1} satisfying $\rho\left(a_{m1}\right) = \lambda/|\kappa|$. The Hubble rate defined by the physical metric $H \equiv \dot{a}/a$, where the dot denotes the derivative with respect to t, reads [358]

$$H^2 \approx \frac{8N^2\left(a - a_{m1}\right)}{3|\kappa|a_{m1}}\,, \tag{13.3}$$

when $a \to a_{m1}$. By assuming a constant lapse function N, it can be proven that the big bang singularity in the physical metric is replaced with a bouncing solution in the sense that (13.3) can be integrated to get $a - a_{m1} \propto t^2$. To study the behavior of the auxiliary metric when $a \to a_{m1}$, we rewrite (13.1) as follows

$$\frac{\lambda^2}{Y^4} = \left(\lambda + \kappa\rho\right)\left(\lambda - \kappa w\rho\right)\,, \qquad \frac{X^4}{\lambda^2} = \frac{\lambda + \kappa\rho}{\left(\lambda - \kappa w\rho\right)^3}\,. \tag{13.4}$$

When $\rho \to \lambda/|\kappa|$ and $a \to a_{m1}$, (13.4) can be written as

$$b = \frac{a}{Y} \approx \frac{a_{m1}\left(1+w\right)^{1/4}}{\lambda^{1/4}}\left(\lambda + \kappa\rho\right)^{1/4} \to 0\,, \qquad X = \frac{N}{M} \approx \frac{b}{a_{m1}\left(1+w\right)} \to 0\,. \tag{13.5}$$

Therefore, at the bounce where $a = a_{m1}$, the auxiliary scale factor b vanishes. On the other hand, the scalar curvature defined by the auxiliary metric is given by

$$R[q] \equiv q^{\mu\nu}R_{(\mu\nu)} = \frac{1}{\kappa}\left(4\lambda - X^2 - 3Y^2\right)\,. \tag{13.6}$$

When $a = a_{m1}$, it can be seen that $R[q]$ diverges because $Y \to \infty$. Also, by suitably choosing the lapse functions, it can be shown that this divergence happens at a finite time t. Therefore, there is a big bang singularity in the auxiliary metric when $b = 0$.

13.2.2 The big bang singularity in the auxiliary metric with $\kappa > 0$

If κ is positive, the big bang singularity in the physical metric is again avoided in the EiBI gravity but in a different manner. In this case, according to (13.1), the energy density of the perfect fluid ρ is bounded from above by

$$\lambda - \kappa w\rho \geq 0\,, \qquad \Longrightarrow \qquad \kappa\rho \leq \frac{\lambda}{w}\,. \tag{13.7}$$

Therefore, the physical scale factor has a minimum value a_{m2} satisfying $\rho\left(a_{m2}\right) = \lambda/\left(w\kappa\right)$. The Hubble rate defined by the physical metric can be approximated as [358]

$$H^2 \approx \frac{8N^2\left(a - a_{m2}\right)^2}{3\kappa a_{m2}^2}\,, \tag{13.8}$$

when $a \to a_{m2}$. By assuming a constant lapse function N, the expression (13.8) can be integrated to get $a - a_{m2} \propto e^t$. It can be seen that the scale factor a takes its minimum value when $t \to -\infty$. The big bang singularity in the physical metric is thus avoided.

Regarding the asymptotic behavior of the auxiliary metric when $a \to a_{m2}$, we use (13.4) and consider the limit where $\rho \to \lambda/(w\kappa)$ to get

$$b \approx \frac{a_{m2}\,(1+w)^{1/4}}{(w\lambda)^{1/4}}\,(\lambda - \kappa w \rho)^{1/4} \to 0\,, \qquad X \approx \frac{(1+w)\,a_{m2}^3}{w b^3} \to \infty\,. \tag{13.9}$$

Therefore, the auxiliary scale factor b vanishes and it can be shown that the auxiliary curvature diverges when $b \to 0$. Also, by suitably choosing the lapse functions, it can be proven that this divergence happens at a finite time t. Therefore, there is a big bang singularity in the auxiliary metric.

13.2.3 The instability of linear perturbations

In the EiBI gravity, the big bang singularity in the physical metric can be avoided in the sense that the matter field is minimally coupled with the physical metric, hence the physical observers can only see the geometry of that metric, which is free of the big bang singularity. However, non-singular behaviors of the physical metric in the EiBI gravity are still problematic because of the tensor instabilities. Actually, it has been proven in [138] that these tensor instabilities are highly related to the singular behaviors of the auxiliary metric. In other words, the propagation of gravitational waves would be affected by the geometry of the auxiliary metric. The tensor instabilities in the EiBI gravity were firstly found in [134]. In addition, the instabilities of scalar mode and vector mode perturbations have been discovered in [135]. In this subsection, we will briefly review the tensor instabilities of the non-singular solutions in the EiBI gravity and it will become clear that these instabilities are indeed related to the singularity in the auxiliary metric.

Considering the tensor perturbations of the metrics such that the perturbed metrics are $\delta g_{ij} = a^2 h_{ij}$ and $\delta q_{ij} = b^2 \gamma_{ij}$, it has been proven in [389] that in the absence of any anisotropic stress, the transverse-traceless tensor perturbations of the two metrics are equivalent, that is, $h_{ij} = \gamma_{ij}$. The evolution of the tensor perturbation is described by the following equation [134, 135, 137, 138]:

$$\begin{aligned} &\ddot{h}_{ij} + \left(\frac{3\dot{b}}{b} - \frac{\dot{M}}{M}\right)\dot{h}_{ij} - \frac{M^2}{b^2}\nabla^2 h_{ij} \\ =&\ddot{h}_{ij} + \left(3H - \frac{3\dot{Y}}{Y} - \frac{\dot{N}}{N} + \frac{\dot{X}}{X}\right)\dot{h}_{ij} - \frac{N^2 Y^2}{X^2 a^2}\nabla^2 h_{ij} = 0\,. \end{aligned} \tag{13.10}$$

It can be seen that the propagation of the tensor mode is able to see the geometry of the auxiliary metric. When $\kappa < 0$, by using (13.3) and (13.5), it can be proven that the coefficient of the friction term in (13.10), that is, the $3\dot{b}/b - \dot{M}/M$ term, is proportional to $1/b^2$ when $b \to 0$. The coefficient of the last term, i.e., M^2/b^2, is proportional to $1/b^4$ in the same limit. Therefore, these two terms diverge and the tensor perturbation is severely unstable at the physical bounce. On the other hand, for a positive κ, the coefficients of both the friction term and the last term are proportional to b^4 when $b \to 0$. In this regard, the tensor mode behaves linearly in time.

Therefore, when approaching the loitering stage at $t \to -\infty$, the tensor mode grows linearly backward in time and it diverges in the asymptotic past.

As can be seen above and according to the results in [138], the instabilities of the tensor perturbations in the EiBI gravity indeed result from the divergence of the auxiliary metric. Even though the physical observers can only see the non-singular metric, the linear instabilities still jeopardise the validity of the theory. This motivates us to study whether the hidden singularity in the auxiliary metric can be resolved by including some sorts of quantum effects and we will address this issue in the following sections.

13.3 The WDW equation: perfect fluid

As mentioned in the previous section, the instability of linear perturbations in the EiBI gravity is highly associated with the divergences appearing in the auxiliary metric. Therefore, as long as such a singularity can be ameliorated by quantum effects, the instability problems can be naturally resolved. To address this issue, we shall consider a quantum geometrodynamical approach in which the WDW equation plays a central role. To derive the WDW equation, one is supposed to start with the correct classical Hamiltonian $\mathcal{H}_T$, which gives the classical equations of motion, and then promote the Hamiltonian to a quantum operator: $\mathcal{H}_T \to \hat{\mathcal{H}}_T$. In this regard, it can be proven that the Hamiltonian stands for a first class constraint, indicating that it corresponds to a restriction on the Hilbert space, more precisely, $\hat{\mathcal{H}}_T|\psi\rangle = 0$.

As we have done in the previous chapter, we use the action (7.15) which corresponds to the original EiBI action (7.11) transformed into its Einstein frame via a Legendre transformation [126, 381]. Therefore, for a system where the matter sector is described by means of a perfect fluid, the Lagrangian is given by (7.17) while the Hamiltonian, which represents a primary constraint of the system, it is given by (11.10). We remind that as in the previous chapter, there are six constraints, p_M, p_X, p_Y, C_M, C_X and C_Y (cf. (7.18)-(7.22)), where only p_M is first class constraint while the others are second class.

In [246], a thorough constraint analysis of this system has been carried out. Similarly, we have prceded in the same way in chapter 11. In the previous chapter 12, an improved investigation has been done in which the matter sector is assumed to be a scalar field rather than a perfect fluid. As expected, the Hamiltonian itself is a first class constraint and at the quantum level, it would be treated as a restriction on the Hilbert space, giving rise to the WDW equation. In addition, the equations of motion (13.1), which relate algebraically the metrics and the energy-momentum tensor, are exactly the secondary constraints of the system and they are second class constraints. In the presence of second class constraints, one has to resort to the Dirac brackets to promote the phase space functions to quantum operators [312]. By doing so, the second class constraints can be directly regarded as zero operators and the WDW equation can be significantly simplified.

In contrast as we did in chapter 11, we choose a basis $\langle b|$ rather than $\langle XYb|$ to write down the WDW equation $\langle b|\hat{\mathcal{H}}_T|\psi\rangle = 0$ as follows

$$\frac{-1}{24\lambda}\langle b|\frac{\hat{p}_b^2}{b}|\psi\rangle + V(b)\langle b|\psi\rangle = 0\,, \tag{13.11}$$

where the potential is the same given in (11.14). Note that the variables X and Y can be expressed as functions of b by imposing the second class constraints given by (13.1) in this model (see also (3.9) and (3.10) in [246]). Therefore, the potential $V(b)$ can be expressed as follows

$$V(b) = \frac{2\lambda^2 b^3}{\kappa} + \frac{\lambda}{\kappa} b^3 X^2(b) - \frac{3\lambda}{\kappa} b^3 Y^2(b)\,. \tag{13.12}$$

13.3.1 The WDW equation for $\kappa < 0$

In the perfect fluid description, the differential equation (13.11) and the potential (13.12) stands for a general expression of the WDW equation of the EiBI gravity. The explicit expression of $X(b)$ and $Y(b)$ are given by the constraints (13.1) and they depend on the cosmological solutions under consideration. In this subsection, we focus on the approximated cosmological solutions of the bouncing scenario for a negative κ, which has been discussed in subsection 13.2.1. In this case, we insert the approximated behaviors (13.5) to the potential $V(b)$ and the potential can be approximated as

$$V(b) = -\frac{2\lambda^2 b^3}{|\kappa|} - \frac{\lambda b^5}{|\kappa| a_{m1}^2 \left(1+w\right)^2} + \frac{3\lambda a_{m1}^2 b}{|\kappa|}\,, \tag{13.13}$$

when $b \to 0$. It can be also seen that when $b \to 0$, the last term on the right hand side dominates. We choose the following factor ordering

$$\frac{\hat{p}_b^2}{b} = -\hbar^2 \left(\frac{1}{\sqrt{b}}\frac{\partial}{\partial b}\right)\left(\frac{1}{\sqrt{b}}\frac{\partial}{\partial b}\right) \tag{13.14}$$

and introduce a new variable

$$y = (c_1 b)^{3/2}\,, \qquad \text{where} \qquad c_1^4 = \frac{a_{m1}^2 \lambda^2}{|\kappa|\hbar^2}\,. \tag{13.15}$$

The WDW equation when $b \to 0$ ($y \to 0$) can be written as

$$\left(\frac{d^2}{dy^2} + 32 y^{\frac{2}{3}}\right)\psi(y) = 0\,. \tag{13.16}$$

Note that only the last term on the right hand side of (13.13) is considered because it dominates the potential when $b \to 0$.

13.3.2 The WDW equation for $\kappa > 0$

In this subsection, we shall derive the approximated WDW equation when $b \to 0$ in the EiBI gravity with a positive κ. In this case, we insert the asymptotic equations (13.9) into the potential (13.12), and the potential can be approximated as

$$V(b) = \frac{2\lambda^2 b^3}{\kappa} + \frac{\lambda \left(1+w\right)^2 a_{m2}^6}{\kappa w^2 b^3} - \frac{3\lambda a_{m2}^2 b}{\kappa}\,. \tag{13.17}$$

It can be seen that when $b \to 0$, the second term on the right hand side dominates. To proceed, we choose the same factor ordering as given in (13.14), and introduce a new variable

$$z = b^{3/2}\,. \tag{13.18}$$

The WDW equation when $b \to 0$ ($z \to 0$) can be written as

$$\left(\frac{d^2}{dz^2} + \frac{c_2}{z^2}\right)\psi(z) = 0\,, \tag{13.19}$$

where c_2 is a positive constant and it is defined as

$$c_2 = \frac{32\lambda^2\left(1+w\right)^2 a_{m2}^6}{3\kappa\hbar^2 w^2}\,. \tag{13.20}$$

Note that only the second term on the right hand side of (13.17) is considered since it dominates the potential when $b \to 0$.

13.4 The WDW equation: scalar field

In the previous section, we have derived the WDW equations near the singularity of the auxiliary metric by using a perfect fluid description. The quantum system has only one degree of freedom in the sense that the WDW equation turns out to be an ordinary differential equation of a single variable, the scale factor b. However, the assumption of the perfect fluid description is just for convenience and may not be complete to describe the quantum evolution of the Universe in a satisfactory manner. For the sake of completeness, in this section we will introduce an additional degree of freedom, the scalar field ϕ minimally coupled to the EiBI gravity, to describe the matter sector of the gravitational system. In the classical regime, it is well-known that the properties of a perfect fluid, including its EoS and evolution, can be described by a scalar field when a corresponding potential $V(\phi)$ is chosen. In the quantum regime, on the other hand, the two degrees of freedom from the geometrical sector and from the matter sector do not necessarily relate to each other as in the classical regime. In this regard, the WDW equation becomes a partial differential equation of two variables b and ϕ. To have a more complete picture of the quantum behavior of the Universe near the singularity, we will solve the wave function and investigate how the wave function evolves in the two dimensional (b, ϕ) space. We shall mention that in [189], the quantum avoidance of the big rip singularity in the EiBI gravity has been studied by solving the WDW equation with two degrees of freedom, one from the geometrical sector and the other is the phantom scalar field from the matter sector.

Considering a homogeneous and isotropic metric and assuming a scalar field minimally coupled to the gravity sector, the reduced Lagrangian is given in (7.25) while the corresponding Hamiltonian, obtained by making use of the conjugate momenta defined in (7.26) and (7.26), it is given in (7.29).

The complete constraint analysis of this system has been carried out in chapter 7. It turns out that the Hamiltonian is again a first class constraint as expected and it becomes a restriction in the Hilbert space at the quantum level. p_M is another first class constraint and it corresponds to a gauge degree of freedom which can be fixed by assuming the lapse function M to be a constant. It should be stressed that in the EiBI theory, there are two additional second class constraints which correspond to two algebraic relations in the theory. In the perfect fluid description, these second class constraints are given by (13.1). In the scalar field description, on the other hand, these constraints are also given by (13.1) but one has to substitute the energy density and the pressure by their scalar field counterparts, ρ_ϕ and p_ϕ, respectively. The explicit expressions of

these second class constraints are given in (7.29) and (7.30). Essentially, once we introduce the Dirac brackets to promote the phase space functions to quantum operators, the second class constraints can be regarded as zero operators [312]. As a result, the total Hamiltonian can be significantly simplified [189]

$$\mathcal{H}_T = M\left(-\frac{p_b^2}{24\lambda b}+\frac{X}{Y^3}\frac{p_\phi^2}{4b^3}+\frac{2\lambda b^3}{\kappa}\left(\lambda-Y^2\right)\right)+\lambda_X p_X+\lambda_Y p_Y\,. \tag{13.21}$$

Note that at the quantum level, the last two terms can be omitted since p_X and p_Y are also second class constraints. We shall emphasise that (13.21) is still not the final expression of the WDW equation that we are going to study. The final expression of the WDW equation is expected to be a partial differential equation of b and ϕ. After inserting $p_X \sim 0$ and $p_Y \sim 0$, there remain two variables X and Y in (13.21). Technically, we have to use again the second class constraints to relate these two variables to the phase space variables b, p_b, ϕ, and p_ϕ. It can be expected that these relations would depend on the cosmological models under consideration and also on the scalar field potential that we choose in the model. Different choices of the cosmological solutions and potentials certainly change the expressions of the second class constraints, hence change the quantisation of the system and also the expression of the WDW equation. In the following two subsections, we will first consider the cosmological solution near the singularity of the auxiliary metric for a negative κ and rewrite the WDW equation as a partial differential equation from which the wave function can be solved. A similar study for a positive κ will be presented in the subsection 13.4.2.

13.4.1 The WDW equation for $\kappa < 0$

The energy density, ρ_ϕ, and its pressure, p_ϕ, can be described by a scalar field ϕ and its potential $V(\phi)$ as given in (12.2) and (12.3). Note that we have used a lower index ϕ to highlight that the energy density and the pressure are described through the dynamics of a scalar field. For the EiBI gravity with a negative κ, the physical Hubble rate near the bounce $a \to a_{m1}$ $(b \to 0)$ is approximated as in (13.3). On the other hand, the conservation of the energy-momentum tensor implies that the energy density and the pressure, if expressed as a function of the scale factor a, read $\rho_\phi \approx \rho_0 a^{-3(1+w)}$ and $p_\phi \approx w\rho_0 a^{-3(1+w)}$, respectively, where ρ_0 is an integration constant and w stands for the EoS defined by $w \equiv p_\phi/\rho_\phi$. Using the approximated Hubble rate (13.3) and (12.2)-(12.3), we obtain the asymptotic expression of the scalar field as a function of the scale factor a near the bounce:

$$\phi\left(\delta a\right) = \phi_0 + 2A\sqrt{\delta a}\,, \tag{13.22}$$

where $\delta a \equiv a - a_{m1}$ and

$$A \equiv \sqrt{\frac{3|\kappa|\rho_0\left(1+w\right)a_{m1}^{-3(1+w)-1}}{8}} = \sqrt{\frac{3\lambda\left(1+w\right)}{8a_{m1}}}\,. \tag{13.23}$$

On the above equations, ϕ_0 is an integration constant and it is the value of the scalar field when $\delta a = 0$. Furthermore, using again (12.2) and (12.3), the scalar field potential can be expressed with the EoS parameter w and it approaches a constant

$$V\left(\phi\right) \approx \frac{\lambda}{2|\kappa|}\left(1-w\right)\,, \tag{13.24}$$

when $\delta a \to 0$.

Now, we shall rewrite the WDW equation (13.21) in such a way that it only contains the phase space variables b, ϕ, and their conjugate momenta. According to (13.5), we get the following approximated equations:

$$\frac{X}{Y^3} \approx \frac{b^4}{(1+w)\, a_{m1}^4}\,, \qquad Y^2 \approx \frac{a_{m1}^2}{b^2}\,, \tag{13.25}$$

when $b \to 0$. Using (13.25), the Hamiltonian can be written as

$$\mathcal{H}_T = M\left[-\frac{p_b^2}{24\lambda b} + \frac{b}{4\,(1+w)\, a_{m1}^4} p_\phi^2 - \frac{2\lambda b^3}{|\kappa|}\left(\lambda - \frac{a_{m1}^2}{b^2}\right)\right] + \lambda_X p_X + \lambda_Y p_Y\,. \tag{13.26}$$

We would like to stress again that if we use the Dirac brackets to promote the phase space functions to quantum operators, the second class constraints can be treated as zero operators. That is why we can use (13.25) to simplify the WDW equation. Actually, the second class constraints that correspond to the above substitutions are secondary constraints, which are also the equations of motion of the theory, i.e., (13.4). More strictly speaking, one should first use the Dirac brackets to promote the phase space functions to quantum operators, obtaining the Hamiltonian operator $\hat{\mathcal{H}}_T$. Then one regards the second class constraints as zero quantum operators and make the substitutions mentioned above. In the aforementioned procedures, it looks like we are doing it the other way around, that is, making substitutions at the classical level then promoting the phase space functions to operators. In either case, the final expression of the WDW equation is the same. Therefore, we will use the Hamiltonian (13.26) to construct the WDW equation.

After promoting the phase space functions to quantum operators and simplifying the Hamiltonian operator with the second class constraints, we construct the WDW equation as follows

$$\langle b\phi | \frac{\hat{\mathcal{H}}_T}{b} |\psi\rangle = 0\,, \tag{13.27}$$

and choose the following factor ordering

$$\begin{aligned}\left(\frac{\hat{p}_b}{b}\right)^2 &= -\hbar^2\left(\frac{1}{b}\frac{\partial}{\partial b}\right)\left(\frac{1}{b}\frac{\partial}{\partial b}\right) = -\hbar^2\left(\frac{\partial}{\partial x}\right)\left(\frac{\partial}{\partial x}\right)\,,\\ \hat{p}_\phi^2 &= -\hbar^2\left(\frac{\partial}{\partial \phi}\right)\left(\frac{\partial}{\partial \phi}\right)\,.\end{aligned} \tag{13.28}$$

Note that we have defined a new variable

$$x = \frac{b^2}{2}\,, \tag{13.29}$$

to label the scale factor of the auxiliary metric. Finally, the WDW equation becomes

$$\left[\frac{\hbar^2}{24\lambda}\partial_x^2 - \frac{\hbar^2}{4\,(1+w)\, a_{m1}^4}\partial_\phi^2 - \frac{4\lambda x}{|\kappa|}\left(\lambda - \frac{a_{m1}^2}{2x}\right)\right]\psi(x,\phi) = 0\,. \tag{13.30}$$

Near the singularity ($x \to 0$) of the auxiliary metric, the WDW equation (13.30) can be further approximated as

$$\left[\frac{\hbar^2}{24\lambda}\partial_x^2 - \frac{\hbar^2}{4\,(1+w)\, a_{m1}^4}\partial_\phi^2 + \frac{2\lambda}{|\kappa|}a_{m1}^2\right]\psi(x,\phi) = 0\,. \tag{13.31}$$

In the next section, we will solve this equation (13.31) to get the asymptotic behavior of the wave function $\psi(x,\phi)$ near the singularity ($x \to 0$, $\phi \to \phi_0$) with a negative κ.

13.4.2 The WDW equation for $\kappa > 0$

As shown explicitly in section 13.2, the EiBI theory of gravity with a positive κ resolves the big bang singularity quite differently as compared with the situation for a negative κ. When $\kappa > 0$, the asymptotic behavior of the physical Hubble function is given by (13.8) when the physical scale factor approaches its minimum value $a \to a_{m2}$ ($b \to 0$). Note that this happens at $t \to -\infty$ for a constant lapse function N. If the density and pressure of the fluid are related via a constant EoS parameter effectively, that is, $p_\phi = w\rho_\phi$, their relations with the physical scale factor can be obtained from the conservation equation: $\rho_\phi \approx \rho_0 a^{-3(1+w)}$ and $p_\phi \approx w\rho_0 a^{-3(1+w)}$. Combining (13.8), (12.2) and (12.3), we obtain the asymptotic expression of the scalar field as a function of $\delta a \equiv a - a_{m2}$ as follows

$$\phi(\delta a) = \sqrt{B}\ln \delta a\,, \tag{13.32}$$

where

$$B \equiv \frac{3\kappa\rho_0\,(1+w)\,a_{m2}^{-3(1+w)}}{8} = \frac{3\lambda\,(1+w)}{8w}\,. \tag{13.33}$$

It can be seen that $\phi \to -\infty$ when δa and b vanish. The scalar field potential approaches a constant when $a \to a_{m2}$ and its value depends on the EoS parameter w:

$$V(\phi) \approx \frac{\lambda}{2\kappa w}\,(1-w)\ . \tag{13.34}$$

Similar to what we have done in the previous subsection, we have to express X/Y^3 and Y^2 in (13.21) in terms of b, ϕ, and their conjugate momenta. To do this, we use (13.9) to get

$$\frac{X}{Y^3} \approx \frac{1+w}{w}\,, \qquad Y^2 \approx \frac{a_{m2}^2}{b^2}\,. \tag{13.35}$$

Substituting (13.35) into the Hamiltonian, we obtain

$$\mathcal{H}_T = M\left[-\frac{p_b^2}{24\lambda b} + \left(\frac{1+w}{4w}\right)\frac{p_\phi^2}{b^3} + \frac{2\lambda b^3}{\kappa}\left(\lambda - \frac{a_{m2}^2}{b^2}\right)\right] + \lambda_X p_X + \lambda_Y p_Y\,. \tag{13.36}$$

To proceed, we use the following factor ordering:

$$\langle b\phi|b^3\hat{\mathcal{H}}_T|\psi\rangle = 0\,, \tag{13.37}$$

and

$$b^2\hat{p}_b^2 \;\; = -\hbar^2\left(b\tfrac{\partial}{\partial b}\right)\left(b\tfrac{\partial}{\partial b}\right) = -\hbar^2\left(\tfrac{\partial}{\partial z}\right)\left(\tfrac{\partial}{\partial z}\right)\,, \tag{13.38}$$

$$\hat{p}_\phi^2 \qquad\qquad = -\hbar^2\left(\tfrac{\partial}{\partial\phi}\right)\left(\tfrac{\partial}{\partial\phi}\right)\,. \tag{13.39}$$

Note that we have defined a new variable

$$z = \ln b\,, \tag{13.40}$$

and it can be seen that $z \to -\infty$ when $b \to 0$. Finally, the WDW equation can be expressed as

$$\left[\frac{\hbar^2}{24\lambda}\partial_z^2 - \frac{(1+w)\,\hbar^2}{4w}\partial_\phi^2 - \frac{2\lambda a_{m2}^2 e^{4z}}{\kappa}\right]\psi(z,\phi) = 0\,. \tag{13.41}$$

13.5 The wave functions in the perfect fluid description

In the previous sections, we have obtained the asymptotic expressions of the WDW equation near the singularity ($b \to 0$) of the auxiliary metric or equivalently the physical connection. For a negative κ, we have derived the WDW equations (13.16) and (13.31), by assuming that the matter field is governed by a perfect fluid and a scalar field, respectively. On the other hand, for a positive κ, the corresponding WDW equations with a perfect fluid and a scalar field have been obtained in (13.19) and (13.41), respectively. We will solve the wave functions for all these WDW equations and see whether the wave functions satisfy the DW boundary condition, i.e., the wave functions vanish, near the configuration of the singularity of the auxiliary metric. Let us first consider the cases in which the matter field is described by a perfect fluid and solve the WDW equations (13.16) and (13.19).

13.5.1 The $\kappa < 0$ case

When the matter content is governed by a perfect fluid, the WDW equation for a negative κ that we will take into account is given by (13.16). The general solution can be written as a linear combination of two independent solutions as follows

$$\psi\,(y) = y^{\frac{1}{2}}\left[C_1 J_{\frac{3}{8}}\left(3\sqrt{2}y^{\frac{4}{3}}\right) + C_2 Y_{\frac{3}{8}}\left(3\sqrt{2}y^{\frac{4}{3}}\right)\right], \tag{13.42}$$

where C_1 and C_2 are constants. The functions $J_\nu\,[f\,(y)]$ and $Y_\nu\,[f\,(y)]$ are Bessel functions of first kind and second kind, respectively, with order $\nu = 3/8$ and argument $f\,(y) = 3\sqrt{2}y^{\frac{4}{3}}$. Near the singularity, i.e., $y \to 0$, the two independent solutions can be approximated as follows [307]:

$$y^{\frac{1}{2}} J_{\frac{3}{8}}\left(3\sqrt{2}y^{\frac{4}{3}}\right) \approx \frac{3^{3/8}}{2^{3/16}\Gamma\left(\frac{11}{8}\right)}y\,, \qquad y^{\frac{1}{2}} Y_{\frac{3}{8}}\left(3\sqrt{2}y^{\frac{4}{3}}\right) \approx -\frac{2^{3/16}\Gamma\left(\frac{3}{8}\right)}{3^{3/8}\pi}\,. \tag{13.43}$$

It can be seen that when $y \to 0$, the solution $\sqrt{y}\,J_{3/8}\,[f\,(y)]$ vanishes, while the other solution $\sqrt{y}\,Y_{3/8}\,[f\,(y)]$ approaches a non-zero constant. Therefore, the wave function (13.42) satisfies the DW condition near the singularity as long as one assumes $C_2 = 0$.

13.5.2 The $\kappa > 0$ case

On the other hand, the WDW equation for a positive κ within the perfect fluid description is given by (13.19). Depending on the value of the parameter c_2, which is positive (see (13.20)), the general solution can be categorised as follows

$$\psi\,(z) = z^{\frac{1}{2}}\left(\tilde{D}_1 z^{\frac{1}{2}\sqrt{1-4c_2}} + \tilde{D}_2 z^{-\frac{1}{2}\sqrt{1-4c_2}}\right), \qquad \text{if} \quad 0 < c_2 < \tfrac{1}{4}\,, \tag{13.44}$$

$$\psi\,(z) = z^{\frac{1}{2}}\left(\bar{D}_1 + \bar{D}_2 \ln z\right), \qquad \text{if} \quad c_2 = \tfrac{1}{4}\,, \tag{13.45}$$

$$\psi\,(z) = z^{\frac{1}{2}}\left(D_1 z^{\frac{i}{2}\sqrt{|1-4c_2|}} + D_2 z^{-\frac{i}{2}\sqrt{|1-4c_2|}}\right), \qquad \text{if} \quad c_2 > \tfrac{1}{4}\,, \tag{13.46}$$

where D_1, D_2, $\tilde{D}_1$, $\tilde{D}_2$, $\bar{D}_1$, and $\bar{D}_2$ are integration constants. Next, we will consider different values of c_2 and investigate whether the wave function is able to satisfy the DW boundary condition near the singularity where $z \to 0$.

- If $0 < c_2 < 1/4$, the general solution of the wave function is given by (13.44). It can be shown that for each independent solution, the variable z has a positive power. Therefore, the general solution vanishes when $z \to 0$, satisfying the DW condition at the singularity.

- If $c_2 = 1/4$, the general solution is given by (13.45) and the DW condition at $z \to 0$ is unambiguously satisfied due to the factor $\sqrt{z}$.

- If $c_2 > 1/4$, the general solution is given by (13.46) and the power of z is complex. In consequence, the wave function acquires an oscillating behavior described by the imaginary part of the power of z. However, the modulus of the wave function behaves as $|\psi| \approx \sqrt{z}$. Therefore, when $z \to 0$, the modulus of the wave function vanishes and the DW condition is fulfilled.

Consequently, in a perfect fluid description and when $\kappa > 0$, the wave function always satisfies the DW condition at the singularity of the auxiliary metric.

13.6 The wave functions in the scalar field description

For the scalar field description, the asymptotic expressions of the WDW equations near the singularity are given by (13.31) and (13.41), corresponding to a negative and a positive value of κ, respectively. The WDW equations are partial differential equations with two independent variables. We will prove that even in these general cases in which one more degree of freedom is included into the system, the DW boundary condition can still be satisfied near the singularity of the auxiliary metric.

13.6.1 The $\kappa < 0$ case

The WDW equation in the scalar field description with a negative κ is given by the partial differential (13.31). The general solution to (13.31) can be obtained by using the separation of variables such that the total wave function can be decomposed as a series of products of two single variable functions

$$\psi(x,\phi) = \sum_k C_k(x)\,\varphi_k(\phi)\,, \tag{13.47}$$

where $C_k(x)$ and $\varphi_k(\phi)$ are the solutions to the following two ordinary differential equations

$$\left(\frac{\hbar^2}{24\lambda}\partial_x^2 + \frac{2\lambda}{|\kappa|}a_{m1}^2 - k\right) C_k(x) = 0\,, \qquad \left[-\frac{\hbar^2}{4(1+w)\,a_{m1}^4}\partial_\phi^2 + k\right]\varphi_k(\phi) = 0\,, \tag{13.48}$$

and k corresponds to the decoupling constant. The above ordinary differential equations (13.48) can be solved to get the solution of the gravitational part $C_k(x)$

$$C_k(x) = \left\{E_{1,k}\exp\left[\sqrt{\frac{24\lambda}{\hbar^2}\left(k - \frac{2\lambda}{|\kappa|}a_{m1}^2\right)}x\right] + E_{2,k}\exp\left[-\sqrt{\frac{24\lambda}{\hbar^2}\left(k - \frac{2\lambda}{|\kappa|}a_{m1}^2\right)}x\right]\right\}\,, \tag{13.49}$$

and the solution of the matter part $\varphi_k(\phi)$

$$\varphi_k(\phi) = \left\{ F_{1,k} \exp\left[\frac{2a_{m1}^2\sqrt{(1+w)\,k}}{\hbar}\phi \right] + F_{2,k} \exp\left[-\frac{2a_{m1}^2\sqrt{(1+w)\,k}}{\hbar}\phi \right] \right\} . \tag{13.50}$$

It should be stressed that near the singularity of the auxiliary metric, the scalar field approaches a constant and the auxiliary scale factor vanishes, i.e., $\phi \to \phi_0$ and $x \to 0$. Therefore, the matter part of the wave function $\varphi_k(\phi)$ is well-defined and the gravitational part tends to a constant value $E_{1,k} + E_{2,k}$. Since the total wave function is constructed by the product of C_k and φ_k, the DW boundary condition can be satisfied as long as one requires $E_{1,k} = -E_{2,k}$.

13.6.2 The $\kappa > 0$ case

For a positive value of κ, the asymptotic expression of the WDW equation in the scalar field description near the singularity of the auxiliary metric is given by (13.41). Again, the partial differential equation can be solved by using the separation of variables. The total wave function can be decomposed as a series of products of the solutions corresponding to the gravitational part and matter part:

$$\psi(z,\phi) = \sum_m Q_m(z)\,\xi_m(\phi) , \tag{13.51}$$

where $Q_m(z)$ and $\xi_m(\phi)$ are, respectively, the gravitational and matter part of the wave function. In this regard, the WDW equation (13.41) can be decoupled into two ordinary differential equations as follows

$$\left(\frac{\hbar^2}{24\lambda}\partial_z^2 - \frac{2\lambda a_{m2}^2 e^{4z}}{\kappa} - m \right) Q_m(x) = 0 , \qquad \left[-\frac{(1+w)\,\hbar^2}{4w}\partial_\phi^2 + m \right] \xi_m(\phi) = 0 , \tag{13.52}$$

where m is the value of the decoupling constant. The general solution to the gravitational part can be written in terms of the modified Bessel functions $I_\mu[g(z)]$ and $K_\mu[g(z)]$ as follows [307]:

$$Q_m(z) = G_{1,m} I_\mu[g(z)] + G_{2,m} K_\mu[g(z)] , \tag{13.53}$$

where $G_{1,m}$ and $G_{2,m}$ are integration constants. The order μ and the argument $g(z)$ of the modified Bessel functions can be explicitly expressed as

$$\mu = \frac{\sqrt{6\lambda m}}{\hbar} , \tag{13.54}$$

$$g(z) = \sqrt{\frac{12\lambda^2 a_{m2}^2}{\hbar^2\kappa}}\, e^{2z} . \tag{13.55}$$

On the other hand, the solution of the matter part can be solved as follows

$$\xi_m(\phi) = \left\{ H_{1,m} \exp\left[\frac{2}{\hbar}\sqrt{\frac{wm}{(1+w)}}\phi \right] + H_{2,m} \exp\left[-\frac{2}{\hbar}\sqrt{\frac{wm}{(1+w)}}\phi \right] \right\} , \tag{13.56}$$

where $H_{1,m}$ and $H_{2,m}$ are integration constants. Note that the scalar field $\phi \to -\infty$ near the singularity of the auxiliary metric.

To further proceed, we assume that the decoupling constant m is a real number. This assumption is fully physical as m has dimension of energy. Under this assumption, the order μ acquires either a non-negative real value when $m \geq 0$, or a purely imaginary value when $m < 0$. Depending on

the value of m, the asymptotic expressions of the modified Bessel functions at small arguments ($z \to -\infty$ and $g(z) \to 0$) are given as follows [307]

$$I_\mu\left[g\left(z\right)\right] \approx \frac{1}{\Gamma\left(\mu+1\right)}\left[\frac{g\left(z\right)}{2}\right]^\mu \qquad \text{when } \mu \neq -1,-2,-3,\ldots, \tag{13.57}$$

$$K_\mu\left[g\left(z\right)\right] \approx \frac{\Gamma\left(\mu\right)}{2}\left[\frac{g\left(z\right)}{2}\right]^{-\mu} \qquad \text{when } \mu \text{ is real and positive}, \tag{13.58}$$

$$K_\mu\left[g\left(z\right)\right] \approx -\ln\left[g\left(z\right)\right] \qquad \text{when } \mu = 0, \tag{13.59}$$

$$K_\mu\left[g\left(z\right)\right] \approx -\left[\frac{\pi}{\nu\sinh\left(\pi\nu\right)}\right]^{\frac{1}{2}}\sin\left[\nu\ln\left(\frac{g(z)}{2}\right)\right] \qquad \text{when } \mu = i\nu \text{ is purely imaginary}, \tag{13.60}$$

where $\Gamma\left(\alpha\right)$ stands for the Gamma function. In the following, we will investigate the behaviors of the total wave function for different values of the decoupling constant m.

- If $m < 0$, the matter part of the wave function (13.56) turns out to be a plane wave solution whose oscillating amplitude is constant. As for the gravitational part, the order μ becomes imaginary, and therefore according to (13.57) and (13.60), the modified Bessel functions $I_\mu\left[g\left(z\right)\right]$ and $K_\mu\left[g\left(z\right)\right]$ are both rapidly oscillating functions with a non-zero constant modulus. In consequence, for $m < 0$ the total wave function does not vanish at the singularity and the DW condition cannot be satisfied.

- If $m = 0$, the solution to the matter part is given by

$$\xi_0\left(\phi\right) = \tilde{H}_{1,0} + \tilde{H}_{2,0}\phi\,, \tag{13.61}$$

  where $\tilde{H}_{1,0}$ and $\tilde{H}_{2,0}$ are integration constants. On the other hand, the asymptotic expressions of the modified Bessel functions with a zero order are given by (13.57) and (13.59). Obviously, as $z \to -\infty$ and $\phi \to -\infty$, we get $I_0\left(0\right) \to 1$, $K_0\left(0\right) \to \infty$, and $\xi_0\left(-\infty\right) \to \pm\infty$. Therefore, the DW condition cannot be satisfied.

- If $m > 0$, the matter part of the wave function turns out to be exponential functions. If we assume $H_{2,m} = 0$, the growing part of the solution when $\phi \to -\infty$ is removed. On the other hand, the order μ of the modified Bessel functions in the gravitational part is a positive and real number. In this case, it can be seen from (13.57) and (13.58) that the modified Bessel function $I_\mu\left[g\left(z\right)\right]$ vanishes when $g(z) \to 0$, while $K_\mu\left[g\left(z\right)\right]$ diverges. Consequently, one has to further choose $G_{2,m} = 0$ in order to ensure the DW condition near the singularity of the auxiliary metric.

In summary, we have found that if $m \leq 0$, it is impossible to obtain a wave function satisfying the DW boundary condition at the singularity of the auxiliary metric. In fact, one is supposed to impose an additional condition on the decoupling constant, i.e., $m > 0$, such that the DW condition is able to be satisfied.

13.7 Conclusions

In the context of the EiBI gravity, it has been shown that the propagation of gravitational waves would be affected by the geometry of the auxiliary metric, which is compatible with the affine connection of the theory. Therefore, even though the big bang singularity can be resolved, the singularity is present in the auxiliary metric and it has an important consequence on the behavior

of the linear perturbations. The linear perturbations, including the tensor modes, turn out to be unstable in the non-singular solutions within the EiBI theory. In this chapter, we consider the quantum geometrodynamical approach in the context of the EiBI gravity. Note that the Born-Infeld type of theories seem to have intrinsic Noether symmetries as shown recently in [386]. This also supports the choice of the EiBI action in this chapter. Our motivation is to see whether or not the singularity in the auxiliary metric can be ameliorated by quantum effects. It turns out the answer is yes and therefore, the linear instabilities of the physical metric, which are associated with the singular behavior of the auxiliary metric, would be resolved by the same token.

For the sake of completeness, we have considered two descriptions regarding the matter sector of the theory. In the perfect fluid description, the matter field is governed by a perfect fluid with a positive and constant EoS parameter. In the homogeneous and isotropic Universe, the system is characterised by a single variable b, the scale factor of the auxiliary metric. In the second description, that is, the scalar field description, we introduce a scalar field degree of freedom to incorporate the matter sector which, in the classical level, describes the evolution of the corresponding perfect fluid in the perfect fluid description. In this setup, the system contains two canonical degrees of freedom, the scale factor b and the scalar field ϕ, spanning a two dimensional configuration space.

In the framework of quantum geometrodynamical approach, the building block is the WDW equation describing the quantum evolution of the Universe as a whole. Essentially, we start with the alternative EiBI action in the Einstein frame and derive the classical Hamiltonian for both descriptions mentioned above. The Hamiltonian constraint, which is a first class constraint, is regarded as a restriction on the Hilbert space and the WDW equation is derived by promoting all phase space functions to quantum operators. The commutation relations are constructed by using the Dirac brackets which are necessary for a system containing second class constraints. We have derived the asymptotic expressions of the WDW equations for the two matter descriptions, and for positive and negative values of the Born-Infeld parameter κ. For a negative value of κ, the physical metric bounces in the past at the classical level. The asymptotic expressions of the WDW equations near the bounce are given by (13.16) and (13.31), for the perfect fluid and the scalar field descriptions, respectively. For a positive value of κ, the physical metric acquires its minimum scale factor in the asymptotic past (the loitering effect). The approximated WDW equations are given by (13.19) and (13.41), for the perfect fluid and the scalar field descriptions, respectively.

After deriving the WDW equations, we have studied the quantum behavior of the Universe by solving the wave function as a solution to the WDW equations. We have found that for each WDW equation under consideration, wave functions which satisfy the DW boundary conditions at the singularity of the auxiliary metric can always be obtained. Therefore, the hidden singularity in the auxiliary metric is expected to be avoided at the quantum level and the linear instabilities are not harmful in the quantum world.

14

Conclusions and outlook

Don't let it end like this. Tell them I said something

– Pancho Villa

Conclusions

Dark energy (DE), together with dark matter(DM), represent the most intriguing open problems in the current stage of modern cosmology. Surprisingly, both components represent the major part of the Universe's energy budget, being DE dominant at present. While the existence of DM was postulated in the first half of the XX century, the discovery of DE is relatively recent. That is why, over the last two decades the problem about the nature of DE has gained much attention. The unexpected discovery of the speed up of the Universe has brought the flourishing of new research fields, as it is the case of future cosmological singularities. The future of the Universe is still an enigma, the smallest deviation from the standard cosmological model ΛCDM could induce a range of different cosmic doomsdays.

In this thesis, we have studied in deep three genuine phantom models, coined as model A, model B and model C. The backgrounds described by these paradigms stand as interesting alternatives to the widely known ΛCDM model. Model A includes a deviation from ΛCDM in the fact that the EoS parameter stays constant but below -1. Model B also differs from ΛCDM by adding a term proportional to the root square of the energy density to the EoS parameter, while in model C the proposed modification consists simply in adding a constant. Therefore, the ΛCDM model is recovered in model A by taking the limit $w \to -1$ in (2.10), while in models B and C we retrieve ΛCDM by taking the limits $\mathcal{B} \to 0$ in (2.13) and $\mathcal{C} \to 0$ in (2.16), respectively. We recall that, despite inducing small differences in the background at present, each of these models induce a particular future abrupt event. Among the three possible final fates under study in the present thesis, the BR (induced in model A) is the the strongest event. In addition, the divergence of the cosmological functions, as for instance, the energy density or the Hubble rate, occur at a finite cosmic time, this is why we regard BR as a true singularity. On the other hand, we regard the LR and LS as abrupt events (induced by the models B and C, respectively), since the divergence of the cosmological functions occurs at infinite cosmic time. Despite the LS and LR abrupt events are smoother than a BR, an effective cosmic doomsday would take place at a finite cosmic time, since the total destruction of bound structures will occur inevitably sooner or later.

The study comprised in this thesis is separated into two parts: (i) the classical part, where we describe DE by means of a perfect fluid in a classical FLRW Universe, and (ii), the quantum part, where we deal with singularity avoidance by adopting a quantum approach.

In the classical part, we address the perturbations and forecast mainly the current matter power spectrum and growth rate of matter perturbations for different models. These observables,

compared with the available data, allow us to better describe the current speed up of the Universe and, in consequence, the phenomenon known as DE. In addition, we have performed an observational fit with its corresponding statistical analysis obtaining constraints on the parameters characterising the models. These parameters describe the backgrounds of the DE models under study, including as well the ΛCDM model which is used as a guideline, given its consistent results. The main conclusion reached, when comparing the outputs of the genuine phantom models considered here with the current observational data is that, despite ΛCDM still provides good results, the models analysed also fit the data such that it is very difficult to distinguish between them, even when computing relative differences. The main departures between this thesis's models and ΛCDM have been computed up to the relative differences in such a way that, at present, the results are too small to be measured beyond present observational data statistical errors. Notwithstanding, the models addressed in the present thesis describe consistently the current speed up of the Universe.

In summary, we have analysed in detail the deviations of three genuine phantom models looking for the imprints characterising each paradigm. We can presume to be able to distinguish the phenomenology of every model at the background level, however, at present time and with the current dataset, it is hard to favour a particular model over the others at a perturbative level. By performing a statistical analysis, we found that ΛCDM model still gives the best fit. Among the studied models, we have found that at a background level, the model A is the one that better fits the observations closely followed by the models B and C, respectively. However, when performing the cosmological perturbations with the constraints obtained after fitting the background, what we have found is that those that less differ from ΛCDM fit more conveniently the data. Therefore, at a perturvative level, the model C is the one that better fits observations followed by model B and finally by model A. Not by accident, the LS abrupt event (induced by model C), is considered the less harming scenario while the BR (induced by model A), is by far, the strongest phantom singularity. In between, the behaviour found in model B shows always intermediate results. All these findings are in accordance with the fact that the EoS parameter, measured by different observations, slightly favours a phantom Universe, $w < -1$, rather than a non-phantom one, $w \geq -1$ [18].

In addition, we have computed the perturbations for the three models changing the $c^2_{s\mathsf{d}}$ parameter from 0 to 1. We found that the most important effects, concerning the perturbations to the background, occur in the DE sector. The smaller is the $c^2_{s\mathsf{d}}$ value, the larger is the clustering of DE. Vanishing values of $c^2_{s\mathsf{d}}$ parameter predict a DE clustering located in the recent past not yet observed, so we exclude this possibility. On the one hand, for values in the interval $0.2 < c^2_{s\mathsf{d}} < 1$, perturbations in the DE sector forecast a lower clustering reconcilable with observations. On the other hand, we have not found important differences, comparing to previous works, when $c^2_{s\mathsf{d}} = 1$. We conclude that perturbations in the DE sector slightly affect the growth of matter perturbations, in consequence, the different DE models studied here barely induce detectable footprints on the growth of matter structures.

Despite the fact that, at present, the models exhibit a high similarity and no important differences are found, every model drives a particular cosmic event in the future, and therefore, some footprints at very large scale factors could be expected. Moreover, there is a remarkable issue to point out: The sign switch of the gravitational potential. This effect is induced mainly by the phantom nature of the DE content. First, the presence of DE is considered almost negligible,

at the radiation dominated era, when we impose initial adiabatic conditions (2.37). As opposed to standard DE models, the sign of the phantom DE density contrast is fixed negative while the rest of the components contribute with a positive matter density contrast. Initially, the gravitational potential keep its attractive nature, however, when DE totally overtake the Universe energy budget, the gravitational potential switches its sign. We recall that the magnitudes we mention relate to their Fourier transforms, and therefore, we consider that the gravitational potential is repulsive from a particular distance onwards. We have found that this event will happen earlier in models where the induced singularity is stronger and vice versa. In addition, the value of the effective speed of sound parameter could strongly affect such an event. For vanishing $c^2_{s\mathsf{d}}$ parameter, the sign switch occurs for all the modes at the same cosmic time. For non-vanishing values, the smallest modes; i.e. small k, feel the effect before the larger ones (see figure 6.5). As expected, the repulsive effect happens progressively, firstly, at large lengths and then, for shorter distances.

Whether this effect will be physically observable by future observers depends on the size of the horizon when the gravitational potential switches the sign. At distances larger than the horizon, it will be theoretically undetectable. On the contrary, if the gravitational potential switch occurs before the horizon exit, far objects will look like under the influence of a repulsive gravitational effect. We emphasise that these conclusions depend on the conditions assumed in the present work. Those conditions involve some approximations at the radiation dominated epoch and the adiabatic conditions that ultimately fix the signs of the different perturbations components.

We could visualise this effect as another horizon, which would be defined at the distance where the gravitational potential becomes positive. This horizon moves from infinitely large lengths to shorter distances. If we compare the growth of this horizon with the comoving Hubble horizon, what we find is that the distance between both horizons is asymptotically constant (see figure 6.6). On the one hand, for a vanishing parameter $c^2_{s\mathsf{d}}$, the repulsive effect would be observable since it would be manifested at shorter distances than the comoving Hubble horizon. On the other hand, for large enough values of $c^2_{s\mathsf{d}}$, the repulsive effect would be nonphysical since it would manifest at distances that stand outside the comoving Hubble horizon. Therefore, we conclude that there must be an intermediate value of $c^2_{s\mathsf{d}}$ where both horizons coincide and move as a single one, we find such a particular value around $c^2_{s\mathsf{d}} \simeq 2.1 \times 10^{-3}$.

The observational value of parameter c^2_s is still uncertain and hopefully will be fixed by more accurate data, as it is expected from the forthcoming Euclid mission, conceived to measure other quantities as for example, a non-vanishing DE fluid viscosity parameter [104]. The upcoming missions will provide useful data allowing to unravel the DE sector. A range of new results for DE models could arise upon a detailed analysis of the perturbations speed and its key role with respect to the matter growth and DE clustering. For example, a future project could consist in considering a multi DE fluid where the pressure of each new component should be splitted into adiabatic and non-adiabatic contributions. In addition, a time dependent parameter c^2_s could also be an interesting idea to address, in this sense, extra conditions could be imposed and compared with more accurate future observations.

As mentioned above, a better observational fit will allow to seriously consider or neglect different DE models. Consequently, we could get a clearer picture of what will be the ultimate fate of our Universe. Furthermore, we could have a better understanding of the hypothetical rip of

all the bound structures in the Universe. However, this would not mean that all the features of the final doomsday would be classical. It is expected that quantum effects should determine the last phases of the Universe if a doomsday is approached, as they did at its very early stages, deep inside the inflationary era. Therefore, we are dealing with the most dramatic features of a potential second quantum era of the Universe. For the sake of completeness, the second part of the present thesis is aimed to address the issue of cosmological singularities by means of QM.

Despite the fact that we lack a consistent gravitational quantum theory to address this issue, we can pursue some approaches that could give us some hints about the quantum avoidance of singularities and abrupt events afflicting the classical theory of GR. In particular, in the current thesis, we have focused on the WDW equation, which consists in quantising the metric variables throughout space-time diffeomorphism constraints such that after obtaining the solution to the differential equation, i.e. the wave function of the Universe, the latter should vanish at the singularity vicinity. This requirement is known as the DW boundary condition and, in this thesis, it is used as the main quantum argument to avoid classical singularities.

We have obtained the WDW equation from the fundamental Hilbert-Einstein action minimally coupled with a matter field. Such a matter content is described, (i) by a perfect fluid, and (ii), by a scalar field. In addition, we have applied different factor orderings. Notice that we have followed the same methodology to quantise GR but within the EiBI context as well. That is, we have considered another starting point: The action inspired by the Eddington's functional endowed with a Born-Infeld like structure. Since at classical level, the emerging auxiliary metric could assimilate the divergences present in the physical metric, this possibility gives an interesting option to address the issue of cosmological singularities. We should bear in mind that within an EiBI quantum context, the true dynamical variable is the auxiliary metric while the scale factor of the physical metric plays the role of a parameter. However, the divergence in the auxiliary metric is still present and we deal with it by means of WDW equation and checking, once again, the fulfillment of DW boundary condition. For example, we have studied the LR and LS abrupt events obtained in a scenario with a perfect fluid. Here, we have computed the expected value of the auxiliary scale factor near the abrupt event for different factor orderings. For the sake of completeness, we have also addressed a BR singularity driven by a scalar field.

In addition, we have addressed as well the Big Bang primordial singularity in the context of EiBI theory, where the matter content is played by a perfect fluid or a scalar field. In this situation, we have analysed the cases for a positive and a negative EiBI constant parameter, κ, that characterises the theory. As mentioned above, within the EiBI approach the divergences in the physical metric move to the auxiliary metric, so the EiBI theory by itself could alleviate the classical singularities present in GR. However, those divergences could affect the tensor sector inducing instabilities on, for example, the gravitational waves production. The goal consisted in avoiding those divergences from the auxiliary metric by means of a suitable quantum approach. In such a way that the vanishing of the total wave function close to the Big Bang singularity will ensure the mitigation of tensor instabilities.

When the content is given by a scalar field, the system is extended with a second degree of freedom. Therefore, we should consider a wave function spreading over a two-dimensional variable space defined by both the auxiliary metric and the scalar field. Often, we have made use of the BO approximation. The BO approximation, in principle was suggested to compute the total

wave function of molecules, where the back-reaction of the electrons over the protons is negligible due to the large mass difference. Its cosmological analogue would consists on avoiding the back-reaction of the matter over the gravitational part. Consequently, the total wave function becomes the product of two separated wave functions. The solution of the gravitational part only depends on the metric variable, while the solution of the matter part is a two dimensional wave function. In this sense, the DW condition is considered satisfied if the total wave function vanishes at the vicinity of the singular event. We have shown that, in all the cases analysed in the present thesis, the WDW equation provides a vanishing solutions near the singularity. That is, there is a wave function that fulfills the DW boundary condition and, therefore, the criteria for singularity avoidance is satisfied.

As already stressed, we do not have a fully consistent quantum theory of gravity. This fact becomes evident when selecting a factor ordering since we lack a particular choice dictated by a self-consistent method compatible with such a gravitational quantum theory. Different factor orderings recover the same classical picture of the Universe by taking the limit $\hbar \to 0$. In the current thesis, we have followed different factor orderings to check whether the same cosmic event can be alleviated through quantum effects. In all the cases studied, the obtained wave function contemplates, at least, a vanishing solution at large scale factors where the cosmic doomsday takes place. The existence of a vanishing solution ensures the singularity avoidance in a quantum realm, nevertheless, this fact should be taken with precaution and understood as a hint of singularity avoidance rather than a prove in itself.

In this sense, an interesting question that arises is: *is it possible that all the factor orderings result in a vanishing solution of the wave function?* or using the opposite inquiry, *is there a particular factor ordering where the wave function only produces non-vanishing solutions?*. If the answer to the later one is yes, we will be facing a case where it would be impossible to fullfill the DW boundary condition, and therefore, dealing with a situation where the quantum avoidance via the WDW equation is not valid, or where the factor ordering selected is not the correct one. It should be interesting to analyse those family of factor orderings and corresponding wave functions where the DW boundary condition is always fulfilled and identify those ones where such a condition is unavoidably broken.

In order to understand which factor ordering is the true one in such a quantum theory, we should take a look at the quantum effects, that actually have not yet been detected due to our technological and engineering capabilities limits. Taking into account the lack of observational data in this context, one could ask *What kind of measurable observable could be induced by quantum effects?* If they exist, they could give us some hints about what kind of factor orderings are the corrects ones, reducing the vast number of options to a few ones. An interesting alternative could be computing quantum perturbations, where as a first approach, we would consider that DE quantum perturbations ignore the quantum perturbations of matter. We hope to address this issue in the near future.

Finally, the models studied in the present thesis could be understood as deviations from the standard ΛCDM model, and therefore, good candidates to describe suitably the current speed up of the Universe. Despite some models are slightly favoured by current observations, we have not yet enough evidences to clearly point out to a favorite cosmological paradigm. Therefore, we can not forecast clearly about a particular future cosmic doomsday. Every kind of event deserves

to be studied in detail, mostly, when all scenarios are currently on the table. If the Universe would face a future cosmic abrupt event, we could ensure that under the WDW approach, we can always find a wave function compatible with DW boundary condition, and therefore, it could be interpreted as singularity avoidance from the quantum point of view. Unfortunately, we have not yet a consistent quantum theory of gravity. It constitutes nowadays the holy grail of theoretical physics. The WDW equation, used in the present thesis, is just a useful tool to approach results that could capture some aspects of a fundamental quantum theory of gravity.

Not by accident, the hunger for acknowledge has pushed the scientific development not only in the observational context but in the theoretical one as well. On the one hand, future missions are encouraged to scrutinise the dark sector being currently *Euclid* one of the most popular. These efforts will be recognised by the vast amount of data likely useful to detect new hints in the mysterious nature of DE. On the other hand, several interesting ideas have been proposed in theoretical physics. As it is the case of modified theories of gravity inspired by the EiBI theory, considered in this thesis. In the end, our endeavor is to uncover the correct path to a consistent theoretical description.

Despite the Universe could look more dark than ever, we will continue shedding light, up to the last corner. From the vast kingdom of the emptiness to the smallest (or not so small) quantum scales. Hopefully, fast enough to reveal the hidden essence of the cosmos before the ruthless doomsday catches us.

Appendices

Appendix A

Statefinder parameters

A.1 Statefinder parameters in wCDM

For a wCDM model with a radiation component the statefinder parameters defined in (5.2), (5.3) , (5.4) and (5.5) read

$$S_3^{(1)} = \quad 1 + \frac{2\Omega_{\mathsf{r},0}\frac{a_0}{a} + \frac{9}{2}w(1+w)\Omega_{\mathsf{d},0}\left(\frac{a_0}{a}\right)^{3w}}{\Omega_{\mathsf{r},0}\frac{a_0}{a} + \Omega_{\mathsf{m},0} + \Omega_{\mathsf{d},0}\left(\frac{a_0}{a}\right)^{3w}}\,, \tag{A.1}$$

$$\begin{aligned} S_4^{(1)} = 1 - \left[\Omega_{\mathsf{r},0}\frac{a_0}{a} + \Omega_{\mathsf{m},0} + \Omega_{\mathsf{d},0}\left(\frac{a_0}{a}\right)^{3w}\right]^{-2} \Bigg\{ \Bigg[10\Omega_{\mathsf{r},0}\frac{a_0}{a} + 9\Omega_{\mathsf{m},0} \\ + \left(9 + \frac{3}{2}w\left(14 + 3w\left(7 + 3w\right)\right)\right)\Omega_{\mathsf{d},0}\left(\frac{a_0}{a}\right)^{3w}\Bigg] + \frac{9}{4}w\left(1+w\right) \\ \times \left[\left(7+6w\right)\Omega_{\mathsf{m},0} + \left(7+9w\right)\Omega_{\mathsf{d},0}\left(\frac{a_0}{a}\right)^{3w}\right]\Omega_{\mathsf{d},0}\left(\frac{a_0}{a}\right)^{3w}\Bigg\}, \end{aligned} \tag{A.2}$$

$$\begin{aligned} S_5^{(1)} = 1 + \left[\Omega_{\mathsf{r},0}\frac{a_0}{a} + \Omega_{\mathsf{m},0} + \Omega_{\mathsf{d},0}\left(\frac{a_0}{a}\right)^{3w}\right]^{-2} \Bigg\{ \Bigg[76\Omega_{\mathsf{r},0}\frac{a_0}{a} + 60\Omega_{\mathsf{m},0} \\ + \left(60 + \frac{3}{2}w\big(37 + w\left(59 + 39w + 9w^2\right)\big)\right)\Omega_{\mathsf{d},0}\left(\frac{a_0}{a}\right)^{3w}\Bigg]\Omega_{\mathsf{r},0}\frac{a_0}{a} + \frac{9}{4}w\left(1+w\right) \\ \times \left[\left(41+3w\left(17+6w\right)\right)\Omega_{\mathsf{m},0} + \left(41 + 87w + 54w^2\Omega_{\mathsf{d},0}\left(\frac{a_0}{a}\right)^{3w}\right]\Omega_{\mathsf{d},0}\left(\frac{a_0}{a}\right)^{3w}\Bigg\}. \end{aligned} \tag{A.3}$$

$$s = \frac{4\Omega_{\mathsf{r},0}\frac{a_0}{a} + 9w(1+w)\Omega_{\mathsf{d},0}\left(\frac{a_0}{a}\right)^{3w}}{3\Omega_{\mathsf{r},0}\frac{a_0}{a} + 9w\Omega_{\mathsf{d},0}\left(\frac{a_0}{a}\right)^{3w}}. \tag{A.4}$$

Due to the Friedmann constraint $1 = \Omega_{\mathsf{r},0} + \Omega_{\mathsf{m},0} + \Omega_{\mathsf{d},0}$ we can eliminate one of the fractional energy density parameters. It can be checked that for the ΛCDM model, where $\Omega_{\mathrm{r},0} = 0$ and $w = -1$ the previous expressions reduce to $S_n^{(1)} = 1$ and $s = 0$.

Appendix B

Cosmological perturbations

In this appendix we disclose the main methods followed to describe a classical Universe. The mathematical content involves the analysis of the perturbations addressed in the present thesis, (i) theoretical calculation of the perturbed quantities up to first order, (ii) computation of the matter power spectrum and f_{σ_8}, and (iii) decomposition of the pressure in its adiabatic and non-adabatic contributions. In addition, we obtain the scalar field potential when mapping the models studied in the present thesis to a a scalar field and present the corresponding cosmological perturbations.

B.1 Perturbed equations for a single fluid

B.1.1 The Newtonian gauge

We start by considering the FLRW spacetime metric,

$$ds^2 = -dt^2 + a^2(t)d\mathbf{x}^2, \tag{B.1}$$

where $a(t)$ is the scale factor with t being the cosmic time, $\mathbf{x}$ is three dimensional space vector. The curvature perturbation $\zeta\left(t,\,\mathbf{x}\right)$ in the comoving gauge is defined by the perturbation of the spatial part of the metric. We will consider just first order scalar perturbations. We will start by convenience using the *Newtonian* or *longitudinal gauge*. Therefore, the perturbed line element is written as [23, 92]

$$ds^2 = a^2\left[-\left(1+2\Psi\right)d\eta^2 + \left(1+2\Phi\right)\delta_{ij}dx^i dx^j\right], \tag{B.2}$$

where Ψ and Φ are scalars functions which describe the deviation from the background metric and can depend on time and space, since we are dealing with perturbations, they are regarded as small quantities, i.e. $\Psi, \Phi \ll 1$. As usual, η is the conformal time. Note that from now on, we will refer the time derivatives as

$$dt = a\;d\eta \;\;,\;\; \partial_t = \frac{1}{a}\partial_\eta \;\; \text{or} \;\; \{\}^{\cdot} = \frac{1}{a}\{\}'. \tag{B.3}$$

Therefore,

$$H = \frac{1}{a}\mathcal{H} \qquad , \qquad \dot{H} = \frac{1}{a^2}\left(\mathcal{H}' - \mathcal{H}^2\right) \tag{B.4}$$

where H is the Hubble parameter and $\mathcal{H}$ is the conformal Hubble parameter. The dot stands for derivatives respect to the cosmic time while prime stands for derivatives respect to the conformal time. Starting from the line element, (B.2), we will write the metric tensor and its inverse, via

$$g_{\mu\nu}g^{\mu\nu} = \mathbb{I}. \tag{B.5}$$

where we will apply the taylor expansion up to first order, more generally:

$$(1+\alpha)^{-1} \approx 1 - \alpha + \mathcal{O}\left(\alpha^2\right). \tag{B.6}$$

Therefore, the metric and its inverse can be written as

$$g_{\mu\nu} = a^2 \begin{bmatrix} -(1+2\Psi) & 0 \\ 0 & (1+2\Phi) \end{bmatrix}, \qquad g^{\mu\nu} = a^{-2} \begin{bmatrix} -(1-2\Psi) & 0 \\ 0 & (1-2\Phi) \end{bmatrix}, \tag{B.7}$$

where this metric is the sum of the background metric and perturbed one. From now on, we will use a *bar* over the background quantity to distinguish it from the total quantity, writing the perturbed quantity preceded by δ.

$$g^{\mu\nu} = \overline{g}^{\mu\nu} + \delta g^{\mu\nu}. \tag{B.8}$$

Therefore, the perturbed and background metric can be written as [23, 92]

$$\delta g_{\mu\nu} = a^2 \begin{bmatrix} -2\Psi & 0 \\ 0 & 2\Phi \end{bmatrix}, \qquad \delta g^{\mu\nu} = a^{-2} \begin{bmatrix} 2\Psi & 0 \\ 0 & -2\Phi \end{bmatrix}, \tag{B.9}$$

$$\overline{g}_{\mu\nu} = a^2 \eta_{\mu\nu}, \;\; \overline{g}^{\mu\nu} = a^{-2}\eta^{\mu\nu} \;\; \text{where} \;\; \eta_{\nu\mu} = \eta^{\nu\mu} = \begin{bmatrix} -1 & 0 \\ 0 & 1 \end{bmatrix}. \tag{B.10}$$

Once we have the perturbed metric, the first step consists in writing the Christoffel symbols. Then, we will obtain the Ricci tensor and its scalar following by the Einstein tensor. Finally, we will equal the energy-momentum tensor to the Einstein tensor. Although we are interested in perturbations, we will conserve the background expressions for all these quantities because they will be necessary for further calculations.

B.1.2 Christoffel symbols

Now, we will proceed to calculate the Christoffel symbols, which are defined as follows

$$\Gamma^{\mu}_{\nu\lambda} = \frac{1}{2} g^{\mu\alpha} \left(\partial_\lambda g_{\alpha\nu} + \partial_\nu g_{\alpha\lambda} - \partial_\alpha g_{\mu\lambda}\right), \tag{B.11}$$

whose perturbation can be written as

$$\delta\Gamma^{\mu}_{\nu\lambda} = \frac{1}{2}\delta g^{\mu\alpha}\left(\partial_\lambda \overline{g}_{\alpha\nu} + \partial_\nu \overline{g}_{\alpha\lambda} - \partial_\alpha \overline{g}_{\mu\lambda}\right) + \frac{1}{2}\overline{g}^{\mu\alpha}\left(\partial_\lambda \delta g_{\alpha\nu} + \partial_\nu \delta g_{\alpha\lambda} - \partial_\alpha \delta g_{\mu\lambda}\right). \tag{B.12}$$

We write the background quantities instead of the unperturbed quantities in order to avoid the second order approximations which are neglected. As the perturbed metric remains diagonal, those Christoffel symbols with three different indexes vanishes. These are the non vanishing

terms [23]:

$$\begin{aligned}
\delta\Gamma^0_{00} &= \Psi' \quad , \quad \overline{\Gamma}^0_{00} = \frac{a'}{a}. \\
\delta\Gamma^0_{0i} &= \Psi_{,i} \quad , \quad \overline{\Gamma}^0_{0i} = 0. \\
\delta\Gamma^i_{00} &= \Psi_{,i} \quad , \quad \overline{\Gamma}^i_{00} = 0. \\
\delta\Gamma^i_{0j} &= \Phi'\delta^i_j \quad , \quad \overline{\Gamma}^i_{0j} = \frac{a'}{a}\delta^i_j. \\
\delta\Gamma^0_{ij} &= \left[2\mathcal{H}\left(\Phi-\Psi\right)+\Phi'\right]\delta_{ij} \quad , \quad \overline{\Gamma}^0_{ij} = \frac{a'}{a}\delta_{ij}. \\
\delta\Gamma^i_{kl} &= \Phi_{,l}\delta^i_k + \Phi_{,k}\delta^i_l - \Phi_{,i}\delta_{kl} \quad , \quad \overline{\Gamma}^i_{kl} = 0,
\end{aligned} \tag{B.13}$$

where we have made use of Latin characters to refer to spatial indexes and the subscript 0 for time indexes. The bar stands for background quantities.

B.1.3 Ricci curvature tensor and scalar

The Ricci tensor is written in terms of Christoffel symbols as follows

$$R_{\mu\nu} = \partial_\alpha\Gamma^\alpha_{\mu\nu} - \partial_\nu\Gamma^\alpha_{\mu\alpha} + \Gamma^\alpha_{\mu\nu}\Gamma^\beta_{\alpha\beta} - \Gamma^\alpha_{\mu\beta}\Gamma^\beta_{\alpha\nu}, \tag{B.14}$$

while the perturbed Ricci tensor is written as

$$\delta R_{\mu\nu} = \partial_\alpha\delta\Gamma^\alpha_{\mu\nu} - \partial_\nu\delta\Gamma^\alpha_{\mu\alpha} + \delta\Gamma^\alpha_{\mu\nu}\overline{\Gamma}^\beta_{\alpha\beta} + \overline{\Gamma}^\alpha_{\mu\nu}\delta\Gamma^\beta_{\alpha\beta} - \delta\Gamma^\alpha_{\mu\beta}\overline{\Gamma}^\beta_{\alpha\nu} - \overline{\Gamma}^\alpha_{\mu\beta}\delta\Gamma^\beta_{\alpha\nu}. \tag{B.15}$$

Using the latter equation and the definitions for Christoffel symbols defined in (B.13) we get [23, 92]

$$\begin{aligned}
\delta R_{00} &= \nabla^2\Psi - 3\Phi'' + 3\mathcal{H}\left(\Psi'-\Phi'\right) \quad , \quad \overline{R}_{00} = -3\mathcal{H}'. \\
\delta R_{0i} &= 2\left[\mathcal{H}\Psi - \Phi'\right]_{,i} \quad , \quad \overline{R}_{0i} = 0. \\
\delta R_{ij} &= \left[\Phi'' - \nabla^2\Phi + \mathcal{H}\left(5\Phi'-\Psi'\right)\right. \\
&\left.+2\left(\Phi-\Psi\right)\left(\mathcal{H}'+2\mathcal{H}^2\right)\right]\delta_{ij} - \left[\Psi+\Phi\right]_{,ij} \quad , \quad \overline{R}_{ij} = \left(\mathcal{H}'+2\mathcal{H}^2\right)\delta_{ij}.
\end{aligned} \tag{B.16}$$

To raise the indexes we cannot contract directly with the metric tensor, we should depart from the unperturbed definition and contract with the metric tensor to latter calculate the perturbation, so

$$R^\mu_\nu = g^{\alpha\mu}R_{\alpha\nu} \ , \ \delta R^\mu_\nu = \delta g^{\alpha\mu}\overline{R}_{\alpha\nu} + \overline{g}^{\alpha\mu}\delta R_{\alpha\nu}. \tag{B.17}$$

Therefore, the perturbed and background Ricci tensor with an index up and one down can be written as [23, 92]

$$\begin{aligned}
\delta R^0_0 &= a^{-2}\left[-\nabla^2\Phi + 3\Phi'' - 3\mathcal{H}\left(\Phi'-\Psi'\right) - 6\mathcal{H}'\Psi\right] \quad , \quad \overline{R}^0_0 = -3a^{-2}\mathcal{H}'. \\
\delta R^i_0 &= 2a^{-2}\left[\mathcal{H}\Psi - \Phi'\right]_{,i} \quad , \quad \overline{R}^i_0 = 0. \\
\delta R^0_i &= -2a^{-2}\left[\mathcal{H}\Psi - \Phi'\right]_{,i} \quad , \quad \overline{R}^0_i = 0. \\
\delta R^i_j &= a^{-2}\left[\Phi'' - \nabla^2\Phi + \mathcal{H}\left(5\Phi'-\Psi'\right)\right. \\
&\left.-\left(\mathcal{H}'+2\mathcal{H}^2\right)\Psi\right]\delta^i_j - a^{-2}\left[\Psi+\Phi\right]_{,ij} \quad , \quad \overline{R}^i_j = \left(\mathcal{H}'+2\mathcal{H}^2\right)\delta^i_j.
\end{aligned} \tag{B.18}$$

Finally the Ricci scalar and its perturbation are defined as

$$R = g^{\mu\nu}R_{\mu\nu} \quad , \quad \delta R = \delta g^{\mu\nu}\overline{R}_{\mu\nu} + \overline{g}^{\mu\nu}\delta R_{\mu\nu}, \tag{B.19}$$

where the result for the Ricci scalar (perturbed and background) is

$$\begin{aligned} \delta R =& a^{-2}\left[-\nabla^2\left(\Psi+2\Phi\right)+6\Phi''+6\mathcal{H}\left(3\Phi'-\Psi'\right)-12\Psi\left(\mathcal{H}'+\mathcal{H}^2\right)\right], \\ \overline{R} =& 6a^{-2}\left(\mathcal{H}'+\mathcal{H}^2\right). \end{aligned} \tag{B.20}$$

B.1.4 Einstein tensor

The following step consists on obtaining the perturbation for the Einstein tensor, we will start from the general definition and then we will compute the perturbation,

$$G_{\mu\nu} = R_{\mu\nu} - \frac{1}{2}g_{\mu\nu}R \qquad , \qquad \delta G_{\mu\nu} = \delta R_{\mu\nu} - \frac{1}{2}\left(\delta g_{\mu\nu}\overline{R} + \overline{g}_{\mu\nu}\delta R\right). \tag{B.21}$$

Combining the latter equation with the equations defined in (B.16) we get [23, 92]

$$\begin{aligned} \delta G_{00} &= -2\nabla^2\Psi + 6\mathcal{H}\Phi' \qquad , \qquad \overline{G}_{00} = -3\mathcal{H}^2. \\ \delta G_{0i} &= 2\left[\mathcal{H}\Psi - \Phi'\right]_{,i} \qquad , \qquad \overline{G}_{0i} = 0. \\ \delta G_{ij} &= \left[-2\Phi'' + \nabla^2\left(\Psi+\Phi\right) + 2\mathcal{H}\left(\Psi'-2\Phi'\right)\right. \\ &\left.+2\left(\Phi-\Psi\right)\left(\mathcal{H}'+2\mathcal{H}^2\right)\right]\delta_{ij} - \left[\Psi+\Phi\right]_{,ij} \qquad , \qquad \overline{G}_{ij} = \left(-2\mathcal{H}'+\mathcal{H}^2\right)\delta_{ij}. \end{aligned} \tag{B.22}$$

Similarly to what was done in equation (B.17) we rise the index in the following way:

$$G^{\mu}_{\nu} = g^{\alpha\mu}G_{\alpha\nu} \quad , \quad \delta G^{\mu}_{\nu} = \delta g^{\alpha\mu}\overline{G}_{\alpha\nu} + \overline{g}^{\alpha\mu}\delta G_{\alpha\nu}. \tag{B.23}$$

Finally, we get the following equations [23, 92]

$$\begin{aligned} \delta G^0_0 &= 2a^{-2}\left[\nabla^2\Phi + 3\mathcal{H}\left(\Psi\mathcal{H}-\Phi'\right)\right] \qquad , \qquad \overline{G}^0_0 = -3a^{-2}\mathcal{H}. \\ \delta G^i_0 &= 2a^{-2}\left[\mathcal{H}\Psi - \Phi'\right]_{,i} \qquad , \qquad \overline{G}^i_0 = 0. \\ \delta G^0_i &= -2a^{-2}\left[\mathcal{H}\Psi - \Phi'\right]_{,i} \qquad , \qquad \overline{G}^0_i = 0. \\ \delta G^i_j &= a^{-2}\left[-\Phi'' + \nabla^2\left(\Phi+\Psi\right) + 2\mathcal{H}\left(\Psi'-2\Phi'\right)\right. \\ &\left.+2\Psi\left(2\mathcal{H}'+\mathcal{H}^2\right)\right]\delta^i_j - a^{-2}\left[\Psi+\Phi\right]_{,ij} \qquad , \qquad \overline{G}^i_j = -2a^{-2}\left(2\mathcal{H}'+\mathcal{H}^2\right)\delta^i_j. \end{aligned} \tag{B.24}$$

B.1.5 Energy-momentum tensor

The general expression for the energy momentum tensor can be written as

$$T^{\mu}_{\nu} = \left(\rho + p\right)u^{\mu}u_{\nu} + p\delta^{\mu}_{\nu}. \tag{B.25}$$

Perturbing the above equation equation we get [23, 92]

$$\delta T^{\mu}_{\nu} = \left(\delta\rho + \delta p\right)\overline{u}^{\mu}\overline{u}_{\nu} + \left(\rho+p\right)\left(\delta u^{\mu}\overline{u}_{\nu} + \overline{u}^{\mu}\delta u_{\nu}\right) + \delta p\delta^{\mu}_{\nu}. \tag{B.26}$$

We will calculate the perturbations for the four-velocity vector, u^{μ}, u_{ν}, to obtain the perturbed energy momentum tensor. In the background, due to the isotropy the four velocity only contain

a single non-vanishing term which corresponds to the time axis,

$$\overline{u}^{\mu} = \frac{1}{a}(1,0) \qquad , \qquad \overline{u}_{\mu} = a(-1,0), \tag{B.27}$$

while the perturbed quantities up to first order read

$$\delta u^{\mu} = \frac{1}{a}\left(-\Psi, v^{i}\right) \qquad , \qquad \delta u_{\mu} = a(-\Psi, v_{i}). \tag{B.28}$$

We can get the result for the perturbed energy momentum tensor replacing the equations (B.27) and (B.28) into (B.26). Therefore,

$$\begin{aligned} \delta T_{0}^{0} &= -\delta\rho \qquad , \qquad \overline{T}_{0}^{0} = -\rho. \\ \delta T_{0}^{i} &= -(p+\rho)\, v^{i} \qquad , \qquad \overline{T}_{0}^{i} = 0. \\ \delta T_{i}^{0} &= (p+\rho)\, v_{i} \qquad , \qquad \overline{T}_{i}^{0} = 0. \\ \delta T_{j}^{i} &= \delta p \delta_{j}^{i} \qquad , \qquad \overline{T}_{j}^{i} = p\delta_{j}^{i}. \end{aligned} \tag{B.29}$$

In the same way, the perturbed metric fulfills the conservation equation

$$\overline{T}_{\nu;\mu}^{\mu} = 0 \qquad \text{therefore,} \qquad \delta T_{\nu;\mu}^{\mu} = 0. \tag{B.30}$$

The covariant derivation of the energy momentum tensor reads

$$T_{\nu;\mu}^{\mu} = \partial_{\mu} T_{\nu}^{\mu} - \Gamma_{\nu\beta}^{\alpha} T_{\alpha}^{\beta} + \Gamma_{\beta\alpha}^{\alpha} T_{\nu}^{\beta}, \tag{B.31}$$

and its perturbation leads to [23, 92]

$$\delta T_{\nu;\mu}^{\mu} = \partial_{\mu}\delta T_{\nu}^{\mu} - \delta\Gamma_{\nu\beta}^{\alpha}\overline{T}_{\alpha}^{\beta} - \overline{\Gamma}_{\nu\beta}^{\alpha}\delta T_{\alpha}^{\beta} + \delta\Gamma_{\beta\alpha}^{\alpha}\overline{T}_{\nu}^{\beta} + \overline{\Gamma}_{\beta\alpha}^{\alpha}\delta T_{\nu}^{\beta}. \tag{B.32}$$

We will separate the above expression into time and spatial components, i.e. $\nu = 0$ and $\nu = i$, [23, 92]

$$(\delta\rho)' + 3\mathcal{H}(\delta\rho + \delta p) + (\rho + p)\left(\nabla_{i} v^{i} + 3\Phi'\right) = 0, \tag{B.33}$$

$$4\mathcal{H}(\rho + p)\, v^{i} + \left[(\rho + p)\, v^{i}\right] + \delta p_{,i} + (\rho + p)\,\Psi_{,i} = 0. \tag{B.34}$$

We will use the next definitions in order to simplify the latter equations:

$$\delta = \frac{\delta\rho}{\rho} \qquad , \qquad \theta = \nabla_{i} v^{i}. \tag{B.35}$$

Therefore, the equations (B.33) and (B.34) can be written as [23, 92]

$$\delta' + 3\mathcal{H}\left(\frac{\delta p}{\delta\rho} - \frac{p}{\rho}\right)\delta + \left(1 + \frac{p}{\rho}\right)(\theta + 3\Phi') = 0, \tag{B.36}$$

$$4\mathcal{H}(\rho + p)\,\theta + \left[(\rho + p)\,\theta\right]' + \nabla^{2}\left[\delta p + (\rho + p)\,\Psi\right] = 0, \tag{B.37}$$

where we have applied the divergence over the equation (B.34).

B.1.6 Equation of evolution for perturbed quantities

Einstein tensor is proportional to the energy momentum tensor. Therefore, Einstein tensor and its perturbation satisfy

$$G^{\mu}_{\nu} = 8\pi G T^{\mu}_{\nu} \qquad , \qquad \delta G^{\mu}_{\nu} = 8\pi G \delta T^{\mu}_{\nu}. \tag{B.38}$$

We combine the equations (B.29) and (B.24) to get [23]

$$\begin{aligned} \nabla^2\Phi + 3\mathcal{H}\left(\mathcal{H}\Psi - \Phi'\right) &= -4\pi G a^2 \delta\rho, \\ \left[\mathcal{H}\Psi - \Phi'\right]_{,i} &= -4\pi G a^2 \left(\rho + p\right) v^i, \\ \left[-2\Phi'' + \nabla^2\left(\Psi + \Phi\right) + 2\mathcal{H}\left(\Psi' - 2\Phi'\right)\right. & \\ \left. + 2\Psi\left(2\mathcal{H}' + \mathcal{H}^2\right)\right]\delta^i_j - \left(\Psi + \Phi\right)_{,ij} &= 8\pi G \delta p \delta^i_j. \end{aligned} \tag{B.39}$$

As we have assumed a vanishing shear stress tensor, i.e., the non-diagonal elements of the spatial part (those with diferent latin indexes) in the energy momentum tensor vanish, therefore, we obtain $\left(\Psi + \Phi\right)_{,ij} = 0$. Replacing this equivalence, $\Psi = -\Phi$, in the set of equations (B.39) we finally have [23]

$$\begin{aligned} \nabla^2\Phi - 3\mathcal{H}\left(\mathcal{H}\Phi + \Phi'\right) &= -4\pi G a^2 \delta\rho, \\ -\nabla^2\left(\mathcal{H}\Phi + \Phi'\right) &= -4\pi G a^2 \left(\rho + p\right)\theta, \\ \Phi'' + 3\mathcal{H}\Phi' + \Phi\left(2\mathcal{H}' + \mathcal{H}^2\right) &= -4\pi G a^2 \delta p, \end{aligned} \tag{B.40}$$

where we have applied the divergence for the second equation using the definition given in equation (B.35). Finally, combining the first and third expressions of the latter set of equations (B.40), we can obtain an equation for Φ alone [23]

$$\Phi'' + 3\mathcal{H}\left(1 + c_s^2\right)\Phi' + \left[3\mathcal{H}^2\left(c_s^2 - w\right) - c_s^2\nabla^2\right]\Phi = 0, \tag{B.41}$$

where we have made use of the following relations

$$w \equiv \frac{p}{\rho} \quad , \quad c_s^2 \equiv \frac{\delta p}{\delta\rho} \quad , \quad \mathcal{H}' = -\frac{1}{2}\left(1 + 3w\right). \tag{B.42}$$

On the same way, we can use the first and second equation of (B.40) to obtain the so called Poisson equation [23]:

$$\nabla^2\Phi = -4\pi G a^2 \rho\left[\delta - 3\mathcal{H}\left(1 + w\right)v\right], \tag{B.43}$$

where we have replaced the relation $\theta = \nabla^2 v$, where v is the velocity potential. Therefore, we can define the *total matter variable*, δ^*_m, as [23]

$$\delta^*_m = \delta - 3\mathcal{H}\left(1 + w\right)v. \tag{B.44}$$

In a similar way to what we have done for the gravitational part, we can find an equation for δ^*_m alone by combining the equations (B.36) and (B.41) together with the relations given in equation (B.42),

$$\delta^{*\prime\prime}_m + \mathcal{H}\left(1 + 3c_s^2 - 6w\right)\delta^{*\prime}_m - \left[\frac{3}{2}\mathcal{H}\left(1 - 6c_s^2 - 3w^2 + 8w\right) + c_s^2\nabla^2\right]\delta^*_m = 0, \tag{B.45}$$

where we have employed the following extra useful relations

$$w' \equiv -3\mathcal{H}\left(1+w\right)\left(c_s^2-w\right)\ ,\ \frac{\rho'}{\rho} \equiv -3\mathcal{H}\left(1+w\right)\ ,\ \frac{\rho''}{\rho} \equiv 3\mathcal{H}^2\left(1+w\right)\left[\frac{3}{2}\left(1+w\right)+c_s^2\right]. \quad \text{(B.46)}$$

B.2 Perturbed equations in Fourier space

As we will proceed later on, in order to get a suitable set of equations to compare with the observational data it is convenient to apply the Fourier transform to the set of equations (B.39) and (B.40). Bear in mind that observational data for matter power spectrum is given in terms of k modes, where k is the corresponding wave number of a length. By definition, the Fourier transform of some quantity, let us say, $\psi_k(x,\eta)$, is related with the original function, $\psi(x,\eta)$, as

$$\psi(x,\eta) = \frac{V}{\left(2\pi\right)^3}\int e^{i\mathbf{k}\cdot\mathbf{r}}\psi_k(x,\eta)\ d^3k, \quad \text{(B.47)}$$

while the inverse transform is written as

$$\psi_k(x,\eta) = \frac{1}{V}\int e^{-i\mathbf{k}\cdot\mathbf{r}}\psi(x,\eta)\ d^3x. \quad \text{(B.48)}$$

Each perturbation variable can be written as the sum of plane waves, since the equations are linear, each mode have the same equation with a different wave number k. Therefore, for practical purposes, we can replace each perturbed variable by

$$\psi(x,\eta) \to e^{i\mathbf{k}\cdot\mathbf{r}}\psi_k(\eta), \qquad \nabla^2\psi(x,\eta) \to -k^2 e^{i\mathbf{k}\cdot\mathbf{r}}\psi_k(\eta), \quad \text{(B.49)}$$

where those quantities with a Laplace operator are simply transformed by replacing $-k^2$ times the Fourier transform. We will use this transform, for example, with the velocity fields. Therefore the quantity θ can be written as [23, 92]

$$\theta = \nabla_i v^i = \nabla^2 v \qquad , \qquad \nabla^2 v \to -k^2 e^{i\mathbf{k}\cdot\mathbf{r}} v_k. \quad \text{(B.50)}$$

On the one hand, from now on we will incorporate Fourier transform for all the equations, where we will drop the subindex k for notation convenience. On the other hand, we will apply the following change of variable:

$$N \equiv \ln\left(a\right)\ \ ,\ \ dN = \frac{da}{a}\ \ ,\ \ \{\}' = \{\}_N\,\mathcal{H}\ \ ,\ \ \{\}'' = \{\}_{NN}\,\mathcal{H}^2 + \{\}_N\,\mathcal{H}', \quad \text{(B.51)}$$

where the subscript N denotes the derivative over the variable N. Using the set of relations written in this subsection, we will rewrite the equations of perturbations for a multi fluid system.

B.3 Perturbed equations for two fluids

Once we have the evolution equations of the perturbation in the case of a single fluid model, we will follow addressing the task for a system with more than a one fluid. On the one hand, we will assume that the fluids are conserved separately, therefore, equations (B.33) and (B.34) which are obtained from the conservation equation can be handled independently. On the other hand, we should be careful with those equations involving the perturbed quantity Φ, which is

related with the total contribution of the different fluids.

Let us define some quantities that relate the total and partial contribution for each fluid. we will use a and b subscripts to denote two arbitrary fluids, while for the total contribution we will use a notation without subscripts.

$$\begin{aligned}
&\rho = \rho_a + \rho_b \ , \ \Omega_a = \frac{\rho_a}{\rho} \ , \ \Omega_b = \frac{\rho_b}{\rho}, \\
&w = \Omega_a w_a + \Omega_b w_b, \\
&\theta = \frac{1}{1+w}\left[(1+w_a)\,\omega_a\theta_a + (1+w_b)\,\omega_b\theta_b\right], \\
&\delta = \Omega_a\delta_a + \Omega_b\delta_b \ \ , \ \ \delta_a = \frac{\delta\rho_a}{\rho_a} \ \ , \ \ \delta_b = \frac{\delta\rho_b}{\rho_b},
\end{aligned} \tag{B.52}$$

where $\Omega_{\text{a,b}}$ describes the energy density fraction for each fluid. The w and θ quantities (without subscripts) represent the effective EoS parameter and the divergence of velocity field, respectively. The equations of conservation for each fluid lead to the following set of equations [23]:

$$\begin{aligned}
\delta_a' + 3\mathcal{H}\left(c_{sa}^2 - w_a\right)\delta_a &= -\left(1+w_a\right)\left(\theta + 3\Phi'\right), \\
\theta_a' + \left[\mathcal{H}\left(1-3w_a\right) + w_a'\right]\theta_a &= -\nabla^2\left[\frac{c_{sa}^2}{1+w_a}\delta_a - \Phi\right], \\
\delta_b' + 3\mathcal{H}\left(c_{sb}^2 - w_b\right)\delta_b &= -\left(1+w_b\right)\left(\theta + 3\Phi'\right), \\
\theta_b' + \left[\mathcal{H}\left(1-3w_b\right) + w_b'\right]\theta_b &= -\nabla^2\left[\frac{c_{sb}^2}{1+w_b}\delta_b - \Phi\right],
\end{aligned} \tag{B.53}$$

while the equations for the gravitational potential, Φ, related with the above equations read [23]

$$\begin{aligned}
\nabla^2\Phi - 3\mathcal{H}\left(\mathcal{H}\Phi + \Phi'\right) &= -4\pi G a^2\rho\delta, \\
-\nabla^2\left(\mathcal{H}\Phi + \Phi'\right) &= -4\pi G a^2\left(1+w\right)\rho\theta, \\
\Phi'' + 3\mathcal{H}\Phi' + \Phi\left(2\mathcal{H}' + \mathcal{H}^2\right) &= -4\pi G a^2 c_s^2\rho\delta.
\end{aligned} \tag{B.54}$$

B.3.1 Perturbed equations for radiation and matter

We will start choosing the contents of radiation and matter, using the subscripts r and m, respectively. The corresponding values for independent EoS parameters, ($c_{sr}^2 = w_r = 1/3$ for radiation and $c_{sm}^2 = w_m = 0$ for matter), will be incorporated. In addition, we will use the following Friedmann equation that allow us to simplify the equation for the gravitational scalar perturbation,

$$\rho = \frac{3a^2\mathcal{H}^2}{8\pi G} \tag{B.55}$$

Therefore, the equations for the gravitational perturbation can be rewritten as follows [23]

$$\begin{aligned}
&\Phi_N + \Phi\left(1 + \frac{k^2}{3\mathcal{H}^2}\right) = \frac{1}{2}\delta, \\
&\Phi_N + \Phi = \frac{3}{2}\mathcal{H}v\left(1+w\right), \\
&\Phi_{NN} + \left[3 - \frac{1}{2}\left(1+3w\right)\right]\Phi_N - 3w\Phi = -\frac{3}{2}c_s^2\delta.
\end{aligned} \tag{B.56}$$

In the same way that we have done previously, combining the first and third equation in (B.56) we can get an equation for Φ alone [23]

$$\Phi_{NN} + \left[3\left(1+c_s^2\right) - \frac{1}{2}\left(1+3w\right)\right]\Phi_N + \left[3\left(c_s^2 - w\right) + \frac{c_s^2 k^2}{\mathcal{H}^2}\right]\Phi = 0. \tag{B.57}$$

Finally, the equations for matter perturbations and velocities are [23, 92]

$$\begin{aligned} \delta_{m,N} &= \left[\frac{k^2}{\mathcal{H}} v_m + 3\Psi_N\right] \quad , \quad \delta_{r,N} = \frac{4}{3}\left[\frac{k^2}{\mathcal{H}} v_r + 3\Psi_N\right], \\ v_{m,N} &= -\left[v_m + 3\frac{\Psi}{\mathcal{H}}\right] \quad , \quad v_{r,N} = -\frac{1}{\mathcal{H}}\left[\frac{\delta_r}{4} + \Psi\right], \end{aligned} \tag{B.58}$$

where the effective EoS parameter, w, and the total contribution for velocity and matter perturbations read

$$w = \frac{\Omega_r}{3} \quad , \quad v = \frac{1}{1+w}\left(\frac{4}{3}\Omega_r v_r + \Omega_m v_m\right) \quad , \quad \delta = \Omega_r \delta_r + \Omega_m \delta_m. \tag{B.59}$$

The set of equations obtained in this section describe a fluid mixture of radiation and matter. However, it is easy to incorporate more fluids by considering, for example, a DE fluid with a well defined EoS. In the present thesis, we have incorporated the DE fluid by considering a third component in the mixture with a EoS parameter that always stands below -1. Bear in mind that for each a new fluid incorporated the set of dynamical equation (B.58) is broaden with two more equations, giving rise to the set of equations (2.33). Therefore, there will be two more initial conditions to be fixed.

B.3.2 Initial conditions

Once the dynamical equation system is defined, it only remains to fix the initial conditions. In the present thesis, we have fixed the initial conditions in the early Universe deep inside the radiation dominated era. Within this scenario, the presence of DE and matter is regardless[i] and we could apply some approximations. One of them is that all the relevant modes considered at present are small comparing with the comoving Hubble parameter at the radiation dominated epoch, i.e $k \ll \mathcal{H}(N)$ where $N \to -\infty$. For example, neglecting the term $k/\mathcal{H}$ in (B.57) we have [23]

$$\Phi_{NN} + \left[3\left(1+c_s^2\right) - \frac{1}{2}\left(1+3w\right)\right]\Phi_N \approx 0. \tag{B.60}$$

Therefore $\Phi = constant$ is a solution. Applying this result to the equation set (B.56), we get [23]

$$\begin{aligned} \Phi &\approx \frac{1}{2}\delta, \\ \Phi &\approx \frac{3}{2}\mathcal{H} v \left(1+w\right). \end{aligned} \tag{B.61}$$

This means that the total matter perturbation, δ, and the quantity $\mathcal{H}v\left(1+w\right)$, are constant at the beginning, i.e. when $N \to -\infty$. On the other hand, during the radiation dominated epoch, the contribution of the other fluids can be disregarded, i.e. $\Omega_r \approx 1$. Therefore, the effective

[i] However, we will consider a very small portion of matter and DE since they are necessary at the time to impose adiabatic condition as we will see later on.

EoS, the total matter density contrast and velocity can be approximated as

$$w \approx w_r = \frac{1}{3} \quad , \quad v \approx v_r \quad , \quad \delta \approx \delta_r. \tag{B.62}$$

Finally, the imposition of adiabatic condition at the beginning leads to [23]

$$\frac{\delta_m}{1+w_m} = \frac{\delta_r}{1+w_r} = \frac{\delta}{1+w}. \tag{B.63}$$

If a third fluid is considered, which is indeed the case of the present thesis with a DE content, the adiabatic condition is written as (2.37). Note that in order to have a complete set of initial condition, still remains to impose the initial value of δ. However, for a linear set of dynamical system, the total solution is a linear combination of independent solutions. We have made use of this property writing all the initial conditions proportional to the initial total matter perturbation, δ. Therefore,

$$\delta_m\left(N_*\right) \approx \frac{3}{4}\delta_r\left(N_*\right) \approx \frac{3}{4}\delta\left(N_*\right), \tag{B.64}$$

where N_* denotes the initial value. On the other hand, the adiabatic condition is also valid for the total matter density contrast (see (B.44)), therefore, it follows from the gauge difference [92] that

$$\frac{\delta_m\left(N_*\right) - 3\mathcal{H}v_m\left(N_*\right)}{1+w_m} = \frac{\delta_r\left(N_*\right) - 3\mathcal{H}v_r\left(N_*\right)}{1+w_r}. \tag{B.65}$$

Finally, using the equations (B.64) and (B.65) we obtain

$$v_m\left(N_*\right) = v_m\left(N_*\right) \approx \frac{\delta}{3\mathcal{H}\left(1+w\right)}, \tag{B.66}$$

where we have made use of the approximation given in (B.61). Once we have the initial conditions for each perturbation variable, we solve the system for $\Phi\left(N_*\right) = 1$ (that means $\delta\left(N_*\right) = 2$) and then, multiply all solutions by the physical value of $\delta\left(N_*\right)$ which is given by the observational fit. The same methodology could be applied if a third fluid were involved, as it is the case of the present thesis where the initial conditions for a mixture with three fluids give rise to the set of initial conditions given in section 2.3.1

B.4 Two point correlation function

The two point correlation function is a mathematical tool used in statistics to quantify the fluctuations. In cosmology it is often applied to describe the distribution of galaxies, in this sense, the total matter density contrast is the quantity usually used. The two point correlation function, $\xi_\zeta\left(\mathbf{x}\right)$, by definition is written as [ii]

$$\xi_\zeta\left(\mathbf{r}\right) = \frac{1}{V}\int_V \zeta^*\left(\mathbf{x}\right)\zeta\left(\mathbf{x}+\mathbf{r}\right)d^3\mathbf{x}, \tag{B.67}$$

where the script * denotes the complex conjugate and $\zeta\left(\mathbf{x}+\mathbf{r}\right)$ is the value of ζ at the position $\mathbf{x}+\mathbf{r}$. In other words, it can be said that the correlation function is a tool to know how much is a function similar with itself. For example, the correlation function of a an amount that remains

[ii] As we will see later on, ζ will coincide with the total matter density contrast, δ.

constant is always equal to one. It is very useful to use the Fourier transform leading to

$$\begin{aligned}\zeta(\mathbf{k}) &= \frac{A}{V}\int e^{-i\mathbf{k}\cdot\mathbf{x}}\zeta(\mathbf{x})\ d^3\mathbf{x},\\ \zeta(\mathbf{x}) &= BV\int e^{i\mathbf{k}\cdot\mathbf{x}}\zeta(\mathbf{k})\ d^3\mathbf{k},\end{aligned} \tag{B.68}$$

where $AB = 1/(2\pi)^3$. Therefore, it is the usual to choice $A = 1$ and $B = 1/(2\pi)^3$. On the other hand, it can be defined the Dirac delta as

$$\delta^D(\mathbf{k}) = AB\int e^{-i\mathbf{k}\cdot\mathbf{x}}d^3\mathbf{x}. \tag{B.69}$$

Applying the Fourier transform on both elements inside the integral (B.67), we get

$$\begin{aligned}\xi_\zeta(\mathbf{r}) &= B^2V\int_V\int e^{-i\mathbf{k}\cdot\mathbf{x}}\zeta^*(\mathbf{k})\ d^3\mathbf{k}\int e^{i\tilde{\mathbf{k}}\cdot(\mathbf{x}+\mathbf{r})}\zeta(\mathbf{k}')\ d^3\mathbf{k}',\\ \xi_\zeta(\mathbf{r}) &= B^2V\int\int\zeta^*(\mathbf{k})\,\zeta(\mathbf{k}')\,d^3\mathbf{k}d^3\mathbf{k}'\int_V e^{i(\mathbf{k}'-\mathbf{k})\cdot\mathbf{x}}\ d^3\mathbf{x},\end{aligned} \tag{B.70}$$

where the last integral term in rhs of (B.70) is proportional to the Dirac delta centered in $\mathbf{k}'$, that is

$$\delta^D(\mathbf{k}-\mathbf{k}') = AB\int e^{i(\mathbf{k}'-\mathbf{k})}d^3\mathbf{x}. \tag{B.71}$$

Making use of the Dirac delta we obtain

$$\xi_\zeta(\mathbf{r}) = \frac{BV}{A}\int|\zeta(\mathbf{k})|^2\,e^{i\mathbf{k}\cdot\mathbf{r}}d^3\mathbf{k}. \tag{B.72}$$

Just for notation convenience, we will define

$$P_\zeta(\mathbf{k}) \equiv \frac{1}{A}|\zeta(\mathbf{k})|^2 \tag{B.73}$$

$$\xi_\zeta(\mathbf{r}) \equiv BV\int P_\zeta(\mathbf{k})\,e^{i\mathbf{k}\cdot\mathbf{r}}d^3\mathbf{k}. \tag{B.74}$$

If we assume a homogeneous and isotropic Universe at large scales, there is not dependence on the direction, only the distances are important. In order to perform the integral (B.74), we will chose the axis such that the direction of $\mathbf{r}$ coincides with that of the z axis, in such a way that

$$d^3\mathbf{k} = k^2\sin\theta_k\ dk\ d\theta_k\ d\varphi_k \qquad , \qquad \mathbf{k}\cdot\mathbf{r} = k\ r\cos\theta_k, \tag{B.75}$$

therefore, the integral (B.70) is written as

$$\xi_\zeta(r) = BV\int_0^\infty\int_0^\pi\int_0^{2\pi}P_\zeta(k)\,e^{ikr\cos\theta_k}k^2\sin\theta_k\ dk\ d\theta_k\ d\varphi_k. \tag{B.76}$$

Integrating (B.76) over the solid angle we get

$$\xi_\zeta(r) = 4\pi BV\int_0^\infty P_\zeta(k)\,\frac{k}{r}\sin kr\ dk. \tag{B.77}$$

This expression can be rewritten as

$$\xi_\zeta(r) = V\int_0^\infty \Delta_\zeta^2(k)\,\frac{\sin kr}{kr}\,d[\ln k]\,,\quad \text{where}\quad \Delta_\zeta^2(k) = 4\pi B k^3 P_\zeta(k) \tag{B.78}$$

B.4.1 Matter power spectrum

We have fixed the initial conditions on a regime where the radiation totally dominates over the the other components in such a way that all the relevant modes lie outside the horizon. For practical purposes, it is often used the *primordial power spectrum*, Δ_ζ^2, instead of the *power spectrum*, P_ζ. These two functions are related as follows (see the previous section B.4)

$$\Delta_\zeta^2 = \frac{k^3}{2\pi^2}\,|\zeta|^2\,, \tag{B.79}$$

The quantity usually used to set the initial conditions is the comoving curvature perturbation, $R = -(\Phi + v\mathcal{H})$. The observational fit for the curvature perturbation coincides with the following empirical formula

$$\Delta_R^2 = A_s(k_*)\left(\frac{k}{k_*}\right)^{n_s(k_*)-1}, \tag{B.80}$$

where the quantities A_s and n_s depend on the value for the chosen pivot wave-number k_*. Equating the observational results (B.80) with the theoretical one (B.79), we can get a suitable value for the curvature perturbation within a radiation dominated era (see (B.61)) which can be approximated to the total matter perturbation, i.e. $R \approx \delta$. Therefore,

$$|\delta| \approx \frac{4\pi}{3}\sqrt{2A_s}\,k^{-\frac{3}{2}}\left(\frac{k}{k_*}\right)^{\frac{n_s-1}{2}}. \tag{B.81}$$

B.4.2 Physical value of the initial total matter density contrast

Once the set of dynamical equation is defined and the set of the initial conditions is fixed, the initial values of all the perturbation variables are proportional to the initial total matter density contrast, $\delta^\star$. Therefore, it remains only to fix the physical value of $\delta^\star$. This value is fixed through the Planck data for a single field inflation which can be written as [13, 15]

$$\delta^\star = \frac{4\pi}{3}\sqrt{2A_\mathsf{s}}\left[\frac{k}{k_\mathsf{pivot}}\right]^{\frac{n_\mathsf{s}-1}{2}} k^{-\frac{3}{2}}, \tag{B.82}$$

where the pivot wave-number is $k_\mathsf{pivot} = 0.05\ \mathsf{Mpc}^{-1}$. In addition, A_s and n_s are the amplitude and the spectral index, respectively. We have used different values of A_s and n_s corresponding with the latest data of Planck missions available at the time of publishing the works [13, 15].

B.5 Decomposition of a non-adiabatic pressure

We first consider a gauge transformation from the rest frame to the Newtonian gauge. Therefore, the physical quantities in both gauges are related as [16, 92, 101]

$$\delta p_\ell = \delta p_\ell|_{\mathsf{r.f.}} - p'_\ell\delta\eta\ \ ,\ \ \delta\rho_\ell = \delta\rho_\ell|_{\mathsf{r.f.}} - \rho'_\ell\delta\eta\ \ ,\ \ (v_\ell + B) = (v_\ell + B)|_{\mathsf{r.f.}} + \delta\eta, \tag{B.83}$$

where ℓ stands for a given DE fluid, subscript r.f denotes the rest frame and no subscript refers to the Newtonian gauge. In the rest frame, $v_{\ell\text{r.f.}} = 0$ and $B_{\text{r.f.}} = 0$, while in the Newtonian gauge it is set $B = 0$. Therefore, this implies $v_\ell = \delta\eta$. On the other hand, we consider that the total pressure perturbation is given by its adiabatic and non-adiabatic contributions,

$$\delta p_\ell = \delta p_{\ell\text{ad}} + \delta p_{\ell\text{nad}}, \tag{B.84}$$

where by definition, $\delta p_{\ell\text{ad}} = c_{a\ell}^2 \delta\rho_\ell$ is the adiabatic part. We compute the gauge difference on both sides of the equality (B.84) using the equations (B.83). First, we deduce that the non adiabatic part is gauge invariant, i.e. $\delta p_{\ell\text{nad}} = \delta p_{\ell\text{nad}}|_{\text{r.f.}}$. Therefore, we get

$$\delta p_{\ell\text{nad}} = \left(c_{s\ell}^2 - c_{a\ell}^2\right) \delta\rho_\ell|_{\text{r.f.}}\,, \qquad \delta p_\ell = c_{s\ell}^2 \delta\rho_\ell + \left(c_{s\ell}^2 - c_{a\ell}^2\right) \rho_\ell' \delta\eta. \tag{B.85}$$

Finally, making use of the conservation equation, $\rho_\ell' = -3\mathcal{H}\left(1 + w_\ell\right)\rho_\ell$, the non-adiabatic contribution and the total pressure perturbation can be written as [16, 101, 231]

$$\begin{aligned} \delta p_{\ell\text{nad}} &= \left(c_{s\ell}^2 - c_{a\ell}^2\right)\left[\delta\rho_\ell - 3\mathcal{H}\left(1 + w_\ell\right)\rho_\ell v_\ell\right], \\ \delta p_\ell &= c_{s\ell}^2 \delta\rho_\ell + \left(c_{a\ell}^2 - c_{s\ell}^2\right) 3\mathcal{H}\left(1 + w_\ell\right)\rho_\ell v_\ell. \end{aligned} \tag{B.86}$$

B.6 Classical perturbations for a Universe containing an adiabatic fluid with a negative speed of sound

On the following appendix, we remind why a Universe filled with a DE fluid with a negative speed of sound, like it is the case of a phantom fluid with a constant EoS parameter, the linear perturbations of DE blow up. We begin by recalling the evolution equations (2.30) for the pair δ_A and v_A in Fourier space:

$$\begin{aligned} \delta_A' &= 3\mathcal{H}\left(w_A - c_{sA}^2\right)\delta_A + \left(1 + w_A\right)\left[9\mathcal{H}^2\left(c_{sA}^2 - c_{aA}^2\right) + k^2\right] v_A + 3\left(1 + w_A\right)\Psi', \\ v_A' &= \left(3c_{sA}^2 - 1\right)\mathcal{H} v_A - \frac{c_{sA}^2}{1 + w_A}\delta_A - \Psi\,. \end{aligned} \tag{B.87}$$

We can combine these equations into a single second order inhomogeneous differential equation for δ_A by differentiating (B.87) and then using (B.87) and (B.87) to eliminate v_A and v_A'

$$\begin{aligned} &\delta_A'' + \left[\left(1 - 6w_A + 3c_{aA}^2\right) - \frac{\mathcal{H}\left(c_{sA}^2 - c_{aA}^2\right)' + 2\mathcal{H}'\left(c_{sA}^2 - c_{aA}^2\right)}{\mathcal{H}^2\left(c_{sA}^2 - c_{aA}^2\right) + \frac{k^2}{9}}\right]\mathcal{H}\delta_A' \\ &- 3\Bigg[\mathcal{H}'\left(w_A - c_{sA}^2\right) + \mathcal{H}\left(w_A - c_{sA}^2\right)' + \mathcal{H}^2\left(1 - 3w_A\right)\left(w_A - c_{sA}^2\right) + 3\mathcal{H}^2 w_A\left(c_{aA}^2 - c_{sA}^2\right) \\ &+ \mathcal{H}^2\left(c_{sA}^2 - w_A\right)\frac{\mathcal{H}\left(c_{sA}^2 - c_{aA}^2\right)' + 2\mathcal{H}'\left(c_{sA}^2 - c_{aA}^2\right)}{\mathcal{H}^2\left(c_{sA}^2 - c_{aA}^2\right) + \frac{k^2}{9}} - \frac{k^2}{3}c_{sA}^2\Bigg]\delta_A \\ &= 3\left(1 + w_A\right)\Bigg\{\Psi'' + \left[\left(1 - 3c_{sA}^2\right) - \frac{\mathcal{H}\left(c_{sA}^2 - c_{aA}^2\right)' + 2\mathcal{H}'\left(c_{sA}^2 - c_{aA}^2\right)}{\mathcal{H}^2\left(c_{sA}^2 - c_{aA}^2\right) + \frac{k^2}{9}}\right]\mathcal{H}\Psi' \\ &- \left[3\mathcal{H}^2\left(c_{sA}^2 - c_{aA}^2\right) + \frac{k^2}{3}\right]\Psi\Bigg\}\,. \end{aligned} \tag{B.88}$$

This is a wave equation with a variable damping term, λ_A, and mass, m_A, and with an external source, $\mathcal{S}_A$:

$$\delta_A'' + \lambda_A \delta_A' + m_A^2 \delta_A = \mathcal{S}_A \,, \tag{B.89}$$

where

$$\lambda_A \;= \left[\left(1 - 6w_A + 3c_{aA}^2\right) - \frac{\mathcal{H}\left(c_{sA}^2 - c_{aA}^2\right)' + 2\mathcal{H}'\left(c_{sA}^2 - c_{aA}^2\right)}{\mathcal{H}^2\left(c_{sA}^2 - c_{aA}^2\right) + \frac{k^2}{9}} \right] \mathcal{H}, \tag{B.90}$$

$$\begin{aligned} m_A^2 \;= k^2 c_{sA}^2 - 3 \Bigg[& \mathcal{H}'\left(w_A - c_{sA}^2\right) + \mathcal{H}\left(w_A - c_{sA}^2\right)' + \mathcal{H}^2\left(1 - 3w_A\right)\left(w_A - c_{sA}^2\right) \\ & + 3\mathcal{H}^2 w_A\left(c_{aA}^2 - c_{sA}^2\right) + \mathcal{H}^2\left(c_{sA}^2 - w_A\right) \frac{\mathcal{H}\left(c_{sA}^2 - c_{aA}^2\right)' + 2\mathcal{H}'\left(c_{sA}^2 - c_{aA}^2\right)}{\mathcal{H}^2\left(c_{sA}^2 - c_{aA}^2\right) + \frac{k^2}{9}} \Bigg], \end{aligned} \tag{B.91}$$

$$\begin{aligned} \mathcal{S}_A \;= 3\left(1 + w_A\right) \Bigg\{ & \Psi'' + \left[\left(1 - 3c_{sA}^2\right) - \frac{\mathcal{H}\left(c_{sA}^2 - c_{aA}^2\right)' + 2\mathcal{H}'\left(c_{sA}^2 - c_{aA}^2\right)}{\mathcal{H}^2\left(c_{sA}^2 - c_{aA}^2\right) + \frac{k^2}{9}} \right] \mathcal{H}\Psi' \\ & - \left[3\mathcal{H}^2\left(c_{sA}^2 - c_{aA}^2\right) + \frac{k^2}{3} \right] \Psi. \end{aligned} \tag{B.92}$$

To leading order in k^2, we have $m_A^2 \simeq k^2 c_{sA}^2$. Therefore, for sufficiently large k, the mass becomes imaginary if $c_{sA}^2 < 0$ and the solutions of the homogeneous equation comprise a decaying and a growing mode, with the latter leading to the instabilities. As such, barotropic fluids with negative adiabatic squared speed of sound, for which $c_{sA}^2 = c_{aA}^2$, are stricken by instabilities at the linear level in perturbations. The growth of δ_A can be particularly intense during the matter era, when most relevant modes are inside the Hubble horizon, i.e., $k^2 \gg \mathcal{H}^2$, and $\Psi \sim const.$

B.7 Mapping to a phantom scalar field

The phantom scalar field, which was first introduced in [30] as a way of obtaining an EoS parameter with $w < -1$, can be seen as a minimally coupled scalar field with the sign of the kinetic term in the Lagrangian switched, i.e.: [iii]

$$L_\varphi = \frac{1}{2} g^{\mu\nu} \partial_u \varphi \partial_\nu \varphi - V(\varphi) \,. \tag{B.93}$$

In this sense, the phantom scalar field can be viewed as a particular case of the K-essence models with $K = -X$ [24]. The change of sign in the Lagrangian with regards to the usual scalar field is propagated to the energy density and pressure, which for the phantom field case in a FLRW background are given by the expressions:

$$\begin{aligned} \rho_\varphi &= -\frac{1}{2}\dot{\varphi}^2 + V(\varphi) \,, \\ p_\varphi &= -\frac{1}{2}\dot{\varphi}^2 - V(\varphi) \,. \end{aligned} \tag{B.94}$$

[iii] Here, we remind the reader that on this work we employ the metric signature $(-\,+\,+\,+)$. This is the reason that the sign of the kinetic term in the Lagrangian does not coincide with the one in [30], which uses the signature $(+\,-\,-\,-)$.

Likewise, the term of the equation of motion of the field that depends on the derivative of the potential suffers a change of sign:

$$\ddot{\varphi} + 3H\dot{\varphi} - \frac{dV}{d\varphi} = 0\,. \tag{B.95}$$

From equations (B.94) we find that for positive valued potentials the parameter of EoS of the phantom scalar field, $w_\varphi = p_\varphi/\rho_\varphi$, can evolve dynamically in the interval $(-\infty,\, -1]$, while from the equation of motion (B.95) we find that the field tends to climb the potential towards a state of higher energy [30].

In Section 2.2, we have reviewed three phantom DE models that lead to abrupt events in the future: model A leads to a BR; model B leads to a LR; model C leads to a LS. At the background level, these models can be mapped to a phantom scalar field through the identifications

$$\begin{aligned} \dot{\varphi}^2 &= -\left(1 + w_{\mathsf{d}}\right)\rho_{\mathsf{d}}\,, \\ V(\varphi) &= \frac{1}{2}\left(1 - w_{\mathsf{d}}\right)\rho_{\mathsf{d}}\,. \end{aligned} \tag{B.96}$$

Once the background evolution is imposed, the shape of the potential can be found by integrating the first equation of (B.96)

$$\varphi(t) - \varphi(t_*) = \int_t^{t_*} d\tilde{t}\sqrt{-\left(1 + w_{\mathsf{d}}\right)\rho_{\mathsf{d}}}\,, \tag{B.97}$$

inverting the expression obtained to find $\rho(\varphi)$ and finally plugging the result in the second equation of (B.96) we get $V(\varphi)$. For the three models at hand, we can solve (B.97) analytically well inside the DE dominated regime, i.e., for $t \geq t_*$ we have $H^2 \approx (\kappa^2/3)\rho_{\mathsf{d}}$, obtaining for each case the potential [42, 70, 202, 390, 391]

$$\begin{aligned} &\text{Model A,} \qquad V(\varphi) = \rho_{\mathsf{d},*}\frac{1 - w_{\mathsf{d}}}{2}\exp\left[\sqrt{-3(1 + w_{\mathsf{d}})}\kappa\left(\varphi - \varphi_*\right)\right]\,; \\ &\text{Model B,} \qquad V(\varphi) = \rho_{\mathsf{d},*}\left\{\left[1 + \frac{3}{4}\left(\frac{\Omega_{\mathsf{lr}}}{\Omega_{\mathsf{d},*}}\right)^{1/4}\kappa\left(\varphi - \varphi_*\right)\right]^2 + \frac{1}{2}\left(\frac{\Omega_{\mathsf{lr}}}{\Omega_{\mathsf{d},*}}\right)^{1/2}\right\} \\ &\qquad\qquad\qquad \times\left[1 + \frac{3}{4}\left(\frac{\Omega_{\mathsf{lr}}}{\Omega_{\mathsf{d},*}}\right)^{1/4}\kappa\left(\varphi - \varphi_*\right)\right]^2\,; \\ &\text{Model C,} \qquad V(\varphi) = \rho_{\mathsf{d},*}\left\{\left[1 + \frac{1}{2}\left(\frac{\Omega_{\mathsf{lsbr}}}{\Omega_{\mathsf{d},*}}\right)^{1/2}\kappa\left(\varphi - \varphi_*\right)\right]^2 + \frac{1}{6}\left(\frac{\Omega_{\mathsf{lsbr}}}{\Omega_{\mathsf{d},*}}\right)^{1/2}\right\}\,. \end{aligned} \tag{B.98}$$

We now look at the evolution of the linear scalar perturbations of such models. In the phantom scalar field description, the evolution of the perturbation $\delta\varphi$ in the Newtonian gauge is given by [30, 392]

$$\delta\varphi'' + 2\mathcal{H}\delta\varphi' + \left(k^2 - a^2\frac{d^2V}{d\varphi^2}\right)\delta\varphi = 2a^2\frac{dV}{d\varphi}\Phi + \varphi'\left(\Phi' - 3\Psi'\right)\,. \tag{B.99}$$

As long as the squared mass term $k^2 - a^2 d^2V/d\varphi^2$ is positive, then the perturbation $\delta\varphi$ is free of instabilities [30]. However, for the three models considered in this work, the second derivative of the potential is always positive; in fact, from (B.98) we find that for the models (i) and (ii) $d^2V/d\varphi^2$ goes to infinity as the field climbs the potential, while for the model (iii) it is a positive

constant. Therefore, in all cases as the Universe expands the effective mass of the perturbation $\delta\varphi$ becomes imaginary and the unstable regime sets in.

As discussed above, for the three models considered in this work there is an instability at the perturbative level that leads $\delta\varphi$ to extremely large values in the far future, as the Universe evolves towards a cosmological singularity or abrupt event. However, as we will see next, if we describe the linear perturbations of the scalar field from an hydrodynamical point of view, this instability is not displayed for $\delta_\varphi = \delta\rho_\varphi/\rho_\varphi$ or for the gravitational potential Ψ. Let us begin by reviewing the perturbations of the energy density, pressure and the peculiar velocity of the phantom scalar, which in the Newtonian gauge read

$$\begin{aligned}
\delta\rho_\varphi &= -\frac{1}{a^2}\varphi'\left(\delta\varphi' - \varphi'\Phi\right) + \frac{dV}{d\varphi}\delta\varphi\,, \\
\delta p_\varphi &= -\frac{1}{a^2}\varphi'\left(\delta\varphi' - \varphi'\Phi\right) - \frac{dV}{d\varphi}\delta\varphi\,, \\
v_\varphi &= -\frac{\delta\varphi}{\varphi'}\,.
\end{aligned} \tag{B.100}$$

From these equations we find that

$$\delta p_\varphi = \delta\rho_\varphi - 2\frac{dV}{d\varphi}\delta\varphi = \delta\rho_\varphi + 2\frac{dV}{d\varphi}\varphi' v_\varphi\,, \tag{B.101}$$

Since the adiabatic squared speed of sound is $c^2_{a\varphi} = \dot{p_\varphi}/\dot{\rho_\varphi} = 1 - 2a^2/(3\mathcal{H}\varphi')(dV/d\varphi)$ a comparison of (B.101) with (2.26) leads to the conclusion that at the perturbative level the phantom scalar field corresponds to a non-adiabatic fluid with effective speed of sound $c^2_{s\varphi} = 1$. The same result can be reached by using the definitions (2.27) and (B.100) and noting that in the rest frame of the field $\delta\varphi = 0$.

To show that the divergence of $\delta\varphi$ does not necessarily translate into a divergence of δ_φ, we now look at the evolution of the gravitational potential Ψ. Since at late-time the contribution of matter and radiation to the potential is suppressed by the factors Ω_{m} and Ω_{r}, respectively, then we can assume that in the future the potential is generated only by the DE perturbations. By combining (B.40), (B.95), (B.100) and (B.101) and changing from η-derivatives to x-derivatives [iv], we arrive at the following evolution equation for each Fourier mode

$$\Psi_{xx} + \left(2 + \frac{\mathcal{H}'}{\mathcal{H}^2} - 2\frac{\varphi''}{\mathcal{H}\varphi'}\right)\Psi_x + 2\left(\frac{\mathcal{H}'}{\mathcal{H}^2} - \frac{\varphi''}{\mathcal{H}\varphi'} + \frac{k^2}{\mathcal{H}^2}\right)\Psi \quad = 0\,. \tag{B.102}$$

At this point, we note that $\mathcal{H}'/\mathcal{H}^2 = -(1+3w)/2$ and $\varphi''/(\mathcal{H}\varphi') = -(1+3c^2_{a\varphi})/2$ and that the term in k^2 can be dropped, since in a phantom dominated (or in general in an inflating) Universe all the modes end up outside of the Hubble horizon. We can then approximate (B.102) as:

$$\Psi_{xx} + \frac{1}{2}\left[2 + 3\left(1 + c^2_{a\varphi}\right) + 3\left(c^2_{a\varphi} - w_\varphi\right)\right]\Psi_x + 3\left(c^2_{a\varphi} - w_\varphi\right)\Psi \quad \approx 0\,. \tag{B.103}$$

Therefore, there is no instability at the level of the gravitational potential as long as the mass term in the previous equation is positive. To check whether or not this is the case in the models at hand, we use the relation $c^2_a = w + \rho(w'/\rho')$ and recall that for model (i) $w'_\varphi = 0$ while for models (ii) and (iii) w_φ is approaching -1 from below and ρ_φ grows continuously as the

[iv] We remind the reader that by definition $x = \log(a/a_0)$.

Universe expands. Thus we find that in all three cases Ψ remains bounded and slowly varying with x. Finally, from the perturbed Einstein equations (2.34), we conclude that $\delta_\varphi = -2\Psi$ is also bounded at late-time. This is the behaviour in the far future that we find in figures 3.1 and 3.2.

Appendix C

Detailed calculations for the quantum part

In this appendix we show a detailed calculation of the main approximations used in the present thesis when solving the WDW equation. On the one hand, the WKB approximation up to the first order is carried several times for a one dimensional differential equation. On the other hand, the BO approximation is carried when dealing with a phantom scalar field. These two approximation engross the methods for obtaining a suitable solution to the WDW equation. Finally, we show detailed calculations of the solutions to the differential equation (9.38) within the context of the Symanzik scaling law.

C.1 The WKB approximation

We next review briefly the WKB method for second order differential equation

$$\left[\frac{d^2}{dy^2} + V_{\text{eff}}\left(y\right)\right]\psi(y) = 0\ , \tag{C.1}$$

where y is defined such that it is a dimensionless degree of freedom and where the effective potential can be written as

$$V_{\text{eff}}\left(y\right) = \tilde{\eta}^2 g(y)\ . \tag{C.2}$$

Moreover, $\tilde{\eta}$ is a dimensionless parameter related with the constants of the system. The zero order WKB approximation reads

$$\psi_0(y) \approx B_1 e^{iS_0(y)} + B_2 e^{-iS_0(y)}, \tag{C.3}$$

where B_1 and B_2 are constants and

$$S_0(y) = \tilde{\eta}\int_{y_1}^{y}\sqrt{g(y)}dy. \tag{C.4}$$

On the other hand, the general expression for the WKB approximated solution up to first order, reads [339]

$$\psi_I(y) \approx \left[-\tilde{\eta}^2 g\left(y\right)\right]^{-\frac{1}{4}}\left[B_1 e^{iS_0(y)} + B_2 e^{-iS_0(y)}\right], \tag{C.5}$$

Note that the first order WKB approximation is a product of the function $\tilde{\eta}^{-\frac{1}{2}} g\left(y\right)^{-\frac{1}{4}}$ and the zero order WKB approximation, which is just a sinusoidal function, $\psi_0(y) \approx B_1 e^{iS_0(y)} + B_2 e^{-iS_0(y)}$. As can be seen, the first order WKB approximation just modulates the zero order WKB approximation.

C.1.1 Validity of the WKB approximation

The zero order WKB approximation, given by (C.3), is valid as far the following inequality is fulfilled [334, 339]

$$\frac{1}{\tilde{\eta}}\left|\frac{\dot{g}(y)}{g^{\frac{3}{2}}(y)}\right| \ll 1. \tag{C.6}$$

For example, the WKB approximation for a constant potential returns the exact solution since the inequality (C.6) is fully fulfilled. On the contrary, the approximation is not valid when the effective potential (C.2) vanishes since the output of (C.6) returns very large values. On the other hand, the WKB approximation up to the first order, given by (C.5), is valid as long as the inequality

$$\frac{1}{\tilde{\eta}^2}\left|\frac{5\dot{g}^2(y)-4\ddot{g}(y)g(y)}{16g^3(y)}\right| \ll 1, \tag{C.7}$$

is fulfilled [44, 339]. When the left hand side of (C.7) goes to zero we can be sure that the behavior of the exact solution in this regime matches almost perfectly with the WKB approximation.

C.1.2 Justification for the WKB approximation

We have used the WKB approximation several times to solve the second order differential equation as that given in (C.1). For example, in (8.14) the WKB approximation is justified due to the large values of the parameter $\tilde{\eta}^2$ in the region where the approximation was applied. Then, in (8.18) the WKB approximation is justified since the effective potential of DE as given in Eq (8.17) returns a vanishing value at very large scale factors when replacing it in (C.7).

Furthermore, the approximations used in section 9.3 for the first and the second quantisation procedures, corresponds to an effective potential whose general shape reads

$$V_{\text{eff}}\,(y) \equiv \tilde{\eta}\; y^n\left[1+\gamma\ln(y)\right], \tag{C.8}$$

where for each quantisation procedure we have that:

- First quantisation procedure:

$$\tilde{\eta} = \frac{2}{3}\sqrt{\Omega_{d0}}\eta \qquad , \qquad n=2 \qquad , \qquad \gamma = \sqrt{6}b. \tag{C.9}$$

- Second quantisation procedure:

$$\tilde{\eta} = \sqrt{\Omega_{d0}}\eta \qquad , \qquad n=1 \qquad , \qquad \gamma = \sqrt{\frac{8}{3}}b. \tag{C.10}$$

The necessary condition for the approximation to be valid reads

$$\begin{aligned}&\left|\left\{n^2\,(9-4n)+\frac{4\gamma n\,(1-6n-2\gamma)}{[1+\gamma\ln(y)]}\right.\right.\\&\left.\left.+\;\frac{\gamma^2\,(36-32n-16\gamma)}{[1+\gamma\ln(y)]^2}\right\}\frac{1}{16y^{n+2}\,[1+\gamma\ln(y)]^2}\right|\frac{1}{\tilde{\eta}^2}\ll 1.\end{aligned} \tag{C.11}$$

Finally, in the approximations used in section 10.3 only the parameters s, b and $\tilde{\eta}$ depend on the factor ordering:

1. For the first quantisation procedure used in section 10.3, we use the operator $a\hat{\mathcal{H}}(a,\hat{\pi}_a)$. Then, the parameters above are written as follows

$$s=2,\quad b=\Omega_A,\quad \tilde{\eta}=\frac{3\pi a_0^3 H_0}{2G\hbar}. \tag{C.12}$$

2. For the second factor ordering choice, which corresponds to the operator $\hat{\mathcal{H}}(a,\hat{\pi}_a)$, the parameters are written as

$$s=1,\quad b=\frac{2}{3}\Omega_A,\quad \tilde{\eta}=\frac{\pi a_0^3 H_0}{G\hbar}. \tag{C.13}$$

The integral in (C.4) is given by

$$S_0(y)\equiv\int_{y_1}^{y}\tilde{\eta}y^s\left[\Omega_\Lambda+b\ln(y)\right]^{\frac{1}{2}}dy, \tag{C.14}$$

after performing an integral by parts we get

$$S_0(y)=\tilde{\eta}\frac{y^{s+1}}{s+1}\left[\Omega_\Lambda+b\ln(y)\right]^{\frac{1}{2}}\Big|_{y_1}^{y}-\int_{y_1}^{y}\tilde{\eta}\frac{by^s}{2\,(s+1)}\left[\Omega_\Lambda+b\ln(y)\right]^{-\frac{1}{2}}dy. \tag{C.15}$$

The integral of the second term can be done defining an auxiliary variable $t=i\sqrt{\frac{s+1}{b}\left[\Omega_\Lambda+b\ln(y)\right]}$. This leads to

$$\begin{aligned}S_0(y)=&\,\tilde{\eta}\frac{y^{s+1}}{s+1}\left[\Omega_\Lambda+b\ln(y)\right]^{\frac{1}{2}}-\tilde{\eta}\frac{\sqrt{\pi b}e^{-\frac{\Omega_\Lambda}{b}(s+1)}}{2\,(s+1)^{\frac{3}{2}}}\left\{\text{erfi}\left[\left(\frac{s+1}{b}\right)^{\frac{1}{2}}\sqrt{\Omega_\Lambda+b\ln(y)}\right]\right\}\\&-\tilde{\eta}\frac{y_1^{s+1}}{s+1}\left[\Omega_\Lambda+b\ln(y_1)\right]^{\frac{1}{2}}+\tilde{\eta}\frac{\sqrt{\pi b}e^{-\frac{\Omega_\Lambda}{b}(s+1)}}{2\,(s+1)^{\frac{3}{2}}}\left\{\text{erfi}\left[\left(\frac{s+1}{b}\right)^{\frac{1}{2}}\sqrt{\Omega_\Lambda+b\ln(y_1)}\right]\right\},\end{aligned} \tag{C.16}$$

where y_1 is an arbitrary integration constant such that a_1 (corresponding to y_1) is larger than a_0. The function erfi(z) is the "imaginary error function", which is related with the error function (the expression 7.1.1 of page 297 in [307]) through $\mathrm{erfi}(z)=-i\mathrm{erf}(iz)$. The second term on the rhs in (C.16) is much smaller than the first term for large values of y (as it can be noted considering the expression 7.1.23 of page 298 in [307]), and the third and four terms can, of course, be dismissed in this limit. Therefore, we can neglect it for big values of y.

$$S_0(y)\approx\tilde{\eta}\frac{y^{s+1}}{s+1}\left[\Omega_\Lambda+b\ln(y)\right]^{\frac{1}{2}}. \tag{C.17}$$

The approximation (C.17) is then applied in equations (10.13) and (10.19), where the value of the parameters are written in (C.12) and (C.13), for the first and the second quantisation procedures, respectively. For both of the cases mentioned above, the LR and LS occur for large values of the variable y, where the latter expressions go to zero when $y\to\infty$; i.e. the WKB approximated solution is valid. The inequality (C.7) is a necessary condition for the first order WKB approximation. Being $g(y)=\left[\gamma+\beta\ln(y)\right]y^{2s}$, we get

$$\dot{g}(y)=\left\{\beta+2s\left[\gamma+\beta\ln(y)\right]\right\}y^{2s-1}, \tag{C.18}$$

$$\ddot{g}(y) = \{(2s-1)\{\beta + 2s[\gamma + \beta\ln(y)]\} + 2s\beta\}\, y^{2s-2}, \tag{C.19}$$

so for the zeroth order approximation we have

$$\frac{1}{\tilde{\eta}}\left|\frac{\{\beta + 2s[\gamma + \beta\ln(y)]\}}{2[\gamma + \beta\ln(y)]^{\frac{3}{2}}} y^{-(s+1)}\right| \ll 1, \tag{C.20}$$

and for the first order approximation we get

$$\begin{aligned}\left|\left\{\frac{5}{16}\frac{\{\beta + 2s[\gamma + \beta\ln(y)]\}^2}{[\gamma + \beta\ln(y)]} - \frac{1}{4}\{(2s-1)\{\beta + 2s[\gamma + \beta\ln(y)]\}\}\right.\right. \\ \left.\left. -\frac{s\beta}{2}\right\}\left\{\frac{y^{-2(s+1)}}{[\gamma + \beta\ln(y)]^2}\right\}\right| \frac{1}{\tilde{\eta}^2} \ll 1,\end{aligned} \tag{C.21}$$

which is clearly verified when $y \to \infty$ because $-1 < s$, for both cases and for the two quantisation methods. Here γ and β are constants which for the zeroth and first orders are given in (10.11) and (10.18), respectively.

C.2 Detailed calculations for the matter part of the WDW equation given by equation (10.24)

The matter part of the WDW equation, given in (10.24), can be rewritten as

$$\frac{\partial^2\varphi_k(\alpha, z)}{\partial z^2} + \left(\frac{1}{4}z^2 - \beta\right)\varphi_k(\alpha, z) = 0, \tag{C.22}$$

where

$$\beta = -\frac{1}{2\hbar(\pi G)^{1/2}}\left[\frac{\mathcal{C}^{1/2}a_0^3 e^{3\alpha}}{6} - \frac{E_k}{\mathcal{C}^{1/2}a_0^3 e^{3\alpha}}\right], \tag{C.23}$$

and

$$z = \frac{2a_0^{3/2}e^{3\alpha/2}(\pi G\mathcal{C})^{1/4}}{\hbar^{1/2}}(\phi - \phi_1). \tag{C.24}$$

The expression given in (C.22) corresponds to the expression 19.1.3 of page 686 in [307]. Thus, its solutions are the following parabolic cylinder functions:

$$\begin{aligned}\varphi_k^{(1)}(\alpha, \phi) &= W(\beta, z), \qquad \varphi_k^{(2)}(\alpha, \phi) = W(\beta, -z), \\ \varphi_k^{(3)}(\alpha, \phi) &= E(\beta, z), \qquad \varphi_k^{(4)}(\alpha, \phi) = E^*(\beta, z),\end{aligned} \tag{C.25}$$

with

$$E(\alpha, \phi) = K^{-1/2}W(\beta, z) + iK^{1/2}W(\beta, -z), \tag{C.26}$$

and

$$K = \sqrt{1 + e^{2\pi\beta}} - e^{\pi\beta}. \tag{C.27}$$

We are interested on the behaviour of these functions for arbitrary values of the field and very large values of α. It can be noted that $\beta \to -\infty$ when $\alpha \to \infty$. Defining

$$X = \sqrt{z^2 - 4\beta} = \frac{\sqrt{2}\, a_0^{3/2} e^{3\alpha/2}}{\hbar^{1/2}(\pi G\mathcal{C})^{1/4}} \sqrt{2\pi G\mathcal{C}(\phi - \phi_1)^2 + \frac{\mathcal{C}}{6} - \frac{E_k}{a_0^6 e^{6\alpha}}}, \tag{C.28}$$

it can be noted that $X \to \infty$ when $\alpha \to \infty$. Thus, we focus our attention on the case $\beta < 0$ and $X^2 \gg 0$. The real solutions for this regime are given by (see equations 19.23.10 and 19.23.11 of page 694 in [307])

$$W(\beta,\, z) = \sqrt{2K} e^{v_r} \cos(\pi/4 + \theta + v_i), \tag{C.29}$$

and

$$W(\beta,\, -z) = \sqrt{2/K} e^{v_r} \sin(\pi/4 + \theta + v_i), \tag{C.30}$$

with

$$\begin{aligned} \theta =& \frac{1}{4} zX - \beta \ln\left(\frac{z+X}{2\sqrt{|\beta|}}\right) \\ =& \frac{a_0^3 e^{3\alpha}}{2\hbar\sqrt{\pi\, G\mathcal{C}}} \left\{ \sqrt{\pi\, G\mathcal{C}}(\phi - \phi_1) \sqrt{2\pi G\mathcal{C}(\phi - \phi_1)^2 + \frac{\mathcal{C}}{6} - \frac{E_k}{a_0^6 e^{6\alpha}}} \right. \\ & \left. + \left[\frac{\mathcal{C}}{6} - \frac{E_k}{a_0^6 e^{6\alpha}}\right] \ln\left[\frac{\sqrt{\pi\, G\mathcal{C}}(\phi - \phi_1) + \sqrt{2\pi G\mathcal{C}(\phi - \phi_1)^2 + \frac{\mathcal{C}}{6} - \frac{E_k}{a_0^6 e^{6\alpha}}}}{\sqrt{\frac{\mathcal{C}}{6} - \frac{E_k}{a_0^6 e^{6\alpha}}}} \right] \right\}, \end{aligned} \tag{C.31}$$

and v_i and v_r are defined by series that go as $v_r \approx -1/2 \ln X$ and $v_i \approx 0$ for very large values of X (see equation 19.23.4 of [307]). Moreover, using (C.27) and (C.31), it can be seen that θ diverges as $e^{3\alpha}$ and $K \to 1$ for $\alpha \to \infty$. For large values of α, we can approximate (C.29) as

$$W(\beta,\, z) \approx \sqrt{2}\, X^{-1/2} \cos\left[\frac{\pi}{4} + \frac{1}{4} zX - \beta \ln\left(\frac{z+X}{2\sqrt{|\beta|}}\right)\right]. \tag{C.32}$$

Thus, we have

$$W(\beta,\, z) \sim e^{-3\alpha/4} \cos(e^{3\alpha}) \to 0, \tag{C.33}$$

and

$$W(\beta,\, -z) \sim e^{-3\alpha/4} \sin(e^{3\alpha}) \to 0, \tag{C.34}$$

for $\alpha \to \infty$. On the other hand, taking into account (C.33) and (C.34) into (C.26), one can conclude that the imaginary solutions also vanish in the asymptotic limit.

C.3 The BO approximation

Consider the case of a WDW equation (7.10), where the total wave function is written as (12.19), i.e. the total wave function is a product of the gravitational part, $C_k(\alpha)$, and the matter part,

$\varphi_k(\alpha,\phi)$. Therefore, the WDW equation (7.10) can now be written as

$$\frac{\hbar^2}{2}\frac{\kappa^2}{6}\left(C_k\frac{\partial^2\varphi_k}{\partial\alpha^2}+\varphi_k\frac{\partial^2 C_k}{\partial\alpha^2}+2\frac{\partial C_k}{\partial\alpha}\frac{\partial\varphi_k}{\partial\alpha}\right)+\frac{\hbar^2}{2}C_k\frac{\partial^2\varphi_k}{\partial\phi^2}+a_0^6e^{6\alpha}V(\phi)C_k\varphi_k=0. \tag{C.35}$$

The BO approximation assumes that the first and third terms inside the parenthesis of the latter equation can be neglected in comparison with the second term. That is, it considers that the gravitational part, $C_k(\alpha)$, varies faster with the scale factor than the matter part, $\varphi_k(\alpha,\phi)$, in such a way that

$$\frac{\partial^2\varphi_k(x,\tilde{\phi})}{\partial x^2}C_k(x),\frac{\partial\varphi_k(x,\tilde{\phi})}{\partial x}\frac{\partial C_k(x)}{\partial x}\ll\frac{\partial^2 C_k(x)}{\partial x^2}\varphi_k(x,\tilde{\phi}). \tag{C.36}$$

This assumption leads to the separation of the initial equation (7.10) into two coupled equations $C(x)$ and $\varphi(x,\tilde{\phi})$. Once these differential equations are solved, it is necessary to justify whether the obtained solutions $C(x)$ and $\varphi(x,\tilde{\phi})$ fulfill the inequality (C.36).

C.3.1 Validity of the BO approximation

The validity of this approximation can be explored using expansions with respect to κ (see [48] and references cited there). For Example, in the geometric part of (10.23), we get

$$C_k\sim\mathcal{O}(\kappa^0),\quad \dot{C}_k\sim\mathcal{O}(\kappa^{-1}),\quad \ddot{C}_k\sim\mathcal{O}(\kappa^{-2}), \tag{C.37}$$

with $\dot{}\equiv\partial/\partial\alpha$. The matter part is given in terms of parabolic cylinder functions. In order to get its expansion in terms of κ and A in a simple way, we use the approximation for large values of the scale factor given by (C.32). We should also keep track of the dependence on α. Noting that

$$\beta\sim\theta\sim\mathcal{O}(\kappa^{-1}\mathcal{C}^{1/2}a_0^3)\,e^{3\alpha},\quad z\sim X\sim\mathcal{O}(\kappa^{-1/2}\mathcal{C}^{1/4}a_0^{3/2})e^{3\alpha/2}, \tag{C.38}$$

we get

$$\varphi_k(\alpha,\phi)\sim E(\alpha,\phi)=\sqrt{2}\,\exp\left[h(\alpha,\phi)\right], \tag{C.39}$$

where

$$h(\alpha)\sim\mathcal{O}\left(1\right)\,\alpha+\mathcal{O}\left(\kappa^{-1}\mathcal{C}^{1/2}a_0^3\right)e^{3\alpha}, \tag{C.40}$$

and the quantity $\kappa^{-1/2}A^{1/4}a_0^{3/2}$ is dimensionless. Thus, we have

$$\frac{C_k\ddot{\varphi}_k}{\ddot{C}_k\varphi_k}\sim\mathcal{O}(\kappa^2)\left[\dot{h}^2+\ddot{h}\right]\sim\mathcal{O}(\kappa^2)+\mathcal{O}(\kappa\,\mathcal{C}^{1/2}\,a_0^3)\,e^{3\alpha}+\mathcal{O}(\mathcal{C}\,a_0^6)\,e^{6\alpha}, \tag{C.41}$$

and

$$\frac{\dot{C}_k\dot{\varphi}_k}{\ddot{C}_k\varphi_k}\sim\mathcal{O}(\kappa)\,\dot{h}\sim\mathcal{O}(\kappa^1)+\mathcal{O}(\mathcal{C}^{1/2}a_0^3)\,e^{3\alpha}. \tag{C.42}$$

Thus, the B.O. approximation is fulfilled as long as $\mathcal{C}a_0^6e^{6\alpha}\ll\kappa^2$; i.e. this approach is valid for sufficiently small value of $\mathcal{C}$, i.e. the fluid (2.16) is close enough to a cosmological constant and for large enough values of a but not infinite value of a, that is within a semiclassical regime.

On the other hand, the asymptotic behavior of the terms in (12.19) can be written as

$$\frac{\partial^2 C_k}{\partial x^2}\varphi_k \sim \frac{48}{\kappa\hbar^2}e^{6x}C_k\varphi_k, \tag{C.43}$$

$$\frac{\partial\varphi_k}{\partial x}\frac{\partial C_k}{\partial x} \sim \frac{24\sqrt{6}}{\hbar^2\kappa^2\rho_0}\left[f\left(w\right)\right]^{\frac{1}{2}}e^{6x}\tilde{\phi}^2 C_k\varphi_k, \tag{C.44}$$

$$\frac{\partial^2\varphi_k}{\partial x^2}C_k \sim \frac{18f(w)}{\hbar^2\kappa^3\rho_0^2}e^{6x}\tilde{\phi}^4 C_k\varphi_k. \tag{C.45}$$

It should be stressed that although the parabolic cylinder functions obtained in (12.26) depend on the metric for both the order and the argument, the order approaches a constant parameter when $x \to \infty$ (see the expression (12.27)). Therefore, one can derive (C.43), (C.44) and (C.45) by calculating the corresponding derivatives of the asymptotic expression obtained in (12.31). In this regard, the BO approximation method is valid as far as

$$\frac{\tilde{\phi}}{\sqrt{\kappa\rho_0}} \ll 1. \tag{C.46}$$

The term $\kappa\rho_0$ is dimensionless and it quantifies the current value of the phantom DE density normalised with the EiBI coupling constant κ. In any case, the inverse of $\tilde{\phi}$ should be very large (at least much larger than the EiBI scale and very close to the Planck scale) near the BR singularity. This then justifies the BO approximation. In principle, the smaller the value of $\tilde{\phi}$ is, the better is the BO approximation. Despite that the BO method breaks down for large values of $\tilde{\phi}$, we can ensure that such an approach is still valid close to the region given by the classical trajectory, i.e., $x \to \infty$ and $\tilde{\phi} \to 0$.

C.4 Justification for the approximation done in the equation (9.43)

The approximation done for the differential equation (9.43) consists into disregarding the first three terms after the change of variable realised in (9.40). Once these terms are neglected, the resulting differential equation is separable and the approximation is valid if

$$\frac{\hbar^2\kappa^2}{24\pi^2}e^{-2z}\left[\varphi^2\partial_\varphi^2 + \varphi\partial_\varphi + 2\varphi\partial_\varphi\partial_z\right]C\left(z\right)U\left(\varphi\right) \ll \frac{\hbar^2\kappa^2}{24\pi^2}e^{-2z}\partial_z^2 C\left(z\right)U\left(\varphi\right), \tag{C.47}$$

and

$$\frac{\hbar^2\kappa^2}{24\pi^2}e^{-2z}\left[\varphi^2\partial_\varphi^2 + \varphi\partial_\varphi + 2\varphi\partial_\varphi\partial_z\right]C\left(z\right)U\left(\varphi\right) \ll \frac{\hbar^2}{4\pi^2}\partial_\varphi^2 C\left(z\right)U\left(\varphi\right), \sigma\varphi^4 C\left(z\right)U\left(\varphi\right). \tag{C.48}$$

As a result of the performed approximation, the last two terms in the rhs of the above inequality have the same order of magnitude for large values of z and φ or ϕ and x (See (C.49)). In fact, the dominant terms that we keep reads

$$\frac{\hbar^2}{4\pi^2}\partial_\varphi^2 C\left(z\right)U\left(\varphi\right), \sigma\varphi^4 C\left(z\right)U\left(\varphi\right) \sim \frac{\hbar}{2\pi}\left(\frac{\kappa^2}{6k}\right)^{\frac{1}{4}}\sigma^{\frac{3}{4}}\varphi^3 e^{-\frac{1}{2}z} = \frac{\hbar}{2\pi}\left(\frac{\kappa^2}{6k}\right)^{\frac{1}{4}}\sigma^{\frac{3}{4}}\phi^3 e^{\frac{5}{2}x}, \tag{C.49}$$

$$\frac{\hbar^2\kappa^2}{24\pi^2}e^{-2z}\partial_z^2 C\left(z\right)U\left(\varphi\right)\sim\frac{\hbar}{2\pi}\left(\frac{\kappa^2k^3}{6}\right)^{\frac{1}{4}}\sigma^{-\frac{1}{4}}\varphi^{-1}e^{-\frac{1}{2}z}=\frac{\hbar}{2\pi}\left(\frac{\kappa^2k^3}{6}\right)^{\frac{1}{4}}\sigma^{-\frac{1}{4}}\phi^{-1}e^{-\frac{3}{2}x},\tag{C.50}$$

while the neglected terms evolve asymptotically as

$$\frac{\hbar^2\kappa^2}{24\pi^2}e^{-2z}\varphi^2\partial_\varphi^2 C\left(z\right)U\left(\varphi\right)\sim\frac{\hbar}{12\pi}\left(\frac{\kappa^{10}}{6k}\right)^{\frac{1}{4}}\sigma^{\frac{3}{4}}\varphi^5e^{-\frac{5}{2}z}=\frac{\hbar}{12\pi}\left(\frac{\kappa^{10}}{6k}\right)^{\frac{1}{4}}\sigma^{\frac{3}{4}}\phi^5e^{\frac{5}{2}x},\tag{C.51}$$

$$\frac{\hbar^2\kappa^2}{24\pi^2}e^{-2z}\varphi\partial_\varphi C\left(z\right)U\left(\varphi\right)\sim\frac{\hbar^2}{24\pi^2}\left(\frac{\kappa^{10}}{6k}\right)^{\frac{1}{4}}\sigma^{\frac{1}{4}}\varphi^2e^{-\frac{5}{2}z}=\frac{\hbar^2}{24\pi^2}\left(\frac{\kappa^{10}}{6k}\right)^{\frac{1}{4}}\sigma^{\frac{1}{4}}\phi^2e^{-\frac{1}{2}x},\tag{C.52}$$

$$\frac{\hbar^2\kappa^2}{12\pi^2}e^{-2z}\varphi\partial_\varphi\partial_z C\left(z\right)U\left(\varphi\right)\sim\frac{\hbar}{6\pi}\left(\frac{3\kappa^6k}{8}\right)^{\frac{1}{4}}\sigma^{\frac{1}{4}}\varphi^2e^{-\frac{3}{2}z}=\frac{\hbar}{6\pi}\left(\frac{3\kappa^6k}{8}\right)^{\frac{1}{4}}\sigma^{\frac{1}{4}}\phi^2e^{\frac{1}{2}x}.\tag{C.53}$$

Therefore, in order to obtain the suitable region for the realised approximation we compare the smallest of the saved terms with the largest between the neglected ones, that is

$$\begin{aligned}&\frac{\hbar}{12\pi}\left(\frac{\kappa^{10}}{6k}\right)^{\frac{1}{4}}\sigma^{\frac{3}{4}}\phi^5e^{\frac{5}{2}x}\ll\frac{\hbar}{2\pi}\left(\frac{\kappa^2k^3}{6}\right)^{\frac{1}{4}}\sigma^{-\frac{1}{4}}\phi^{-1}e^{-\frac{3}{2}x},\\ \implies\quad&\frac{\kappa^2\sigma}{6k}\phi^6e^{4x}\ll1.\end{aligned}\tag{C.54}$$

Finally, the realised approximation is valid as long as $\left(\kappa^2\sigma/6k\right)\phi^6e^{4x}\ll1$. This means that for sufficiently small values of σ; i.e. for small values[i] of $\mathcal{C}$, which is indeed the observationally preferred situation, and large values of x; i.e. $x\gg1$ (but finite), the approximation we have used is valid.

C.5 Scalar field eigenstates and Symanzik scaling behavior

In this Appendix we analyse the expression (9.38) in the context of the Symanzik scaling law, following the results found in [393–395]. We start by performing, in the aforementioned equation, the following change of variables,

$$x=c_1\bar{x}\ ,\quad \phi=c_2\bar{\phi}\ ,\tag{C.55}$$

where c_1 and c_2 are constants. We obtain

$$\left\{\frac{\hbar^2}{4\pi^2}\left[\frac{\kappa^2}{6c_1^2}\partial_{\bar{x}}^2+\frac{1}{c_2^2}\partial_{\bar{\phi}}^2\right]+\sigma e^{6c_1\bar{x}}\,c_2^4\bar{\phi}^4\right\}\Psi(\bar{x},\,\bar{\phi})=0\ ,\tag{C.56}$$

where by imposing

$$c_1=\frac{\hbar}{2\sqrt{6}\pi}\kappa\ ,\quad c_2=i\frac{\hbar}{2\pi}\ ,\tag{C.57}$$

we get

$$\left[\partial_{\bar{x}}^2-\partial_{\bar{\phi}}^2+\frac{\hbar^4}{16\pi^4}\sigma e^{\frac{\sqrt{6}}{2\pi}\hbar\kappa\bar{x}}\bar{\phi}^4\right]\Psi(\bar{x},\,\bar{\phi})=0\ ,\tag{C.58}$$

[i] Small values of $\mathcal{C}$ implies small deviations of our model from the ΛCDM scenario.

which is precisely given by equation (1) of [393]. As done in [393], we conclude that the general solutions of (C.58) can be expressed as

$$\Psi(\bar{x},\,\bar{\phi}) = \sum_{n=0}^{+\infty} A_n\left(\bar{x}\right)\Phi_n\left(\bar{x},\,\bar{\phi}\right)\ , \tag{C.59}$$

which can be rewritten in a vectorial notation as

$$\Psi(\bar{x},\,\bar{\phi}) = \mathbf{\Phi}^T\left(\bar{x},\,\bar{\phi}\right)\cdot\mathbf{A}\left(\bar{x}\right)\ , \tag{C.60}$$

where the scalar part wave functions satisfy

$$\left[\partial^2_{\bar{\phi}} + E_n\left(\bar{x}\right) - \frac{\hbar^4}{16\pi^4}\sigma e^{\frac{\sqrt{6}}{2\pi}\hbar\kappa\bar{x}}\bar{\phi}^4\right]\Phi_n\left(\bar{x},\,\bar{\phi}\right) = 0\ . \tag{C.61}$$

Notice that the scalar part solutions depend on the scale factor. Using the Symanzik scaling law [393–395], we have that

$$\begin{aligned}\Phi_n\left(\bar{x},\,\bar{\phi}\right) &= \left[\frac{\hbar^4}{16\pi^4}\sigma e^{\frac{\sqrt{6}}{2\pi}\hbar\kappa\bar{x}}\right]^{\frac{1}{12}} f_n\left(\bar{\chi}\right)\ ,\\ E_n\left(\bar{x}\right) &= \left[\frac{\hbar^4}{16\pi^4}\sigma e^{\frac{\sqrt{6}}{2\pi}\hbar\kappa\bar{x}}\right]^{\frac{1}{3}}\varepsilon_n\ ,\end{aligned} \tag{C.62}$$

where

$$\bar{\chi} = \left[\frac{\hbar^4}{16\pi^4}\sigma e^{\frac{\sqrt{6}}{2\pi}\hbar\kappa\bar{x}}\right]^{\frac{1}{12}}\bar{\phi}\ . \tag{C.63}$$

Furthermore, the vectorial scalar field wave equation can be used to define a coupling matrix $\mathbf{\Omega}$ as [393–395]

$$\frac{\partial\mathbf{\Phi}}{\partial\bar{x}} = \mathbf{\Omega}\mathbf{\Phi}\left(\bar{x},\,\bar{\phi}\right)\ . \tag{C.64}$$

Given that $\{\Phi_n\}$ are an orthonormal basis, we can conclude that

$$\Omega_{mn} = \frac{\varepsilon_m - \varepsilon_n}{4}\int d\bar{\chi}\,\bar{\chi}^2 f_m\left(\bar{\chi}\right) f_n\left(\bar{\chi}\right)\ . \tag{C.65}$$

References

[1] A. Einstein, "The Foundation of the General Theory of Relativity," *Annalen Phys.* **49** no. 7, (1916) 769–822. [Annalen Phys.14,517(2005); ,65(1916); Annalen Phys.354,no.7,769(1916)].

[2] **LIGO Scientific, Virgo** Collaboration, B. P. Abbott *et al.*, "Observation of Gravitational Waves from a Binary Black Hole Merger," *Phys. Rev. Lett.* **116** no. 6, (2016) 061102, arXiv:1602.03837 [gr-qc].

[3] E. Hubble, "A relation between distance and radial velocity among extra-galactic nebulae," *Proceedings of the National Academy of Sciences* **15** no. 3, (1929) 168–173, https://www.pnas.org/content/15/3/168.full.pdf. https://www.pnas.org/content/15/3/168.

[4] E. P. Hubble, "Extragalactic nebulae," *Astrophys. J.* **64** (1926) 321–369.

[5] A. G. Lemaître, "A Homogeneous Universe of Constant Mass and Increasing Radius accounting for the Radial Velocity of Extra-galactic Nebulæ," *Monthly Notices of the Royal Astronomical Society* **91** no. 5, (03, 1931) 483–490, https://academic.oup.com/mnras/article-pdf/91/5/483/3079971/mnras91-0483.pdf. https://doi.org/10.1093/mnras/91.5.483.

[6] A. A. Penzias and R. W. Wilson, "A Measurement of excess antenna temperature at 4080-Mc/s," *Astrophys. J.* **142** (1965) 419–421.

[7] F. Zwicky, "On the Masses of Nebulae and of Clusters of Nebulae," *Astrophys. J.* **86** (1937) 217–246.

[8] V. C. Rubin and W. K. Ford, Jr., "Rotation of the Andromeda Nebula from a Spectroscopic Survey of Emission Regions," *Astrophys. J.* **159** (1970) 379–403.

[9] D. Clowe, M. Bradac, A. H. González, M. Markevitch, S. W. Randall, C. Jones, and D. Zaritsky, "A direct empirical proof of the existence of dark matter," *Astrophys. J.* **648** (2006) L109–L113, arXiv:astro-ph/0608407 [astro-ph].

[10] **Supernova Cosmology Project** Collaboration, S. Perlmutter *et al.*, "Measurements of Omega and Lambda from 42 high redshift supernovae," *Astrophys. J.* **517** (1999) 565–586, arXiv:astro-ph/9812133 [astro-ph].

[11] **Supernova Search Team** Collaboration, A. G. Riess *et al.*, "Observational evidence from supernovae for an accelerating universe and a cosmological constant," *Astron. J.* **116** (1998) 1009–1038, arXiv:astro-ph/9805201 [astro-ph].

[12] **Supernova Cosmology Project** Collaboration, S. Perlmutter *et al.*, "Cosmology from Type Ia supernovae," *Bull. Am. Astron. Soc.* **29** (1997) 1351, arXiv:astro-ph/9812473 [astro-ph].

[13] **Planck** Collaboration, P. A. R. Ade *et al.*, "Planck 2015 results. XIV. Dark energy and modified gravity," *Astron. Astrophys.* **594** (2016) A14, arXiv:1502.01590 [astro-ph.CO].

[14] **Planck** Collaboration, P. A. R. Ade *et al.*, "Planck 2015 results. XIII. Cosmological parameters," *Astron. Astrophys.* **594** (2016) A13, arXiv:1502.01589 [astro-ph.CO].

[15] **Planck** Collaboration, N. Aghanim *et al.*, "Planck 2018 results. VI. Cosmological parameters," arXiv:1807.06209 [astro-ph.CO].

[16] R. Bean and O. Dore, "Probing dark energy perturbations: The Dark energy equation of state and speed of sound as measured by WMAP," *Phys. Rev.* **D69** (2004) 083503, arXiv:astro-ph/0307100 [astro-ph].

[17] **WMAP** Collaboration, E. Komatsu *et al.*, "Five-Year Wilkinson Microwave Anisotropy Probe (WMAP) Observations: Cosmological Interpretation," *Astrophys. J. Suppl.* **180** (2009) 330–376, arXiv:0803.0547 [astro-ph].

[18] *Planck 2015 Results: Cosmological Parameter Tables:*. https://wiki.cosmos.esa.int/planckpla2015/images/0/07/Paramstable2015limit95.pdf.

[19] L.-M. Wang and P. J. Steinhardt, "Cluster abundance constraints on quintessence models," *Astrophys. J.* **508** (1998) 483–490, arXiv:astro-ph/9804015 [astro-ph].

[20] A. Yu. Kamenshchik, U. Moschella, and V. Pasquier, "An Alternative to quintessence," *Phys. Lett.* **B511** (2001) 265–268, arXiv:gr-qc/0103004 [gr-qc].

[21] H. Stefancic, "Dark energy transition between quintessence and phantom regimes - An Equation of state analysis," *Phys. Rev.* **D71** (2005) 124036, arXiv:astro-ph/0504518 [astro-ph].

[22] K. Bamba, S. Capozziello, S. Nojiri, and S. D. Odintsov, "Dark energy cosmology: the equivalent description via different theoretical models and cosmography tests," *Astrophys. Space Sci.* **342** (2012) 155–228, arXiv:1205.3421 [gr-qc].

[23] L. Amendola and S. Tsujikawa, *Dark Energy: Theory and Observations*. Cambridge University Press, 2010.

[24] C. Armendariz-Picon, V. F. Mukhanov, and P. J. Steinhardt, "A Dynamical solution to the problem of a small cosmological constant and late time cosmic acceleration," *Phys. Rev. Lett.* **85** (2000) 4438–4441, arXiv:astro-ph/0004134 [astro-ph].

[25] E. J. Copeland, M. Sami, and S. Tsujikawa, "Dynamics of dark energy," *Int. J. Mod. Phys.* **D15** (2006) 1753–1936, arXiv:hep-th/0603057 [hep-th].

[26] R. Saitou and S. Nojiri, "The unification of inflation and late-time acceleration in the frame of k-essence," *Eur. Phys. J.* **C71** (2011) 1712, arXiv:1104.0558 [hep-th].

[27] W. de Sitter, "On the relativity of inertia. Remarks concerning Einstein's latest hypothesis," *Koninklijke Nederlandse Akademie van Wetenschappen Proceedings Series B Physical Sciences* **19** (Mar, 1917) 1217–1225.

[28] R. R. Caldwell, M. Kamionkowski, and N. N. Weinberg, "Phantom energy and cosmic doomsday," *Phys. Rev. Lett.* **91** (2003) 071301, arXiv:astro-ph/0302506 [astro-ph].

[29] A. A. Starobinsky, "Future and origin of our universe: Modern view," *Grav. Cosmol.* **6** (2000) 157–163, arXiv:astro-ph/9912054 [astro-ph].

[30] R. R. Caldwell, "A Phantom menace?," *Phys. Lett.* **B545** (2002) 23–29, arXiv:astro-ph/9908168 [astro-ph].

[31] S. M. Carroll, M. Hoffman, and M. Trodden, "Can the dark energy equation - of - state parameter w be less than -1?," *Phys. Rev.* **D68** (2003) 023509, arXiv:astro-ph/0301273 [astro-ph].

[32] L. P. Chimento and R. Lazkoz, "On the link between phantom and standard cosmologies," *Phys. Rev. Lett.* **91** (2003) 211301, arXiv:gr-qc/0307111 [gr-qc].

[33] M. P. Dabrowski, T. Stachowiak, and M. Szydlowski, "Phantom cosmologies," *Phys. Rev.* **D68** (2003) 103519, arXiv:hep-th/0307128 [hep-th].

[34] P. F. González-Díaz, "K-essential phantom energy: Doomsday around the corner?," *Phys. Lett.* **B586** (2004) 1–4, arXiv:astro-ph/0312579 [astro-ph].

[35] P. F. González-Díaz, "Axion phantom energy," *Phys. Rev.* **D69** (2004) 063522, arXiv:hep-th/0401082 [hep-th].

[36] P. F. González-Díaz, "Wormholes and ringholes in a dark - energy universe," *Phys. Rev.* **D68** (2003) 084016, arXiv:astro-ph/0308382 [astro-ph].

[37] P. F. González-Díaz, "You need not be afraid of phantom energy," *Phys. Rev.* **D68** (2003) 021303, arXiv:astro-ph/0305559 [astro-ph].

[38] D.-j. Liu and X.-z. Li, "Born-Infeld type phantom on the brane world," *Phys. Rev.* **D68** (2003) 067301, arXiv:hep-th/0307239 [hep-th].

[39] L. P. Chimento and M. G. Richarte, "Interacting dark matter and modified holographic Ricci dark energy plus a noninteracting cosmic component," **85** no. 12, (Jun, 2012) 127301, arXiv:1207.1492 [astro-ph.CO].

[40] M. Li, "A Model of holographic dark energy," *Phys. Lett.* **B603** (2004) 1, arXiv:hep-th/0403127 [hep-th].

[41] M. Bouhmadi-López and J. A. Jiménez Madrid, "Escaping the big rip?," *JCAP* **0505** (2005) 005, arXiv:astro-ph/0404540 [astro-ph].

[42] M. P. Dabrowski, C. Kiefer, and B. Sandhöfer, "Quantum phantom cosmology," *Phys. Rev.* **D74** (2006) 044022, arXiv:hep-th/0605229 [hep-th].

[43] J. de Haro, "Does loop quantum cosmology replace the big rip singularity by a non-singular bounce?," *JCAP* **1211** (2012) 037, arXiv:1207.3621 [gr-qc].

[44] I. Albarran and M. Bouhmadi-López, "Quantisation of the holographic Ricci dark energy model," *JCAP* **1508** no. 08, (2015) 051, arXiv:1505.01353 [gr-qc].

[45] S. Nojiri and S. D. Odintsov, "The Final state and thermodynamics of dark energy universe," *Phys. Rev.* **D70** (2004) 103522, arXiv:hep-th/0408170 [hep-th].

[46] M. Bouhmadi-López, P. F. González-Díaz, and P. Martín-Moruno, "Worse than a big rip?," *Phys. Lett.* **B659** (2008) 1–5, arXiv:gr-qc/0612135 [gr-qc].

[47] S. Nojiri, S. D. Odintsov, and S. Tsujikawa, "Properties of singularities in (phantom) dark energy universe," *Phys. Rev.* **D71** (2005) 063004, arXiv:hep-th/0501025 [hep-th].

[48] M. Bouhmadi-López, C. Kiefer, B. Sandhöfer, and P. Vargas Moniz, "On the quantum fate of singularities in a dark-energy dominated universe," *Phys. Rev.* **D79** (2009) 124035, arXiv:0905.2421 [gr-qc].

[49] V. Gorini, A. Yu. Kamenshchik, U. Moschella, and V. Pasquier, "Tachyons, scalar fields and cosmology," *Phys. Rev.* **D69** (2004) 123512, arXiv:hep-th/0311111 [hep-th].

[50] M. Cataldo, L. P. Chimento, and M. G. Richarte, "Finite time future singularities in the interacting dark sector," *Phys. Rev. D* **95** no. 6, (2017) 063510, arXiv:1702.07743 [gr-qc].

[51] A. Kamenshchik, C. Kiefer, and B. Sandhöfer, "Quantum cosmology with big-brake singularity," *Phys. Rev.* **D76** (2007) 064032, arXiv:0705.1688 [gr-qc].

[52] J. D. Barrow, A. B. Batista, J. C. Fabris, M. J. S. Houndjo, and G. Dito, "Sudden singularities survive massive quantum particle production," *Phys. Rev.* **D84** (2011) 123518, arXiv:1110.1321 [gr-qc].

[53] L. Fernández-Jambrina and R. Lazkoz, "Geodesic behaviour of sudden future singularities," *Phys. Rev.* **D70** (2004) 121503, arXiv:gr-qc/0410124 [gr-qc].

[54] J. D. Barrow, "Sudden future singularities," *Class. Quant. Grav.* **21** (2004) L79–L82, arXiv:gr-qc/0403084 [gr-qc].

[55] H. Stefancic, "Expansion around the vacuum equation of state - Sudden future singularities and asymptotic behavior," *Phys. Rev.* **D71** (2005) 084024, arXiv:astro-ph/0411630 [astro-ph].

[56] S. Nojiri and S. D. Odintsov, "Quantum escape of sudden future singularity," *Phys. Lett.* **B595** (2004) 1–8, arXiv:hep-th/0405078 [hep-th].

[57] A. Y. Kamenshchik and S. Manti, "Classical and quantum Big Brake cosmology for scalar field and tachyonic models," *Phys. Rev.* **D85** (2012) 123518, arXiv:1202.0174 [gr-qc].

[58] S. Nojiri and S. D. Odintsov, "The Future evolution and finite-time singularities in F(R)-gravity unifying the inflation and cosmic acceleration," *Phys. Rev.* **D78** (2008) 046006, arXiv:0804.3519 [hep-th].

[59] S. Nojiri and S. D. Odintsov, "Inhomogeneous equation of state of the universe: Phantom era, future singularity and crossing the phantom barrier," *Phys. Rev.* **D72** (2005) 023003, arXiv:hep-th/0505215 [hep-th].

[60] M. Bouhmadi-López, P. F. González-Díaz, and P. Martín-Moruno, "On the generalised Chaplygin gas: Worse than a big rip or quieter than a sudden singularity?," *Int. J. Mod. Phys.* **D17** (2008) 2269–2290, arXiv:0707.2390 [gr-qc].

[61] M. Bouhmadi-López, C. Kiefer, and P. Martín-Moruno, "Phantom singularities and their quantum fate: general relativity and beyond—a CANTATA COST action topic," *Gen. Rel. Grav.* **51** no. 10, (2019) 135, arXiv:1904.01836 [gr-qc].

[62] K. Bamba, S. Nojiri, and S. D. Odintsov, "The Universe future in modified gravity theories: Approaching the finite-time future singularity," *JCAP* **0810** (2008) 045, arXiv:0807.2575 [hep-th].

[63] M. Bouhmadi-López, C. Kiefer, and M. Krämer, "Resolution of type IV singularities in quantum cosmology," *Phys. Rev.* **D89** no. 6, (2014) 064016, arXiv:1312.5976 [gr-qc].

[64] T. V. Ruzmaikina and A. A. Ruzmaikin, "Quadratic Corrections to the Lagrangian Density of the Gravitational Field and the Singularity," *Soviet Journal of Experimental and Theoretical Physics* **30** (1969) 372.

[65] M. Bouhmadi-López, "Phantom-like behaviour in dilatonic brane-world scenario with induced gravity," *Nucl. Phys.* **B797** (2008) 78–92, arXiv:astro-ph/0512124 [astro-ph].

[66] P. H. Frampton, K. J. Ludwick, and R. J. Scherrer, "The Little Rip," *Phys. Rev.* **D84** (2011) 063003, arXiv:1106.4996 [astro-ph.CO].

[67] I. Brevik, E. Elizalde, S. Nojiri, and S. D. Odintsov, "Viscous Little Rip Cosmology," *Phys. Rev.* **D84** (2011) 103508, arXiv:1107.4642 [hep-th].

[68] A. N. Makarenko, S. D. Odintsov, and G. J. Olmo, "Little Rip, ΛCDM and singular dark energy cosmology from Born-Infeld-$f(R)$ gravity," *Phys. Lett.* **B734** (2014) 36–40, arXiv:1404.2850 [gr-qc].

[69] M. Bouhmadi-López, A. Errahmani, P. Martín-Moruno, T. Ouali, and Y. Tavakoli, "The little sibling of the big rip singularity," *Int. J. Mod. Phys.* **D24** no. 10, (2015) 1550078, arXiv:1407.2446 [gr-qc].

[70] I. Albarran, M. Bouhmadi-López, F. Cabral, and P. Martín-Moruno, "The quantum realm of the "Little Sibling" of the Big Rip singularity," *JCAP* **1511** no. 11, (2015) 044, arXiv:1509.07398 [gr-qc].

[71] M. Bouhmadi-López, D. Brizuela, and I. Garay, "Quantum behavior of the "Little Sibling" of the Big Rip induced by a three-form field," *JCAP* **1809** no. 09, (2018) 031, arXiv:1802.05164 [gr-qc].

[72] Y. Shtanov and V. Sahni, "Unusual cosmological singularities in brane world models," *Class. Quant. Grav.* **19** (2002) L101–L107, arXiv:gr-qc/0204040 [gr-qc].

[73] L. P. Chimento and R. Lazkoz, "Duality extended Chaplygin cosmologies with a big rip," *Class. Quant. Grav.* **23** (2006) 3195–3204, arXiv:astro-ph/0505254 [astro-ph].

[74] M. P. Dabrowski, K. Marosek, and A. Balcerzak, "Standard and exotic singularities regularized by varying constants," *Mem. Soc. Ast. It.* **85** no. 1, (2014) 44–49, arXiv:1308.5462 [astro-ph.CO].

[75] F. J. Tipler, "Singularities in conformally flat spacetimes," *Phys. Lett.* **A64** (1977) 8–10.

[76] A. Krolak, "Towards the proof of the cosmic censorship hypothesis," *Classical and Quantum Gravity* **3** no. 3, (May, 1986) 267–280. https://doi.org/10.1088%2F0264-9381%2F3%2F3%2F004.

[77] L. Fernández-Jambrina and R. Lazkoz, "Singular fate of the universe in modified theories of gravity," *Phys. Lett.* **B670** (2009) 254–258, arXiv:0805.2284 [gr-qc].

[78] L. Fernández-Jambrina and R. Lazkoz, "Cosmological singularities and modified theories of gravity," *AIP Conf. Proc.* **1122** no. 1, (2009) 264–267, arXiv:0903.4775 [gr-qc].

[79] M. Bouhmadi-López, J. Marto, J. Morais, and C. M. Silva, "Cosmic infinity: A dynamical system approach," *JCAP* **1703** (2017) 042, arXiv:1611.03100 [gr-qc].

[80] M. Chevallier and D. Polarski, "Accelerating universes with scaling dark matter," *Int. J. Mod. Phys.* **D10** (2001) 213–224, arXiv:gr-qc/0009008 [gr-qc].

[81] E. V. Linder, "Exploring the expansion history of the universe," *Phys. Rev. Lett.* **90** (2003) 091301, arXiv:astro-ph/0208512 [astro-ph].

[82] L. R. Abramo, R. C. Batista, L. Liberato, and R. Rosenfeld, "Physical approximations for the nonlinear evolution of perturbations in inhomogeneous dark energy scenarios," *Phys. Rev.* **D79** (2009) 023516, arXiv:0806.3461 [astro-ph].

[83] R. J. Scherrer, "Mapping the Chevallier-Polarski-Linder parametrization onto Physical Dark Energy Models," *Phys. Rev.* **D92** no. 4, (2015) 043001, arXiv:1505.05781 [astro-ph.CO].

[84] E. R. M. Tarrant, E. J. Copeland, A. Padilla, and C. Skordis, "The Dark Energy Cosmic Clock: A New Way to Parametrise the Equation of State," *JCAP* **1312** (2013) 013, arXiv:1304.5532 [astro-ph.CO].

[85] J. Beltran Jiménez, R. Lazkoz, D. Sáez-Gómez, and V. Salzano, "Observational constraints on cosmological future singularities," *Eur. Phys. J.* **C76** no. 11, (2016) 631, arXiv:1602.06211 [gr-qc].

[86] J.-Z. Ma and X. Zhang, "Probing the dynamics of dark energy with novel parametrizations," *Phys. Lett.* **B699** (2011) 233–238, arXiv:1102.2671 [astro-ph.CO].

[87] S. Capozziello, R. D'Agostino, and O. Luongo, "Cosmic acceleration from a single fluid description," *Phys. Dark Univ.* **20** (2018) 1–12, arXiv:1712.04317 [gr-qc].

[88] A. Balcerzak and T. Denkiewicz, "Density preturbations in a finite scale factor singularity universe," *Phys. Rev.* **D86** (2012) 023522, arXiv:1202.3280 [astro-ph.CO].

[89] T. Denkiewicz, "Dark energy and dark matter perturbations in singular universes," *JCAP* **1503** (2015) 037, arXiv:1411.6169 [astro-ph.CO].

[90] T. Denkiewicz, "Dynamical dark energy models with singularities in the view of the forthcoming results of the growth observations," arXiv:1511.04708 [astro-ph.CO].

[91] T. Denkiewicz and V. Salzano, "Scale-dependent perturbations finally detectable by future galaxy surveys and their contribution to cosmological model selection," arXiv:1702.01291 [astro-ph.CO].

[92] H. Kurki-Suonio, *Cosmological Perturbation Theory (lecture notes)*. University of Helsinki, 2003. https://www.mv.helsinki.fi/home/hkurkisu/CosPer.pdf.

[93] P. G. Ferreira and M. Joyce, "Cosmology with a primordial scaling field," *Phys. Rev.* **D58** (1998) 023503, arXiv:astro-ph/9711102 [astro-ph].

[94] P. G. Ferreira and M. Joyce, "Structure formation with a selftuning scalar field," *Phys. Rev. Lett.* **79** (1997) 4740–4743, arXiv:astro-ph/9707286 [astro-ph].

[95] L. Amendola and D. Tocchini-Valentini, "Stationary dark energy: The Present universe as a global attractor," *Phys. Rev.* **D64** (2001) 043509, arXiv:astro-ph/0011243 [astro-ph].

[96] W. Zimdahl and D. Pavon, "Interacting quintessence," *Phys. Lett.* **B521** (2001) 133–138, arXiv:astro-ph/0105479 [astro-ph].

[97] L. P. Chimento, A. S. Jakubi, D. Pavon, and W. Zimdahl, "Interacting quintessence solution to the coincidence problem," *Phys. Rev.* **D67** (2003) 083513, arXiv:astro-ph/0303145 [astro-ph].

[98] S. M. Carroll, A. De Felice, V. Duvvuri, D. A. Easson, M. Trodden, and M. S. Turner, "The Cosmology of generalized modified gravity models," *Phys. Rev.* **D71** (2005) 063513, arXiv:astro-ph/0410031 [astro-ph].

[99] **EUCLID** Collaboration, R. Laureijs *et al.*, "Euclid Definition Study Report," arXiv:1110.3193 [astro-ph.CO].

[100] L. Amendola *et al.*, "Cosmology and fundamental physics with the Euclid satellite," *Living Rev. Rel.* **21** no. 1, (2018) 2, arXiv:1606.00180 [astro-ph.CO].

[101] J. Väliviita, E. Majerotto, and R. Maartens, "Instability in interacting dark energy and dark matter fluids," *JCAP* **0807** (2008) 020, arXiv:0804.0232 [astro-ph].

[102] S. Nojiri and S. D. Odintsov, "Unifying phantom inflation with late-time acceleration: Scalar phantom-non-phantom transition model and generalized holographic dark energy," *Gen. Rel. Grav.* **38** (2006) 1285–1304, arXiv:hep-th/0506212 [hep-th].

[103] M. Kunz and D. Sapone, "Crossing the Phantom Divide," *Phys. Rev.* **D74** (2006) 123503, arXiv:astro-ph/0609040 [astro-ph].

[104] D. Sapone, E. Majerotto, M. Kunz, and B. Garilli, "Can dark energy viscosity be detected with the Euclid survey?," *Phys. Rev.* **D88** (2013) 043503, arXiv:1305.1942 [astro-ph.CO].

[105] I. Albarran, M. Bouhmadi-López, and J. Morais, "Cosmological perturbations in an effective and genuinely phantom dark energy Universe," *Phys. Dark Univ.* **16** (2017) 94–108, arXiv:1611.00392 [astro-ph.CO].

[106] I. Albarran, M. Bouhmadi-López, and J. Morais, "What if gravity becomes really repulsive in the future?," *Eur. Phys. J.* **C78** no. 3, (2018) 260, arXiv:1706.01484 [gr-qc].

[107] A. Bouali, I. Albarran, M. Bouhmadi-López, and T. Ouali, "Cosmological constraints of phantom dark energy models," *Phys. Dark Univ.* **26** (2019) 100391, arXiv:1905.07304 [astro-ph.CO].

[108] A. A. Starobinsky, "Spectrum of relict gravitational radiation and the early state of the universe," *JETP Lett.* **30** (1979) 682–685. [Pisma Zh. Eksp. Teor. Fiz.30,719(1979)].

[109] S. Bahamonde, S. D. Odintsov, V. K. Oikonomou, and M. Wright, "Correspondence of $F(R)$ Gravity Singularities in Jordan and Einstein Frames," *Annals Phys.* **373** (2016) 96–114, arXiv:1603.05113 [gr-qc].

[110] A. Alonso-Serrano, M. Bouhmadi-López, and P. Martín-Moruno, "$f(R)$ quantum cosmology: avoiding the Big Rip," *Phys. Rev.* **D98** no. 10, (2018) 104004, arXiv:1802.03290 [gr-qc].

[111] E. Elizalde and D. Sáez-Gómez, "F(R) cosmology in presence of a phantom fluid and its scalar-tensor counterpart: Towards a unified precision model of the universe evolution," *Phys. Rev.* **D80** (2009) 044030, arXiv:0903.2732 [hep-th].

[112] S. Nojiri, S. D. Odintsov, and N. Shirai, "Variety of cosmic acceleration models from massive $F(R)$ bigravity," *JCAP* **1305** (2013) 020, arXiv:1212.2079 [hep-th].

[113] S. Nojiri, S. D. Odintsov, and D. Sáez-Gómez, "Cyclic, ekpyrotic and little rip universe in modified gravity," *AIP Conf. Proc.* **1458** no. 1, (2012) 207–221, arXiv:1108.0767 [hep-th].

[114] D. Sáez-Gómez, "Cosmological evolution, future singularities and Little Rip in viable f(R) theories and their scalar-tensor counterpart," *Class. Quant. Grav.* **30** (2013) 095008, arXiv:1207.5472 [gr-qc].

[115] R. D. Boko, M. J. S. Houndjo, and J. Tossa, "Interacting cosmological viscous fluid with Little Rip and Pseudo Rip solutions in f(R) gravity," *Int. J. Geom. Meth. Mod. Phys.* **15** no. 02, (2017) 1850028.

[116] P. Xi, X.-H. Zhai, and X.-Z. Li, "Alternative mechanism of avoiding the big rip or little rip for a scalar phantom field," *Phys. Lett.* **B706** (2012) 482–489, arXiv:1111.6355 [gr-qc].

[117] T. Borislavov Vasilev, M. Bouhmadi-López, and P. Martín-Moruno, "Classical and quantum fate of the little sibling of the big rip in $f(R)$ cosmology," *Phys. Rev.* **D100** no. 8, (2019) 084016, arXiv:1907.13081 [gr-qc].

[118] I. I. Shapiro, M. E. Ash, R. P. Ingalls, W. B. Smith, D. B. Campbell, R. B. Dyce, R. F. Jurgens, and G. H. Pettengill, "Fourth test of general relativity - new radar result," *Phys. Rev. Lett.* **26** (1971) 1132–1135.

[119] E. Berti *et al.*, "Testing General Relativity with Present and Future Astrophysical Observations," *Class. Quant. Grav.* **32** (2015) 243001, arXiv:1501.07274 [gr-qc].

[120] C. M. Will, "The Confrontation between General Relativity and Experiment," *Living Rev. Rel.* **17** (2014) 4, arXiv:1403.7377 [gr-qc].

[121] J. W. Dyson, "The mathematical theory of relativity. by a. s. eddington. 2nd edition. pp. ix 270. 20s. net. 1924. (cam. univ. press.)," *The Mathematical Gazette* **12** no. 175, (1925) 351–352.

[122] M. Bañados and P. G. Ferreira, "Eddington's theory of gravity and its progeny," *Phys. Rev. Lett.* **105** (2010) 011101, arXiv:1006.1769 [astro-ph.CO]. [Erratum: Phys. Rev. Lett.113,no.11,119901(2014)].

[123] M. Born and L. Infeld, "Foundations of the new field theory," *Proc. Roy. Soc. Lond.* **A144** no. 852, (1934) 425–451.

[124] S. Deser and G. W. Gibbons, "Born-Infeld-Einstein actions?," *Class. Quant. Grav.* **15** (1998) L35–L39, arXiv:hep-th/9803049 [hep-th].

[125] P. Pani, T. Delsate, and V. Cardoso, "Eddington-inspired Born-Infeld gravity. Phenomenology of non-linear gravity-matter coupling," *Phys. Rev.* **D85** (2012) 084020, arXiv:1201.2814 [gr-qc].

[126] T. Delsate and J. Steinhoff, "New insights on the matter-gravity coupling paradigm," *Phys. Rev. Lett.* **109** (2012) 021101, arXiv:1201.4989 [gr-qc].

[127] Y. H. Sham, L. M. Lin, and P. T. Leung, "Testing universal relations of neutron stars with a nonlinear matter-gravity coupling theory," *Astrophys. J.* **781** (2014) 66, arXiv:1312.1011 [gr-qc].

[128] P. Pani and T. P. Sotiriou, "Surface singularities in Eddington-inspired Born-Infeld gravity," *Phys. Rev. Lett.* **109** (2012) 251102, arXiv:1209.2972 [gr-qc].

[129] M. Bouhmadi-López, C.-Y. Chen, and P. Chen, "Is Eddington-Born-Infeld theory really free of cosmological singularities?," *Eur. Phys. J.* **C74** (2014) 2802, arXiv:1302.5013 [gr-qc].

[130] M. Bouhmadi-López, C.-Y. Chen, and P. Chen, "Eddington–Born–Infeld cosmology: a cosmographic approach, a tale of doomsdays and the fate of bound structures," *Eur. Phys. J.* **C75** (2015) 90, arXiv:1406.6157 [gr-qc].

[131] M. Bouhmadi-López, C.-Y. Chen, and P. Chen, "Cosmological singularities in Born-Infeld determinantal gravity," *Phys. Rev.* **D90** (2014) 123518, arXiv:1407.5114 [gr-qc].

[132] P. P. Avelino and R. Z. Ferreira, "Bouncing Eddington-inspired Born-Infeld cosmologies: an alternative to Inflation ?," *Phys. Rev.* **D86** (2012) 041501, arXiv:1205.6676 [astro-ph.CO].

[133] I. Cho, H.-C. Kim, and T. Moon, "Precursor of Inflation," *Phys. Rev. Lett.* **111** (2013) 071301, arXiv:1305.2020 [gr-qc].

[134] C. Escamilla-Rivera, M. Bañados, and P. G. Ferreira, "A tensor instability in the Eddington inspired Born-Infeld Theory of Gravity," *Phys. Rev.* **D85** (2012) 087302, arXiv:1204.1691 [gr-qc].

[135] K. Yang, X.-L. Du, and Y.-X. Liu, "Linear perturbations in Eddington-inspired Born-Infeld gravity," *Phys. Rev.* **D88** (2013) 124037, arXiv:1307.2969 [gr-qc].

[136] X.-L. Du, K. Yang, X.-H. Meng, and Y.-X. Liu, "Large Scale Structure Formation in Eddington-inspired Born-Infeld Gravity," *Phys. Rev.* **D90** (2014) 044054, arXiv:1403.0083 [gr-qc].

[137] M. Bouhmadi-López, C.-Y. Chen, and P. Chen, "Primordial Cosmology in Mimetic Born-Infeld Gravity," *JCAP* **1711** (2017) 053, arXiv:1709.09192 [gr-qc].

[138] J. Beltran Jiménez, L. Heisenberg, G. J. Olmo, and D. Rubiera-Garcia, "On gravitational waves in Born-Infeld inspired non-singular cosmologies," *JCAP* **1710** no. 10, (2017) 029, arXiv:1707.08953 [hep-th]. [Erratum: JCAP1808,no.08,E01(2018)].

[139] I. Albarran, M. Bouhmadi-López, C.-Y. Chen, and P. Chen, "Eddington-inspired-Born-Infeld tensorial instabilities neutralized in a quantum approach," *Eur. Phys. J.* **C80** no. 1, (2020) 33, arXiv:1911.03935 [gr-qc].

[140] P. Pani, V. Cardoso, and T. Delsate, "Compact stars in Eddington inspired gravity," *Phys. Rev. Lett.* **107** (2011) 031101, arXiv:1106.3569 [gr-qc].

[141] J. Casanellas, P. Pani, I. Lopes, and V. Cardoso, "Testing alternative theories of gravity using the Sun," *Astrophys. J.* **745** (2012) 15, arXiv:1109.0249 [astro-ph.SR].

[142] P. P. Avelino, "Eddington-inspired Born-Infeld gravity: astrophysical and cosmological constraints," *Phys. Rev.* **D85** (2012) 104053, arXiv:1201.2544 [astro-ph.CO].

[143] P. P. Avelino, "Eddington-inspired Born-Infeld gravity: nuclear physics constraints and the validity of the continuous fluid approximation," *JCAP* **1211** (2012) 022, arXiv:1207.4730 [astro-ph.CO].

[144] T. Harko, F. S. N. Lobo, M. K. Mak, and S. V. Sushkov, "Structure of neutron, quark and exotic stars in Eddington-inspired Born-Infeld gravity," *Phys. Rev.* **D88** (2013) 044032, arXiv:1305.6770 [gr-qc].

[145] G. J. Olmo, D. Rubiera-Garcia, and H. Sanchis-Alepuz, "Geonic black holes and remnants in Eddington-inspired Born-Infeld gravity," *Eur. Phys. J.* **C74** (2014) 2804, arXiv:1311.0815 [hep-th].

[146] S.-W. Wei, K. Yang, and Y.-X. Liu, "Black hole solution and strong gravitational lensing in Eddington-inspired Born-Infeld gravity," *Eur. Phys. J.* **C75** (2015) 253, arXiv:1405.2178 [gr-qc]. [Erratum: Eur. Phys. J.C75,331(2015)].

[147] C. Rovelli, "Time in Quantum Gravity: Physics Beyond the Schrodinger Regime," *Phys. Rev.* **D43** (1991) 442–456.

[148] M. Li, W. Song, Y. Song, and T. Wang, "A Weak gravity conjecture for scalar field theories," *JHEP* **05** (2007) 026, arXiv:hep-th/0606011 [hep-th].

[149] M. Li and Y. Wang, "A Stochastic Measure for Eternal Inflation," *JCAP* **0708** (2007) 007, arXiv:0706.1691 [hep-th].

[150] Z.-Y. Wang, Q. Qiu, and C.-D. Xiong, "Time operator in QFT with Virasoro constraints," *Phys. Lett.* **B718** (2013) 1515–1518, arXiv:1205.5942 [quant-ph].

[151] C. Kiefer, "Quantum gravity: Third edition," *Quantum Gravity: Third Edition* (01, 2012) 1–408.

[152] P. Vargas Moniz, "Supersymmetric quantum cosmology: a 'Socratic' guide," *Gen. Rel. Grav.* **46** (2014) 1618.

[153] D. S. Hajdukovic, "On the gravitational field of a point-like body immersed in a quantum vacuum," *Mon. Not. Roy. Astron. Soc.* **491** no. 4, (2020) 4816–4828.

[154] G. 't Hooft, "A Planar Diagram Theory for Strong Interactions," *Nucl. Phys. B* **72** (1974) 461.

[155] P. Candelas, G. T. Horowitz, A. Strominger, and E. Witten, "Vacuum Configurations for Superstrings," *Nucl. Phys. B* **258** (1985) 46–74.

[156] G. Veneziano, "A Stringy Nature Needs Just Two Constants," *Europhys. Lett.* **2** (1986) 199.

[157] D. Amati, M. Ciafaloni, and G. Veneziano, "Classical and Quantum Gravity Effects from Planckian Energy Superstring Collisions," *Int. J. Mod. Phys. A* **3** (1988) 1615–1661.

[158] D. Amati, M. Ciafaloni, and G. Veneziano, "Can Space-Time Be Probed Below the String Size?," *Phys. Lett. B* **216** (1989) 41–47.

[159] M. Gasperini and G. Veneziano, "Pre - big bang in string cosmology," *Astropart. Phys.* **1** (1993) 317–339, arXiv:hep-th/9211021.

[160] E. Witten, "String theory dynamics in various dimensions," *Nucl. Phys. B* **443** (1995) 85–126, arXiv:hep-th/9503124.

[161] E. Witten, "Anti-de Sitter space and holography," *Adv. Theor. Math. Phys.* **2** (1998) 253–291, arXiv:hep-th/9802150.

[162] J. M. Maldacena, "The Large N limit of superconformal field theories and supergravity," *Adv. Theor. Math. Phys.* **2** (1998) 231–252, arXiv:hep-th/9711200.

[163] J. Polchinski, *String theory. Vol. 1: An introduction to the bosonic string*. Cambridge Monographs on Mathematical Physics. Cambridge University Press, 12, 2007.

[164] J. Polchinski, *String theory. Vol. 2: Superstring theory and beyond*. Cambridge Monographs on Mathematical Physics. Cambridge University Press, 12, 2007.

[165] A. Ashtekar, "New Variables for Classical and Quantum Gravity," *Phys. Rev. Lett.* **57** (1986) 2244–2247.

[166] A. Ashtekar, "New Hamiltonian Formulation of General Relativity," *Phys. Rev. D* **36** (1987) 1587–1602.

[167] A. Ashtekar, J. Lewandowski, D. Marolf, J. Mourao, and T. Thiemann, "Quantization of diffeomorphism invariant theories of connections with local degrees of freedom," *J. Math. Phys.* **36** (1995) 6456–6493, arXiv:gr-qc/9504018.

[168] A. Ashtekar and J. Lewandowski, "Quantum theory of geometry. 1: Area operators," *Class. Quant. Grav.* **14** (1997) A55–A82, arXiv:gr-qc/9602046.

[169] M. Bojowald, "Absence of singularity in loop quantum cosmology," *Phys. Rev. Lett.* **86** (2001) 5227–5230, arXiv:gr-qc/0102069.

[170] A. Ashtekar, M. Bojowald, and J. Lewandowski, "Mathematical structure of loop quantum cosmology," *Adv. Theor. Math. Phys.* **7** no. 2, (2003) 233–268, arXiv:gr-qc/0304074.

[171] A. Ashtekar and J. Lewandowski, "Background independent quantum gravity: A Status report," *Class. Quant. Grav.* **21** (2004) R53, arXiv:gr-qc/0404018.

[172] M. Bojowald, "Loop quantum cosmology," *Living Rev. Rel.* **8** (2005) 11, arXiv:gr-qc/0601085.

[173] A. Ashtekar, T. Pawlowski, and P. Singh, "Quantum Nature of the Big Bang: Improved dynamics," *Phys. Rev. D* **74** (2006) 084003, arXiv:gr-qc/0607039.

[174] M. Bojowald, "Loop quantum cosmology," *Living Rev. Rel.* **11** (2008) 4.

[175] A. Ashtekar, "Introduction to loop quantum gravity and cosmology," *Lect. Notes Phys.* **863** (2013) 31–56, arXiv:1201.4598 [gr-qc].

[176] B. S. DeWitt, "Quantum Theory of Gravity. 1. The Canonical Theory," *Phys. Rev.* **160** (1967) 1113–1148. [3,93(1987)].

[177] B. S. DeWitt, "The Everett-Wheeler interpretation of quantum mechanics," in *Battelle rencontres - 1967 lectures in mathematics and physics: Seattle, WA, USA, 16 - 31 July 1967*, pp. 318–332. 1968.

[178] S. W. Hawking, "The Quantum State of the Universe," *Nucl. Phys.* **B239** (1984) 257. [Adv. Ser. Astrophys. Cosmol.3,236(1987)].

[179] J. B. Hartle and S. W. Hawking, "Wave Function of the Universe," *Phys. Rev.* **D28** (1983) 2960–2975. [Adv. Ser. Astrophys. Cosmol.3,174(1987)].

[180] J. J. Halliwell and S. W. Hawking, "The Origin of Structure in the Universe," *Phys. Rev.* **D31** (1985) 1777. [Adv. Ser. Astrophys. Cosmol.3,277(1987)].

[181] A. O. Barvinsky, "Unitarity approach to quantum cosmology," *Phys. Rept.* **230** (1993) 237–367.

[182] T. Padmanabhan, "Some Fundamental Aspects of Semiclassical and Quantum Gravity," *Int. J. Mod. Phys.* **A4** (1989) 4735–4818.

[183] A. O. Barvinsky and A. Yu. Kamenshchik, "Selection rules for the Wheeler-DeWitt equation in quantum cosmology," *Phys. Rev.* **D89** no. 4, (2014) 043526, arXiv:1312.3147 [gr-qc].

[184] P. A. M. Dirac, "Generalized Hamiltonian dynamics," *Can. J. Math.* **2** (1950) 129–148.

[185] C. Kiefer, "Wave Packets in Minisuperspace," *Phys. Rev.* **D38** (1988) 1761–1772.

[186] C. Bertoni, F. Finelli, and G. Venturi, "The Born-Oppenheimer approach to the matter - gravity system and unitarity," *Class. Quant. Grav.* **13** (1996) 2375–2384, arXiv:gr-qc/9604011 [gr-qc].

[187] F. Finelli, G. P. Vacca, and G. Venturi, "Chaotic inflation with a scalar field in nonclassical states," *Phys. Rev.* **D58** (1998) 103514, arXiv:gr-qc/9712098 [gr-qc].

[188] I. Albarran, M. Bouhmadi-López, C.-Y. Chen, and P. Chen, "Doomsdays in a modified theory of gravity: A classical and a quantum approach," *Phys. Lett.* **B772** (2017) 814–818, arXiv:1703.09263 [gr-qc].

[189] I. Albarran, M. Bouhmadi-López, C.-Y. Chen, and P. Chen, "Quantum cosmology of Eddington-Born–Infeld gravity fed by a scalar field: The big rip case," *Phys. Dark Univ.* **23** (2019) 100255, arXiv:1811.05041 [gr-qc].

[190] V. Sahni and A. A. Starobinsky, "The Case for a positive cosmological Lambda term," *Int. J. Mod. Phys.* **D9** (2000) 373–444, arXiv:astro-ph/9904398 [astro-ph].

[191] S. M. Carroll, "The Cosmological constant," *Living Rev. Rel.* **4** (2001) 1, arXiv:astro-ph/0004075 [astro-ph].

[192] S. Weinberg, "The Cosmological Constant Problem," *Rev. Mod. Phys.* **61** (1989) 1–23. [,569(1988)].

[193] T. Padmanabhan, "Cosmological constant: The Weight of the vacuum," *Phys. Rept.* **380** (2003) 235–320, arXiv:hep-th/0212290 [hep-th].

[194] S. Tsujikawa, "Dark energy: investigation and modeling," arXiv:1004.1493 [astro-ph.CO].

[195] V. Faraoni and S. Capozziello, *Beyond Einstein Gravity*, vol. 170. Springer, Dordrecht, 2011. http://www.springerlink.com/content/hl1805/#section=801705&page=1.

[196] J. Morais, M. Bouhmadi-López, and S. Capozziello, "Can $f(R)$ gravity contribute to (dark) radiation?," *JCAP* **1509** no. 09, (2015) 041, arXiv:1507.02623 [gr-qc].

[197] **DES** Collaboration, T. Abbott *et al.*, "The Dark Energy Survey: more than dark energy - an overview," *Mon. Not. Roy. Astron. Soc.* **460** no. 2, (2016) 1270–1299, arXiv:1601.00329 [astro-ph.CO].

[198] C. Deffayet, O. Pujolas, I. Sawicki, and A. Vikman, "Imperfect Dark Energy from Kinetic Gravity Braiding," *JCAP* **1010** (2010) 026, arXiv:1008.0048 [hep-th].

[199] O. Pujolas, I. Sawicki, and A. Vikman, "The Imperfect Fluid behind Kinetic Gravity Braiding," *JHEP* **11** (2011) 156, arXiv:1103.5360 [hep-th].

[200] D. A. Easson and A. Vikman, "The Phantom of the New Oscillatory Cosmological Phase," arXiv:1607.00996 [gr-qc].

[201] M. Bouhmadi-López, P. Chen, and Y.-W. Liu, "Tradeoff between smoother and sooner 'little rip'," *Eur. Phys. J.* **C73** (2013) 2546, arXiv:1302.6249 [gr-qc].

[202] I. Albarran, M. Bouhmadi-López, C. Kiefer, J. Marto, and P. Vargas Moniz, "Classical and quantum cosmology of the little rip abrupt event," *Phys. Rev.* **D94** no. 6, (2016) 063536, arXiv:1604.08365 [gr-qc].

[203] M. Bouhmadi-López and C.-Y. Chen, "Towards the Quantization of Eddington-inspired-Born-Infeld Theory," *JCAP* **1611** no. 11, (2016) 023, arXiv:1609.00700 [gr-qc].

[204] A. Y. Kamenshchik, "Quantum cosmology and late-time singularities," *Class. Quant. Grav.* **30** (2013) 173001, arXiv:1307.5623 [gr-qc].

[205] J. Morais, M. Bouhmadi-López, K. Sravan Kumar, J. Marto, and Y. Tavakoli, "Interacting 3-form dark energy models: distinguishing interactions and avoiding the Little Sibling of the Big Rip," *Phys. Dark Univ.* **15** (2017) 7–30, arXiv:1608.01679 [gr-qc].

[206] D. Baumann, *Cosmology: Part III Mathematical Tripos (lecture notes)*. University of Chicago, 2016. http://theory.uchicago.edu/~liantaow/my-teaching/dark-matter-472/lectures.pdf.

[207] J. M. Bardeen, "Gauge Invariant Cosmological Perturbations," *Phys. Rev.* **D22** (1980) 1882–1905.

[208] C.-P. Ma and E. Bertschinger, "Cosmological perturbation theory in the synchronous and conformal Newtonian gauges," *Astrophys. J.* **455** (1995) 7–25, arXiv:astro-ph/9506072 [astro-ph].

[209] G. Ballesteros and J. Lesgourgues, "Dark energy with non-adiabatic sound speed: initial conditions and detectability," *JCAP* **1010** (2010) 014, arXiv:1004.5509 [astro-ph.CO].

[210] D. Wands and A. Slosar, "Scale-dependent bias from primordial non-Gaussianity in general relativity," *Phys. Rev.* **D79** (2009) 123507, arXiv:0902.1084 [astro-ph.CO].

[211] M. Bruni, R. Crittenden, K. Koyama, R. Maartens, C. Pitrou, and D. Wands, "Disentangling non-Gaussianity, bias and GR effects in the galaxy distribution," *Phys. Rev.* **D85** (2012) 041301, arXiv:1106.3999 [astro-ph.CO].

[212] E. V. Linder, "Cosmic growth history and expansion history," *Phys. Rev.* **D72** (2005) 043529, arXiv:astro-ph/0507263 [astro-ph].

[213] E. V. Linder and R. N. Cahn, "Parameterized Beyond-Einstein Growth," *Astropart. Phys.* **28** (2007) 481–488, arXiv:astro-ph/0701317 [astro-ph].

[214] Y.-S. Song and W. J. Percival, "Reconstructing the history of structure formation using Redshift Distortions," *JCAP* **0910** (2009) 004, arXiv:0807.0810 [astro-ph].

[215] Y. Wang *et al.*, "Designing a space-based galaxy redshift survey to probe dark energy," *Mon. Not. Roy. Astron. Soc.* **409** (2010) 737, arXiv:1006.3517 [astro-ph.CO].

[216] M. J. Hudson and S. J. Turnbull, "The growth rate of cosmic structure from peculiar velocities at low and high redshifts," *Astrophys. J.* **751** (2013) L30, arXiv:1203.4814 [astro-ph.CO].

[217] F. Beutler, C. Blake, M. Colless, D. H. Jones, L. Staveley-Smith, G. B. Poole, L. Campbell, Q. Parker, W. Saunders, and F. Watson, "The 6dF Galaxy Survey: z $\approx$ 0 measurement of the growth rate and σ_8," *Mon. Not. Roy. Astron. Soc.* **423** (2012) 3430–3444, arXiv:1204.4725 [astro-ph.CO].

[218] C. Howlett, A. Ross, L. Samushia, W. Percival, and M. Manera, "The clustering of the SDSS main galaxy sample – II. Mock galaxy catalogues and a measurement of the growth of structure from redshift space distortions at $z = 0.15$," *Mon. Not. Roy. Astron. Soc.* **449** no. 1, (2015) 848–866, arXiv:1409.3238 [astro-ph.CO].

[219] **2dFGRS** Collaboration, W. J. Percival *et al.*, "The 2dF Galaxy Redshift Survey: Spherical harmonics analysis of fluctuations in the final catalogue," *Mon. Not. Roy. Astron. Soc.* **353** (2004) 1201, arXiv:astro-ph/0406513 [astro-ph].

[220] C. Blake *et al.*, "The WiggleZ Dark Energy Survey: the growth rate of cosmic structure since redshift z=0.9," *Mon. Not. Roy. Astron. Soc.* **415** (2011) 2876, arXiv:1104.2948 [astro-ph.CO].

[221] L. Samushia, W. J. Percival, and A. Raccanelli, "Interpreting large-scale redshift-space distortion measurements," *Mon. Not. Roy. Astron. Soc.* **420** (2012) 2102–2119, arXiv:1102.1014 [astro-ph.CO].

[222] R. Tojeiro *et al.*, "The clustering of galaxies in the SDSS-III Baryon Oscillation Spectroscopic Survey: measuring structure growth using passive galaxies," *Mon. Not. Roy. Astron. Soc.* **424** (2012) 2339, arXiv:1203.6565 [astro-ph.CO].

[223] H. Gil-Marín *et al.*, "The clustering of galaxies in the SDSS-III Baryon Oscillation Spectroscopic Survey: RSD measurement from the LOS-dependent power spectrum of DR12 BOSS galaxies," *Mon. Not. Roy. Astron. Soc.* **460** no. 4, (2016) 4188–4209, arXiv:1509.06386 [astro-ph.CO].

[224] **SDSS** Collaboration, M. Tegmark *et al.*, "Cosmological Constraints from the SDSS Luminous Red Galaxies," *Phys. Rev.* **D74** (2006) 123507, arXiv:astro-ph/0608632 [astro-ph].

[225] C. Blake *et al.*, "The WiggleZ Dark Energy Survey: Joint measurements of the expansion and growth history at z < 1," *Mon. Not. Roy. Astron. Soc.* **425** (2012) 405–414, arXiv:1204.3674 [astro-ph.CO].

[226] C.-H. Chuang *et al.*, "The clustering of galaxies in the SDSS-III Baryon Oscillation Spectroscopic Survey: single-probe measurements from CMASS anisotropic galaxy clustering," *Mon. Not. Roy. Astron. Soc.* **461** no. 4, (2016) 3781–3793, arXiv:1312.4889 [astro-ph.CO].

[227] L. Guzzo *et al.*, "A test of the nature of cosmic acceleration using galaxy redshift distortions," *Nature* **451** (2008) 541–545, arXiv:0802.1944 [astro-ph].

[228] S. de la Torre *et al.*, "The VIMOS Public Extragalactic Redshift Survey (VIPERS). Galaxy clustering and redshift-space distortions at z=0.8 in the first data release," *Astron. Astrophys.* **557** (2013) A54, arXiv:1303.2622 [astro-ph.CO].

[229] H. Okada *et al.*, "The Subaru FMOS Galaxy Redshift Survey (FastSound). II. The Emission Line Catalog and Properties of Emission Line Galaxies," *Publ. Astron. Soc. Jap.* **68** no. 3, (2016) 47, arXiv:1504.05592 [astro-ph.GA].

[230] **BOSS** Collaboration, S. Satpathy *et al.*, "The clustering of galaxies in the completed SDSS-III Baryon Oscillation Spectroscopic Survey: On the measurement of growth rate using galaxy correlation functions," *Mon. Not. Roy. Astron. Soc.* **469** no. 2, (2017) 1369–1382, arXiv:1607.03148 [astro-ph.CO].

[231] Y.-H. Li and X. Zhang, "Large-scale stable interacting dark energy model: Cosmological perturbations and observational constraints," *Phys. Rev.* **D89** no. 8, (2014) 083009, arXiv:1312.6328 [astro-ph.CO].

[232] *CAMB code for anisotropies*. http://camb.info/.

[233] J. Lesgourgues, "The Cosmic Linear Anisotropy Solving System (CLASS) I: Overview," arXiv:1104.2932 [astro-ph.IM].

[234] A. V. Astashenok and S. D. Odintsov, "Confronting dark energy models mimicking ΛCDM epoch with observational constraints: future cosmological perturbations decay or future Rip?," *Phys. Lett.* **B718** (2013) 1194–1202, arXiv:1211.1888 [gr-qc].

[235] E. Macaulay, I. K. Wehus, and H. K. Eriksen, "Lower Growth Rate from Recent Redshift Space Distortion Measurements than Expected from Planck," *Phys. Rev. Lett.* **111** no. 16, (2013) 161301, arXiv:1303.6583 [astro-ph.CO].

[236] R. A. Battye, T. Charnock, and A. Moss, "Tension between the power spectrum of density perturbations measured on large and small scales," *Phys. Rev.* **D91** no. 10, (2015) 103508, arXiv:1409.2769 [astro-ph.CO].

[237] S. D. H. Hsu, A. Jenkins, and M. B. Wise, "Gradient instability for w < -1," *Phys. Lett.* **B597** (2004) 270–274, arXiv:astro-ph/0406043 [astro-ph].

[238] S. Dubovsky, T. Gregoire, A. Nicolis, and R. Rattazzi, "Null energy condition and superluminal propagation," *JHEP* **03** (2006) 025, arXiv:hep-th/0512260 [hep-th].

[239] H. Stefancic, "Generalized phantom energy," *Phys. Lett.* **B586** (2004) 5–10, arXiv:astro-ph/0310904 [astro-ph].

[240] E. Elizalde, S. Nojiri, S. D. Odintsov, D. Sáez-Gómez, and V. Faraoni, "Reconstructing the universe history, from inflation to acceleration, with phantom and canonical scalar fields," *Phys. Rev.* **D77** (2008) 106005, arXiv:0803.1311 [hep-th].

[241] V. Sahni, A. Shafieloo, and A. A. Starobinsky, "Model independent evidence for dark energy evolution from Baryon Acoustic Oscillations," *Astrophys. J.* **793** no. 2, (2014) L40, arXiv:1406.2209 [astro-ph.CO].

[242] S. Vagnozzi, S. Dhawan, M. Gerbino, K. Freese, A. Goobar, and O. Mena, "Constraints on the sum of the neutrino masses in dynamical dark energy models with $w(z) \geq -1$ are tighter than those obtained in ΛCDM," *Phys. Rev.* **D98** no. 8, (2018) 083501, arXiv:1801.08553 [astro-ph.CO].

[243] U. Alam, S. Bag, and V. Sahni, "Constraining the Cosmology of the Phantom Brane using Distance Measures," *Phys. Rev.* **D95** no. 2, (2017) 023524, arXiv:1605.04707 [astro-ph.CO].

[244] V. Sahni and Y. Shtanov, "Brane world models of dark energy," *JCAP* **0311** (2003) 014, arXiv:astro-ph/0202346 [astro-ph].

[245] F. Contreras, N. Cruz, E. Elizalde, E. González, and S. Odintsov, "Linking little rip cosmologies with regular early universes," *Phys. Rev.* **D98** no. 12, (2018) 123520, arXiv:1808.06546 [gr-qc].

[246] M. Bouhmadi-López, C.-Y. Chen, and P. Chen, "On the Consistency of the Wheeler-DeWitt Equation in the Quantized Eddington-inspired Born-Infeld Gravity," *JCAP* **1812** no. 12, (2018) 032, arXiv:1810.10918 [gr-qc].

[247] E. Elizalde, S. Nojiri, and S. D. Odintsov, "Late-time cosmology in (phantom) scalar-tensor theory: Dark energy and the cosmic speed-up," *Phys. Rev.* **D70** (2004) 043539, arXiv:hep-th/0405034 [hep-th].

[248] E. Elizalde, S. Nojiri, S. D. Odintsov, and P. Wang, "Dark energy: Vacuum fluctuations, the effective phantom phase, and holography," *Phys. Rev.* **D71** (2005) 103504, arXiv:hep-th/0502082 [hep-th].

[249] H. Velten and R. Fazolo, "Revealing the nonadiabatic nature of dark energy perturbations from galaxy clustering data," *Phys. Rev.* **D96** no. 8, (2017) 083502, arXiv:1707.03224 [astro-ph.CO].

[250] A. Maeder and V. G. Gueorguiev, "The growth of the density fluctuations in the scale-invariant vacuum theory," *Phys. Dark Univ.* **25** (2019) 100315, arXiv:1811.03495 [astro-ph.CO].

[251] J. Mifsud and C. Van De Bruck, "Probing the imprints of generalized interacting dark energy on the growth of perturbations," *JCAP* **1711** no. 11, (2017) 001, arXiv:1707.07667 [astro-ph.CO].

[252] J. Dutta, W. Khyllep, and N. Tamanini, "Dark energy with a gradient coupling to the dark matter fluid: cosmological dynamics and structure formation," *JCAP* **1801** (2018) 038, arXiv:1707.09246 [gr-qc].

[253] E. G. M. Ferreira, G. Franzmann, J. Khoury, and R. Brandenberger, "Unified Superfluid Dark Sector," *JCAP* **1908** (2019) 027, arXiv:1810.09474 [astro-ph.CO].

[254] R. A. Battye, B. Bolliet, and F. Pace, "Do cosmological data rule out $f(\mathcal{R})$ with $w \neq -1$?," *Phys. Rev.* **D97** no. 10, (2018) 104070, arXiv:1712.05976 [astro-ph.CO].

[255] R. Arjona, W. Cardona, and S. Nesseris, "Unraveling the effective fluid approach for $f(R)$ models in the subhorizon approximation," *Phys. Rev.* **D99** no. 4, (2019) 043516, arXiv:1811.02469 [astro-ph.CO].

[256] A. de la Macorra and E. Almaraz, "Theoretical and Observational Constraints of Bound Dark Energy with Precision Cosmological Data," *Phys. Rev. Lett.* **121** no. 16, (2018) 161303, arXiv:1805.01510 [astro-ph.CO].

[257] D. M. Scolnic *et al.*, "The Complete Light-curve Sample of Spectroscopically Confirmed SNe Ia from Pan-STARRS1 and Cosmological Constraints from the Combined Pantheon Sample," *Astrophys. J.* **859** no. 2, (2018) 101, arXiv:1710.00845 [astro-ph.CO].

[258] Z. Zhai and Y. Wang, "Robust and model-independent cosmological constraints from distance measurements," *JCAP* **1907** no. 07, (2019) 005, arXiv:1811.07425 [astro-ph.CO].

[259] L. Kazantzidis, L. Perivolaropoulos, and F. Skara, "Constraining power of cosmological observables: blind redshift spots and optimal ranges," *Phys. Rev.* **D99** no. 6, (2019) 063537, arXiv:1812.05356 [astro-ph.CO].

[260] **BOSS** Collaboration, L. Anderson *et al.*, "The clustering of galaxies in the SDSS-III Baryon Oscillation Spectroscopic Survey: baryon acoustic oscillations in the Data Releases 10 and 11 Galaxy samples," *Mon. Not. Roy. Astron. Soc.* **441** no. 1, (2014) 24–62, arXiv:1312.4877 [astro-ph.CO].

[261] F. Beutler, C. Blake, M. Colless, D. H. Jones, L. Staveley-Smith, L. Campbell, Q. Parker, W. Saunders, and F. Watson, "The 6dF Galaxy Survey: Baryon Acoustic Oscillations and the Local Hubble Constant," *Mon. Not. Roy. Astron. Soc.* **416** (2011) 3017–3032, arXiv:1106.3366 [astro-ph.CO].

[262] A. J. Ross, L. Samushia, C. Howlett, W. J. Percival, A. Burden, and M. Manera, "The clustering of the SDSS DR7 main Galaxy sample – I. A 4 per cent distance measure at $z = 0.15$," *Mon. Not. Roy. Astron. Soc.* **449** no. 1, (2015) 835–847, arXiv:1409.3242 [astro-ph.CO].

[263] E. A. Kazin *et al.*, "The WiggleZ Dark Energy Survey: improved distance measurements to z = 1 with reconstruction of the baryonic acoustic feature," *Mon. Not. Roy. Astron. Soc.* **441** no. 4, (2014) 3524–3542, arXiv:1401.0358 [astro-ph.CO].

[264] **BOSS** Collaboration, S. Alam *et al.*, "The clustering of galaxies in the completed SDSS-III Baryon Oscillation Spectroscopic Survey: cosmological analysis of the DR12 galaxy sample," *Mon. Not. Roy. Astron. Soc.* **470** no. 3, (2017) 2617–2652, arXiv:1607.03155 [astro-ph.CO].

[265] C. Zhang, H. Zhang, S. Yuan, S. Liu, T.-J. Zhang, and Y.-C. Sun, "Four new observational H(z) data from luminous red galaxies in the Sloan Digital Sky Survey data release seven," *Research in Astronomy and Astrophysics* **14** no. 10, (Oct, 2014) 1221–1233, arXiv:1207.4541 [astro-ph.CO].

[266] D. Stern, R. Jiménez, L. Verde, M. Kamionkowski, and S. A. Stanford, "Cosmic Chronometers: Constraining the Equation of State of Dark Energy. I: H(z) Measurements," *JCAP* **1002** (2010) 008, arXiv:0907.3149 [astro-ph.CO].

[267] M. Moresco *et al.*, "Improved constraints on the expansion rate of the Universe up to z 1.1 from the spectroscopic evolution of cosmic chronometers," *JCAP* **1208** (2012) 006, arXiv:1201.3609 [astro-ph.CO].

[268] C.-H. Chuang and Y. Wang, "Modeling the Anisotropic Two-Point Galaxy Correlation Function on Small Scales and Improved Measurements of $H(z)$, $D_A(z)$, and $\beta(z)$ from the Sloan Digital Sky Survey DR7 Luminous Red Galaxies," *Mon. Not. Roy. Astron. Soc.* **435** (2013) 255–262, arXiv:1209.0210 [astro-ph.CO].

[269] M. Moresco, "Raising the bar: new constraints on the Hubble parameter with cosmic chronometers at z ¤ 2," *Mon. Not. Roy. Astron. Soc.* **450** no. 1, (2015) L16–L20, arXiv:1503.01116 [astro-ph.CO].

[270] M. Moresco, L. Pozzetti, A. Cimatti, R. Jiménez, C. Maraston, L. Verde, D. Thomas, A. Citro, R. Tojeiro, and D. Wilkinson, "A 6% measurement of the Hubble parameter at $z \sim 0.45$: direct evidence of the epoch of cosmic re-acceleration," *JCAP* **1605** no. 05, (2016) 014, arXiv:1601.01701 [astro-ph.CO].

[271] P. Stöcker, M. Krämer, J. Lesgourgues, and V. Poulin, "Exotic energy injection with ExoCLASS: Application to the Higgs portal model and evaporating black holes," *JCAP* **1803** no. 03, (2018) 018, arXiv:1801.01871 [astro-ph.CO].

[272] **SNLS** Collaboration, A. Conley *et al.*, "Supernova Constraints and Systematic Uncertainties from the First 3 Years of the Supernova Legacy Survey," *Astrophys. J. Suppl.* **192** (2011) 1, arXiv:1104.1443 [astro-ph.CO].

[273] D. J. Fixsen, "The Temperature of the Cosmic Microwave Background," *Astrophys. J.* **707** (2009) 916–920, arXiv:0911.1955 [astro-ph.CO].

[274] W. Hu and N. Sugiyama, "Small scale cosmological perturbations: An Analytic approach," *Astrophys. J.* **471** (1996) 542–570, arXiv:astro-ph/9510117 [astro-ph].

[275] **SDSS** Collaboration, D. J. Eisenstein *et al.*, "Detection of the Baryon Acoustic Peak in the Large-Scale Correlation Function of SDSS Luminous Red Galaxies," *Astrophys. J.* **633** (2005) 560–574, arXiv:astro-ph/0501171 [astro-ph].

[276] D. J. Eisenstein and W. Hu, "Baryonic features in the matter transfer function," *Astrophys. J.* **496** (1998) 605, arXiv:astro-ph/9709112 [astro-ph].

[277] E. Gaztanaga, A. Cabre, and L. Hui, "Clustering of Luminous Red Galaxies IV: Baryon Acoustic Peak in the Line-of-Sight Direction and a Direct Measurement of H(z)," *Mon. Not. Roy. Astron. Soc.* **399** (2009) 1663–1680, arXiv:0807.3551 [astro-ph].

[278] R. Jiménez and A. Loeb, "Constraining cosmological parameters based on relative galaxy ages," *Astrophys. J.* **573** (2002) 37–42, arXiv:astro-ph/0106145 [astro-ph].

[279] H. Akaike, *A new look at the statistical model identification*. Institute of Electrical and Electronics Engineers, Institute of Statistical Mathematics, Minato-ku, Tokyo, Japan, 1974. hhttps://ieeexplore.ieee.org/document/1100705.

[280] S. Basilakos and S. Nesseris, "Conjoined constraints on modified gravity from the expansion history and cosmic growth," *Phys. Rev.* **D96** no. 6, (2017) 063517, arXiv:1705.08797 [astro-ph.CO].

[281] B. Sagredo, J. S. Lafaurie, and D. Sapone, "Comparing Dark Energy models with Hubble versus Growth Rate data," arXiv:1808.05660 [astro-ph.CO].

[282] S. Nesseris, G. Pantazis, and L. Perivolaropoulos, "Tension and constraints on modified gravity parametrizations of $G_{\rm eff}(z)$ from growth rate and Planck data," *Phys. Rev.* **D96** no. 2, (2017) 023542, arXiv:1703.10538 [astro-ph.CO].

[283] L. Kazantzidis and L. Perivolaropoulos, "Evolution of the $f\sigma_8$ tension with the Planck15/ΛCDM determination and implications for modified gravity theories," *Phys. Rev.* **D97** no. 10, (2018) 103503, arXiv:1803.01337 [astro-ph.CO].

[284] M. Davis, A. Nusser, K. Masters, C. Springob, J. P. Huchra, and G. Lemson, "Local Gravity versus Local Velocity: Solutions for β and nonlinear bias," *Mon. Not. Roy. Astron. Soc.* **413** (2011) 2906, arXiv:1011.3114 [astro-ph.CO].

[285] S. J. Turnbull, M. J. Hudson, H. A. Feldman, M. Hicken, R. P. Kirshner, and R. Watkins, "Cosmic flows in the nearby universe from Type Ia Supernovae," *Mon. Not. Roy. Astron. Soc.* **420** (2012) 447–454, arXiv:1111.0631 [astro-ph.CO].

[286] D. Huterer, D. Shafer, D. Scolnic, and F. Schmidt, "Testing ΛCDM at the lowest redshifts with SN Ia and galaxy velocities," *JCAP* **1705** no. 05, (2017) 015, arXiv:1611.09862 [astro-ph.CO].

[287] M. Feix, A. Nusser, and E. Branchini, "Growth Rate of Cosmological Perturbations at z~ 0.1 from a New Observational Test," *Phys. Rev. Lett.* **115** no. 1, (2015) 011301, arXiv:1503.05945 [astro-ph.CO].

[288] C. Blake *et al.*, "Galaxy And Mass Assembly (GAMA): improved cosmic growth measurements using multiple tracers of large-scale structure," *Mon. Not. Roy. Astron. Soc.* **436** (2013) 3089, arXiv:1309.5556 [astro-ph.CO].

[289] A. G. Sanchez *et al.*, "The clustering of galaxies in the SDSS-III Baryon Oscillation Spectroscopic Survey: cosmological implications of the full shape of the clustering wedges in the data release 10 and 11 galaxy samples," *Mon. Not. Roy. Astron. Soc.* **440** no. 3, (2014) 2692–2713, arXiv:1312.4854 [astro-ph.CO].

[290] A. Pezzotta *et al.*, "The VIMOS Public Extragalactic Redshift Survey (VIPERS): The growth of structure at $0.5 < z < 1.2$ from redshift-space distortions in the clustering of the PDR-2 final sample," *Astron. Astrophys.* **604** (2017) A33, arXiv:1612.05645 [astro-ph.CO].

[291] M. Visser, "Cosmography: Cosmology without the Einstein equations," *Gen. Rel. Grav.* **37** (2005) 1541–1548, arXiv:gr-qc/0411131 [gr-qc].

[292] C. Cattoen and M. Visser, "The Hubble series: Convergence properties and redshift variables," *Class. Quant. Grav.* **24** (2007) 5985–5998, arXiv:0710.1887 [gr-qc].

[293] S. Capozziello, V. F. Cardone, and V. Salzano, "Cosmography of f(R) gravity," *Phys. Rev.* **D78** (2008) 063504, arXiv:0802.1583 [astro-ph].

[294] V. Sahni, T. D. Saini, A. A. Starobinsky, and U. Alam, "Statefinder: A New geometrical diagnostic of dark energy," *JETP Lett.* **77** (2003) 201–206, arXiv:astro-ph/0201498 [astro-ph]. [Pisma Zh. Eksp. Teor. Fiz.77,249(2003)].

[295] U. Alam, V. Sahni, T. D. Saini, and A. A. Starobinsky, "Exploring the expanding universe and dark energy using the Statefinder diagnostic," *Mon. Not. Roy. Astron. Soc.* **344** (2003) 1057, arXiv:astro-ph/0303009 [astro-ph].

[296] M. Arabsalmani and V. Sahni, "The Statefinder hierarchy: An extended null diagnostic for concordance cosmology," *Phys. Rev.* **D83** (2011) 043501, arXiv:1101.3436 [astro-ph.CO].

[297] J. Li, R. Yang, and B. Chen, "Discriminating dark energy models by using the statefinder hierarchy and the growth rate of matter perturbations," *JCAP* **1412** no. 12, (2014) 043, arXiv:1406.7514 [gr-qc].

[298] R. de Putter, D. Huterer, and E. V. Linder, "Measuring the Speed of Dark: Detecting Dark Energy Perturbations," *Phys. Rev.* **D81** (2010) 103513, arXiv:1002.1311 [astro-ph.CO].

[299] A. Yu. Kamenshchik, E. O. Pozdeeva, S. Yu. Vernov, A. Tronconi, and G. Venturi, "Transformations between Jordan and Einstein frames: Bounces, antigravity, and crossing singularities," *Phys. Rev.* **D94** no. 6, (2016) 063510, arXiv:1602.07192 [gr-qc].

[300] S. Bag, A. Viznyuk, Y. Shtanov, and V. Sahni, "Cosmological perturbations on the Phantom brane," *JCAP* **1607** no. 07, (2016) 038, arXiv:1603.01277 [gr-qc].

[301] H. A. Rizwan ul and S. Unnikrishnan, "Effect of dark energy sound speed and equation of state on CDM power spectrum," *J. Phys. Conf. Ser.* **484** (2014) 012048, arXiv:1407.4079 [astro-ph.CO].

[302] S. Nesseris and D. Sapone, "Accuracy of the growth index in the presence of dark energy perturbations," *Phys. Rev.* **D92** no. 2, (2015) 023013, arXiv:1505.06601 [astro-ph.CO].

[303] D. Pietrobon, A. Balbi, M. Bruni, and C. Quercellini, "Affine parameterization of the dark sector: costraints from WMAP5 and SDSS," *Phys. Rev.* **D78** (2008) 083510, arXiv:0807.5077 [astro-ph].

[304] M. S. Linton, A. Pourtsidou, R. Crittenden, and R. Maartens, "Variable sound speed in interacting dark energy models," *JCAP* **1804** no. 04, (2018) 043, arXiv:1711.05196 [astro-ph.CO].

[305] T. Koivisto and D. F. Mota, "Dark energy anisotropic stress and large scale structure formation," *Phys. Rev.* **D73** (2006) 083502, arXiv:astro-ph/0512135 [astro-ph].

[306] A. Mehrabi, S. Basilakos, and F. Pace, "How clustering dark energy affects matter perturbations," *Mon. Not. Roy. Astron. Soc.* **452** no. 3, (2015) 2930–2939, arXiv:1504.01262 [astro-ph.CO].

[307] M. Abramowitz and I. A. Stegun, *Handbook of mathematical functions with formulas, graphs, and mathematical tables*. 1965.

[308] C. Kiefer, "On the Avoidance of Classical Singularities in Quantum Cosmology," *J. Phys. Conf. Ser.* **222** (2010) 012049.

[309] A. Kamenshchik, C. Kiefer, and N. Kwidzinski, "Classical and quantum cosmology of Born-Infeld type models," *Phys. Rev.* **D93** no. 8, (2016) 083519, arXiv:1602.01319 [gr-qc].

[310] R. M. Wald, *General Relativity*. Chicago Univ. Pr., Chicago, USA, 1984.

[311] M. Henneaux and C. Teitelboim, *Quantization of gauge systems*. 1992.

[312] P. A. M. Dirac, *Lectures on Quantum Mechanics*. Belfer Graduate School Sci. Mono. Belfer Graduate School of Science, New York, NY, 1964. https://cds.cern.ch/record/113811. Photocopy.

[313] P. J. E. Peebles and B. Ratra, "The Cosmological constant and dark energy," *Rev. Mod. Phys.* **75** (2003) 559–606, arXiv:astro-ph/0207347 [astro-ph]. [,592(2002)].

[314] W. Fischler and L. Susskind, "Holography and cosmology," arXiv:hep-th/9806039 [hep-th].

[315] J. D. Bekenstein, "A Universal Upper Bound on the Entropy to Energy Ratio for Bounded Systems," *Phys. Rev.* **D23** (1981) 287.

[316] P. F. González-Díaz, "BOUNDS ON THE ENTROPY," *Phys. Rev.* **D27** (1983) 3042–3043.

[317] A. G. Cohen, D. B. Kaplan, and A. E. Nelson, "Effective field theory, black holes, and the cosmological constant," *Phys. Rev. Lett.* **82** (1999) 4971–4974, arXiv:hep-th/9803132 [hep-th].

[318] S. D. H. Hsu, "Entropy bounds and dark energy," *Phys. Lett.* **B594** (2004) 13–16, arXiv:hep-th/0403052 [hep-th].

[319] R. Horvat, "Holography and variable cosmological constant," *Phys. Rev.* **D70** (2004) 087301, arXiv:astro-ph/0404204 [astro-ph].

[320] R.-G. Cai, "A Dark Energy Model Characterized by the Age of the Universe," *Phys. Lett.* **B657** (2007) 228–231, arXiv:0707.4049 [hep-th].

[321] C. Gao, F. Wu, X. Chen, and Y.-G. Shen, "A Holographic Dark Energy Model from Ricci Scalar Curvature," *Phys. Rev.* **D79** (2009) 043511, arXiv:0712.1394 [astro-ph].

[322] L. N. Granda and A. Oliveros, "Infrared cut-off proposal for the Holographic density," *Phys. Lett.* **B669** (2008) 275–277, arXiv:0810.3149 [gr-qc].

[323] I. Duran and D. Pavon, "A model of interacting holographic dark energy at the Ricci's scale," *Phys. Rev.* **D83** (2011) 023504, arXiv:1012.2986 [astro-ph.CO].

[324] L. P. Chimento and M. G. Richarte, "Interacting dark matter and modified holographic Ricci dark energy induce a relaxed Chaplygin gas," *Phys. Rev.* **D84** (2011) 123507, arXiv:1107.4816 [astro-ph.CO].

[325] L. P. Chimento, M. Forte, and M. G. Richarte, "Modified holographic Ricci dark energy coupled to interacting dark matter and a non interacting baryonic component," *Eur. Phys. J.* **C73** no. 1, (2013) 2285, arXiv:1301.2737 [gr-qc].

[326] C.-J. Feng, "Statefinder Diagnosis for Ricci Dark Energy," *Phys. Lett.* **B670** (2008) 231–234, arXiv:0809.2502 [hep-th].

[327] M. Bouhmadi-López and Y. Tavakoli, "Why is the running vacuum energy more benign than the holographic Ricci dark energy?," *Phys. Rev.* **D87** no. 2, (2013) 023515.

[328] S. Ghaffari, A. Sheykhi, and M. H. Dehghani, "Statefinder diagnosis for holographic dark energy in the DGP braneworld," *Phys. Rev.* **D91** no. 2, (2015) 023007, arXiv:1504.04008 [gr-qc].

[329] M. Suwa, K. Kobayashi, and H. Oshima, "The interacting generalized Ricci dark energy model in non-flat universe," *J. Mod. Phys.* **6** (2015) 327, arXiv:1412.5241 [astro-ph.CO].

[330] L. Xu and Y. Wang, "Observational Constraints to Ricci Dark Energy Model by Using: SN, BAO, OHD, fgas Data Sets," *JCAP* **1006** (2010) 002, arXiv:1006.0296 [astro-ph.CO].

[331] C. Kiefer and B. Sandhöfer, "Quantum Cosmology," arXiv:0804.0672 [gr-qc].

[332] M. Bouhmadi-López, L. J. Garay, and P. F. González-Díaz, "Quantum behavior of FRW radiation filled universes," *Phys. Rev.* **D66** (2002) 083504, arXiv:gr-qc/0204072 [gr-qc].

[333] M. Bouhmadi-López and P. Vargas Moniz, "FRW quantum cosmology with a generalized Chaplygin gas," *Phys. Rev.* **D71** (2005) 063521, arXiv:gr-qc/0404111 [gr-qc].

[334] M. Bouhmadi-López and P. Vargas Moniz, "Quantisation of Parameters and the String Landscape Problem," *JCAP* **0705** (2007) 005, arXiv:hep-th/0612149 [hep-th].

[335] S. del Campo, J. C. Fabris, R. Herrera, and W. Zimdahl, "Cosmology with Ricci dark energy," *Phys. Rev.* **D87** no. 12, (2013) 123002, arXiv:1303.3436 [astro-ph.CO].

[336] Y. Tavakoli and J. C. Fabris, "Creation of particles in a cyclic universe driven by loop quantum cosmology," *Int. J. Mod. Phys.* **D24** no. 08, (2015) 1550062, arXiv:1412.0775 [gr-qc].

[337] C. Kiefer, "Quantum geometrodynamics: whence, whither?," *Gen. Rel. Grav.* **41** (2009) 877–901, arXiv:0812.0295 [gr-qc].

[338] C. Kiefer and H. D. Zeh, "Arrow of time in a recollapsing quantum universe," *Phys. Rev.* **D51** (1995) 4145–4153, arXiv:gr-qc/9402036 [gr-qc].

[339] J. J. M. Mathews, Mathews and R. L. Walker., *Mathematical methods of physics*.

[340] C. M. Bender, D. C. Brody, J.-H. Chen, H. F. Jones, K. A. Milton, and M. C. Ogilvie, "Equivalence of a Complex PT-Symmetric Quartic Hamiltonian and a Hermitian Quartic Hamiltonian with an Anomaly," *Phys. Rev.* **D74** (2006) 025016, arXiv:hep-th/0605066 [hep-th].

[341] A. Prudnikov, Y. Brychkov, O. Marichev, and R. Romer, "Integrals and series," *American Journal of Physics - AMER J PHYS* **56** (01, 1988) 957–958.

[342] A. O. Barvinsky, A. Yu. Kamenshchik, C. Kiefer, and I. V. Mishakov, "Decoherence in quantum cosmology at the onset of inflation," *Nucl. Phys.* **B551** (1999) 374–396, arXiv:gr-qc/9812043 [gr-qc].

[343] S. W. Hawking and R. Penrose, "The Singularities of gravitational collapse and cosmology," *Proc. Roy. Soc. Lond.* **A314** (1970) 529–548.

[344] S. Hawking and R. Penrose, "The nature of space and time," *The Nature of Space and Time by Stephen Hawking and Roger Penrose. Princeton University Press, 2010. ISBN: 978-0-691-14570-9* **275** (01, 2010) .

[345] V. Sahni, "Dark matter and dark energy," *Lect. Notes Phys.* **653** (2004) 141–180, arXiv:astro-ph/0403324 [astro-ph]. [,141(2004)].

[346] S. Weinberg, "The Cosmological constant problems," in *Sources and detection of dark matter and dark energy in the universe. Proceedings, 4th International Symposium, DM 2000, Marina del Rey, USA, February 23-25, 2000*, pp. 18–26. 2000. arXiv:astro-ph/0005265 [astro-ph]. http://www.slac.stanford.edu/spires/find/books/www?cl=QB461:I57:2000.

[347] J. Frieman, M. Turner, and D. Huterer, "Dark Energy and the Accelerating Universe," *Ann. Rev. Astron. Astrophys.* **46** (2008) 385–432, arXiv:0803.0982 [astro-ph].

[348] M. C. Bento, O. Bertolami, and A. A. Sen, "Generalized Chaplygin gas model: Dark energy - dark matter unification and CMBR constraints," *Gen. Rel. Grav.* **35** (2003) 2063–2069, arXiv:gr-qc/0305086 [gr-qc].

[349] A. A. Costa, X.-D. Xu, B. Wang, E. G. M. Ferreira, and E. Abdalla, "Testing the Interaction between Dark Energy and Dark Matter with Planck Data," *Phys. Rev.* **D89** no. 10, (2014) 103531, arXiv:1311.7380 [astro-ph.CO].

[350] V. Salvatelli, N. Said, M. Bruni, A. Melchiorri, and D. Wands, "Indications of a late-time interaction in the dark sector," *Phys. Rev. Lett.* **113** no. 18, (2014) 181301, arXiv:1406.7297 [astro-ph.CO].

[351] S. Nojiri, S. D. Odintsov, V. K. Oikonomou, and E. N. Saridakis, "Singular cosmological evolution using canonical and ghost scalar fields," *JCAP* **1509** (2015) 044, arXiv:1503.08443 [gr-qc].

[352] J. D. Barrow and A. A. H. Graham, "New Singularities in Unexpected Places," *Int. J. Mod. Phys.* **D24** no. 12, (2015) 1544012, arXiv:1505.04003 [gr-qc].

[353] K. Bamba, J. de Haro, and S. D. Odintsov, "Future Singularities and Teleparallelism in Loop Quantum Cosmology," *JCAP* **1302** (2013) 008, arXiv:1211.2968 [gr-qc].

[354] C.-I. Kuo and L. H. Ford, "Semiclassical gravity theory and quantum fluctuations," *Phys. Rev.* **D47** (1993) 4510–4519, arXiv:gr-qc/9304008 [gr-qc].

[355] P. Martín-Moruno and M. Visser, "Semiclassical energy conditions for quantum vacuum states," *JHEP* **09** (2013) 050, arXiv:1306.2076 [gr-qc].

[356] P. Martín-Moruno and M. Visser, "Classical and quantum flux energy conditions for quantum vacuum states," *Phys. Rev.* **D88** no. 6, (2013) 061701, arXiv:1305.1993 [gr-qc].

[357] R. Bousso, Z. Fisher, J. Koeller, S. Leichenauer, and A. C. Wall, "Proof of the Quantum Null Energy Condition," *Phys. Rev.* **D93** no. 2, (2016) 024017, arXiv:1509.02542 [hep-th].

[358] J. H. C. Scargill, M. Bañados, and P. G. Ferreira, "Cosmology with Eddington-inspired Gravity," *Phys. Rev.* **D86** (2012) 103533, arXiv:1210.1521 [astro-ph.CO].

[359] F. Arroja, C.-Y. Chen, P. Chen, and D.-h. Yeom, "Singular Instantons in Eddington-inspired-Born-Infeld Gravity," *JCAP* **1703** no. 03, (2017) 044, arXiv:1612.00674 [gr-qc].

[360] A. N. Makarenko, S. Odintsov, and G. J. Olmo, "Born-Infeld-$f(R)$ gravity," *Phys. Rev.* **D90** (2014) 024066, arXiv:1403.7409 [hep-th].

[361] S. D. Odintsov, G. J. Olmo, and D. Rubiera-Garcia, "Born-Infeld gravity and its functional extensions," *Phys. Rev.* **D90** (2014) 044003, arXiv:1406.1205 [hep-th].

[362] J. Beltran Jiménez, L. Heisenberg, and G. J. Olmo, "Infrared lessons for ultraviolet gravity: the case of massive gravity and Born-Infeld," *JCAP* **1411** (2014) 004, arXiv:1409.0233 [hep-th].

[363] C.-Y. Chen, M. Bouhmadi-López, and P. Chen, "Modified Eddington-inspired-Born-Infeld Gravity with a Trace Term," *Eur. Phys. J.* **C76** (2016) 40, arXiv:1507.00028 [gr-qc].

[364] M. Bouhmadi-López, Y. Tavakoli, and P. Vargas Moniz, "Appeasing the Phantom Menace?," *JCAP* **1004** (2010) 016, arXiv:0911.1428 [gr-qc].

[365] R. Penrose, "Gravitational collapse and space-time singularities," *Phys. Rev. Lett.* **14** (1965) 57–59.

[366] S. W. Hawking and G. F. R. Ellis, *The Large Scale Structure of Space-Time*. Cambridge Monographs on Mathematical Physics. Cambridge University Press, 2011.

[367] S. Capozziello and M. De Laurentis, "Extended Theories of Gravity," *Phys. Rept.* **509** (2011) 167–321, arXiv:1108.6266 [gr-qc].

[368] I. Cho, H.-C. Kim, and T. Moon, "Universe Driven by Perfect Fluid in Eddington-inspired Born-Infeld Gravity," *Phys. Rev.* **D86** (2012) 084018, arXiv:1208.2146 [gr-qc].

[369] S.-L. Li and H. Wei, "Stability of the Einstein static universe in Eddington-inspired Born-Infeld theory," *Phys. Rev.* **D96** no. 2, (2017) 023531, arXiv:1705.06819 [gr-qc].

[370] H. Sotani and U. Miyamoto, "Properties of an electrically charged black hole in Eddington-inspired Born-Infeld gravity," *Phys. Rev.* **D90** (2014) 124087, arXiv:1412.4173 [gr-qc].

[371] H. Sotani and U. Miyamoto, "Strong gravitational lensing by an electrically charged black hole in Eddington-inspired Born-Infeld gravity," *Phys. Rev.* **D92** no. 4, (2015) 044052, arXiv:1508.03119 [gr-qc].

[372] C.-Y. Chen and P. Chen, "Quasinormal modes of massless scalar fields for charged black holes in the Palatini-type gravity," *Phys. Rev.* **D98** no. 4, (2018) 044042, arXiv:1806.09500 [gr-qc].

[373] M. Roshan, A. Kazemi, and I. De Martino, "Local fragmentation of thin discs in Eddington-inspired gravity," *Mon. Not. Roy. Astron. Soc.* **479** no. 1, (2018) 1287–1296, arXiv:1806.07414 [astro-ph.HE].

[374] R. Shaikh, "Wormholes with nonexotic matter in Born-Infeld gravity," *Phys. Rev.* **D98** no. 6, (2018) 064033, arXiv:1807.07941 [gr-qc].

[375] S. Jana, G. K. Chakravarty, and S. Mohanty, "Constraints on Born-Infeld gravity from the speed of gravitational waves after GW170817 and GRB 170817A," *Phys. Rev.* **D97** no. 8, (2018) 084011, arXiv:1711.04137 [gr-qc].

[376] A. Delhom, G. J. Olmo, and M. Ronco, "Observable traces of non-metricity: new constraints on metric-affine gravity," *Phys. Lett.* **B780** (2018) 294–299, arXiv:1709.04249 [hep-th].

[377] Y.-X. Liu, K. Yang, H. Guo, and Y. Zhong, "Domain Wall Brane in Eddington Inspired Born-Infeld Gravity," *Phys. Rev.* **D85** (2012) 124053, arXiv:1203.2349 [hep-th].

[378] K. Fernandes and A. Lahiri, "Kaluza Ansatz applied to Eddington inspired Born-Infeld Gravity," *Phys. Rev.* **D91** no. 4, (2015) 044014, arXiv:1405.2172 [gr-qc].

[379] C.-Y. Chen, M. Bouhmadi-López, and P. Chen, "Black hole solutions in mimetic Born-Infeld gravity," *Eur. Phys. J.* **C78** no. 1, (2018) 59, arXiv:1710.10638 [gr-qc].

[380] Ping-Li, J.-C. Ding, Q.-Q. Fan, X.-R. Hu, and J.-B. Deng, "The Varying Speed of Light in Eddington-inspired Born-Infield Gravity with Rainbow Metric," arXiv:1808.00801 [gr-qc].

[381] J. Beltran Jiménez, L. Heisenberg, G. J. Olmo, and D. Rubiera-Garcia, "Born–Infeld inspired modifications of gravity," *Phys. Rept.* **727** (2018) 1–129, arXiv:1704.03351 [gr-qc].

[382] M. Bouhmadi-López, C.-Y. Chen, P. Chen, and D.-h. Yeom, "Regular Instantons in the Eddington-inspired-Born-Infeld Gravity: Lorentzian Wormholes from Bubble Nucleations," *JCAP* **1810** no. 10, (2018) 056, arXiv:1809.06579 [gr-qc].

[383] E. T. Whittaker and G. N. Watson, *A Course of Modern Analysis*. Cambridge Mathematical Library. Cambridge University Press, 4 ed., 1996.

[384] C.-Y. Chen, M. Bouhmadi-López, and P. Chen, "Probing Palatini-type gravity theories through gravitational wave detections via quasinormal modes," *Eur. Phys. J.* **C79** no. 1, (2019) 63, arXiv:1811.12494 [gr-qc].

[385] V. I. Afonso, G. J. Olmo, E. Orazi, and D. Rubiera-Garcia, "Mapping nonlinear gravity into General Relativity with nonlinear electrodynamics," *Eur. Phys. J.* **C78** no. 10, (2018) 866, arXiv:1807.06385 [gr-qc].

[386] S. Capozziello, M. De Laurentis, and R. Myrzakulov, "Noether symmetry approach for Dirac–Born–Infeld cosmology," *Int. J. Geom. Meth. Mod. Phys.* **12** no. 05, (2015) 1550065, arXiv:1411.7523 [gr-qc].

[387] M. Bouhmadi-López, S. Capozziello, and P. Martín-Moruno, "Self-acceleration and matter content in bicosmology from Noether Symmetries," *Gen. Rel. Grav.* **50** no. 4, (2018) 36, arXiv:1610.07346 [gr-qc].

[388] S. Capozziello, R. De Ritis, C. Rubano, and P. Scudellaro, "Noether symmetries in cosmology," *Riv. Nuovo Cim.* **19N4** (1996) 1–114.

[389] J. Beltran Jiménez, L. Heisenberg, and G. J. Olmo, "Tensor perturbations in a general class of Palatini theories," *JCAP* **1506** (2015) 026, arXiv:1504.00295 [gr-qc].

[390] J.-g. Hao and X.-z. Li, "An Attractor solution of phantom field," *Phys. Rev.* **D67** (2003) 107303, arXiv:gr-qc/0302100 [gr-qc].

[391] J.-G. Hao and X.-z. Li, "Phantom cosmic dynamics: Tracking attractor and cosmic doomsday," *Phys. Rev.* **D70** (2004) 043529, arXiv:astro-ph/0309746 [astro-ph].

[392] J.-c. Hwang and H. Noh, "Classical evolution and quantum generation in generalized gravity theories including string corrections and tachyon: Unified analyses," *Phys. Rev.* **D71** (2005) 063536, arXiv:gr-qc/0412126 [gr-qc].

[393] S. P. Kim and D. N. Page, "Wormhole spectrum of a quantum Friedmann-Robertson-Walker cosmology minimally coupled to a power law scalar field and the cosmological constant," *Phys. Rev.* **D45** (1992) R3296–R3300.

[394] S. P. Kim, "Quantum mechanics of conformally and minimally coupled Friedmann-Robertson-Walker cosmology," *Phys. Rev.* **D46** (1992) 3403–3434.

[395] S. P. Kim and W. Kim, "Will quantum cosmology resurrect chaotic inflation model?," *Int. J. Mod. Phys. Conf. Ser.* **43** (2016) 1660205, arXiv:1603.08087 [gr-qc].